Biosynthesis of protein filaments for the creation of a minimal cell

Kattan, Johannes

DOI
10.4233/uuid:724f70a9-efd9-4598-9a24-064aa77db509

Publication date
2020

Document Version
Final published version

Citation (APA)
Kattan, J. (2020). *Biosynthesis of protein filaments for the creation of a minimal cell*. [Dissertation (TU Delft), Delft University of Technology]. https://doi.org/10.4233/uuid:724f70a9-efd9-4598-9a24-064aa77db509

Biosynthesis of protein filaments for the creation of a minimal cell

Biosynthesis of protein filaments for the creation of a minimal cell

Dissertation

for the purpose of obtaining the degree of doctor
at Delft University of Technology
by the authority of the Rector Magnificus Prof.dr.ir. T.H.J.J. van der Hagen
chair of the Board for Doctorates
to be defended publicly
on Friday 12th June 2020 at 10:00 o'clock

by

Johannes Michael Kattan

Master of Science in Biology, Julius-Maximilians-Universität Würzburg, Germany
born in Lauf, Germany.

This dissertation has been approved by the promotors.

Composition of the doctoral committee:

Rector Magnificus,	chairperson
Dr. C.J.A. Danelon	Delft University of Technology, promotor
Prof. dr. M. Dogterom	Delft University of Technology, promotor

Independent members:

Prof.dr. M. Théry	Inst. Recherce Saint Louise
Prof.dr. W.H. Roos	RU Groningen
Prof.dr. H.A.E. Zwart	EU Rotterdam
Prof.dr. J.H. van Esch	Delft University of Technology
Prof.dr.ir. S.J. Tans	Delft University of Technology, reserve member

Keywords: synthetic biology, liposomes, minimal cell, synthetic cell, cell-free gene expression, microtubules, ESCRT-III, bacterial tubulin, Cdv-system

Printed by: Riddenprint

Cover by: Johannes Kattan, program applied for Mandelbrot forms taken from juliasets.dk

Casimir PhD-series, Delft-leiden 2020-13

ISBN: 978-90-8593-440-0

An electronic copy of this dissertation is available at
http://repository.tudelft.nl/

If only there were evil people somewhere insidiously committing evil deeds, and it were necessary only to separate them from the rest of us and destroy them. But the line dividing good and evil cuts through the heart of every human being. And who is willing to destroy a piece of his own heart?

Alexander Solzhenitsyn, The Gulag Archipelago

But the worst enemy you can face will always be yourself.

Friedrich Nietzsche, Thus Spoke Zarathustra

Contents

Chapter 1

Introduction

Was man an der Natur Geheimnisvolles pries,
Das wagen wir verständig zu probieren,
Und was sie sonst organisieren ließ,
Das lassen wir kristallisieren.

The mysteries Nature was praised for,
Through reason we dare to analyse,
And what she otherwise organises
We now let crystalize.

Johann Wolfgang von Goethe, Faust II

1

1.1 Artificial cells

1.1.1 The minimal cell and other artificial cell systems

Synthetic and artificial cells can be understood as umbrella terms and are applied in a heterogenic manner for a variety of systems that have not evolved on their own, but were instead designed intentionally. Most of these artificial systems are emulating certain cellular functions, but without being able to self-replicate or evolve. Thus, primarily mimicking cell functions and attributes, we termed these model systems here mimetic cells to differentiate them from other artificial cell-like systems. Mimetic cells vary significantly in their nature. They can be composed of organic or inorganic components and their compartments can be chambers, aqueous droplets in oil, or vesicles. Examples of mimetic cells are lipid vesicles encapsulating a gene expression system [1], oil droplets containing filaments [2], or vesicles formed from synthetic compounds that can mimic cellular functions like endocytosis [3]. The complexity of such *in vitro* systems is low compared to modern cells, which makes them ideal to study the emulated biological subsystems without interference of the multitude of other processes taking place *in vivo*. However, to understand how biological processes interact and sustain cells in their entirety, it will at some point be necessary to create more complex model systems that share the fundamental characteristics of living cells. Such systems are termed here minimal cells, protocells and abiological cells. An overview of these systems is given in Figure 1.1.

Our aim, and one that gained increasing attention during the last decade, is to recombine biological components and systems in a manner resulting in a cell-like system that can be considered alive. This conceptual entity has been termed a minimal cell, as it would only encompass the cellular processes necessary to engineer a cellular entity. The fundamental nature of this aspiration, which could be phrased as the creation of life, often sparks the need for defining what life is and what sets it apart from non-living matter. This runs into the problem that there are various different definitions of life that have for the longest time been of pragmatic or philosophical origin and applying a scientific framework to these often appears to be of arbitrary nature. Disregarding the implications that this topic has for our view on living organisms and ourselves, we could indeed fall back to the conclusion that the scientific definition of life is simply whatever definition scientists agree upon. However, it should be clarified that the creation of a minimal cell is a more concise aim than the creation of life in general. In case of a minimal cell, we have a specific form of life in mind, namely the cellular life forms that have evolved on our planet and exist today. Therefore, it is technically not necessary that we employ a definition of life that covers all associated processes and organisms. Nevertheless, this does not mean that there is not potentially a characteristic “nature” of living entities and this will be discussed in more detail at the end of this thesis in section 7.4. However, for the purpose of the next six chapters the important question to start with can be phrased as “what are the fundamental traits of a living cell?”.

Regarding the processes that necessarily have to be exerted by an entity to be considered as a living cell, we propose the following ones to be essential:

1. Replication and growth

2. Metabolic synthesis of components

3. The ability to evolve

Replication is an essential cellular process. It is the mechanism by which cellular life spreads and all cells originate from replication events of a precursor, except for the exceptional emergence of life out of non-living matter. Growth can be seen as prerequisite for repetitive replication, as divisions without growth would result in smaller and smaller cells until they would cease to be able of replication. Synthesis of components, which is conducted in biological cells through enzymatic processes, is fundamentally necessary for the creation, regulation and maintenance of any cellular process, including replication and growth. Last, we consider the ability of a system to evolve as a fundamental trait of living cells and likely the most important one at that. As laid out in Chapter 7, the ability to evolve, meaning the change of internal information over time and generations, is the most exclusive trait of living entities as several other structures and phenomena can as well grow and reproduce (crystals, fire, simple machines). The synthesis of components through enzymatic processes in itself is a hallmark of all living cells, but can by now be readily reproduced *in vitro* without being classified as a living system. Another way of defining alive could be the reproduction of an entity based on internal information. However, this would at least on the microscopic scale mean that the internal information is subject to changes due to entropic effects and would at least under any known condition necessarily result in evolutionary processes. Hence, such a definition is not identical, but practically analogues to one based on the potential of evolution.

A minimal cell would be therefore considered as an entity compromising no more biological components than necessary to exert these three functions. Self-maintenance is often referred to as another basic criterion [4–6], but there are two reasons why it can be considered as non-essential. First, it is a rather vague term, because it is not clear what exactly counts as self-maintenance. Cell metabolism is in some cases referred to as equal to self-maintenance, although certain metabolic processes are solely devoted to other functions like growth or reproduction. Second, it might be possible, although maybe unlikely, to create a cell that is able to grow and replicate without any genes responsible for any act of maintenance, assuming that the environment it is growing in is favourable enough. Waste products might be able to leave the cell passively through membrane pores and the DNA does likely not require any repair mechanism to allow for vital offspring over several generations. Overall, self-maintenance can be seen as a mechanism that is responsible for the effectiveness and robustness of a living system, rather than an essential characteristic of living cells. Motility is sometimes stated as another criterion [7], but is one we define here as well as a secondary trait of cellular life, as it is rather a specific adaptation to the environment and several bacterial species are classified as non-motile [8].

In general, the construction of a minimal cell would utilize only existing biological compounds and systems, albeit modified to a certain degree. First, because these are the only systems that we know to be successful in enabling a cell to be alive. Even more important, the application of existing systems for the engineering of a cell-like system is a useful feedback on how well we understand their actual nature and offers us unique chances to learn more about the cellular machineries we are surrounded with and run by. Related to that is the question of how life has emerged from lifeless components at least once in time and an important approach to investigate the origins of life has been the attempt to reconstruct the responsible processes *in vitro*. The ultimate aim in this regard is to discover primitive systems capable of full or partial reproduction, which are often referred to as protocells [9]. The attempt to create such protocells differs from the creation of a minimal cell primarily in that they are limited to the prebiotic components and conditions that are assumed to have been present on earth over 3.5 billion years ago. Thus, a protocell could for example be composed of a fatty acid membrane and utilizing ribozyme based reactions for its metabolism

[9,10]. Contrary to that, the minimal cell would be reconstituted from biological components and systems that are present today in living organisms and that are the product of 3.5 billion years of evolution. Therefore, the aim might be similar, but the applied methods and components inevitably differ. Nevertheless, it is certain that both fields of research will enrich each other considerably and the work towards a minimal cell will likely help us to understand in general how the dynamics of living systems can arise from interactions between its basic material components.

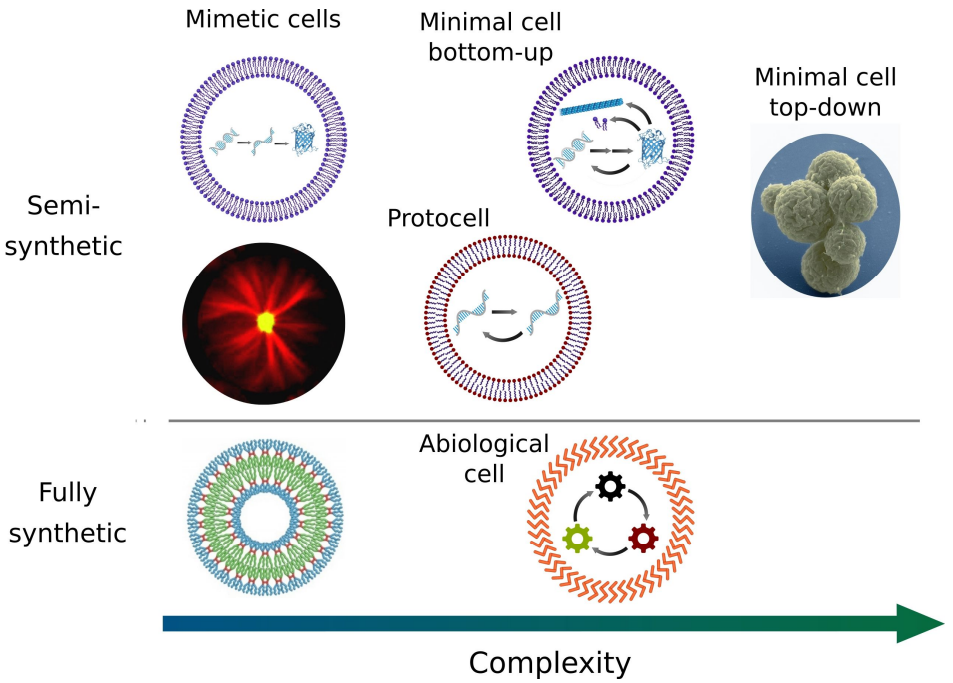

Figure 1.1: Overview of different artificial cell systems ordered by their relative complexity. Mimetic cells represent comparatively simple model systems in which a subset of cell functions are reconstituted or mimicked. Such systems include encapsulation of biological components, such as filaments or a gene expression system, in liposomes or droplets (semi-synthetic) and fully synthetic systems composed of non-organic components which nevertheless can mimic certain cell functions. More complex artificial systems, build from the bottom-up, are envisioned to represent living cells. These living artificial cells are categorized here in minimal cells, protocells and abiologic cells. Minimal cells are defined as a cell-like system, built from biological components present in modern cells. Protocells are made from components that were present when life originated and are aimed to yield plausible explanations for how life emerged. Abiologic cells would be alive in that they are able of reproduction and potentially of evolution, but would not be made from biological components and be only loosely oriented on the mechanisms present in biological cells. Besides these efforts to create cells bottom-up, existing organisms can be reduced in their complexity by a top-down approach to create a minimal cell. The example shown are JCV-syn3.0 cells created by the Craig Venter institute [11].

Besides minimal cells and protocells, which would consist of components that are or have been involved in the function of biological entities, there is also the possibility to engineer a fully synthetic cellular system. This would mean that all or most of the components of the system have little or no resemblance with biological components. DNA and proteins might for example be substituted in such a system by synthetic substances that could transfer information and exert metabolic processes by completely different mechanisms than what has ever been present in biological cells. Due to its unprecedented nature it would be difficult to predict what properties such an abiologic cell would have once it becomes truly alive. How classical synthetic biological system relate to these fully synthetic ones is further discussed in Chapter 7.

1.1.2 The top-down approach

One way of obtaining a minimal cell is by reducing the genome of existing organisms. This approach has been termed top-down approach, as it tries to scale down the complexity of the respective organism. The primary criterion for complexity is in this regard the genome size, as it is the most direct way to quantify the complexity of an organism. The smallest genome of a free-living bacteria is currently attributed to *Pelagibacter ubique* with 1.31 million base pairs (Mbp). For comparison, the size of the *E. coli* genome is 4.6 Mbp, the human genome is 3.1 Gbp, and the largest currently known genome of the Japanese flower plant *Paris japonica* is 149 Gbp. However, several parasitic bacteria possess even smaller genomes, as they can spare enzymes necessary for the synthesis of components that they can draw from their host. The genome of *Mycoplasma genitalium*, a bacterium that infects the urinary tracts in humans, consists of only 0.59 Mbp, which makes it the smallest known organism that is considered still capable of independent growth and reproduction. There are bacteria with smaller genomes, like the endosymbiont *Nasuia deltocephalinicola* with genome sizes as small 0.11 Mbp, but these bacteria are fully dependent on their host for reproduction.

Comparative studies on such organisms can reveal which genes are conserved among different species of bacteria. Thus, they are implicating the respective importance of genes for the fitness of the cell. The genomic comparison between *M. genitalium* and *Haemophilius influenzae* has for example revealed 240 homologous genes and lead to the hypothesis of a minimal genome consisting of 256 genes [12]. This number was later reduced to a theoretical minimal genome size of 206 genes [13]. It should be noted that a substantial number of these genes are involved in translation processes, with ribosomal proteins alone already representing 50 of the listed genes. However, this number of genes is not final and can maybe be further reduced. For example by supplying small compounds like nucleotides (NTPs) and amino acids (AAs) through the outside solution in combination with membrane pores for diffusion into the cell, and by reducing the complexity of the ribosome and other sub-systems [6].

Investigations of the described minimalistic organisms have eventually established the basis for attempts to practically examine the established theories. In 2010, the lab of Craig Venter designed and chemically synthesized a DNA sequence (JCV-syn1.0) based on the genome of *Mycoplasma mycoides*, which has a larger genome than *M. genitalium,* but is more suitable for in vitro experiments due its faster reproduction cycle. The synthesized genome was then transplanted into cells of a closely related bacterial species, *M. capricolum*, which resulted in viable cells [14]. Although only the genome of these cell was man-made, they have been referred to as synthetic, as the treated cells took on the characteristics of *M. mycoides* and after a certain number of replication

events effectively no original components of *M. capricolum* would remain in the offspring. This was followed up by attempts to reduce the size of the 1079 kbp JCV-syn1.0 genome by test cycling. During this process, it became clear who important certain non-coding sequences are for the organisation of the expression of essential genes. Moreover, several genes have been found to be redundant in exerting an identical essential task. Deletion of a single one of these genes is non-lethal, contrary to the deletion of all of them. These synthetic-lethal genes can lead to the false assumption that all of the redundant genes are not essential, which shows a limitation of the predictions generated by comparative and deletion studies. In the end, this process resulted in the creation of a viable, semi-synthetic organism with a genome of 531 kbp (473 genes) [11]. This reduced genome (JCV-syn3.0) was thus smaller as the one of *M. genitalium* and lacked most of the genes necessary for biosynthesis of building blocks like NTPs and AAs, with the retained genes involved in key processes such as transcription and translation. Interestingly, the functions of 149 genes (31% of the genome) remained still largely unknown.

1.2 Our approach for the construction of a minimal cell

We aim at the construction of a minimal cell-like entity by a bottom-up approach. In contrast to the top-down approach, the attempt to decrease the complexity of existing organisms, we reassemble cellular components and reconstitue their respective functions with the aim to increase the complexity of the system until it resembles a living cell. As a compartment we utilize liposomes, while the the information of the system is encoded by DNA and translated into proteins by the PURE cell-free gene expression system (Figure 1.2). Division of the system might be achieved by expression of one or more filament systems interacting with the membrane.

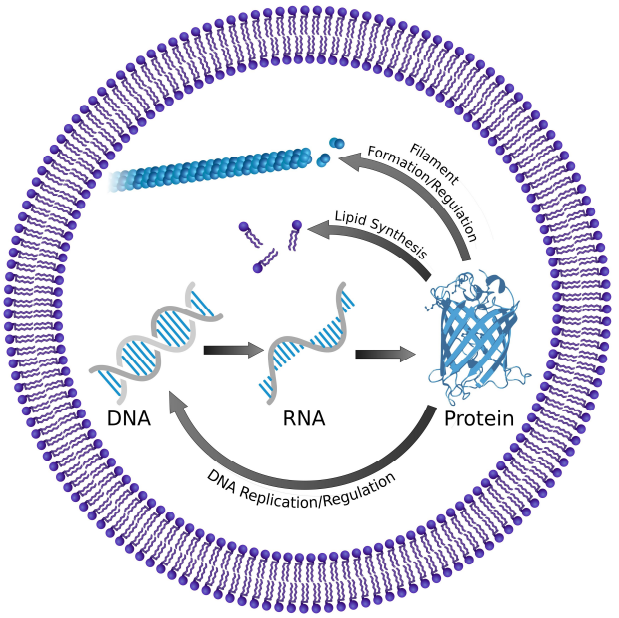

Figure 1.2: Overview of the modules we plan to combine for the creation of a minimal and bottom-up synthetic cell. Primary modules are in this case DNA replication, lipid synthesis, and filament formation.

1.2.1 The PURE system as a platform for cell-free gene expression

The expression of proteins, encoded by DNA, is the most fundamental process of cellular life and the flow of information from DNA to RNA to protein is known as the central dogma of molecular biology. Thus, if we want to create artificial life that represents a minimal version of what can be found in nature, it will necessarily be based on a gene expression system. We apply DNA as the primary information carrier for our approach. From it RNA is produced by transcription, acting as a template for the synthesis of protein by the process of translation (Figure 1.2). RNA itself is in general able to act as a primary information carrier as well, but is less stable than DNA. Moreover, utilizing an RNA based system would distance our approach from the existing mechanisms in modern cells. In general, gene expression is not bound to the cellular compartment and can most easily be achieved by disintegration of cells and removal of unwanted components to produce a cell extract [15]. Cell extracts are cheap, robust and can yield a decent amount of protein (>2 mg/ml)[16–18]. The biggest downside of cell extracts is their crudeness, as they contain a large amount of various cellular components of which some are still uncharacterized. These components can consume nutrients and inhibit gene expression related processes, as well as potentially interfere with the function of expressed proteins. Moreover, the level of complexity inherent in cell extracts effectively prevents a full understanding of all the processes that take place during gene expression and makes them unsuitable for the creation of a minimal cellular system.

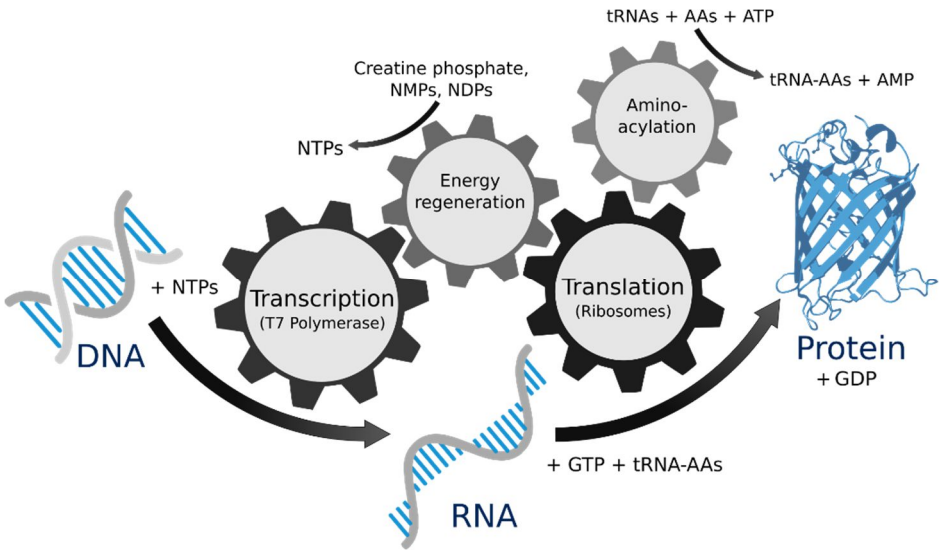

Figure 1.2: Schematic overview of the PURE system and its four main reaction modules: Transcription, translation, tRNA aminoacylation and energy regeneration. Abbreviations: AAs, amino acids; NTPs/NDPs/NMPs, nucleoside triphosphates/diphosphates/ monophosphates.

The alternative to cell extracts are expression systems that consist of separately purified and reconstituted components. Most prominent of these is the PURE system (protein synthesis using recombinant elements) that was developed by the group of Takuya Ueda [19–21]. It contains all components necessary for transcription, translation, tRNA aminoacylation and energy regeneration. Each of those components is purified independently from *E. coli* and recombined at specific

concentrations. The PURE system is commercially available as PURE*frex* and PURE*frex*2.0 from GeneFrontier (Chiba, Japan) and as PURExpress from New England Biolabs. Unlike in the original formulation, the proteins of both PURE*frex* variants are without histidine tags, contrary to PURExpress, in which they are still present. Further, there are modifications of the original composition of the PURE system present in PURE*frex*2.0 and PURExpress that result in higher yields of synthesized protein, but the details of these modifications are currently not disclosed. The main advantage of these systems is that they only contain those components necessary for gene expression and that those are all well characterized. Therefore, it allows for more control over the reaction conditions and, at least theoretically, to model and predict its behaviour.

1.2.2 Liposomes as compartments for minimal cells

Due to their amphiphilic nature, lipids in aqueous solutions tend to arrange themselves into a bilayer in which their hydrophilic head groups are in contact with the solution and their hydrophobic tails are shielded from it. *In vitro*, lipid bilayers can form vesicles, called liposomes, in which the bilayer separates the inside of the vesicle from the outside solution and as such mimics function and morpholology of a cell membrane. Cell-free extracts [22,23] and the PURE system [24,25] can be encapsulated in liposomes, enabling internal expression of proteins. Thus, liposomes can effectively be used as micrometre-sized bioreactors and offer a viable compartment for the bottom-up creation of a minimal cell.

Several methods are available for the generation of liposomes. We employ lipid swelling from glass beads in presence of the PURE system which yields liposomes with a high heterogeneity in size and encapsulation efficiency [25]. It is worth mentioning, that the yield which can be produced inside liposomes was increased distinctly by applying PURE*frex*2.0 compared to the original PURE*frex* expression system and that a small fraction of liposomes shows yields several times higher than the one achieved by expression in bulk [1]. Growth of liposomes can be achieved by fusion of vesicles through electrofusion [26] or through increase of membrane tension caused by osmotic pressure or light activated membrane area reduction [27,28]. Nevertheless, these approaches are not suitable for a minimal cell, as they are either not sustainable or completely mediated from the outside. Therefore, the most suitable approach that is commensurate with the requirements of a minimal cell and reflects the process of membrane growth *in vivo* is the synthesis of phospholipids inside the liposome. It has indeed been demonstrated that it is possible to achieve synthesis of lipids by expression of corresponding enzymes in presence of precursors, albeit currently only at a low level [29].

1.2.3 Division and replication of a minimal cellular system

Self-replication is one of the most fundamental traits of cellular life. A prerequisite for replication of cells is the amplification of all essential components prior to division to avoid death by dilution. For our setup this would at a minimum include all components of the PURE system, the genome of the minimal cell, as well as growth of the liposome itself. Amplification of DNA in cells is mediated by protein complexes including DNA polymerases and has recently been reconstituted inside liposomes by PURE system mediated synthesis of phi29 proteins [30]. Replication of ribosomes by the PURE system on the other hand still remains to be achieved [31].

Once internal components are amplified sufficiently, the liposome has to divide with the compartment retaining its integrity and the components distributed onto the offspring. In cells, division is with a few exceptions orchestrated by specific protein complexes. In eukaryotic cells, division is exerted by a contractile actin-myosin ring complex that facilitates constriction of the membrane [32,33] and a filament complex called ESCRT-III, which finalizes division by severing of the membrane neck [34,35]. The Cdv system is a homologue of the eukaryotic ESCRT system and has been proposed to be responsible for division of archaea of the genus *Crenarchaeota*. In bacteria and several archaea, division is orchestrated predominantly by the tubulin homologue FtsZ, which forms a filament ring at the abscission site. *In vitro* reconstitution has suggested that FtsZ could directly be involved in membrane constriction [36,37]. However, FtsZ polymerization has turned out to be coupled with the cell wall synthesis machinery [38,39], which actually represents the rate limiting step for cytokinesis in *E. coli* [40]. Further, FtsZ is not necessary for division in bacteria lacking a cell wall [41] and it has been suggested that the constriction at the abscission side is in fact mechanically mediated by inward growth of the cell wall, with FtsZ only being involved as an organizer of the process [40,42]. Hence, the exact role of FtsZ for division is currently still unclear [43].

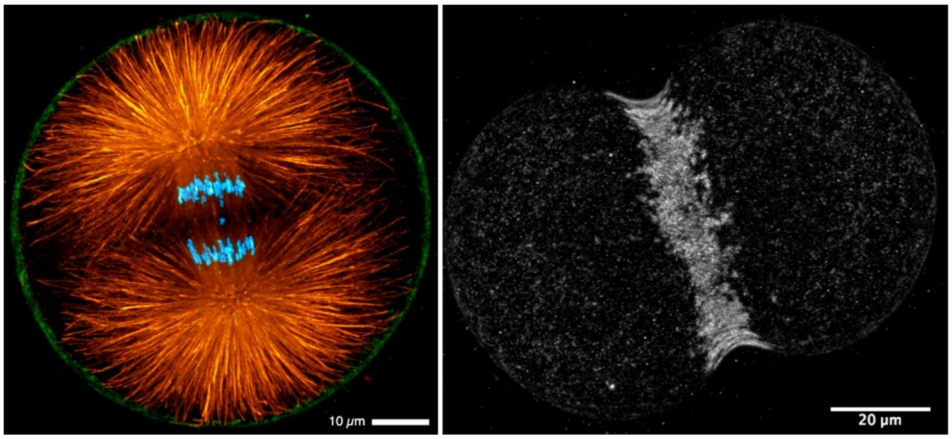

Figure 1.3: Mitosis and cytokinesis in sea urchin cells (*Strongylocentrotus purpuratus*). Left image: Confocal image of a zygote during first anaphase. It shows how microtubules (labelled in orange) separate the chromosomes (labelled in blue) prior to cytokinesis. Myosin is labelled in green. Right image: Signal of labelled myosin of a zygote during first cleavage. Motor activity of myosin is responsible for contraction of the actin ring, leading to the constriction of the cell membrane. Credits to George von Dassow (http://www.gvondassow.com).

All three division machineries predominantly mediate symmetric division in cells, meaning that the daughter cells are near identical in size and composition (Figure 1.5). Aside regular cytokinesis, the ESCRT-III system is also involved in vesicle budding. Therefore, the ESCRT-III system could theoretically also stimulate an asymmetrical division process in which smaller daughter vesicles are generated from the original vesicle. However, it is not clear if a sufficient amount of components could thus be encapsulated. Besides constriction and fusion of the membrane at the abscission site, several other processes are likely necessary for correct function of the divisome and successful replication. One is the separation of the chromosomes, which is orchestrated by microtubules in eukaryotic cells (Figure 1.4) and in case of bacterial plasmids by actin-like filaments of the ParMRC

system [44,45]. Two important processes to prepare for division are shape modulation and polarization of the cell a divisome can likely not be effectively recruited in a symmetric system

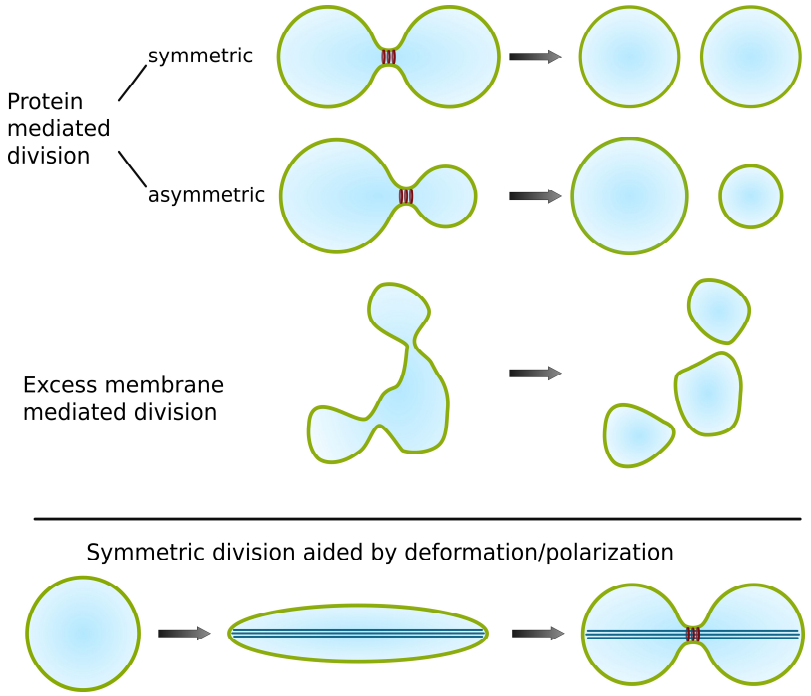

Figure 1.4: Overview of different fundamental divison mechanisms. In most cells, division is orchestrated by a protein machinery (indicated in red) that divides the cell intro two identical daughter cells by symmetric division. Some organisms, as for example budding yeast, undergo an asymmetric division, resulting in a mother and a smaller daughter cell. In L-form bacteria, division is independent of any specific cell division system and occurs due to membrane deformations caused by increased lipid synthesis.

Despite the general importance of the divisome for cell replication, it should be recognized that division of synthetic liposomes can occur without presence of any protein machinery. First, in certain circumstances shear forces of the medium can be already sufficient to divide vesicles into intact daughter vesicles without loss of content [46]. Second, liposomes composed of inverse-cone shaped lipids and subjected to temperature cycling can undergo budding and birthing events [47]. Third, cell division can be triggered by excess membrane synthesis in cell wall deficient bacteria, called L-forms. These bacteria are able to divide completely independent of any divisome machinery or filament system. In these cells, excess membrane synthesis leads to an abnormal cell surface area to volume ratio that drives the cell shape deformations and leads ultimately to scission of the membrane [41]. The latter mechanism is quite promising in regards of creating a minimal cell, as it relies entirely on lipid synthesis and would require no additional machinery. However, even if it turns out that a division machinery is not needed for the creation of a minimal cell, the reconstruction of a division machinery would still be of great importance as it would allow us more insights into one of the most important cellular mechanisms.

The focus in this work has been on the deformation of membranes by forces created through protein filaments. In our lab we already investigated FtsZ and the related Min system [48]. Here we attempted to reconstruct eukaryotic ESCRT and the archaeal Cdv system by cell-free synthesis (Chapter 5 and 6) and investigated their suitability for a reconstituted minimal cell division machinery. We further have explored the membrane deformation capabilities of eukaryotic and bacterial microtubules and to what extent we can regulate or synthesize these filaments by cell-free gene expression (Chapter 3 and 4).

1.3 Physical interactions of filaments with the membrane of cells and liposomes

In absence of a cell wall, as present in most prokaryotic and plant cells, cell shape is determined by interactions between the plasma membrane and the different filament networks, such as actin or microtubules. These filament systems have been studied extensively *in vivo* as well as *in vitro* and their interaction with cell-like membranes has been investigated by encapsulation in liposomes [49,50]. Liposome membranes represent a close model to cell membranes, although they admittedly lack the membrane proteins and a cell cortex present in eukaryotic cells. When tubulin is encapsulated in liposomes and forms microtubules, the most commonly reported morphology is the formation of two long protrusions on opposite sides of the liposome body (Figure 1.6 A and B) [49]. These protrusions are formed by a microtubule bundle that runs from both ends of the protrusions and through the middle of the liposome. Due to the resemblance of this morphology to the letter • , it is referred to as • -shape. Interestingly, a similar morphology of elongated cells with two protrusions extending from the cell body arises when actin is depolymerized in lymphoblasts (Figure 1F) [51]. The protrusions become more pronounced upon addition of the microtubule stabilizing compound paclitaxel (Taxol), which supports the reasoning that this effect is caused by deformation of the membrane through microtubules agglomerated into bundles. These results also indicate that a crucial difference between the encapsulation of microtubules *in vitro* and microtubules growing in cells is the presence of an actin filament network in the latter. When microtubules start growing in spherical liposomes, it was observed that the liposomes first elongate into either ellipsoid (Figure 1.6B) or lemon shapes (Figure 1.6D) before the membrane collapses into two membrane tubes around the filament and forms a • -shape [52]. Furthermore, there is a rare alternative to the • -shape in which the body of the liposome divides along the microtubule bundle and forms what has been termed a pearl-shape (Figure 1.6E) [53].

The tendency of encapsulated microtubules or actin filaments to agglomerate into one thick bundle is caused by the positive feedback introduced by membrane deformations. When a filament forms a minor bulge in the membrane, this bulge acts as a trap for other filaments, as they can grow longer at the side of the bulge without being stalled by resistance of the membrane. The more filaments accumulate in one protrusion of the membrane, the stronger the membrane deformation becomes and thus the more energetically favourable it becomes for microtubules to grow into the protrusion.

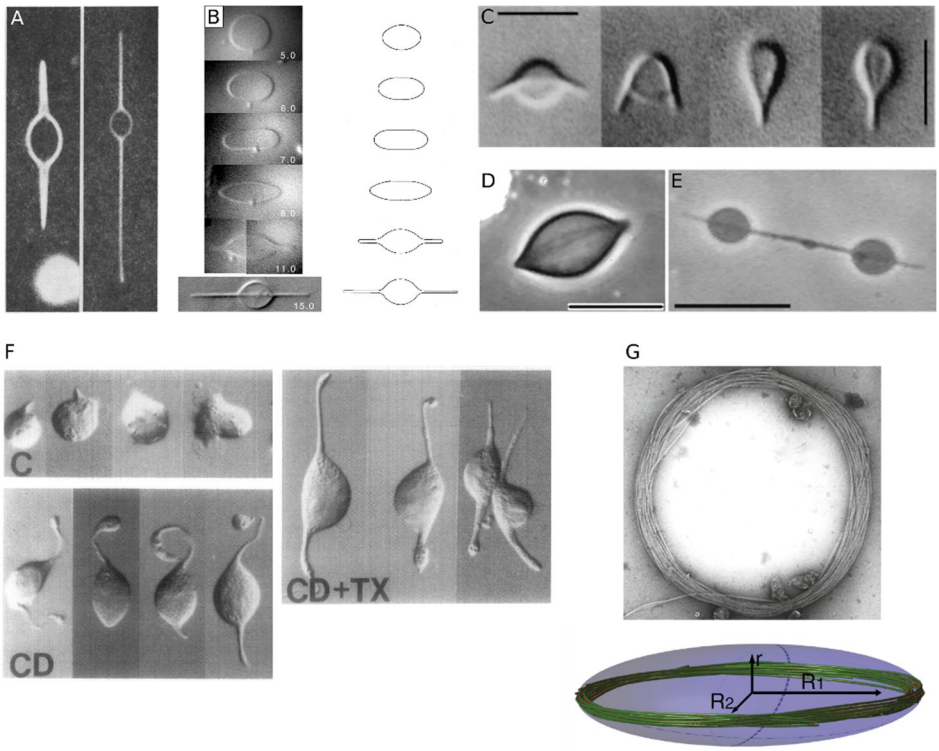

Figure 1.5: Various morphologies of membrane deformation caused by microtubules *in vitro* and *in vivo*. **(A)** Encapsulated microtubules deforming a vesicle into a • -shape. Taken from Hotani and Miyamoto 1990 [49]. **(B)** Changes of vesicle shape through polymerisation of microtubules under low membrane tension. **(C)** Buckling of vesicle in an initially • -shaped liposome. B and C taken from Fygenson et al. 1997 [52]. **(D)** Lemon shape morphology. **(E)** Pearl shape morphology. D and E taken from Emsellem et al. 1998 [53]. **(F)** Morphology of lymphoblasts treated with the actin polymerization inhibitor cytochalasin D (CD). Left upper image C displays regular cell shape, while left lower image displays cells after treatment with CD. Right image CD+TX shows cell treated with both CD and Taxol. Adapted from Bailly et al. 1991 [51]. **(G)** Upper image: Microtubule coil isolated from human plateletafter simultaneous fixation and detergent extraction in suspension. Magnification 313.000x. Taken from White 2013 [54]. Lower image: Schematic representation of the microtubule coil inside a blood cell. Taken from Dmitrieff et al. 2017 [55].

The observed membrane deformations, *in vivo* as well as *in vitro*, are a result of the pushing force of the growing filaments, generated by continuous binding of subunits to their ends. In general, the decrease of free energy accompanying polymerization can be considered as the source for the mechanical force required to deform the membrane. Nevertheless, this does not explain how subunits can polymerize at the tip of the filaments when the tip is simultaneously pushing against the membrane. If both filament and barrier would be unmovable, this would effectively prevent any further attachment of new subunits to the filament by sterically shielding the tip. The fact that filaments are under given conditions still able to exert pushing forces can be explained by a 'Brownian ratchet' model, in which thermal fluctuations allow for sufficient access of subunits to the filament tip for polymerization [56]. When a microtubule polymerizes against a membrane, the

membrane and the microtubule will fluctuate in their position due to Brownian motion. If, as a consequence of thermal fluctuation, a sufficiently large gap occurs, tubulin dimers can enter the gap and be incorporated into the filament. Thus, continued elongation of the filament is possible, although the velocity of growth will decrease proportionally with the force exerted by the filament onto the membrane, as this will increase membrane tension and consequently decrease the degree to which the membrane can fluctuate. The stall force, meaning the force encountered by the barrier at which the growth velocity becomes equal to zero, is determined by $F_s = \frac{k_B T}{\delta} \times ln \frac{k_{on}}{k_{off}}$, where • is the added length per subunit, k_{on} the rate of subunit addition, and k_{off} the rate of subunit detachment. The maximal pushing force generated by growth of single microtubules is in the range of 2.5-4 pN [57] and accumulates linearly when microtubules grow together in a bundle [58]. GTP-bound tubulin concentration is one factor that can influence the pushing force, as the k_{on} rate rises with increasing tubulin concentration. In this regard, it should be considered that in case of • -shaped liposomes containing microtubules, the concentration of GTP-bound tubulin might be lower at the tip of the protrusions than in the liposome body due to diffusion-limited depletion at the microtubule tips. Further, the probability that a single microtubule pushing against the membrane will undergo a catastrophe is dependent on the aging of the GTP-cap, which is influenced by addition or detachment of subunits. The force encountered by the filament growing against the membrane does not affect k_{off}, but does decrease k_{on}, thus increasing the rate of catastrophe events [59]. Moreover, the maximum pushing force can further be limited in case that a microtubule starts to buckle upon encountering the barrier. Buckling takes place when the pushing force of filament growth exceeds the critical force for buckling (F_c), which increases with the number of filaments (N) and the filament rigidity (B) and decreases with the length of the filament or bundle (L): $F_c = N \frac{\pi^2 B}{L^2}$ [52,57]. As buckling increases with the square of filament length, long filaments can generate less pushing forces compared to short ones and will be more likely to buckle upon encountering a barrier.

The resistance a filament growing inside a liposome encounters is effectively the tension of the vesicle membrane and in absence of any other force acting on the vesicle, this tension is determined by the presence of osmotic pressure. Osmotic pressure is the counterforce created by osmosis, the movement of solvent caused by a difference in solute concentration. This means that liposomes containing a higher concentration of solute than the outside solution will undergo an influx of water and an increase in volume. Assuming an already taunt membrane, the surface area will thus increase as well, leading to a lateral tension on the membrane. The membrane tension (•) can be derived from the elastic modulus (resistance towards elastic stretching, ~10^3 N/m^2 in cells [60]) of the membrane (K_m), the change in surface area (• A) and the surface area in absence of any osmotic pressure or deformation (A_0) as: $\sigma = K_m \frac{\Delta A}{A_0}$ [61,62]. When a filament deforms the membrane of a liposome under osmotic pressure and thus further increases the membrane area (• A_{fil}), then this will logically add up to the increase of area through the osmotic pressure (• A_{osm}) and further increase the membrane tension: $\sigma = K_{bil} \frac{\Delta A_{osm} + \Delta A_{fil}}{A_0}$. Since the membrane has properties of a 2D fluid, the membrane tension is expected to equilibrate across the surface [63]. Overall, membrane tension gains recently increasing recognition as an important physical parameter in cell biology, especially in regards of its interplay with filaments and importance for cell shape and motility [60,64,65].

If the force generated by polymerization as well as the counter force of the membrane tension are greater than the critical force for buckling, the filament will bend. With encapsulated microtubules, cases have been observed in which a filament deformed a liposome into a • -shape, but upon further growth (implying increase of filament length and membrane tension) started to buckle and formed a morphology with only a single protrusion (Figure 1.6C) [52]. If the equilibrium between the force necessary for buckling, the filament polymerization force, and the membrane tension is further shifted in favour of the buckling of the filament by increase of the filament length or the tension of the membrane, the filament will not be able to form a protrusion and will instead completely bend along the curvature of the membrane, forming a ring inside the liposome. Through tension of the filaments, the microtubule ring now pushes against the membrane of the liposome along its circumference, deforming it into an oblate spheroid shape. This exact kind of morphology can also be observed in red blood cells where microtubules form a coil, also known as marginal band (Figure 1.6G), which is involved in giving these cells their flattened shape [55,66].

To summarize the relation between morphology and physical parameters in liposomes or cells containing filaments, straight filament protrusions like the • -shape are favoured under conditions of low membrane tension (low osmotic pressure) and low tendency for buckling of the filaments (high rigidity of filaments, small length of filaments/small vesicle diameter, high number of filaments per bundle) while the opposite of these conditions are favouring bending of the filaments into ring-like shapes. The same correlation was observed for actin filaments, in which case the major difference to microtubules is a lower bending rigidity per filament [67].

Our approach was to encapsulate both eukaryotic and bacterial tubulin in liposomes. Compared to most of the presented studies, we applied a more complex lipid compositions and buffer medium for liposome formation and encapsulation, which are closer to the conditions present in bacterial or eukaryotic cells. Nevertheless, our results were in accordance to what has been reported here and are laid out in Chapter 3 for eukaryotic and Chapter 4 for bacterial microtubules.

1.4 Thesis outline

In this work we explored various filament systems *in vitro*, partly to access their applicability for the creation of a minimal cell.

- **In Chapter 2**, we investigated if we can prolong gene expression in the PURE system by application of a semi-permeable set-up.
- **In Chapter 3**, we combined eukaryotic microtubules with the PURE system and expressed the microtubule associated protein Mal3. We further encapsulated microtubules in liposomes under conditions suitable for gene expression.
- **In Chapter 4**, we synthesized bacterial tubulin *de novo* on supported lipid bilayers (SLBs) and inside of liposomes. Additionally, we characterized the interactions of bacterial microtubules with lipid membranes and specifically their potential to deform liposome membranes.
- **In Chapter 5**, we explored if we can reconstitute the membrane modulating functions of the ESCRT-III system by cell-free expression of the respective proteins. Interactions of the synthesized proteins with SLBs and liposome membranes were analysed by fluorescence and electron microscopy, as well as by flotation assays.
- **In Chapter 6**, we attempted to express the Cdv system as well as to purify the respective proteins.
- **In Chapter 7**, we give additional remarks on the possible division mechanisms of a minimal cell and the potential applications and risks of minimal cells. Finally, we will muse about what defines life and what sets it apart from lifeless matter.

1

References

[1] Blanken D, van Nies P, Danelon C. Quantitative imaging of gene-expressing liposomes reveals rare favorable phenotypes. Phys Biol 2019;16:45002.

[2] Vleugel M, Roth S, Groenendijk CF, Dogterom M. Reconstitution of Basic Mitotic Spindles in Spherical Emulsion Droplets. J Vis Exp 2016.

[3] Kostina NY, Rahimi K, Xiao Q, Haraszti T, Dedisch S, Spatz JP, et al. Membrane-Mimetic Dendrimersomes Engulf Living Bacteria via Endocytosis. Nano Lett 2019;19:5732–8.

[4] Murtas G. Artificial assembly of a minimal cell. Mol Biosyst 2009;5:1292–7.

[5] Stano P. Is Research on "Synthetic Cells" Moving to the Next Level? Life (Basel, Switzerland) 2018;9.

[6] Luisi PL, Ferri F, Stano P. Approaches to semi-synthetic minimal cells: a review. Naturwissenschaften 2006;93:1–13.

[7] Schwille P, Spatz J, Landfester K, Bodenschatz E, Herminghaus S, Sourjik V, et al. MaxSynBio: Avenues Towards Creating Cells from the Bottom Up. Angew Chem Int Ed Engl 2018;57:13382–92.

[8] Samad T, Billings N, Birjiniuk A, Crouzier T, Doyle PS, Ribbeck K. Swimming bacteria promote dispersal of non-motile staphylococcal species. ISME J 2017;11:1933–7.

[9] Chen IA, Walde P. From self-assembled vesicles to protocells. Cold Spring Harb Perspect Biol 2010;2:a002170–a002170.

[10] Szostak JW, Bartel DP, Luisi PL. Synthesizing life. Nature 2001;409:387–90.

[11] Hutchison CA 3rd, Chuang R-Y, Noskov VN, Assad-Garcia N, Deerinck TJ, Ellisman MH, et al. Design and synthesis of a minimal bacterial genome. Science 2016;351:aad6253.

[12] Mushegian AR, Koonin E V. A minimal gene set for cellular life derived by comparison of complete bacterial genomes. Proc Natl Acad Sci U S A 1996;93:10268–73.

[13] Gil R, Silva FJ, Peretó J, Moya A. Determination of the core of a minimal bacterial gene set. Microbiol Mol Biol Rev 2004;68:518–37.

[14] Gibson DG, Glass JI, Lartigue C, Noskov VN, Chuang R-Y, Algire MA, et al. Creation of a Bacterial Cell Controlled by a Chemically Synthesized Genome. Science (80-) 2010;329:52 LP – 56.

[15] Nirenberg MW, Matthaei JH. The dependence of cell-free protein synthesis in E. coli upon naturally occurring or synthetic polyribonucleotides. Proc Natl Acad Sci U S A 1961;47:1588–602.

[16] Kwon Y-C, Jewett MC. High-throughput preparation methods of crude extract for robust cell-free protein synthesis. Sci Rep 2015;5:8663.

[17] Krinsky N, Kaduri M, Shainsky-Roitman J, Goldfeder M, Ivanir E, Benhar I, et al. A Simple and Rapid Method for Preparing a Cell-Free Bacterial Lysate for Protein Synthesis. PLoS One 2016;11:e0165137.

[18] Caschera F, Noireaux V. Synthesis of 2.3 mg/ml of protein with an all Escherichia coli cell-free transcription-translation system. Biochimie 2014;99:162–8.

[19] Shimizu Y, Inoue A, Tomari Y, Suzuki T, Yokogawa T, Nishikawa K, et al. Cell-free translation reconstituted with purified components. Nat Biotechnol 2001;19:751–5.

[20] Shimizu Y, Kanamori T, Ueda T. Protein synthesis by pure translation systems. Methods 2005;36:299–304.

[21] Shimizu Y, Kuruma Y, Kanamori T, Ueda T. The PURE system for protein production. Methods Mol Biol 2014;1118:275–84.

[22] Nomura SM, Tsumoto K, Hamada T, Akiyoshi K, Nakatani Y, Yoshikawa K. Gene expression within cell-sized lipid vesicles. Chembiochem 2003;4:1172–5.

[23] Noireaux V, Libchaber A. A vesicle bioreactor as a step toward an artificial cell assembly. Proc Natl Acad Sci U S A 2004;101:17669 LP – 17674.

[24] Murtas G, Kuruma Y, Bianchini P, Diaspro A, Luisi PL. Protein synthesis in liposomes with a minimal set of enzymes. Biochem Biophys Res Commun 2007;363:12–7.

[25] Nourian Z, Roelofsen W, Danelon C. Triggered gene expression in fed-vesicle microreactors with a multifunctional membrane. Angew Chem Int Ed Engl 2012;51:3114–8.

[26] Stoicheva NG, Hui SW. Electrofusion of cell-size liposomes. Biochim Biophys Acta 1994;1195:31–8.

[27] Suzuki Y, Nagai KH, Zinchenko A, Hamada T. Photoinduced Fusion of Lipid Bilayer Membranes. Langmuir 2017;33:2671–6.

[28] Deshpande S, Wunnava S, Hueting D, Dekker C. Membrane Tension-Mediated Growth of Liposomes. Small 2019;15:e1902898.

[29] Scott A, Noga MJ, de Graaf P, Westerlaken I, Yildirim E, Danelon C. Cell-Free Phospholipid Biosynthesis by Gene-Encoded Enzymes Reconstituted in Liposomes. PLoS One 2016;11:e0163058–e0163058.

[30] van Nies P, Westerlaken I, Blanken D, Salas M, Mencia M, Danelon C. Self-replication of DNA by its encoded proteins in liposome-based synthetic cells. Nat Commun 2018;9:1583.

[31] Li J, Haas W, Jackson K, Kuru E, Jewett MC, Fan ZH, et al. Cogenerating Synthetic Parts toward a Self-Replicating System. ACS Synth Biol 2017;6:1327–36.

[32] Mabuchi I. Biochemical aspects of cytokinesis. Int Rev Cytol 1986;101:175–213. https://doi.org/10.1016/s0074-7696(08)60249-1.

[33] Miller AL. The contractile ring. Curr Biol 2011;21:R976–8.

[34] Guizetti J, Schermelleh L, Mantler J, Maar S, Poser I, Leonhardt H, et al. Cortical constriction during abscission involves helices of ESCRT-III-dependent filaments. Science 2011;331:1616–20.

[35] Goliand I, Adar-Levor S, Segal I, Nachmias D, Dadosh T, Kozlov MM, et al. Resolving ESCRT-III Spirals at the Intercellular Bridge of Dividing Cells Using 3D STORM. Cell Rep 2018;24:1756–64.

[36] Osawa M, Erickson HP. Liposome division by a simple bacterial division machinery. Proc Natl Acad Sci 2013;110:11000 LP – 11004.

[37] Osawa M, Anderson DE, Erickson HP. Reconstitution of contractile FtsZ rings in liposomes. Science 2008;320:792–4.

[38] Bisson-Filho AW, Hsu Y-P, Squyres GR, Kuru E, Wu F, Jukes C, et al. Treadmilling by FtsZ filaments drives peptidoglycan synthesis and bacterial cell division. Science 2017;355:739–43.

[39] Yang X, Lyu Z, Miguel A, McQuillen R, Huang KC, Xiao J. GTPase activity-coupled treadmilling of the bacterial tubulin FtsZ organizes septal cell wall synthesis. Science 2017;355:744–7.

[40] Coltharp C, Buss J, Plumer TM, Xiao J. Defining the rate-limiting processes of bacterial cytokinesis. Proc Natl Acad Sci USA 2016;113:E1044-53.

[41] Mercier R, Kawai Y, Errington J. Excess membrane synthesis drives a primitive mode of cell proliferation. Cell 2013;152:997–1007.

[42] Xiao J, Goley ED. Redefining the roles of the FtsZ-ring in bacterial cytokinesis. Curr Opin Microbiol 2016;34:90–6.

[43] Kretschmer S, Ganzinger KA, Franquelim HG, Schwille P. Synthetic cell division via membrane-transforming molecular assemblies. BMC Biol 2019;17:43.

[44] Salje J, Gayathri P, Lowe J. The ParMRC system: molecular mechanisms of plasmid segregation by actin-like filaments. Nat Rev Microbiol 2010;8:683–92.

[45] Moller-Jensen J, Jensen RB, Lowe J, Gerdes K. Prokaryotic DNA segregation by an actin-like filament. EMBO J 2002;21:3119–27.

[46] Zhu TF, Szostak JW. Coupled growth and division of model protocell membranes. J Am Chem Soc 2009;131:5705–13.

[47] Sakuma Y, Imai M. Model system of self-reproducing vesicles. Phys Rev Lett 2011;107:198101.

[48] Godino E, Lopez JN, Foschepoth D, Cleij C, Doerr A, Castella CF, et al. De novo synthesized Min proteins drive oscillatory liposome deformation and regulate FtsA-FtsZ cytoskeletal patterns. Nat Commun 2019;10:4969.

[49] Hotani H, Miyamoto H. Dynamic features of microtubules as visualized by dark-field microscopy. Adv Biophys 1990;26:135–56.

[50] Cortese JD, Schwab B 3rd, Frieden C, Elson EL. Actin polymerization induces a shape change in actin-containing vesicles. Proc Natl Acad Sci U S A 1989;86:5773–7.

[51] Bailly E, Celati C, Bornens M. The cortical actomyosin system of cytochalasin D-treated lymphoblasts. Exp Cell Res 1991;196:287–93.

[52] Fygenson DK, Marko JF, Libchaber A. Mechanics of Microtubule-Based Membrane Extension. Phys Rev Lett 1997;79:4497–500.

[53] Emsellem V, Cardoso O, Tabeling P. Vesicle deformation by microtubules: A phase diagram. Phys Rev E 1998;58:4807–10.

[54] White JG. Chapter 7 - Platelet Structure. In: Michelson ADBT-P (Third E, editor., Academic Press; 2013, p. 117–44.

[55] Dmitrieff S, Alsina A, Mathur A, Nédélec FJ. Balance of microtubule stiffness and cortical tension determines the size of blood cells with marginal band across species. Proc Natl Acad Sci U S A 2017;114:4418–23.

[56] Peskin CS, Odell GM, Oster GF. Cellular motions and thermal fluctuations: the Brownian ratchet. Biophys J 1993;65:316–24.

[57] Dogterom M, Yurke B. Measurement of the Force-Velocity Relation for Growing Microtubules. Science (80-) 1997;278:856 LP – 860.

[58] Laan L, Husson J, Munteanu EL, Kerssemakers JWJ, Dogterom M. Force-generation and dynamic instability of microtubule bundles. Proc Natl Acad Sci 2008;105:8920 LP – 8925.

[59] Janson ME, de Dood ME, Dogterom M. Dynamic instability of microtubules is regulated by force. J Cell Biol 2003;161:1029–34.

[60] Diz-Munoz A, Fletcher DA, Weiner OD. Use the force: membrane tension as an organizer of cell shape and motility. Trends Cell Biol 2013;23:47–53.

[61] Rawicz W, Olbrich KC, McIntosh T, Needham D, Evans E. Effect of chain length and unsaturation on elasticity of lipid bilayers. Biophys J 2000;79:328–39.

[62] Alam Shibly SU, Ghatak C, Sayem Karal MA, Moniruzzaman M, Yamazaki M. Experimental Estimation of Membrane Tension Induced by Osmotic Pressure. Biophys J 2016;111:2190–201.

[63] Kozlov MM, Mogilner A. Model of polarization and bistability of cell fragments. Biophys J 2007;93:3811–9.

[64] Pontes B, Monzo P, Gauthier NC. Membrane tension: A challenging but universal physical parameter in cell biology. Semin Cell Dev Biol 2017;71:30–41.

[65] Simon C, Caorsi V, Campillo C, Sykes C. Interplay between membrane tension and the actin cytoskeleton determines shape changes. Phys Biol 2018;15:65004.

[66] Patel-Hett S, Richardson JL, Schulze H, Drabek K, Isaac NA, Hoffmeister K, et al. Visualization of microtubule growth in living platelets reveals a dynamic marginal band with multiple microtubules. Blood 2008;111:4605–16.

[67] Tsai F-C, Koenderink GH. Shape control of lipid bilayer membranes by confined actin bundles. Soft Matter 2015;11:8834–47.

Chapter 2

Implementation of a semi-open system does not improve PURE system activity

The truth is rarely pure and never simple.

Oscar Wilde, The Importance of Being Earnest

The PURE system represents a powerful tool for the cell-free synthesis of proteins and is a promising candidate for the central machinery of a minimal cell. However, PURE system activity breaks down over time, currently limiting its use for long-term applications. Here we investigated if we can prolong gene expression activity by application of a semi-permeable system. Therefore, we connected a reaction solution, containing the complete PURE system, with a feeding solution over a semi-permeable membrane. Moreover, a buffer solution was prepared to replace the Solution I of PUREfrex in several conditions. Results show that nutrients like amino acids are able to enter from the feeding into the reaction solution, but that this did not influence expression time or yield. These results where further confirmed by experiments done by other group members and prove that neither depletion of nutrients nor accumulation of small inhibitory side products is responsible for cessation of gene expression.

2.1 Introduction

For the reasons described in the previous chapter, we consider the PURE system to be the best protein synthesis platform available at the moment for the assembly of a minimal cell. It does, however, bring with it several limitations compared to cell extracts, such as higher costs of production and lower yield of protein. The latter is likely due to the absence of various cytoplasmic compounds in the PURE system which assist protein synthesis in cell extract. Considering the minimalistic nature, constant concentration of factors between batches, and knowledge of all components, it could be expected that the PURE system would yield more reliable and predictable results than other IVTT systems or in vivo experiments. Contrary to these expectations, the PURE and other IVTT systems suffer from a high batch to batch variability and are resistant to reliable modelling [1,2]. Further, the PURE systems suffer from a breakdown of gene expression activity over time. In bulk reactions at 37°C, PURE*frex* reaches its maximal rate of protein expression about 45 minutes after initiation and stays linear for a short time (Figure 2.1). After 90-120 minutes, the rate of expression decreases until it reaches a plateau after 3-4 h. This is a major limitation, as it prevents us from effectively developing systems that require longer time periods of expression, like genetic oscillators. Not to mention the sustainable activity necessary for a minimal cell.

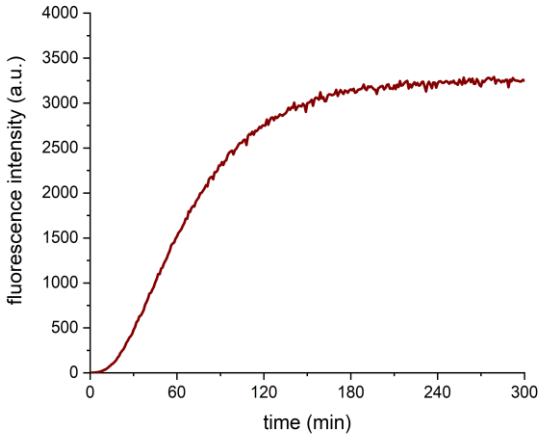

Figure 2.1: Example of a gene expression profile with PURE*frex* 1.0 at 37°C and 7.4 nM of YFP template. Expression has been tracked by measurement of YFP fluorescence over time.

The exact reason for this breakdown of PURE system activity is unfortunately still not known. Two possible causes could be the depletion of nutrients for the reaction (NTPs and AAs) or the accumulation of inhibitory side products. For cell-extracts, it is known that the addition of nutrients can prolong gene expression [3]. Further, there is evidence that the accumulation of inorganic phosphate can inhibit the expression system [4,5]. It has been demonstrated, that both of these limitations can be bypassed by performing gene expression in a semi-open container, or dialysis chamber, in which the reaction solution is in contact with a reservoir that supplies nutrients and takes up side-products [5,6]. With such a semi-open system, the translation rate in a cell extract can be kept constant for more than 40 hours. Interestingly, the molecular cut-offs of the membranes

used in some of the semi-open systems were with 30.000 kDa and 50.000 kDa significantly larger than the size of initiation factors used in the PURE system. Initiation factors are the smallest proteins present in the PURE system, with a size of about 10 kDa and dilution of them through diffusion into the feeding solution is expected to lead to a reduction or breakdown of translation activity. However, gene expression was not impaired to any extend [6]. An explanation could be that, through continuous interactions of the components with each other, dynamic multi-protein complexes are formed, which are too big to be washed out of the reaction compartment. Besides of cell extracts, there is also a report that claims that expression time with the PURE system can be increased through the application of a semi-open system, with a yield 25 times higher than in batch mode [7].

Therefore, we decided to build a dialysis chamber to investigate what effects a semi-open system has on the expression activity of the PURE system. A requirement for this system was that it had to be compatible with real-time fluorescence imaging in order to extract kinetic parameters without harvesting a fraction of the solution. If successful, this system would help us to understand the rate-limiting step and to extend the capabilities of the PURE system. Moreover, we might be able to apply this approach and prolong expression lifespan in liposomes through the formation of membrane pores.

2.2 Results and discussion

2.2.1 Preparation of self-made PURE system solutions

Due to high cost of PURE system components and the high amounts of feeding solution necessary for a semi-open system, we decided to first prepare a self-made PURE buffer. Furthermore, this would also allow us to adjust the several components of the PURE system separately in future experiments. To this end, we prepared a buffer solution and an amino acid mix, which contained together all the components of the commercial buffer (solution I) of PURE*frex*. This substitution first succeeded in yielding an equal amount of YFP compared to the commercial PURE*frex* buffer (Figure 2.2D and 2.2F). Only two months later, however, the same solutions gave a distinctively lower yield of YFP (Figure 2.2E). The amount of expressed RNA, detected by spinach signal was similar to before and to the commercial buffer (Figure 2.2A-C), indicating that the problem was likely linked to the *in vitro* translation. We thus prepared another amino acid mix, for which we used a lower amount of KOH to dissolve the acids. With this solution the yield was lower compared to the commercial solution I (Figure 2.2G) but stayed reproducible for several months. We therefore decided to use this AA solution for further experiments. A remake of the buffer solution proved not successful in recreating a good yield (Figure 2.2H).

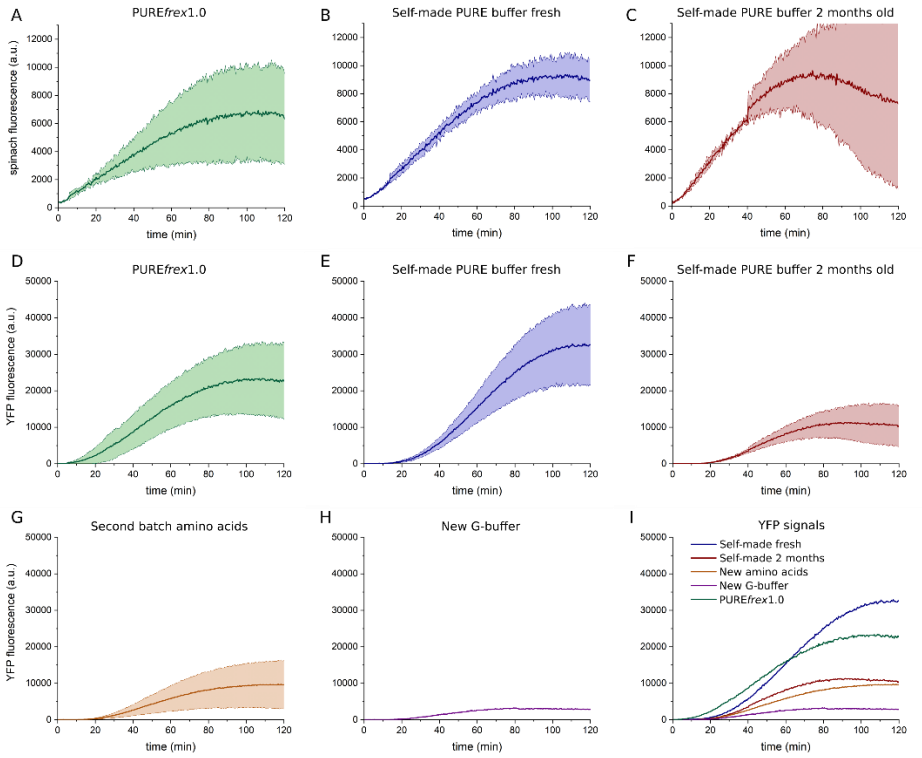

Figure 1.2: Self-made PURE buffer allows for a cheap replacement of the commercial PUREfrex1.0 solution, although ultimately at a lower yield. **A-C**: Signal of LL-Spinach over time. DFHBI was added to expression mix to bind to the spinach sequence on RNA expressed from the eYFP-LL-Spinach gene. The complex formed by the DHFBI and spinach is fluorescent and can thus be used for fluorescence measurement of the RNA concentration. In this case, the measurement was qualitative and not quantitative. **D-I** Signal of expressed eYFP over time. YFP requires a certain time after expression to fold correctly and become fluorescent. Therefore, there is hypothetically a delay of the signal in relation to the expressed protein. **A** and **D**: LL-spinach and YFP signal of the eYFP construct expressed with commercial PUREfrex1.0 solutions (N=3). **B** and **E**: Expression of eYFP with the PUREfrex1.0 solution I substituted with self-made PURE buffer (N=4). **C** and **F**: Expression profile of the same self-made buffer as in **B** and **E**, but two months later (N=2 for RNA and 4 for YFP signal). **G**: Expression profile with second amino acid solution (N=14). **H**: Expression profile with second amino acid solution and a new buffer solution (N=1). I: YFP expression of all five different conditions in direct comparison. All measurements were done by a platereader and with volumes of 10 µl. As the plate was not covered, the expression solution was evaporating over time, leading to a decay of the signal after about 2 hours. This decay was not observed in later experiments during which evaporation was minimized. Shaded areas indicate +/– 1 SD.

2.2.2 Cell-free gene expression in a dialysis chamber

To create a semi-open system, we designed a dialysis device, which primarily consisted of two chambers made from Polymethylmethacrylaat (PMMA) with volumes of 8-10 and 100 µl respectively (figure 2.3 and 2.6). The two chambers were connected over a membrane with a molecular weight cut-off of 20kDa. A silicon sheet was used as a seal between the two chambers

and two microtubes were attached to the opening of the reaction chamber in order to fill it with the PURE system. A reaction solution containing the PURE system,7.4 nM of YFP encoding DNA and a feeding solution consisting of the self-made PURE buffer and amino acid mix were prepared and added to the reaction chamber and the feeding chamber respectively. Next, the chamber was placed in an inverted fluorescence microscope, incubated at 37°C and images of the YFP signal acquired at the focal plane of the reaction chamber.

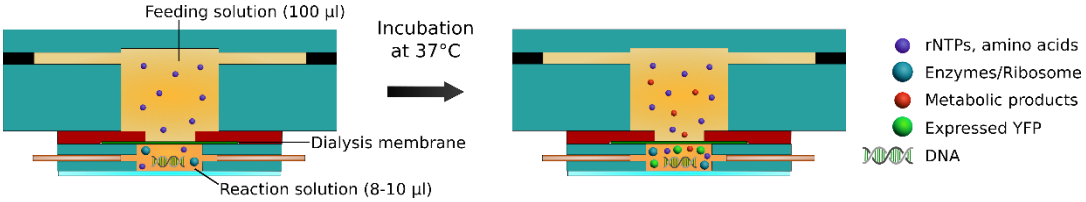

Figure 2.3: Schematic of how our semi-open system should be able to feed the reaction solution with NTPs and amino acids while simultaneously removing waste products.

First, we evaluated if there was diffusion of nutrients between the chambers. Therefore, we omitted the amino acids from the reaction solution and added them only to the feeding solution. If the amino acids would not be able to cross the membrane and diffuse into the reaction solution, no increase of YFP signal would occur. As shown in Figure 2.4A, the YFP signal did start to increase a few minutes after the start of the experiment. It reached a constant rate of expression after about 20 minutes and continued at that for about an hour. Subsequently, the rate of expression was slowly decreasing. If the amino acids were added to the reaction solution from the start, the observed profile of expression (Figure 2.4B) was very similar to the one with none added in the beginning. The average yield was slightly lower and the expression plateaued earlier, but without a substantial difference. To compare the results of the dialysis chamber with normal in bulk expression, we conducted expression in a minimized version of the reaction chamber, which was not in contact with any feeding solution. In this case, expression yield and time (Figure 2.4C and 2.5) were almost as high and long as in the experiments including a feeding solution. We further measured the expression in a cuvette by a fluorescence spectrophotometer (Figure 2.4D), which represents a standard method of conducting expression in bulk. To compare the yields in the dialysis chamber and in the cuvette, several microliters of reaction solution were taken from the dialysis chamber after several hours of expression and measured in the cuvette. This was done two times to gain a rough estimation of how the intensities correspond and the data of the cuvette measurement was adjusted accordingly. In this case, the estimated yield and time of expression were even more similar to the ones of the dialysis chamber. To rule out that the results were specific to our self-made PURE buffer, we conducted a single experiment utilizing only commercial PURE*frex* solutions for reaction and feeding solution, which gave a yield and expression time comparable to the ones of the other conditions (Figure 2.4E). Overall, there was no substantial difference between any condition regarding the final yield and the time until expression plateaued (Figure 2.5).

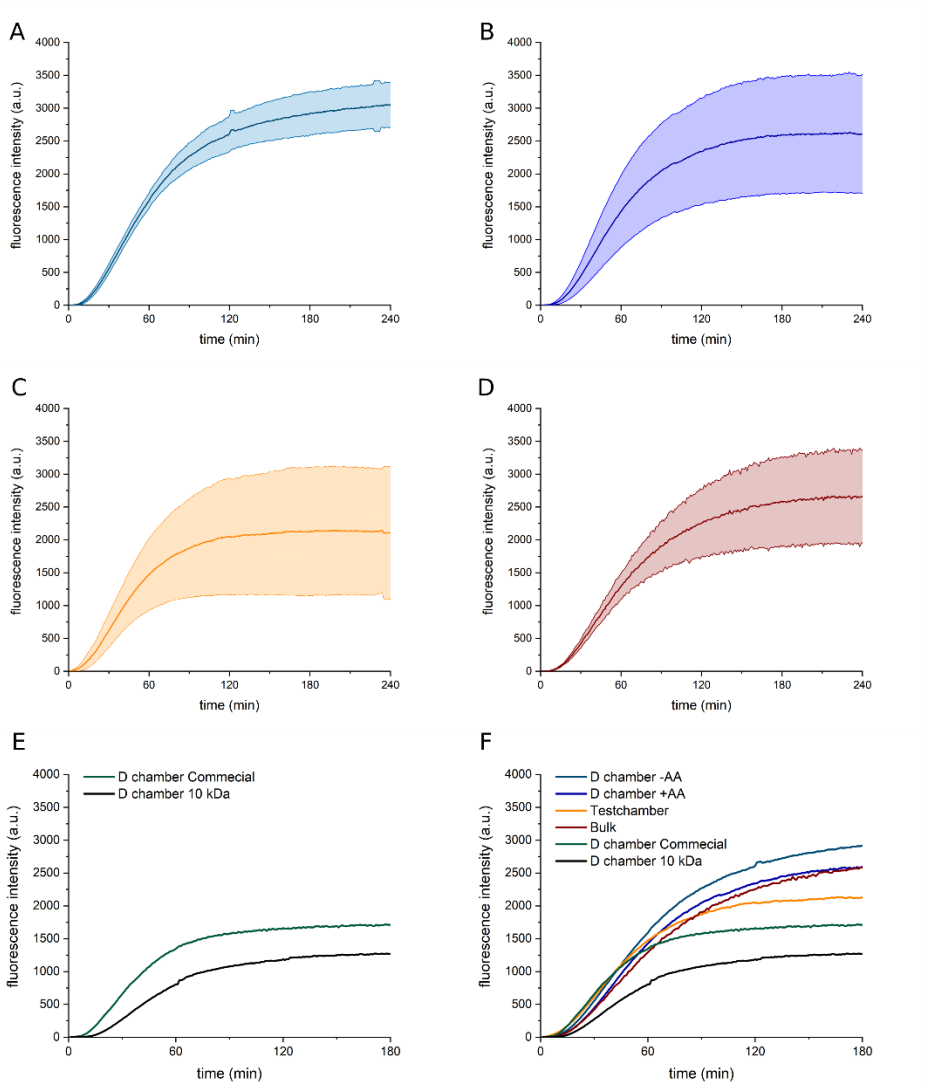

Figure 2.4: Expression yields and times are similar in semi-open and standard expression conditions. **(A)** Signal of eYFP over time in the dialysis chamber without any amino acids present in the reaction solution at the beginning of the experiment. N=5. **(B)** Expression in the dialysis chamber with feeding solution and amino acids present in the reaction solution from the start. N=3. **(C)** Expression inside the reaction solution chamber without contact to any feeding solution. N=3. **(D)** Profile of a standard expression inside a cuvette, measured by a fluorescence spectrophotometer. N=3. E: Expression inside the dialysis chamber with only commercial solutions used for reaction and feeding solution. N=1. **(F)** Direct comparison of all conditions. Shaded areas indicate +/– 1 SD.

When the level of eYFP signal ceased to increase, it would stay at the same level for more than 10 hours. If the chamber was sealed properly, there was no significant evaporation occurring during the same period of time. The observation that gene-expression would take place as fast and as

effective in the condition with no amino acids present in the reaction solution compared to the other conditions proved that the diffusion of amino acids was occurring at a high rate. This represents sufficient validation that the chamber design was working and that small molecules were freely able to migrate between the two solutions, while bigger molecules stayed trapped in the reaction solution. It seems also unlikely that smaller proteins like the initiation factors were lost to the feeding solution at a significant rate. First, as described before, initiation factors were reported to not be lost over time in experiments applying bigger cut-offs than used by us [6]. Second, the expression profile with the dialysis chamber is so similar to what we observed in bulk experiments, that an incidental overlap is at least unlikely. If initiation factors would be lost over time, this should manifest itself in an early decrease of expression rate with a very slow levelling off, as initiation factors would be only slowly diluted to a certain concentration. Third, using a membrane with a smaller cut-off (10.000 kDa) produced the same basic profile of expression (Figure 2.4E).

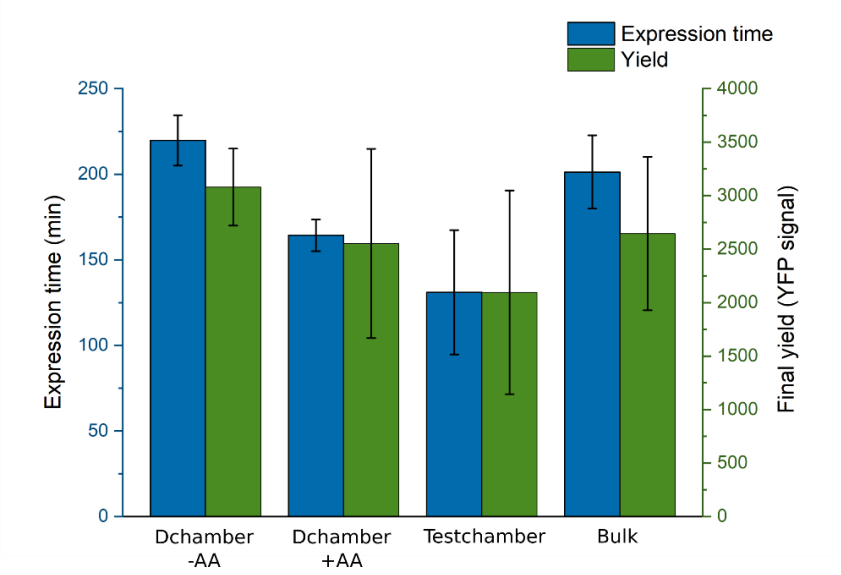

Figure 2.5: Mean values of expression time and yield in dialysis experiments (Dchamber) and controls. No difference was observed between expression in a semi-open system and standard bulk experiments regarding yield and expression time. Sample numbers are N=5 for the Dialysis chamber without AAs and N=3 for the other three conditions. Error bars represent SD.

2.3 Conclusion

The presented results clearly demonstrate that we were successful in creating a semi-open system in which there is an exchange between the reaction and the feeding solution. Thus, there should be a constant supply of nutrients and dilution of low molecular weight waste products. Contrary to what has been claimed [7], this did neither improve the yield of the PURE system nor its stability over time. Thus, accumulation of organic phosphate can in this case be ruled out as a cause for the

breakdown of PURE system activity. The same is true for the depletion of amino acids or NTPs. All of these components should be diluted or supplied by the feeding solution. Further experiments conducted by Anne Doerr in our lab have validated that neither NTPs nor amino acids are depleted to a sufficient amount to explain the decrease of translation [2]. Neither was any significant inactivation of the translation machinery observed over time when the expression mix was incubated for several hours before addition of the template. Instead, other factors that might cause the breakdown of PURE system activity are mRNA inactivation, consecutive sequestration of translation factors and tRNA depletion by peptidyl-tRNA drop-off. What is certain is that the ribosomes in the PURE system function at a low robustness and efficiency and that at least for some DNA constructs a considerable amount of truncated side-products is formed [2]. At some point, when this and other potential problems are identified and solved, it would be worth coming back to the presented semi-open system to check if the expression time can be then further extended. If that's the case, it would be worth to acquire either a commercial kit or develop a system that is easier to use for further experiments. We have limited our experiments overall to PURE*frex*, and it might be that the result would differ with PURE*frex*2.0, as it differs in its components and overall yield. However, it might be worth to wait until the respective composition is disclosed in order to provide an adequate feeding solution. Liposomes can as well function as a semi-open system by incorporation of pore complexes into the membrane, allowing entry of nutrients necessary to maintain metabolic activity of the encapsulated gene expression system and other processes essential for a minimal cell. We have previously realized the successful expression of connexion-43 inside of liposomes, which lead to membrane permeabilization without compromising the yield of co-expressed YFP [8]. Incorporation of a α-hemolysin pore complex in liposomes containing cell lysate has been reported to extend gene expression time [9]. This was not observed for our combination of connexin-43 and PUREfrex and supports the results presented here, indicating that neither nutrients nor metabolic products small enough to pass through the pores are responsible for the limited expression time in PUREfrex.

Generally speaking, the lower robustness of the PURE system compared to cell extracts or gene expression in cells can be seen as a direct result of its minimal setup. Many of the factors present in bacteria and omitted in the PURE system are maybe not essential for gene expression, but they very likely support the effectiveness of the prokaryotic gene expression machinery. In order to create a system that is sufficiently powerful to run all the necessary processes in a minimal cell, it might be necessary to add more components to the PURE system, like chaperones or factors facilitating translation processes. Alternatively, it might be possible to modulate the existing components in order to make them more efficient in the given minimal environment. The prokaryotic enzymes present in the PURE system have evolved for their function inside of cells, where many other enzymes and factors interact with them and probably facilitate their function. However, it might be possible to change their design in ways that make them more efficient on their own and allows to maintain a low number of components. An elegant method for doing so could be the application of an *in vitro* evolution process [10], which would also not necessarily depend on an accurate model of the system in order to improve it.

2.4 Materials and Methods

Preparation of self-made PURE components

A solution containing all PURE system buffer components except NTPs and amino acids was prepared by Andrew Scott. It was prepared at 10x working concentration, named G-solution and only differed from the components used for the commercial buffer in that instead of 10-formyl-tetrahydrofolate we used folinic acid calcium salt hydrate. The pH of the solution was adjusted to 7.4. This solution was diluted to 4x working concentration and the four rNTPs added to receive the F-solution, which was used to replace, together with the amino acid mix and tRNA, the PURE *frex* solution I for the respective experiments. All components and their concentrations can be found in Table 2.1.

Table 2.1: Components of the self-made PURE buffer (G-solution).

Components	G-solution (10x)	F-solution (4x)	Final concentration
HEPES	200 mM	80 mM	20 mM
Potassium glutamate	1800 mM	720 mM	180 mM
Magnesium acetate	140 mM	56 mM	14 mM
DTT	20 mM	8 mM	2 mM
Spermidine	20 mM	8 mM	2 mM
Folinic acid calcium salt hydrate	100 µg/µl	40 µg/µl	10 µg/µl
Sodium phosphocreatine	200 mM	80 mM	20 mM
ATP	-	12	3
GTP	-	12	3
UTP	-	4	1
CTP	-	4	1

The amino acid solution was prepared by dissolving the amino acids in KOH, as several of them are not soluble in water [11]. For the first amino acids solution, all amino acid powders were separately dissolved in 5 mM KOH solution and combined in one solution of 5 mM of each amino acid, which was adjusted to a pH of about 7-8. As described in this chapter, this solution was potent but apparently not stable. In a second preparation of the amino acid solution, a lower amount of KOH was used for dissolving the amino acids, as it was hypothesized that high KOH concentration might decrease amino acid stability. First, single amino acid stock solutions were prepared at a concentration of 500 mM. To the corresponding amount of amino acid powder (Sigma Aldrich) Milli-Q water was added to 0.5 ml. Then, 100 µl of 5 M KOH was added and the solution vortexed for several seconds. This was repeated up to four times, until the amino acids were completely dissolved. The missing amount of liquid was filled up with water to 1 ml total. This was done to avoid higher concentration of KOH than necessary for dissolving the amino acids. Final concentrations of KOH in the stock solutions were ranging between 1 and 2 M. From the 20 amino acid stock solutions, four intermediate mixes were prepared. This was done by mixing 200 µl of five different AA stock solutions and then diluting 500 µl of this mix with 500 µl H_2O. This intermediate stocks contained thus 50 mM of each of the five amino acids. We choose to create this

intermediate mixes in order to facilitate the generation of later amino acid mixes. Of each of the intermediate mixes 100 µl were added to 570 µl H_2O to achieve the final concentration of 0.5 mM of every amino acid. Then, the pH was adjusted between 7-8 by adding acetic acid (1M, 30 µl) and checking the pH with indicator paper (around 20 µl were used for the measuring). At last, the solution was aliquoted, flash frozen with liquid nitrogen, and stored at -80°C. Activity of the self-made buffer and amino acid mix was measured with a platereader (Cary Eclipse, Varian). Excitation and emission was at 460/502 nm for the Spinach aptamer and at 513/535 nm for eYFP respectively.

Gene expression in a dialysis chamber

Dialysis chambers were made of poly(methyl methacrylate) (PMMA) with volumes of 8-10 µl for the reaction chamber and 100 µl for the feeding chamber. Chambers were cleaned by sequential sonication in Hellmanex (2%), KOH (1M), EtOH and milliQ. A silicon sheet with a hole stamped into the middle (about 2 mm Ø) was placed on the opening of the feeding chamber. A piece of dialysis membrane was cut out of a dialysis cassette (Slide-A-Lyzer™, Thermo Scientific) and placed over the hole on the sheet. The reaction chamber was placed on the other side of the sheet, with the openings in alignment and two microtubes are pushed into it. To avoid leakage, a silicon sheet with a hole was placed under the reaction chamber, a glass slide was attached to it and the whole construction pressed together with two clamps. The reaction solution was prepared as described in Table 2.2, including a tRNA mix from New England Biolabs and 7.4 nM of eYFPco-LL-spinach 7.4 nM as DNA template. The 2 µl of amino acid mix were substituted with milliQ for the experiments without amino acids present in the reaction solution. The feeding solution was made from 25 µl F-solution solution, 10 µl amino acid mix, and 65 µl milliQ.

Table 2.2: Components of reaction and feeding solution for dialysis experiments.

Components	Reaction solution	Feeding solution
F-solution	5 µl	25 µl
Amino acid mix	2 µl	10 µl
tRNA (NEB)	2 µl	
PF Sol II	1 µl	
PF Sol III	1 µl	
DFHBI	1 µl	
Superase	0.5 µl	
DNA - eYFP	Amount for 7.4 nM final concentration	
Water (MilliQ)	To 20 µl final volume	65 µl

Next, the reaction solution was added through one of the microtubes by taking up the solution, attaching a short plastic tube to the pipet tip and then pushing the tube over the microtube. The solution was slowly injected into the chamber, with the chamber being held vertically upwards. Subsequently, the feeding chamber was filled with the feeding solution by directly pipetting it through one of the holes. It was optically checked that the membrane was wetted by the reaction solution and that there were no air bubbles present at the membrane. The openings of the feeding chamber and the microtubes were sealed with wax and rubber plugs respectively. For analysis, the chamber was placed in an inverted fluorescence microscope (Olympus IX81, UPlanFLN

20×objective, YFP-2427B-OMF-ZERO filter cube, software Andor iQ3) and incubated at 37°C. To receive the kinetics of YFP production, one image per minute was acquired of the YFP signal at the focal plane of the reaction chamber. Finally, Fiji [12] was used to measure the average signal of each picture. As additional comparison, eYFP expression was measured as well by a fluorescence spectrophotometer (Cary Eclipse, Varian).

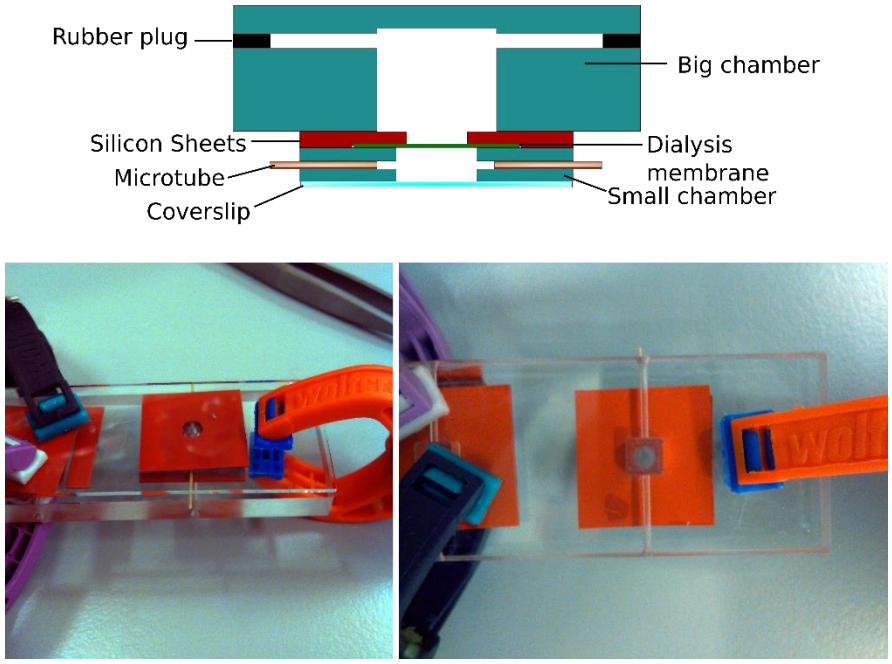

Figure 2.6: Schematic of dialysis chamber components and images of assembled dialysis chamber. The left chamber visible on the photos served as a dummy to stabilize the glass slide which was pressed against the chamber in order to seal it tightly.

References

[1] Takahashi MK, Chappell J, Hayes CA, Sun ZZ, Kim J, Singhal V, et al. Rapidly characterizing the fast dynamics of RNA genetic circuitry with cell-free transcription-translation (TX-TL) systems. ACS Synth Biol 2015;4:503–15.

[2] Doerr A, de Reus E, van Nies P, van der Haar M, Wei K, Kattan J, et al. Modelling cell-free RNA and protein synthesis with minimal systems. Phys Biol 2019;16:25001.

[3] Jewett MC, Swartz JR. Substrate replenishment extends protein synthesis with an in vitro translation system designed to mimic the cytoplasm. Biotechnol Bioeng 2004;87:465–72.

[4] Kim DM, Swartz JR. Prolonging cell-free protein synthesis with a novel ATP regeneration system. Biotechnol Bioeng 1999;66:180–8.

[5] Liu Y, Fritz BR, Anderson MJ, Schoborg JA, Jewett MC. Characterizing and alleviating substrate limitations for improved in vitro ribosome construction. ACS Synth Biol 2015;4:454–62.

[6] Spirin AS, Baranov VI, Ryabova LA, Ovodov SY, Alakhov YB. yield.A continuous cell-free translation system capable of producing polypeptides in high. Science 1988;242:1162–4.

[7] Jackson K, Kanamori T, Ueda T, Fan ZH. Protein synthesis yield increased 72 times in the cell-free PURE system. Integr Biol (Camb) 2014;6:781–8.

[8] Blanken D, van Nies P, Danelon C. Quantitative imaging of gene-expressing liposomes reveals rare favorable phenotypes. Phys Biol 2019;16:45002.

[9] Noireaux V, Libchaber A. A vesicle bioreactor as a step toward an artificial cell assembly. Proc Natl Acad Sci U S A 2004;101:17669 LP – 17674.

[10] Murase Y, Nakanishi H, Tsuji G, Sunami T, Ichihashi N. In Vitro Evolution of Unmodified 16S rRNA for Simple Ribosome Reconstitution. ACS Synth Biol 2018;7:576–83.

[11] Caschera F, Noireaux V. Preparation of amino acid mixtures for cell-free expression systems. Biotechniques 2015;58:40–3.

[12] Schindelin J, Arganda-Carreras I, Frise E, Kaynig V, Longair M, Pietzsch T, et al. Fiji: an open-source platform for biological-image analysis. Nat Methods 2012;9:676–82.

Chapter 3

Combining eukaryotic microtubules and cell-free gene expression

Da steh ich nun, ich armer Tor!
Und bin so klug als wie zuvor.

Johann Wolfgang von Goethe, Faust I

Here we demonstrated that cell-free gene expression through the PURE system and dynamic microtubules can be combined, although the imaging of microtubules under conditions compatible with gene expression proved difficult. Furthermore, we demonstrated that the microtubule associated protein Mal3 can be functionally expressed by the PURE system. Expressed Mal3 is able to bind to microtubules and to recruit the proteins Tea2 and Tip1. It also appears that the expressed Mal3 influences the dynamic properties of the microtubules in accordance to what is reported of purified Mal3. We also were able to encapsulate dynamic microtubules inside liposomes in a manner that allows for simultaneous gene expression. Encapsulated microtubules were deforming the liposome membrane by growth of the filaments and we could demonstrate that the type of deformation could be externally influenced by increase or decrease of the membrane tension.

3.1 Introduction

In section 1.5 we described how filaments encapsulated in lipid vesicles, and in particular microtubules, interact with the membrane they are confined by. In cells growth, positioning, and functions of microtubules are further regulated by microtubule associated proteins (MAPs). A group of MAPs which is heavily involved in interaction of microtubules with the membrane and other filaments are plus-end tracking proteins (+TIP). A member of this group of proteins, as well as of the end-binding (EB) family of MAPs, is EB1. EB1 is able to directly bind to the microtubule lattice and does so predominantly at the plus-end of microtubules as observed *in vivo* [1] as well as *in vitro* [2]. The specific binding of EB1 to the plus-end of growing microtubule is most likely caused by its increased affinity to GTP tubulin, located in the growing cap of the microtubule, compared to GDP tubulin present in the lattice [3,4]. The main function of EB1 is recruitment of other +TIPs that have minor or no native affinity for microtubules to the plus-end [5,6]. Mal3, the homolog of EB1 in the fission yeast Schizosaccharomyces pombe, is for example recruiting a complex of the motor protein Tea2 and the CLIP170 homologue Tip1 to the plus-end of the microtubule [2]. Localization at microtubule ends allows +TIPs to control different aspects of microtubule dynamics, such as the promotion or inhibition of growth and catastrophes, and to link microtubule ends to different cellular structures such as the cell cortex, mitotic kinetochores or actin filaments [6]. Thus, +TIPs play essential roles in mitosis, cell polarity, and cell shape [6,7]. In case of Mal3, it has for example been demonstrated that it is involved in microtubule integrity, DNA segregation and control of cell morphology [8,9].

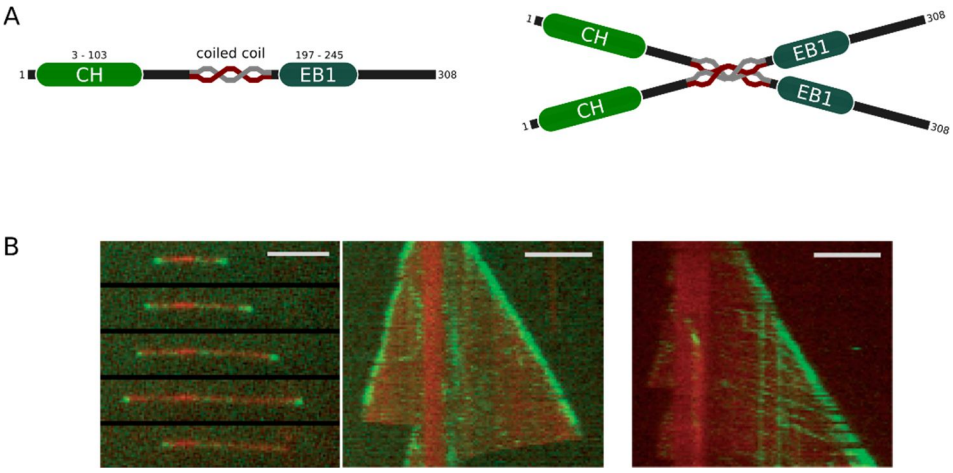

Figure 3.1: Schematic structure of Mal3 and plus-end tracking mediated by Mal3. **(A)** Structure of Mal3. The CH domain mediates binding to microtubules, the coiled coil domain facilitates dimerization and the EB1 domain is important for interactions with binding partners. **(B)** Visualized tip-tracking of microtubules (red) through labelling (in green) of Mal3 (two left images) or Tip1 in presence of Mal3 and Tea2 (right image). Scale bars = 5 µm. Taken from Bieling et al 2007 [2].

Like other EBs, Mal3 is a dimeric protein composed of two highly conserved functional modules, namely an N-terminal calponin homology (CH) domain that mediates binding to the microtubule and a coiled coil domain which facilitates dimerization of Mal3 (Figure 3.1A) [10–12]. The Mal3 dimer binds to GTP tubulin incorporated in the microtubule, but not to tubulin dimers. Unlike *in*

vivo, in which case Mal3 and EB1 stabilize microtubules, both these proteins cause an increase of catastrophe frequency *in vitro* [13–15]. EB1 further strongly promotes growth velocities *in vitro* [16], which was not observed with Mal3 [2]. It was also demonstrated that plus-end tracking by Mal3, Tea2 and Tip1 can be reconstituted *in vitro* [2](Figure 3.1B).

The reviewed examples of *in vitro* systems, such as the encapsulation of microtubules in lipid vesicles or the plus-end tracking through Mal3, Tea2, and Tip1 are set up to be minimalistic in their complexity. This reductionism has proven very useful to explore the given systems, such as the interaction of microtubules with a confining membrane. However, as much as reducing complexity helps us to understand basic biological mechanisms, it also distances those reconstituted systems from how they operate in living cells. A mechanism that is omnipresent in cells and which is in generally omitted in this kind of *in vitro* experiments is gene expression. The regulation of filaments is dependent on a dynamic expression pattern of MAPs and not on fixed concentrations of protein as given in standard *in vitro* assays and it is reasonable to assume that we will have to mimic this dynamic process at some point if we want to create *in vitro* system that represent conditions in living cells more closely. We wondered if we can reintroduce complexity in a functional manner by combining eukaryotic microtubules with cell-free gene expression of MAPs. Therefore, we investigated to what degree we are able to affect microtubules by *de novo* synthesis of proteins such as Mal3 and if we can encapsulate microtubules in liposomes alongside a cell-free gene expression system such as the PURE system.

3.2 Results and discussion

3.2.1 PURE system and eukaryotic microtubule polymerization are compatible

The very first step was to investigate if gene expression activity of the PURE system and polymerization of tubulin can be combined. We therefore added 15 µM of purified tubulin to standard expression mixes of PURE*frex* and PURExpress, and analysed expression kinetics of YFP by fluorescence spectrometry and filament polymerization by TIRF microscopy. Addition of tubulin resulted in only slightly decreased expression yields compared to the control in both PUREsystems (Figure 3.2A and B). This minor difference lies within the range of variations we observe between identical PURE system reactions and did not constitute a limitation for subsequent experiments. When the same mix of PURE system with 15 µM tubulin was analysed by squish assay and TIRF microscopy the polymerization of filaments was observed (Figure 3.3A). However, the imaging quality was sub-standard due to lack of attachment to the surface and additional components usually used in microtubule assays, namely an oxygen scavenger system, methyl cellulose and • -casein.

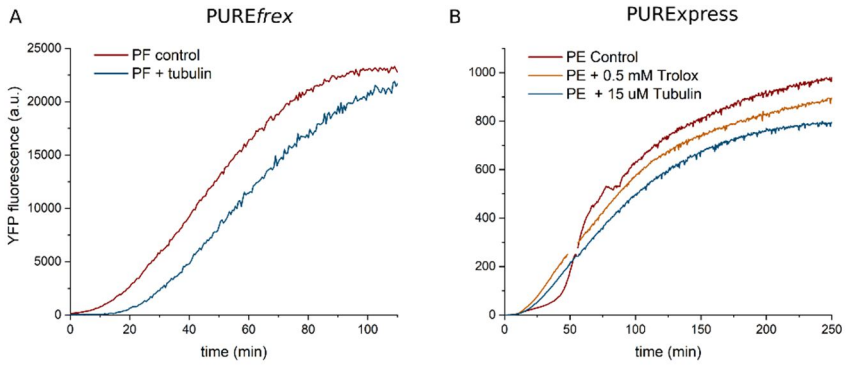

Figure 3.2: Expression of YFP in combination with purified tubulin. **(A)** Expression of YFP by PURE*frex*. The sample with 15 µM of tubulin added (blue line) achieved a similar yield to the control (red line). **(B)** Expression of YFP by PURExpress. Same result was observed as with PURE*frex*. Additionally, the oxygen scavenger trolox (6-hydroxy-2,5,7,8-tetramethylchroman-2-carboxylic acid) was added, which as well did not influence expression yield or kinetics.

Without an oxygen scavenger system, oxygen radicals created by excitation of fluorophores will bleach the fluorophores [17] and cause breakage of the microtubules by disruption of protein-protein interactions [18]. A standard oxygen scavenger system is glucose oxidase coupled with catalase (GODCAT) [19]. When we tested gene expression of YFP in its presence, almost no signal of YFP expression was detected. However, YFP does, like other fluorescent proteins of its class, require molecular oxygen for maturation [20] and it is therefore likely that YFP was expressed, but could not undergo maturation into its fluorescent configuration due to lack of oxygen. Besides this, glucose oxidase activity acidifies the medium, which might at a certain point impede PURE system activity. The expression of fluorescent proteins is the most straightforward method to verify and characterize IVTT activity and thus its incompatibility with the standard microtubule assay posed a problem. An alternative to removal of molecular oxygen is the specific neutralization of oxygen radicals and reactive oxygen species. We therefore applied the antioxidant and Vitamin E analogue Trolox (6-hydroxy-2,5,7,8-tetramethylchroman-2-carboxylic acid) to our assays, which can effectively eliminate both oxygen radicals and reactive oxygen species [21]. When added to PURExpress, Trolox had no distinctive effect on the expression yield (Figure 3.2B). In the microtubule assay, addition of Trolox seemed to yield better results than total omission of any protective system but could not prevent bleaching of the filaments as effectively as the GODCAT system leading to limited imaging time and quality (Figure 3.3B). Although Trolox might remove radicals and reactive oxygen species, it acts likely too slow to effectively prevent oxygen radicals created in the vicinity of fluorophores to react with them and thus complete removal of oxygen is still a more effective method to prevent bleaching and oxidative damage. Furthermore, we tested the protocatechuic acid/protocatechuate-3,4-dioxygenase (PCA/PCD) oxygen scavenging system for imaging, which causes, compared to GODCAT, less acidifaction of the medium [22]. The PCA/PCD system yielded an imaging quality comparable to the GODCAT system (Figure 3.3C).

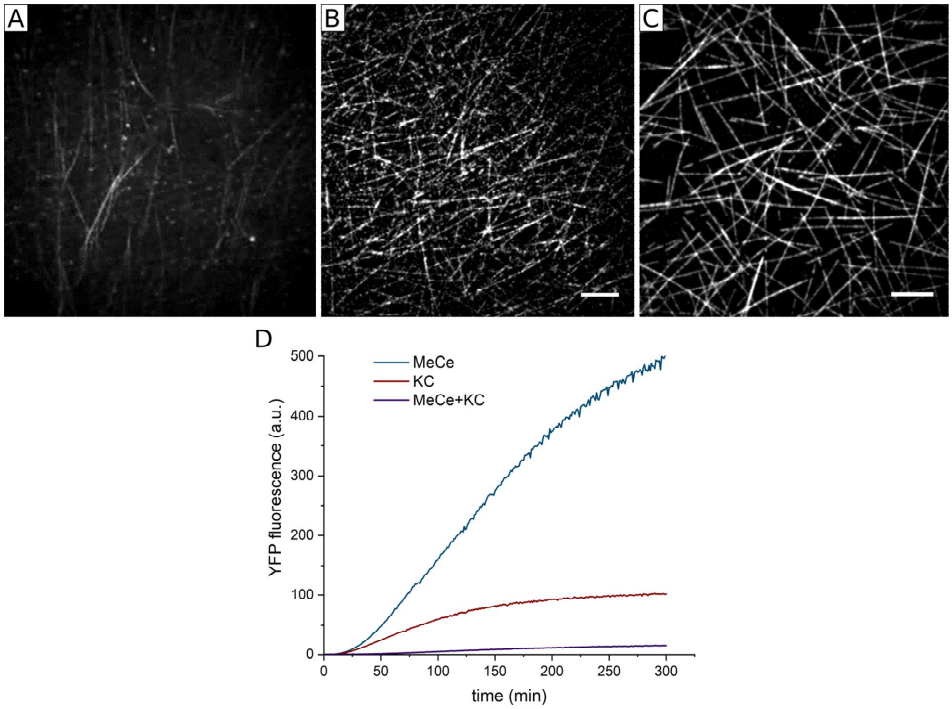

Figure 3.3: TIRF imaging of microtubules and eYFP expression in dependence of additional assay components. **(A)** Squish assay of microtubules in PURE system without additional assay components. To the standard PURE mix 15 µM of tubulin including a fraction of labelled tubulin (HiLyte 635) was added. **(B)** TIRF imaging of microtubules growing from seeds with Troxol added instead of GODCAT. **(C)** TIRF imaging of microtubules growing from seeds with the PCA/PCD system as oxygen scavenger. **(D)** Expression kinetics of eYFP with PURExpress at 30°C and addition of methyl cellulose, • -casein and the combination of both.

Of the other two components normally added in our microtubule assays, methyl cellulose and • -casein, • -casein in particular had a negative effect on expression levels in PURExpress and almost no expression was observed when both were added (Figure 3.3D). Methyl cellulose is used to form a mesh on top of the microtubules on the surface, which prevents microtubules from moving upward and out of focus and • -casein is added to block the glass surface. We tried to find a compromise regarding the concentration of these components, but substantially lower concentrations resulted in poor imaging quality. Thus, although microtubule polymerization and gene expression in the PURE system are compatible, combined gene expression and microtubule imaging perform very poorly under given conditions. As a consequence, we decided that concurrent combination of gene expression and standard microtubule assays is not feasible.

3.2.2 Cell-free gene expression of Mal3

We investigated if when MAP is expressed first seperately from microtubules and subsequently added to them, any interaction of it with the microtubules occurs. We chose Mal3 as a suitable candidate, because its interaction with microtubules is well characterized and it can be purified from *E. coli*, which proofs independence from eukaryotic chaperones and post-translational

modifications. We prepared a linear construct of Mal3 containing a 6xHis-Tag ($Mal3^{His}$) and checked *in vitro* transcription and translation (IVTT) of it by expression with PURE*frex* under addition of fluorescently labelled tRNA (GreenLys) and addition of the product on an SDS-PAGE (Figure 3.). The terminal protein of the phi29 virus (TP) served as a positive control. $Mal3^{His}$ showed clear bands on the GreenLys channel, of which the intensities were comparable to the one of TP. On the coomassie staining, $Mal3^{His}$ was not visible due to overlapping with a band of the PURE*frex* background. Purified Mal3, visible only on the coomassie staining, indicates where the band Mal3 should be on the gel. Expressed Mal3 might be slightly higher due to the His-tag and linker adding about 2 kDa to the size of the protein.

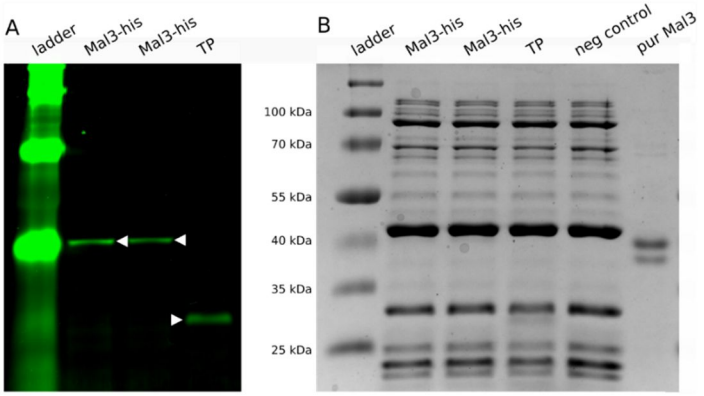

Figure 3.4: SDS-PAGE of Mal3 expressed *in vitro*. A. GreenLys fluorescence signal of expression products. Expression of the terminal protein (TP) was used as a positive control. Synthesized full-length proteins are marked by white arrows. B. Coomassie staining of the same gel. A PURE reaction mix without added DNA was used as negative control and Mal3 purified from *E. coli* added as an additional indication for the height of expressed Mal3 on the gel.

Next, we checked if *de novo* expressed Mal3 is able to interact with microtubules and is possessing full functionality. One of the functions of Mal3 is to recruit other MAPs to the microtubule and an effective and established method to visualize recruitment is the plus-end tracking of microtubules mediated by Mal3, Tea2 and Tip1 [2]. In this assay, Mal3 facilitates recruitment of the kinesin-like protein Tea2 to the microtubule which will subsequently recruit Tip1. Tip1 is tagged with a fluorophore and if both recruitment and motor protein activity occur Tea2 will accumulate at the plus-end of the microtubule, resulting effectively in a labelling of the tip (Figure 3.5A). First, we checked if tip-tracking was working under PURE system conditions, which was positive. We then expressed $Mal3^{His}$ with PURE*frex* under standard conditions for 3 hours at 37°C and afterwards added it to a mix containing all components for the tip-tracking assay except Mal3. This mix was added to a flow cell containing microtubule seeds from which the microtubules could polymerize. Imaging was performed by TIRF microscopy at 30°C. However, this yielded no observable tip-tracking, indicating that the expressed Mal3 was either not able to bind to microtubules or to recruit Tea2. A possible reason for inactivity of expressed protein is incorrect folding and we investigated if addition of chaperones might solve the problem. First, we tried addition of GroE, which gave no positive result either. Next, we added a chaperone mix of DnaK, DnaJ and GrpE (DnaK mix) to the expression solution and consequently observed clear tip-tracking (Figure 3.5B and C).

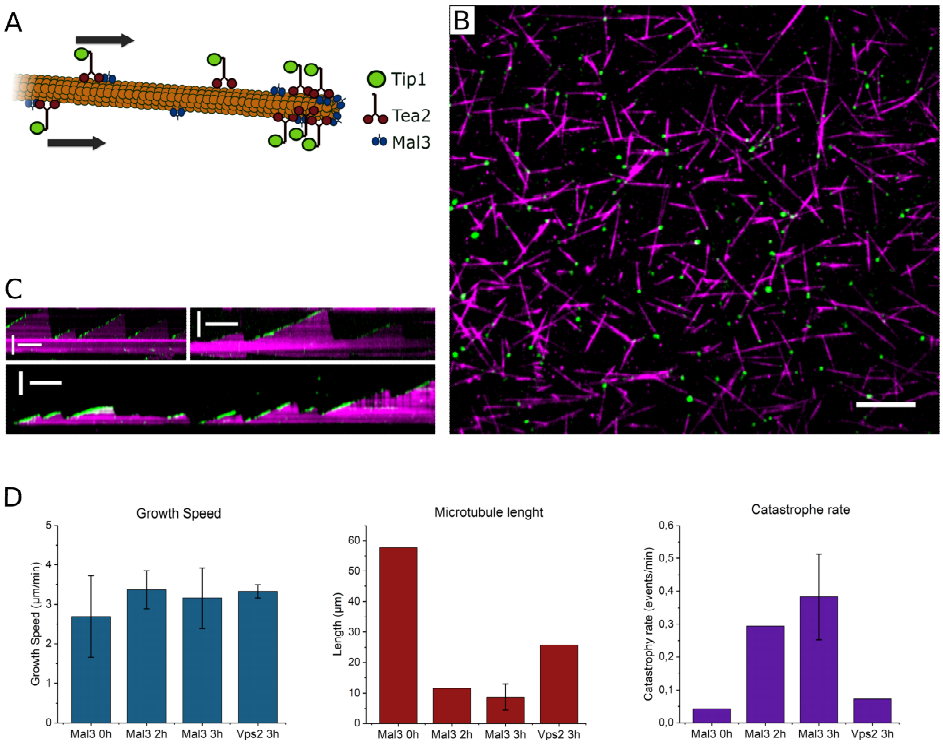

Figure 3.5: Plus-end tracking and influence on microtubule dynamics mediated by synthesized Mal3. **(A)** Scheme of plus-end tip tracking through recruitment of Tip1 to the microtubule tip by Mal3 and Tea2. **(B)** TIRF microscopy image of plus-end tracking mediated by expressed Mal3. Scale bar = 10 µm. **(C)** Kymographs of plus-end tracking. Vertical scale bars represent 5 µm and horizontal scale bars represent 1 minute. **(D)** Influence of expressed Mal3 on microtubule dynamics. Average growth speed, microtubule length and catastrophe rate have been calculated for different time points of Mal3 expression (0, 2 and 3 hours), as well as for Vps2 to check for influence of gene expression in general. Tubulin concentration was 14 µM, except for two repeats of Mal3 3 hours, in which case it was 17 µM. Number of experiments was three for Mal3 3 hours and one for the other three conditions. Total number of measurements was 4 for Vps2, 6 for Mal3 0 hours, 36 for Mal3 2 hours and 86 for Mal3 3 hours. Error bars represent standard deviations.

Besides recruitment of other MAPs, Mal3 is also influencing microtubule dynamics, most prominently the rate of microtubule catastrophes [13–15]. To assess the influence of expressed Mal3, we repeated the assay with different expression times of Mal3 and with expression of the ESCRT protein Vps2 as a negative control. Kymographs were taken and used to calculate average microtubule growth speed, length and catastrophe rate (Figure 3.5D). While average growth speed did not differ between the different conditions, average microtubule length was smaller in the conditions of expressed Mal3 compared to no expression (Mal3 0 hours). Microtubules in the conditions of Vps2 expressed for 3 hours were shorter than those in the condition of no expression (Mal3 0h), but longer than with the expressed Mal3 (Mal3 2h and 3h). Compared to microtubule length, the results of the catastrophe rate were exactly reversed. Average catastrophe rate was

highest in Mal3 expressed for 3 hours, followed by Mal3 2 hours, Vps2 3 hours and lowest for Mal3 0 hours. This indicates that expressed Mal3 causes an increase in microtubule catastrophes, which confirms that Mal3 expressed *de novo* functions in the same manner as the purified protein. Microtubule lengths were moderately smaller and occurrence of catastrophe events was slightly lower in the control of expressed Vps2, indicating that expression might change the buffer conditions and thus affects microtubule dynamics indirectly as well. Nevertheless, in regard of catastrophe rate this effect was much smaller than what was observed with expressed Mal3. However, there were only single experiments performed for the conditions of Mal3 expressed for 0 and 2 hours and expression of Vps2, with only four measurements taken in case of Vps2. Further, the conditions of these experiments were not always exactly the same, partly due to problems of finding one condition in which microtubule length was neither too short nor too long for one subset of experiments. Thus, the amplitude of the effect regarding catastrophe rate and microtubule length might be substantial, but the quantity of the data is low.

3.2.3 Encapsulation of eukaryotic microtubules in liposomes

Next, we investigated to what degree we can achieve combination of cell-free gene expression and microtubule dynamics inside lipid vesicles. As elaborated before, directly linking cell-free gene expression with the classical method for performing microtubule assays proved difficult. In case of encapsulation in vesicles, however, previous problems like the fixation of microtubules in one image plane or the blocking of glass surfaces were not present, making the addition of methyl cellulose and • -casein unnecessary. For encapsulation of tubulin, we utilized natural swelling from lipid-coated beads. Several attempts were made to generate dynamic microtubules from encapsulating tubulin with up to 45 µM of tubulin used in the swelling solution without success. This was surprising as successful encapsulation of microtubules in vesicles was reported with concentrations of 25-30 µM [23]. We eventually managed to obtain microtubules formed in vesicles, but only with 30 µM of tubulin combined with addition of 12.5 µM of Taxol (Figure 3.6A). The problem with this solution was that Taxol prevents shrinkage of microtubules and consequently nearly all tubulin polymerizes into filaments devoid of any dynamics. This does not provide a useful model of microtubules and we thus continued to search for an improvement of the method. We finally achieved formation of microtubules inside liposomes by increasing the concentration of tubulin to 70 µM in the swelling solution. However, the yield was poor as only a single microtubule bundle inside a liposome was found in a whole sample. By chance, it was at this time that our lab applied a new method for liposome swelling. In this new method, we additionally added rhamnose to the lipid mix to promote swelling of solution into the lipid layers. Further, a four time freeze thaw cycle was to the swelling procedure, which should improve encapsulation of components by creating temporary defects in the liposome membrane. With this method, we were indeed able to significantly improve the yield of liposomes containing filaments and to achieve filament formation at lower concentrations of tubulin in the swelling solution (30 µM) (Figure 3.6B).

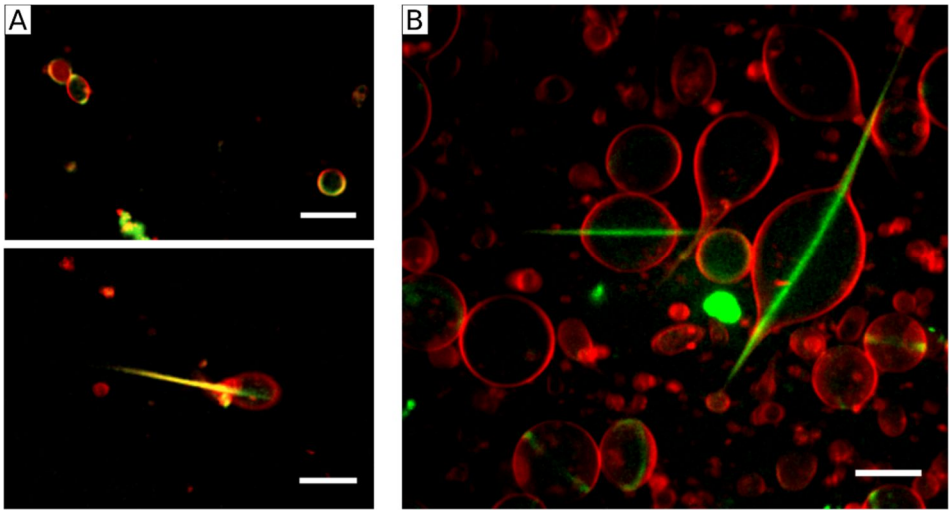

Figure 3.6: Formation of microtubules inside liposomes resulting from encapsulation of tubulin. **(A)** Encapsulation of 50 µM tubulin and Taxol without freeze-thawing after liposome swelling. **(B)** Encapsulation of 30 µM tubulin with freeze-thawing applied. Scale bars = 10 µm.

With this method several experiments at tubulin concentrations between 30 and 50 µM were conducted to further analyse the formation of encapsulated microtubules. Three main morphologies were observed. In one, also known as • -shape, encapsulated microtubules tended to form a single straight bundle that ran through the middle of the liposome and formed two membrane protrusion opposite to each other (Figure3.7A). In the other one, microtubules arranged together into a ring at the liposome membrane that tended to deform the liposome into an oblate spheroid (Figure3.7B). The localisation of the bundle at the membrane is a result of the tension of the bend filaments which competes with the tension of the membrane. Independent of that, membrane binding of eukaryotic microtubules to our lipid composition was never observed and would be highly unlikely as both the membrane and the microtubules are negatively charged. The third morphology was an intermediate between the previous two, in which the microtubule bundle was neither straight nor completely bend along the membrane (Figure3.7C). As laid out in section 1.3, these morphologies have been characterized as well a result of the competitive forces between the membrane tension, the pushing forces of the growing microtubules, and the rigidity of the bundle.

The force exerted by the growing microtubules can be changed by adjusting the concentration of encapsulated tubulin, while the membrane tension is under given conditions dependent on the osmotic pressure acting on the liposome [24]. The rigidity of the bundle depends on the length of the filaments and the number of them therein. We do not know the number of microtubules in a bundle as we cannot be sure that the concentration of tubulin encapsulated is equal to what was added in the swelling solution and we have no immediate way to measure the membrane tension which limits the growth of the microtubules. Moreover, we know neither to what degree the polymerization kinetics differ in the PURE system to standard microtubule assay conditions. However, if we would have information about the concentration and membrane tension, we could theoretically calculate the number of microtubules based on the length of the bundle and the fraction of tubulin that should be polymerized. Considering other reports of encapsulating tubulin in

liposomes of roughly the same size, we assume that the number of microtubules is in the range of about 100 filaments per bundle.

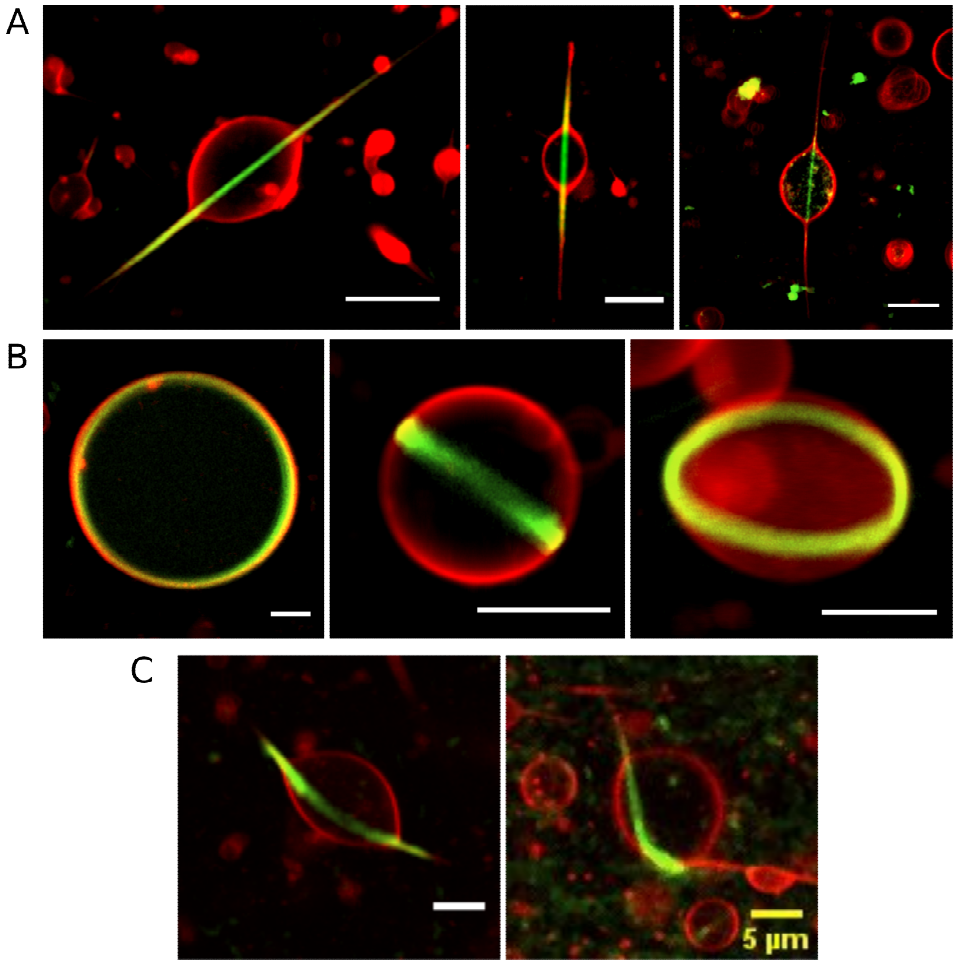

Figure 3.7: Main morphologies observed with encapsulation of microtubules in lipid vesicles. **(A)** Straight filament bundle forming • shaped liposomes. Scale bars = 10 µm. **(B)** Ring shaped bundle inside round/spheroid liposomes. Scale bars = 5 µm. **(C)** Intermediate morphology with partly bend filaments. Images are Z-projections created by ImageJ from Z-stacks. Scale bars = 5 µm.

To explore the influence membrane tension has on the morphology, we prepared a sample of liposomes with encapsulated tubulin in a feeding solution of increased osmolarity. In this case, the majority of liposomes displayed the • -shape morphology (Figure 3.8A). For this condition we measured the size of liposomes (z-projected area) per type of deformation observed (Figure3.8D). In total, about half of the liposomes contained no visible filaments and nearly half of the remaining liposomes displayed straight filament morphologies. Only a small fraction contained buckled or

ring-shaped bundles. It was further observed that liposomes without microtubules were on average of smaller size. Then, whilst imaging, MilliQ water was added to the chamber to lower the osmolarity of the outside solution. After the addition, we observed the buckling of microtubule bundles (Figure3.8C) and the morphology of ring shaped filaments inside spheroid liposomes became dominant (Figure3.8B). This effect could be reversed by exchange with a buffer solution of high osmolarity.

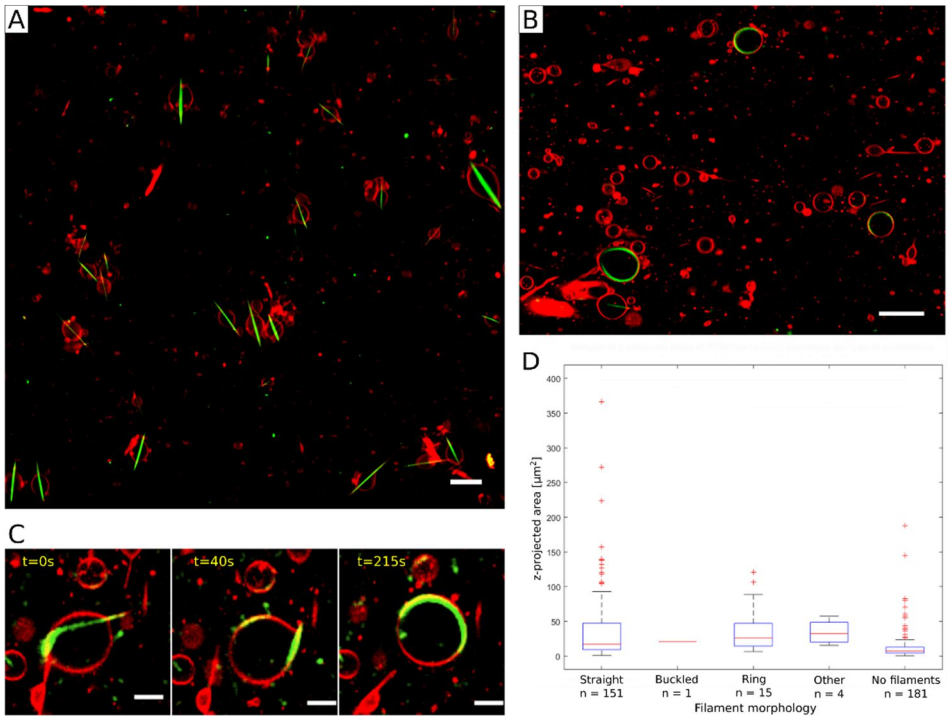

Figure 3.8: Morphology of microtubules encapsulated in liposomes under low membrane tension and during transition to higher membrane tension. **(A)** Overview of liposome sample with encapsulated microtubules under low membrane tension. Scale bar = 20 µm **(B)** Overview of liposomes after addition of MilliQ water. Scale bar = 20 µm **(C)** Transition to higher membrane tension. Imaging started shortly after addition of MilliQ water to the feeding solution. The iniatially buckled filament arranges itself into a ring-shape. Scale bars = 10 µm **(D)** Box plot of filament morphologies under low membrane tension.

There are different methods to influence liposome-microtubule morphology after encapsulation, like the change of membrane tension through a micropipet [25] or the disassembly of microtubules through hydrostatic pressure [26]. The advantage of the method we applied here, the addition of hyper- or hypotonic solution, lies in its simplicity as it requires no adaption of our normal setup. Despite this, it has so far only been demonstrated recently with encapsulated actin filaments [27]. However, our specific approach had two downsides. First, the encapsulation efficiency varies with our method for swelling of liposomes. Second, the exact osmotic concentration of the PURE system is not known to us. As a consequence, we are ignorant about the exact osmotic pressure and thus the membrane tension of the liposomes. We do know the concentration of all essential PURE *frex*

components, but we are not sure of certain buffer components such as glycerol and it might be that there are variations from batch to batch. The exact composition of PURExpress is currently not available, but its osmolarity ranges around 990 mOsm [28]. In comparison to that, the osmolarity of PURE*frex* is lower, but unknown to us. Further, the PURE system differs from other buffers used for microtubule assays, especially in the amount of its components.

In order to make our experiments with the encapsulation of eukaryotic microtubules more controllable and comparable, it would be beneficial to conduct them with a more basic buffer as swelling solution. We therefore tested if our protocol for encapsulation of tubulin works as well with MRB80, the standard buffer for microtubule assays. In the first trial, we simply replaced all PURE solutions with the MRB80 buffer, which resulted in a very poor yield of liposomes and no observation of filaments. Instead, we observed what appeared to be aggregates of the labelled tubulin inside the liposomes, indicating that the freeze thawing caused degradation of the tubulin. Our conclusion was that the PURE system represents likely a protective environment for freeze thawing due to molecular crowding and the presence of glycerol. From experience we know that freeze-thawing reduces the fraction of active tubulin in normal buffer and it is not surprising that MRB80 alone offers not enough freeze protection. Hence, we tried to avoid damaging the tubulin by the freeze-thaw cycles by adding 7.5% glycerol to the swelling solution. In this case, the liposome yield was still low but we observed several cases of encapsulated filaments. Interestingly, we also observed a rare liposome morphology in which the liposome is divided into two along the microtubule bundle (Figure 3.9A). This morphology has been described before as a rare variation named pearls shape [29].

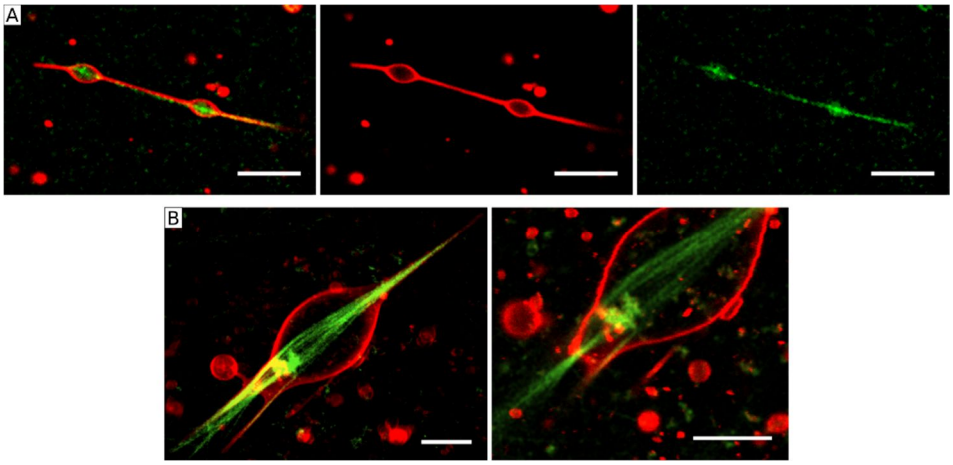

Figure 3.9. Rare morphologies observed with encapsulation of microtubules in lipid vesicles. **(A)** Pearl shaped liposome formed in a swelling solution of MRB80 + glycerol and with 30 µM tubulin. **(B)** Partly independent bundles forming multiple protrusions with one bundle sticking out of the membrane (left image). Swelling solution contained 50 µM tubulin and liposomes were incubated under low osmotic pressure.

There were other few exceptions in shape, like the liposome shown in Figure 3.9B which contains several microtubule bundles creating protrusions partly independent from each other. Most interestingly, one of the bundles has pierced the liposome membrane, without destroying the integrity of the liposome. It appears that the membrane is able to seal the liposome around the bundle. As mentioned, microtubules growing inside liposomes mostly form a single bundle of filaments. In this case the amount of effectively encapsulated tubulin was likely very high and overall there are indications that formation of independent bundles seems to be favoured by high concentration of tubulin, probably because the bundles grow so fast that they can form severe deformations of the membrane rather quickly. A similar correlation with concentration of bacterial tubulin is described in chapter 4.

3.2.4 Encapsulation of eukaryotic microtubules in liposomes combined with cell-free gene expression

After we successfully encapsulated eukaryotic microtubules in lipid vesicles with the same method we commonly apply for cell-free gene expression inside liposomes, we tested if both can be combined. A DNA construct of eYFP and 45 µM tubulin were added to a swelling solution and the generated liposomes were incubated for 3 hours at 37°C. The same was done for a control containing no tubulin. The data of both samples was analysed regarding the size of liposomes and the eYFP signal in the lumen. Figure 3.10A shows that that the addition of tubulin had a moderate effect on the maximal size of liposomes, but none on the average size. In regards of eYFP expression yield inside liposomes, addition of tubulin had no effect (Figure 3.10B). Further, we visualized microtubules and eYFP expression together, which showed that filaments were formed and that they colocalized in several cases with liposomes displaying eYFP expression (Figure 3.10C). Having achieved successful combination of cell-free gene expression and encapsulation of microtubules together in lipid vesicles, our next aim was to express Mal3 inside liposomes to demonstrate that we could influence microtubules by gene expression inside a vesicle. In order to visualise Mal3 expression, we tried to reconstitute plus-end tracking through Mal3, Tea2 and Tip1 in liposomes. This failed as only agglomerations of Tip1 where observed, which is an indication for degradation of the protein.

Overall, effective visualisation of the effect of expressed Mal3 turned out to be difficult with the methods at hand. The effect of Mal3 on microtubule dynamics is significant but not drastic and the encapsulation efficiency varied extremely within samples. Therefore, it would have been very difficult to reliably demonstrate for example a moderate shortening of microtubules through Mal3 expression. The tip-tracking assay would have been a more reliable method to assert Mal3 binding and function, but can currently not be combined with our methods of encapsulation. From working with the tip-tracking assay in flow cell, it was very clear that either Tea2, Tip1, or both proteins are rather unstable and degrade rather quickly. The two hours of swelling on ice together with the freeze thaw cycles were likely sufficient to reduce the amount of active tip-tracking proteins to insufficient levels. The fact that it would take at least an hour at 37°C to produce enough Mal3 to observe tip-tracking would have reduced the chance of observable tip-tracking to practically zero as this time span alone was mostly already sufficient to completely stop visible tip-tracking in respective experiments inside the flow cell.

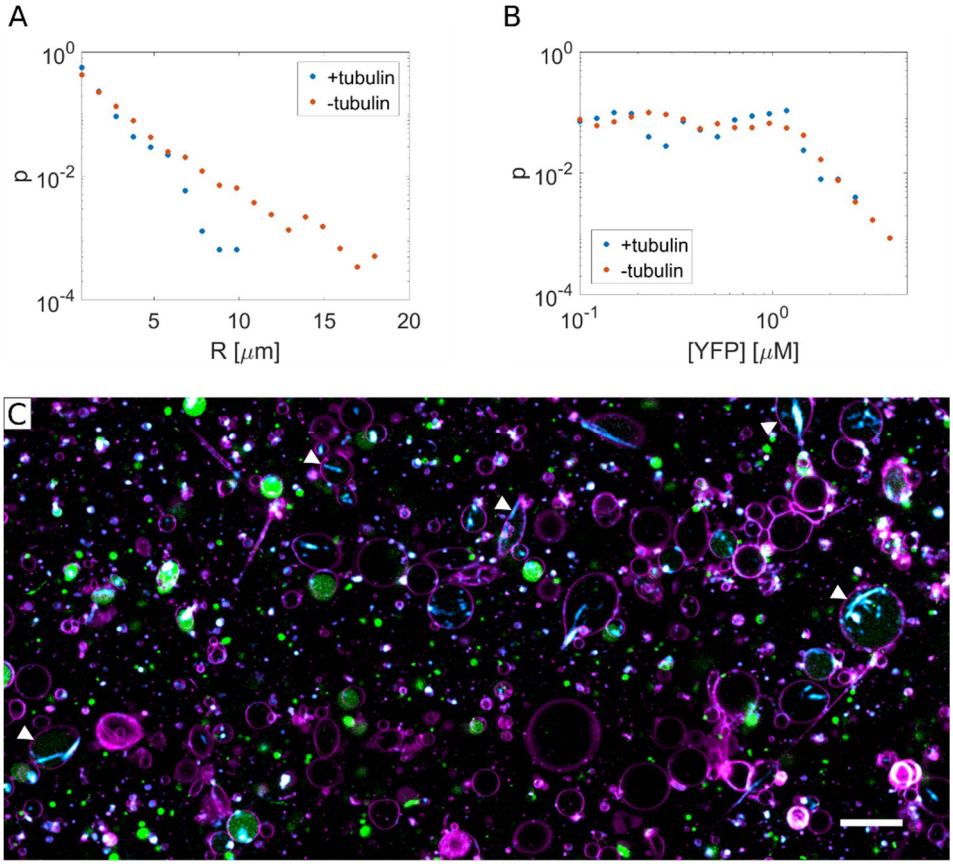

Figure 3.10: Expression of eYFP inside liposomes combined with encapsulation of tubulin. **(A)** Distribution of liposomes (p = probability) depending on their size (R). **(B)** Distribution of liposomes expressing eYFP. Number of analysed liposomes was 1531 for the condition with tubulin, and 5851 for the condition without tubulin. **(C)** Visualization of liposomes (magenta) encapsulating microtubules (cyan) and expressing eYFP (green). Liposomes with a colocalization of filaments and synthesized YFP are marked by white arrow heads.

3.3 Conclusion

Here we demonstrated that the PURE system is fundamentally compatible with polymerization of eukaryotic microtubules and that it is capable of expressing the MAP Mal3 in a manner that allows it to interact with microtubules and to recruit other MAPs. Moreover, we investigated the interaction of microtubules growing inside of liposomes. We found that the adjustment of osmotic pressure is an effective method to alter the morphology of microtubule-containing liposomes. The drastic effect it had on the liposome morphologies also demonstrates how important the feeding solution can be in liposome experiments. The fact that we do not know the exact osmotic concentration of the PURE systems limits our ability to manipulate liposome morphology. The limitation for measuring the osmotic concentration was in our case simply one of monetary costs, as the PURE system is expensive and the volume necessary for measurement would have been too large for the

devices we had available. There are, however, osmometers that can operate with volumes as small as 20 µl. Access to such a device would likely be very beneficial to increase the control over the system in liposome assays.

The alteration of microtubules through expression of Mal3 inside liposomes was not achieved. Not due to an inability to express active Mal3, but due to technical difficulties to analyse the presence of active Mal3. To verify the effect of a MAP on microtubules inside liposomes it would be recommended to instead utilize a protein that has a more severe effect on microtubule dynamics. The facilitation of microtubule growth will not create a very visible difference under the conditions we investigated as there were already very thick microtubule bundles present and even a doubling of microtubule number will likely not cause a large difference in average morphologies. Therefore, it would in this case be more telling to express a MAP that would severely destabilize microtubules when expressed. Several MAPs cannot be purified in *E. coli*, which indicates that the PURE system will not be able to express them as active protein, narrowing down the choice. Destabilizing MAPs that are compatible with expression in *E. coli* would for example be stathmin or katanin. If those proteins could be expressed in liposomes containing microtubules, the filaments should mostly disappear, which could be taken as a proof of activity. However, it is not clear if these proteins might not require chaperones or post-translational modifications present in *E. coli* but not in the PURE system. Alternatively, stabilizing MAPs could be applied if the system could be adjusted so that only a few filaments grow in each liposome as shown for a similar method [23]. In this case, the effect of stabilizing MAPs would be easier to detect. Bundling MAPs, on the other hand, would create no substantially different phenotype either way, because encapsulated microtubules are already attracted to each other due to the energetically favourable state of bundling in response to the elastic membrane tension.

3.4 Materials and Methods

Expression of eYFP in presence of tubulin

The same protocol as described in section 2.5 was applied with 15 µM of tubulin added, including a fraction of labelled tubulin (HiLyte 635).

Preparation of flow cells and microtubule seeds

Flow cells were assembled from two pieces of double-sided sticky tape positioned between a glass slide and a cover slip. Before the experiment, the glass surface of the flow cell is treated by sequential addition of 0.2 mg/ml PLL-PEG-biotin, 0.2 mg/ml streptavidin, 0.5 mg/ml • -casein and finally incubated for 10 minutes with microtubule seeds. The seeds were biotinylated and stabilized by cycling them twice in presence of the GTP analogue GMPCPP.

Microtubule assay and expression of Mal3

For the tip-tracking assay with synthesized Mal3, an PURE*frex* expression mix with the Mal3^{His} construct was assembled as shown in Table 3.1 and incubated for 3 hours. Additional to the standard PURE*frex* components, we have added the DnaK chaperone mix (GeneFrontier Corporation) and a peptidyl-tRNA-hydrolase (PTH). We added PTH2 to our assay because we discovered previously that it can increase the final yield in PURE*frex* [30]. PTH2 was used at a final concentration of 100 nM and of DnaK 1 µl of undiluted mix was added. In parallel to the incubation of the expression mix, the flow cell and microtubule seeds were prepared. Further, a pre-mix of several assay

components shown in Table 3.2 was created. The standard oxygen scavenger system we utilized was GODCAT and consisted of 200 mM DTT, 10 mg/ml catalase and 20 mg/ml glucose oxidase. It was taken care that Tea2 and Tip1 were thawed up just before use and added directly before the pre-mix was added to the assay mix. The assay mix (Table 3.2) consisted of the incubated expression mix, the respective amount of tubulin, labelled tubulin and the pre-mix. Concentration of components and composition of pre- and assay-mix varied between some of the experiments. In case of most experiments focused on the influence of expressed proteins on microtubule dynamics, no Tea2 or Tip1 were added. Right after assembly, the assay mix was added to the flow cell, the channel sealed with wax, and the sample imaged on a TIRF-microscope. The setup consisted of an Ilas^2 system (Roper Scientific) on a Nikon Ti-E inverted microscope with a Nikon CFI Plan Apochromat 100x NA1.45 TIRF oil objective and two Evolve 512 EMCCD camera's (Photometrics) for simultaneous dual-acquisition. The system was operated with MetaMorph 7.8.8.0 (Molecular Device) and the sample kept at 30°C with a custom objective heater.

Table 3.1: Expression mix for synthesis of Mal3^{His}

Expression mix	Volume (µl)
B	10
E	1
R	1
DnaK	1
PTH2 (2µM)	1
Mal3 DNA	0.5
MilliQ	5.5

Table 3.2: Assay mixes for tip-tracking assay with expressed Mal3

Pre-mix	*Stock conc.*	*Volume (µl)*	*Final concentration*
• -casein	5 mg/ml	1.8	225 µg/ml
Methyl cellulose	1 %	2.4	0.06 %
Glucose	40 mM	1	1 mM
GODCAT	-	0.8	-
Tea2	10 µM	0.8	200 nM
Tip1	10 µM	0.64	160 nM
Assay mix	Stock conc.	Volume (μl)	Final concentration
Expression mix	-	12.2	-
Tubulin	100 µM	3.4	17 µM
HiLyte488-tubulin	5 µM	0.7	0.175 µM
Pre-mix	-	3.7	-

Preparation of glass chambers for imaging of liposomes

Glass chambers were made by sandblasting a hole into a glass plate, of which one side was covered by attaching a cover slip (Menzel-Gläser) to it with UV-glue (NOA 61, Norland Products). The height of the glass chamber could be varied by using several glass slides of 1 mm thickness glued on top of another. Chambers were cleaned before experiments by sequential sonication for 10 minutes in chloroform/methanol (1:1 volume), 2% Hellmanex® III (Hellma), 1M KOH, ethanol and milliQ water.

Preparation of lipid beads

The lipid mixture utilized for liposome swelling from lipid beads consisted of DOPC, DOPE, DOPG, cardiolipin, DHPE-TexasRed and DSPE-PEG-biotin (Table 3.3). All lipids were solved in chloroform and supplied by Avanti Polar Lipids, except for the DHPE-TexasRed, which was purchased from Invitrogen. Lipids were mixed in a 25 ml round-bottom glass flask and a solution of 100 mM rhamnose in methanol was added (2.5:1 chloroform-to-methanol volume ratio). Next, 1.5 g of 425-600 µm glass beads (acid washed, Sigma Aldrich) were added and chloroform and methanol were removed from the lipid-bead mixture by rotary evaporation (200 mbar, 2 hours, RT). The lipid-coated beads were then aliquoted, desiccated overnight and stored under argon at –20°C.

Table 3.3: Mixture for lipid beads.

Lipid	Mol%	Concentration (g/l)	Volume (ul)
DOPC	50.8	10	253.8
DOPE	35.6	10	167.8
DOPG	11.5	10	57.9
Cardiolipin	2.1	10	20
Texas Red	-	1	25
PEG-biotin	-	10	5

Encapsulation of tubulin and PURE system in liposomes

For encapsulation of tubulin (30-50 µM) a swelling solution of 10 µl PURE*frex* buffer solution, 1 µl PURE*frex* enzyme solution, 1 µl PURE*frex* ribosome solution, 3-5 µl tubulin (200 µM), 1 µl labelled tubulin (5 µM, HiLyte 488), 0.4 µl GluOx (200mM DTT; 10 mg/ml catalase; 20 mg/ml glucose oxidase), 0.75 µl 1M glucose (Sigma-Aldrich) and 0.85-2.85 µl Milli-Q water was prepared. For encapsulation of tubulin coupled with YFP expression a swelling solution of 10 µl PURE*frex* buffer solution, 1 µl PURE*frex* enzyme solution, 1 µl PURE*frex* ribosome solution, 4.5 µl tubulin (200 µM), 1 µl labelled tubulin (HiLyte 635), 1 µl eYFP Spinach DNA, and 1.5 µl Milli-Q water was utilized. To the respective swelling solution, 20 µg of lipid beads were added and the solution incubated on ice for 2 hours to enable natural swelling without expression activity. During incubation, the tube was a few times gently manually rotated. To further enhance encapsulation efficiency, four freeze-thaw cycles were applied by dipping the tube into liquid nitrogen, followed up by thawing at RT. In the meantime, the glass chamber was sequentially incubated for 5 minutes with a solution of BSA and BSA-biotin (1:1 molar ratio, 1 mg/mL, Thermo Fisher Scientific) and with Neutravidin (1 mg/mL, Sigma Aldrich) to later immobilize the biotinylated liposomes. Swelling solution and dilution buffer (10xG solution, MilliQ and 83 mg/l Proteinase K) were added to the chamber and imaging was performed with a confocal microscope (A1+ from Nikon, ×100 oil immersion objective). During imaging the liposomes were incubated at 37°C.

3.5 Supplementary information

Sequence of *mal3*^{His} (5'→ 3', including T7 promotor and terminator)

TAATACGACTCACTATAGGGGAATTGTGAGCGGATAACAATTCCCCTCTAGAAATAATTTTGATT
TAACTTTAAGAAGGAGATATACCATGAAACATCACCATCACCATCACCCCATGAGCGATTACGA
CATCCCCACTACTGAGAATCTTTATTTTCAGGGCGCCATGGGATCTGAATCTCGGCAAGAGCTCT
TAGCTTGGATCAACCAAGTTACAAGCCTTGGTTTGACCAGGATTGAGGATTGTGGAAAAGGTTA
CGCTATGATACAGATTTTTGACTCCATATATCAAGACATACCACTAAAAAAGGTGAATTTTGAAT
GCAATAATGAGTATCAATATATAAACAATTGGAAAGTTCTTCAACAGGTATTCTTGAAGAAGGG
TATCGATAAAGTTGTAGACCCTGAGAGACTATCGCGTTGTAAAATGCAAGATAATCTGGAGTTC
GTTCAATGGGCCAAACGTTTTTGGGATCAATATTATCCTGGGGGCGATTATGATGCGCTGGCACG
CCGGGGGAATAGAGGACCTGCTAACACTCGTGTTATGAATTCCTCTGCAGGAGCAACTGGCCCT
TCTCGTCGCCGTCAGGTTTCTTCTGGTAGTTCTACACCTTCAATGACTAAGTCATCAGCAAACAA
CAATAACGTGTCTTCGACTGCAAATACTGCGGCAGTGTTAAGGGCAAAGCAAGCACAACAACAA
ATCACTAGTCTTGAAACACAGTTGTACGAAGTTAATGAGACGATGTTTGGTTTGGAGAGAGAAC
GTGATTTCTATTTTAACAAGCTTCGAGAAATTGAAATACTTGTACAAACTCATTTGACCACTTCTC
CTATGTCAATGGAAAATATGTTGGAGCGTATTCAAGCAATACTTTATTCTACTGAGGATGGTTTT
GAGTTACCACCTGATCAACCCGCAGATTTAACTACCGCCCTTACGGACCATGATACTAACAACGT
CGCTGAAGAGGCTCAAATGACTGACCTAAAAGACTCAGAAACTCAACGCGTTCCCTCTGCACCA
GATTTCGTACATGCTAGGCTACAAAGTTTAGAGGTTGATGACGATGAGAATATCACGTTTTAACT
CGAGCACCACCACCACCACCACTGAGATCCGGCTGCTAACAAAGCCCGAAAGGAAGCTGAGTTG
GCTGCTGCCACCGCTGAGCAATAACTAGCATAACCCCTTGGGGCCTCTAAACGGGTCTTGAGGG
GTTTTTTG

References

[1] Busch KE, Brunner D. The microtubule plus end-tracking proteins mal3p and tip1p cooperate for cell-end targeting of interphase microtubules. Curr Biol 2004;14:548–59.

[2] Bieling P, Laan L, Schek H, Munteanu EL, Sandblad L, Dogterom M, et al. Reconstitution of a microtubule plus-end tracking system in vitro. Nature 2007;450:1100–5.

[3] Zanic M, Stear JH, Hyman AA, Howard J. EB1 Recognizes the Nucleotide State of Tubulin in the Microtubule Lattice. PLoS One 2009;4:e7585.

[4] Maurer SP, Bieling P, Cope J, Hoenger A, Surrey T. GTP• S microtubules mimic the growing microtubule end structure recognized by end-binding proteins (EBs). Proc Natl Acad Sci 2011;108:3988 LP – 3993.

[5] Dixit R, Barnett B, Lazarus JE, Tokito M, Goldman YE, Holzbaur ELF. Microtubule plus-end tracking by CLIP-170 requires EB1. Proc Natl Acad Sci 2009;106:492 LP – 497.

[6] Akhmanova A, Steinmetz MO. Microtubule +TIPs at a glance. J Cell Sci 2010;123:3415 LP – 3419. https://doi.org/10.1242/jcs.062414.

[7] Tanabe T, Yamaga M, Kawamukai M, Matsuo Y. Mal3 is a multi-copy suppressor of the sensitivity to microtubule-depolymerizing drugs and chromosome mis-segregation in a fission yeast pka1 mutant. PLoS One 2019;14:e0214803–e0214803.

[8] Beinhauer JD, Hagan IM, Hegemann JH, Fleig U. Mal3, the fission yeast homologue of the human APC-interacting protein EB-1 is required for microtubule integrity and the maintenance of cell form. J Cell Biol 1997;139:717–28.

[9] Polakova S, Benko Z, Zhang L, Gregan J. Mal3, the Schizosaccharomyces pombe homolog of EB1, is required for karyogamy and for promoting oscillatory nuclear movement during meiosis. Cell Cycle 2014;13:72–7.

[10] Akhmanova A, Steinmetz MO. Tracking the ends: a dynamic protein network controls the fate of microtubule tips. Nat Rev Mol Cell Biol 2008;9:309–22.

[11] Buey RM, Mohan R, Leslie K, Walzthoeni T, Missimer JH, Menzel A, et al. Insights into EB1 structure and the role of its C-terminal domain for discriminating microtubule tips from the lattice. Mol Biol Cell 2011;22:2912–23.

[12] des Georges A, Katsuki M, Drummond DR, Osei M, Cross RA, Amos LA. Mal3, the Schizosaccharomyces pombe homolog of EB1, changes the microtubule lattice. Nat Struct Mol Biol 2008;15:1102–8.

[13] Maurer SP, Cade NI, Bohner G, Gustafsson N, Boutant E, Surrey T. EB1 accelerates two conformational transitions important for microtubule maturation and dynamics. Curr Biol 2014;24:372–84.

[14] Komarova Y, De Groot CO, Grigoriev I, Gouveia SM, Munteanu EL, Schober JM, et al. Mammalian end binding proteins control persistent microtubule growth. J Cell Biol 2009;184:691–706.

[15] Duellberg C, Cade NI, Holmes D, Surrey T. The size of the EB cap determines instantaneous microtubule stability. Elife 2016;5:e13470.

[16] Vitre B, Coquelle FM, Heichette C, Garnier C, Chretien D, Arnal I. EB1 regulates microtubule dynamics and tubulin sheet closure in vitro. Nat Cell Biol 2008;10:415–21.

[17] Zheng Q, Jockusch S, Zhou Z, Blanchard SC. The contribution of reactive oxygen species to the photobleaching of organic fluorophores. Photochem Photobiol 2014;90:448–54.

[18] Guo H, Xu C, Liu C, Qu E, Yuan M, Li Z, et al. Mechanism and dynamics of breakage of fluorescent microtubules. Biophys J 2006;90:2093–8.

[19] Aitken CE, Marshall RA, Puglisi JD. An oxygen scavenging system for improvement of dye stability in single-molecule fluorescence experiments. Biophys J 2008;94:1826–35.

[20] Craggs TD. Green fluorescent protein: structure, folding and chromophore maturation. Chem Soc Rev 2009;38:2865–75.

[21] Hamad I, Arda N, Pekmez M, Karaer S, Temizkan G. Intracellular scavenging activity of Trolox (6-hydroxy-2,5,7,8-tetramethylchromane-2-carboxylic acid) in the fission yeast, Schizosaccharomyces pombe. J Nat Sci Biol Med 2010;1:16–21.

[22] Shi X, Lim J, Ha T. Acidification of the oxygen scavenging system in single-molecule fluorescence studies: in situ sensing with a ratiometric dual-emission probe. Anal Chem 2010;82:6132–8.

[23] Kuchnir Fygenson D, Elbaum M, Shraiman B, Libchaber A. Microtubules and vesicles under controlled tension. Phys Rev E 1997;55:850–9.

[24] Alam Shibly SU, Ghatak C, Sayem Karal MA, Moniruzzaman M, Yamazaki M. Experimental Estimation of Membrane Tension Induced by Osmotic Pressure. Biophys J 2016;111:2190–201.

[25] Fygenson DK, Elbaum M, Shraiman B, Libchaber A. Microtubules and vesicles under controlled tension 1997;55:850–9.

[26] Hayashi M, Nishiyama M, Kazayama Y, Toyota T, Harada Y, Takiguchi K. Reversible Morphological Control of Tubulin-Encapsulating Giant Liposomes by Hydrostatic Pressure. Langmuir 2016;32:3794–802.

[27] Tanaka S, Takiguchi K, Hayashi M. Repetitive stretching of giant liposomes utilizing the nematic alignment of confined actin. Commun Phys 2018;1.

[28] Liu Y-J, Hansen GPR, Venancio-Marques A, Baigl D. Cell-free preparation of functional and triggerable giant proteoliposomes. Chembiochem 2013;14:2243–7. https://doi.org/10.1002/cbic.201300501.

[29] Emsellem V, Cardoso O, Tabeling P. Vesicle deformation by microtubules: A phase diagram. Phys Rev E 1998;58:4807–10.

[30] Doerr A, de Reus E, van Nies P, van der Haar M, Wei K, Kattan J, et al. Modelling cell-free RNA and protein synthesis with minimal systems. Phys Biol 2019;16:25001.

Chapter 4

Shaping liposomes by *de novo* synthesis of bacterial microtubules

Im Idealen kommt alles auf die élans,
im Realen auf die Beharrlichkeit an.

In the realm of ideas everything depends on enthusiasm.
In reality all rests on perseverance.

Johann Wolfgang von Goethe, Maximen und Reflexionen

Bacterial microtubules (bMTs) are filaments found in bacteria of the genus *Prosthecobacter* and consist of the tubulins BtubA and BtubB. We investigated bacterial microtubules *in vitro* and discovered that they can attach to lipid membranes independently from other proteins. Further, treadmilling of filaments along the membrane was observed. To move the *in vitro* model closer to the *in vivo* situation, we synthesized the bacterial tubulins with the PURE system. Formation of filaments through the expression of bacterial tubulin was observed on top of a supported lipid bilayers, with filaments displaying treadmilling behaviour. When the genes where encapsulated in liposomes together with the PURE system, filaments polymerized and were able to deform the liposomes. Membrane deformations were reminiscent of those occuring with encapsualted eukaryotic microtubules or actin filaments. The capability of such deformations and a potential polarization of the system could be implemented for the creation of a minimal cell. Moreover, encapsulation and expression in liposomes could prove as an important tool for understanding the role of bacterial microtubules in bacteria.

4.1 Introduction

In eukaryotic cells, microtubules formed from tubulin dimers are an omnipresent structure relevant for a multitude of essential processes. In contrary, bacteria lack any direct counterpart to • - and • -tubulin, indicating that these proteins have evolved after the split between eukaryotes and prokaryotes. Nevertheless, bacteria possess distant tubulin homologues, like FtsZ and TubZ. These proteins share the GTPase activity of eukaryotic tubulin, but the corresponding filaments are very different in their morphologies and functions compared to microtubules [1]. Thus, it was a remarkable discovery that microtubule-like structures are present in bacteria of the genus *Prosthecobacter* [2,3]. Even more so as they are assembled from heterodimers of the proteins BtubA and BtubB in the same manner as eukaryotic microtubules are formed by • - and • -tubulin, with which they share about 40% of their sequence [4,5]. The bacterial microtubules formed by BtubA/B are reported to consist of five protofilaments *in vivo* [5] and of four protofilaments *in vitro* [6]. This makes them strikingly thinner than eukaryotic microtubules, which consist of 13 protofilaments (Figure 4.1A). On the other hand, recent *in vitro* studies demonstrated that bMTs display all the basic characteristics of eukaryotic microtubules, such as dynamic instability and polarity [6,7]. The fact that bacterial tubulin is so similar to its eukaryotic analogue in its structure, assembly dynamics, and sequence while simultaneously not requiring chaperones or cofactors [5] suggests that bacterial tubulin represents an ancient evolutionary stage of eukaryotic tubulin. Therefore, it is assumed that bacterial tubulin has been acquired by horizontal gene transfer from a eukaryotic ancestor [5,8]. The only currently known protein that interacts with bMTs is BtubC (also known as Bklc), which stabilizes bMTs [6] and is proposed to link them to lipid membranes [9]. However, it is still unclear what function bMTs have.

The genus *Prosthecobacter* itself belongs to the Phylum *Verrucomicrobia* and consists of Gram-negative bacteria which exhibit a high degree of compartmentalization [10]. *Prosthecobacter dejongeii* for example possess a major membrane-bounded region, containing the fibrillar nucleoid and all the ribosome-like particles, as well as an intracytoplasmic membrane (Figure 4.1B). Another distinguishing feature of *Prosthecobacter* is the presence of narrowed extensions of the cell wall, called prosthecae. Bacterial microtubules seem to be predominately located in these cell stalks (Figure 4.1C), which suggests that they might be involved in the formation of prosthecae, but no direct evidence has come forth so far.

Besides being independent from chaperones or post-translational modifications, BtubA/B distinguishes itself from eukaryotic tubulin by being functionally expressed in *E. coli* [5]. As a consequence, bacterial tubulin can likely be utilized for a broader array of *in vitro* experiments than its eukaryotic cousin while potentially acting as a simplified model for the later. For instance, eukaryotic tubulin is currently excluded from cell-free gene expression due to its complex posttranslational modifications. Cell-free protein synthesis can be applied to avoid problems associated with protein purification and it enables the dynamic synthesis of target proteins. Moreover, cell-free gene expression is currently one of the most promising tools for the creation of a minimal cell [11,12]. In context of a minimal cell, such bacterial microtubules could potentially be exploited for spatial organisation, polarisation and shape transformation of the system.

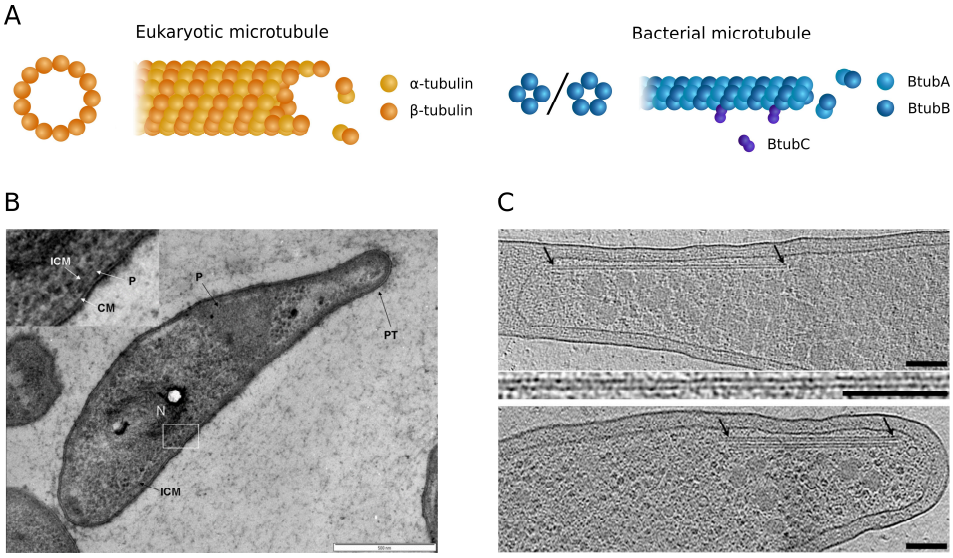

Figure 4.1: **(A)** Schematic comparison of eukaryotic and bacterial microtubule structure. **(B)** TEM image of high-pressure frozen *Prosthecobacter dejongeii* cell, showing prostheca (PT), an intracytoplasmic membrane (ICM) surrounding a region containing a condensed fibrillar nucleoid (N), and a paryphoplasm region (P). Inset: enlarged view of region of cell outlined in the white box showing cytoplasmic membrane (CM), paryphoplasm (P) and ICM. Scale bar: 500 nm. Taken from Lee et al 2009 [10]. **(C)** Electron tomography image of bacterial microtubules in *Prosthecobacter vanneervenii* cells. Scale bars: 100 nm. Taken from Pilhofer et al. 2011 [5].

In this study we investigated the *de novo* synthesis of bacterial tubulin and BtubC with the PURE system [13] in bulk and inside liposomes. Our results demonstrate that bacterial microtubules are suited as a model system for gene-directed filament assembly and liposome deformation. The latter configuration might serve as model system that resembles the *in vivo* situation in baceria more closely than convential *in vitro* assays.

4.2 Results

4.2.1 Bacterial microtubules interact with lipid membranes

First, we investigated the interaction of bacterial microtubules with lipid membranes by addition of 2.5 µM purified bacterial tubulin to a supported lipid bilayer (SLB) consisting of DOPC, DOPE, DOPG, Cardiolipin, and DHPE-TexasRed in a volume ratio of 50:36:12:2:0.2. Here, we observed that the bMTs bind to the membrane on which they were nearly exclusively located compared to the glass surface (Figure 4.2A). Once a bMT attached to the membrane, it mostly remained on it in a stable manner. Interestingly, all this could be observed without any addition of BtubC, which has been reported to mediate the membrane binding of bacterial microtubules [9]. Furthermore, filaments tended to form bundles of multiple filaments over time on the membrane (Figure 4.3C), suggesting lateral binding of microtubules to each other.

Strikingly, single filaments underwent directional movement over the membrane in the direction along their longitudinal axis (Movie 4.1). This behaviour is presumably caused by simultaneous growth and shrinkage on the two ends of the filament, a phenomenon known as treadmilling. To validate this hypothesis, we used dual colour labelling and bleached one of the fluorophores during imaging. Thus, the base of the filament would become dark and only the labelled tubulin that freshly polymerized to the growing ends of the microtubule would be be tracked (Figure 4.2D and E). In most cases, only one tip was tracked and it was almost exclusively on the side towards which the filaments appeared to move (Movie 4.3). Further, single fluorescent spots on the bleached filaments remained immobile. It can therefore be concluded that the observed movement indeed represents polarised growth at one end and shrinkage at the other end of the filaments.

Another observation was that the bMTs could be disassembled through intense illumination. Filaments break apart when excessively exposed to laser light until they completely disintegrate or their fragments detach from the membrane (Figure 4.2B). This effect was dependent on the presence of the corresponding fluorophore used for labelling (Atto488 or Atto565), suggesting a dye-specific photochemical reaction. If illumination was performed with a wavelength outside of the excitation range of the fluorophore, no disassembly was observed under prolonged illumination. Dual labelling confirmed that bMTs truly disintegrated and that their disappearance was not a result of photobleaching (Movie 4.2).

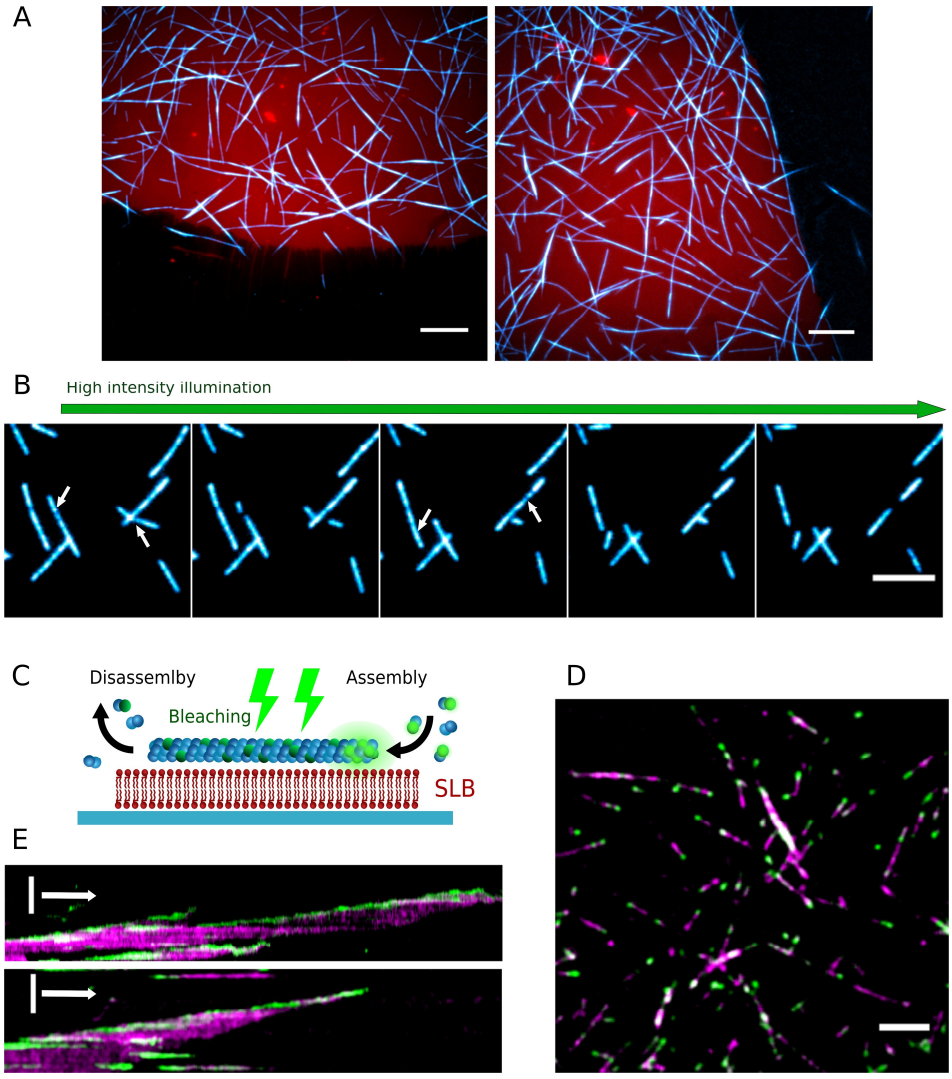

Figure 4.2: Dynamics of bacterial microtubules formed by purified proteins on supported lipid bilayers. **(A)** Selective binding of bMTs (blue) onto a SLB (red). Concentration of bacterial tubulin was 2 µM. Scale bar: 10 µm **(B)** Disassembly of bMTs over time through high intensity illumination. Arrows indicate the locations at which the filaments breaks apart. Duration was 120 seconds between first and last image. Scale bar: 5 µm. **(C)** Scheme of a growing bMT attached to an SLB being bleached. Labelled bacterial tubulin is bleached continuously and thus the only active fluorophores are located at the plus end of the filament, stemming from freshly assembled tubulin. **(D)** Bleached filaments (magenta) display comets originating from continuous addition of fresh, unbleached labelled bacterial tubulin (green). Scale bar: 5 µm. **(E)** Kymographs showing bMT dynamics during bleaching. Vertical scale bar: 5 µm. Horizontal arrow: 1 minute.

4.2.2 Cell-free expressed BtubA/B self-organizes into dynamic microtubules on an SLB

Next, we aimed at expressing bacterial tubulin with the PURE system. First, we verified that the bacterial tubulins could be synthesized at full length. Templates for expression consisted of the *btubA, btubB and btubC* genes from *Prosthecobacter dejongeii*. All three genes were synthesized *de novo* (GenScript) from DNA sequences optimized for expression in an *E. coli* host from which the PURE system translation machinery is derived. Optimization included decreasing the content of GC bases in the first 30 bp of the respective construct without alteration of the amino acid sequence. This was followed by selection of the sequence with the highest value for change in free Gibbs energy (• G) regarding the intramolecular bonds of the RNA around the start codon (Figure 4.7). Lower • G values represent higher melting temperatures of the RNA molecule and high RNA melting temperature is known to be potentially inhibitory of translation in the PURE system [14]. Thus, we selected the sequence with the predicted lowest melting temperature, assuming that this would decrease the occurrence of inhibitory RNA structures involving the ribosome binding site and the start codon.

BtubA and BtubB were expressed from linear DNA constructs with PURE*frex*2.0 and the products were loaded on a SDS-PAGE. Clear bands of the full length proteins were visible, with only a minimal amount of side bands (Figure 4.3A). The intensity of the bands suggests that co-expression of the two genes might yield a lower amount of BtubA compared to BtubB. To quantify expression, we estimated the amount of synthesized protein by comparing it with known concentrations of purified BtubA/B. The comparison gave a yield of about 13 µM for BtubA and 17 µM for BtuB when expressed separately. Co-expression of the two genes yields less total protein and a lower amount of BtubA (3 µM) compared to BtubB (5 µM). It is unclear why co-expression would result in a lower total amount of protein expressed than expression of a single protein, but similar outcomes have been observed with other genes.

The critical protein concentration for the assembly of bMTs is 2.5-5 µM for the given potassium concentration present in the PURE system as reported recently [7]. We have, however, observed filaments already at concentrations of about 1 µM of purified protein in the PURE system (Figure 4.8). Accordingly, the amount of synthesized protein would be sufficient for filament formation if the expressed protein is active.

Consequently, we checked if the synthesized tubulins are capable of forming filaments by expressing BtubA and BtubB separately with PURE*frex*2.0 (3 hours, 37°C) and adding the expression products together with a small fraction of labelled bacterial tubulin (100 nM) to a chamber coated with an SLB. The sample was incubated during imaging at 25°C. As expected, assembly of filaments and recruitment to the SLB was immediately observed after addition of the expressed bacterial tubulin (Figure 4.3C).

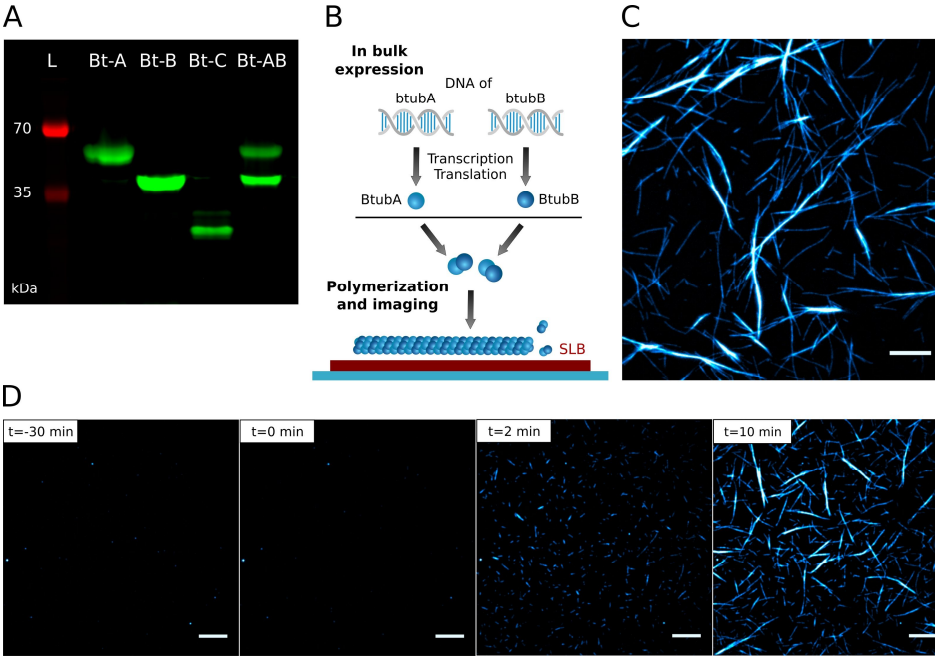

Figure 4.3 Successful cell-free expression of bacterial tubulins with the PURE system. (A) Protein gel of expressed BtubA, BtubB, and BtubC, as well as coexpression of BtubA/B. The proteins were expressed with PURExpress2.0 in the presence of FluoroTect™ GreenLys. (B) Scheme of how the activity of expressed bacterial tubulin was assessed on an SLB. (C) Bacterial microtubules on top of an SLB, polymerized from tubulin expressed by PURExpress2.0. Scale bar: 10 µM. (D) Temporally separated addition of expressed BtubA and BtubB. Expressed BtubA and 100 nM of labelled bacterial tubulin (mix of BtubA/B) were incubated for 30 minutes without filaments observed. At t=0, expressed BtubB was added which was followed by the immediate formation of filaments, proving that the observed filaments originate from the expressed protein. Scale bar: 10 µM.

To validate that filament assembly was not caused by the fraction of labelled tubulin, we imaged a solution of expressed BtubA and 100 nM of labelled bacterial tubulin for 30 minutes. No filaments were observed in this condition. However, filaments immediately started to appear immediately once we added as well expressed BtubB (Figure 4.3D, Movie 4.4). As with the purified protein, dynamic instability, treadmilling on the membrane, as well as bundling of the microtubules were observed.

4.2.3 Synthesized BtubC binds bacterial microtubules to vesicle membranes

To investigate the functionality of expressed BtubC, we assessed the binding of bMTs to lipid vesicles with and without its presence by conducting a liposome flotation assay. In this assay, liposomes, prepared in a solution of lower density than the PURE system, were added to a PURE*frex*2.0 solution containing purified BtubA/B. A fraction of the purified tubulin was labelled with Atto488 to allow for fluorescence gel imaging. The solution was incubated at 30°C for 20 minutes in order to enable for polymerization of microtubules and binding to the vesicles. Then, it was spun down, resulting in a pellet of the liposomes on top of the solution which was separated as

the liposome fraction (LF) from the bottom fraction (BF). When the mix contained expressed BtubC (unlabelled) a clear enrichment of BtubA and BtubB was observed in the liposome fraction compared to the bottom fraction (Figure 4.4A). No such enrichment was visible in absence of BtubC expression, indicating that BtubC expressed by the PURE system is capable of binding either bacterial microtubules, or at least bacterial tubulin dimers to lipid membranes. Further, this result seemingly contradicts the previously observed BtubC independent binding of bMTs to SLB membranes. The most likely explanation is that under given conditions BtubC is facilitating a stronger binding to the membrane than already occuring without it and that in its absence membrane binding was too weak to counter the spin-down force exerted on the bMTs. To check membrane binding of expressed BtubC itself and to assert if expressed BtubA/B is as well recruited by it, we performed a flotation assay with proteins expressed by PURE*frex*2.0 under incorporation of fluorescently labelled lysine. As in case of purified tubulin, expressed BtubA/B on its own did not accumalte in the liposome phase to any discernable degree (Figure4.4B). On the contrary, BtubC accumulated in the liposome phase to the point that it was almost depleted from the bulk solution if expressed alone or together with BtubA/B. When coexpressed with BtubC, BtubA/B appeared to again accumulate in the lipid fraction, although the effect was not as clear as in case of purified BtubA/B. Overall, this results imply that expressed BtubC is fully capable of crosslinking bacterial microtubules and lipid membranes as has been reported for purified BtubC [9]. Thus, the most prominent characteristic of BtubC is active in the synthesized protein.

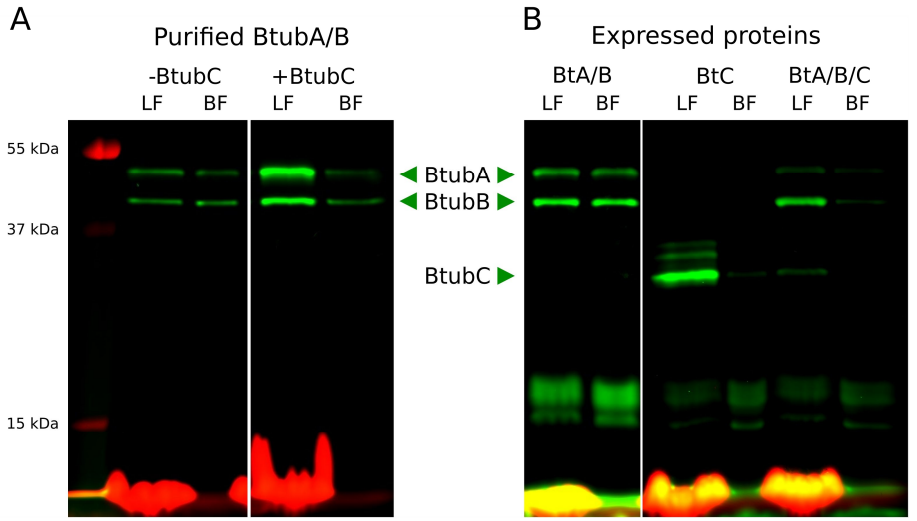

Figure 4.4: Flotation assays of bacterial tubulins. **(A)** Lipid fractions (LF) and bottom fractions (BF) of purified BtubA/B labelled with Atto488 with and without addition of expressed BtubC. **(B)** Greenlys signal of expressed bacterial tubulins and their distribution among LFs and BFs. The red signal at the bottom of the lanes results from the DHPE-TexasRed lipids of the vesicles and is therefore stronger in the LFs.

4.2.4 Liposome morphology can be altered by internally synthesized bacterial tubulin

After it was verified that the expressed bacterial tubulin is functional, we investigated the implementation of bMT synthesis inside of liposomes. The PURE system, the two bacterial tubulin DNA constructs, a DnaK mix and a fraction of labelled tubulin were encapsulated in liposomes by natural swelling. The liposomes were added to a glass chamber, diluted with PURE buffer, and imaged by confocal microscopy at 37°C. At the beginning of imaging, liposomes which had successfully encapsulated the swelling solution displayed an evenly distributed fluorescence signal of the labelled bacterial tubulin (Figure 4.9, t = 60 min). After one hour of incubation, filament-like structures appeared in several liposomes, with number and length of filaments increasing over time (Figure 4.5B, Figure 4.9). It should be mentioned that the fraction of liposomes containing filaments, the time of incubation until their first observation, as well as the amount of filaments in the liposomes differed between experiments. Further, in all experiments, a high liposome-to-liposome heterogeneity was observed regarding the presence and amount of filaments. Among the liposomes containing filaments a large variety of morphologies of liposomes and filaments was observed (Figure 4.5C). Filaments formed various arrangements of straight or bend bundles and meshes, which were located in some cases in the lumen and in others near or at the membrane of the liposome. It is in this regard noteworthy that most liposomes containing filaments exhibited morphological changes compared to their originally spherical shape, like protrusions or global elongation. These deformations can assumed to be a result of the pushing force exerted by the growing filaments on the liposome membrane, as reported for eukaryotic microtubules and actin filaments [15,16].

Such morphologies were neither observed in the liposomes containing no filaments (Figure 4.5B), nor at the start of the experiment (Figure 4.10), nor in the control sample without expression of BtubA/B (Figure 4.10). Similar results were obtained by the encapsulation of 6.6 µM of purified BtubA/B (Figure 4.6). The only recognizable difference between encapsulation of expressed and purified tubulin was that with purified tubulin the amount of filaments seemed higher on average and in rare cases cross-shaped liposomes were observed.

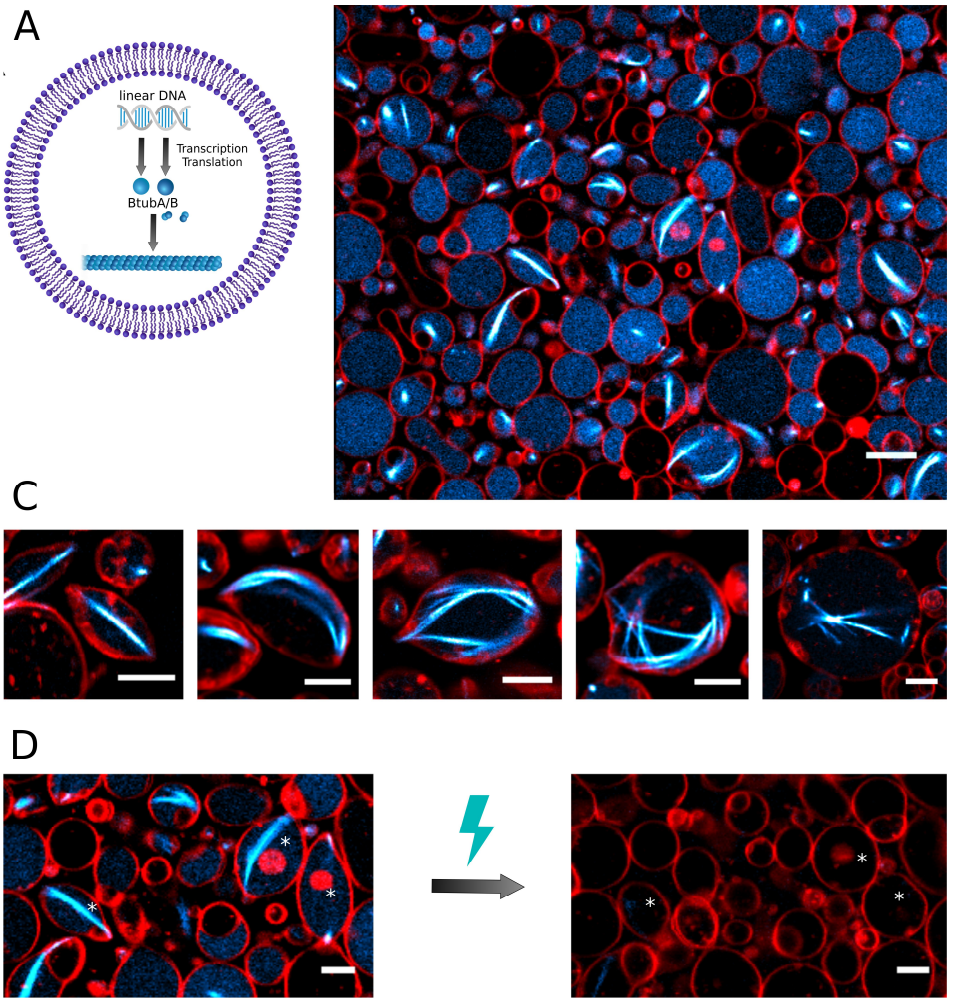

Figure 4.5: Expression of bacterial tubulin inside liposomes. (**A**) Scheme of cell-free expression of BtubA and BtubB inside liposomes with subsequent formation of bacterial microtubules. (**B**) Liposomes (red) expressing BtubA/B, after 4 hours of incubation at 37°C. Bacterial microtububle filaments (cyan) are visible in several liposomes, some of which are deformed by the filaments. Filaments are visualized by 100 nM of purified and labelled bacterial tubulin. Scale bar: 10 µM. (**C**) Examples of different phenotypes of deformed liposomes expressing BtubA/B. Samples were observed after 5 hours of incubation at 37°C. Scale bar: 5 µM. **(D)** Intense illumination of liposomes expressing bacterial tubulin. Scale bar: 5 µM.

To further demonstrate that the microtubules are the cause of the altered shape of the liposome membranes, we disassembled the bacterial microtubules formed by synthesized BtubA/B through high intensity illumination as demonstrated on SLBs in section 4.2.1. After the collapse of filaments, liposomes relaxed to a spherical shape (Figure 4.5D), thus confirming that the filaments are responsible for the deformations of the liposomes and that the deformations are for the most part reversible. An almost identical approach was recently applied to show the reversible nature of

deformations caused by actin filaments [17]. The cases in which the spherical shape of a liposome was not restored were mostly cases in which the liposome membrane was attached to the surface over an extended area, thus preventing it from returning to the original shape. Overall, this demonstrates that bacterial microtubules are capable of deforming liposome membranes.

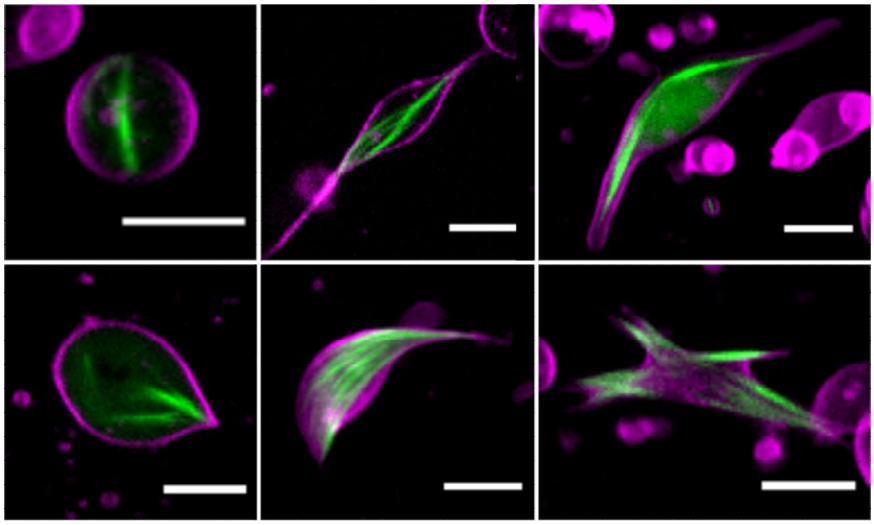

Figure 4.6.: Bacterial microtubules (green) formed by 6.6 µM purified tubulin inside liposomes (red). Scale bars: 5 µm.

4.3 Discussion and conclusions

These results demonstrate that BtubA/B can be synthesized with PURE*frex*2.0 above the concentration threshold for filament assembly and forms dynamic bMTs in bulk and inside liposomes. We further observed that bMTs, formed by synthesized or purified BtubA/B, can attach without co-factors to an SLB membrane. The lipid composition of the membrane contained PE and PG lipids, which can also be found in the membrane of *Prosthecobacter* [18]. Although derived from *E. coli*, the PURE system mimics the buffer conditions of the bacterial cytoplasm more closely than standard *in vitro* experiments do. Polymerisation of bMTs was observed at lower concentrations than reported previously, indicating that the PURE system represents a favourable environment for bMTs polymerisation. Dual colour labelling confirmed that the directional movement of filaments is caused by treadmilling. It has been demonstrated that treadmilling of FtsZ over the inner cell membrane is crucial for cell division [19,20]. Likewise, it is possible that treadmilling of bMTs occurs as well *in vivo* and contributes to their function. However, bMTs visualised by EM imaging in *Prosthecobacter* appear to be too long for effective treadmilling [5].

We also confirmed that expressed BtubC is facilitating binding to vesicle membranes as previously reported for purified BtubC. At least under the given condition, binding of filaments without BtubC to vesicle membranes did either not occur or was much weaker than in presence of BtubC. However, it can not be completely ruled out that the observed effect of increased filament binding to liposomes is a consequence of BtubC facilitating the formation and stability of filaments, which could also lead to a larger fraction of tubulin being bound to the liposomes. If cofactor independent

binding takes place *in vivo* to the degree it does in the PURE system on SLBs, BtubC might act as a regulator of how strong the binding to the membrane is. Overall, these observations might help us to understand the role of bMTs *in vivo*, as well as broaden our understanding of the origins of eukaryotic tubulin.

Synthesized BtubA/B formed dynamic bMTs, which displayed the same properties as observed with purified tubulin. Expression in liposomes lead to the formation of filaments and filament bundles in a substantial fraction of the liposomes. It is noteworthy that this was not observed without the addition of a DnaK chaperone mix, which was not necessary for functional expression of BtubA/B in bulk. It is possible that the confinement inside the liposome or interactions with the membrane are causing aggregation of expressed proteins, which DnaK chaperones might be able to prevent [21]. The high liposome-to-liposome heterogeneity regarding expression efficiency is common for this method and likely the consequence of varying encapsulation efficiency and stochastic effects [22].

The results obtained with bacterial tubulin encapsulated in liposomes are in line with what has been described and observed in Chapter 1 and 3 for eukaryotic microtubules. Different morphologies of the microtubules, formed by purified or synthesized tubulin, and of the liposomes containing them are a result of the pushing forces of the growing microtubules and the agonistic force of the membrane tension. Long and straight filament bundles and membrane deformations are favoured by high amounts of tubulin and low membrane tension, whereas spherical liposomes containing bend or short filaments are observed with higher membrane tension and lower tubulin concentration. This is true for filaments formed by either purified or expressed bacterial tubulin. Very little data is currently available on the physical parameters characterizing bacterial microtubules, but they are very likely less stiff than eukaryotic ones due to their smaller diameter. This seems to be confirmed by the here reported morphologies, as filaments are on average more bend and spread-out than what has been observed with encapsulated eukaryotic microtubules. Morphologies are overall similar to what has been reported with encapsulated actin filaments, bundled together by linker proteins [23]. Therefore, we assume that the rigidity of bacterial microtubules is in the range between eukaryotic microtubules and actin filaments. The comparatively low threshold for polymerization, seemingly rather high rigidity, ability to form bundles without additional cofactors, and suitability for cell-free expression make bMTs a promising candidate for general membrane deformation. The main drawback regarding implementations of the system in a synthetic cell setting is that there are besides BtubC currently no other proteins known to interact with bMTs, which limits the degree to which their functions could be regulated and the range of functions they could be utilized for. However, as *Prosthecobacter* is becoming the focus of investigations only rather recently, it is likely that additional proteins will be revealed to interact with bMTs and thus their potential for applications in synthetic biology might be further extended. In the context of creating a minimal cell, elongation of the liposome, as observed here in a substantial fraction of liposomes expressing bacterial tubulin, might be supportive of other systems involved in polarization and cell division. Reconstitution of the Min system in spherical vesicles for example yielded so far only a small fraction of vesicles showing the pole-to-pole oscillation patterns observed *in vivo* [24,25]. Such oscillation patterns might be influenced by cell-shape and their occurrence could potentially be facilitated by elongation of the vesicle. Further, if more interaction partners with bMTs are discovered, especially end-tracking proteins, they might be used to mediate processes such as chromosome segregation or polarisation of the system.

4.4 Material and Methods

Preparation of DNA constructs

To ensure a high rate of expression, we adjusted the DNA sequence of the three *btub* genes of *Prosthecobacter dejongeii* (*btubA*, *btubB*, *btubC*) with respect to their GC content and intramolecular basepair (bp) binding for the first 30 bp after the start codon. We did so by utilizing a script (Python) that listed all possible DNA sequences of the first 30 bp encoding the same amino acid sequence of the respective gene and then analysed the sequences with the lowest GC content in regards of their melting temperature. This was done by calculating the conformations of the RNA with the highest value for change in free Gibbs energy (• G) regarding the intramolecular bonds of the 30 bp before and 30 bp after the start codon (60 bp total) by mfold [26]. If sequences had similar • G values, the sequence with the least amount of bonds at the ribosome binding site (RBS) and start codon was chosen. An example for of the calculated RNA structure is shown in Figure 4.7. The optimized sequences, including a T7 promotor, RBS and T7 terminator sequence, were sent for gene synthesis to GenScript (United States) and were received in the pUC57 plasmid. Linear constructs were obtained by PCR reactions which were conducted with the reaction mixture displayed in Table 4.1 and utilizing the primers ChD365 and ChD173. The Phusion polymerase (Finnzymes) was added at last to the mix. The temperature settings are reported in Table4.2. Afterwards, the PCR-generated linear constructs were purified by a PCR clean-up kit (Wizard® SV Gel and PCR Clean-Up System), provided by Promega according to the manufacturers protocol. Concentration and purity of the DNA constructs were determined by spectrophotometer measurement (NanoDrop 2000, Thermo Scientific) and they were checked for full length and side products by gel electrophoresis on 1% agarose gels.

Table 4.1: Components of PCR mixture.

Component	Amount (µL)	Concentration
5x HR buffer	10	-
MilliQ water	35.5	-
FW primer	1.0	10 µM
RV primer	1.0	10 µM
PCR Nucleotide mix	1.0	10 mM
DNA Template	1.0	1-10 ng/µL
Phusion polymerase	0.5	2 U/µL
Total volume	50	

Table 4.2: Applied PCR temperature cycle.

Step	Temperature (°C)	Time	Number of cycles
Initial denaturing	98	30 s	1
Denaturing	98	10 s	
Annealing	Min (Tm)	20 s	30
Elongation	72	1min/kb	
Final elongation	72	8 min	1

Protein synthesis of BtubA/B

Cell-free expression for analysis by SDS-PAGE and SLB experiments was performed with PURE*frex*2.0 (GeneFrontier Corporation) according to the supplier's protocol and 5 nM of respective linear DNA. In case of gel analysis, 1 µl of GreenLys solution (FluoroTect™, Promega) was added and gene expression conducted in PCR tubes incubated at 37°C for 3 hours with subsequent denaturing of the proteins by SDS and incubation at 90°C for 10 minutes. Samples were loaded on a 12% SDS-protein gel, run first for 20 minutes at 100 V, and subsequently for 40 minutes at 160 V. Fluorescently labelled proteins were visualized on a fluorescence gel imager (Typhoon, Amersham Biosciences) using a 488• nm laser (Cy2 channel) and a band-pass emission filter of 515 to 535• nm. Subsequently, the gel was stained with InstantBlue™ (expedeon) over night and the protein staining imaged with a ChemiDocTM imaging system (Bio-Rad).

Concentration of purified bacterial tubulin was determined from absorbance at 280 nm (extinction coefficient 103754.2 $M^{-1}cm^{-1}$). Reactions with expressed bacterial tubulin (2.5 nM of DNA construct each encoding for btubA and btubB, expression for 3 hours at 37°C) were loaded onto a 10% stain-free gel, either undiluted or 5-fold diluted. Purified bacterial tubulin was loaded in concentrations ranging from 0.125 µM to 8 µM and a calibration curve was generated from these samples using Fiji [27] to quantify band intensities.

Imaging chambers

SLB and liposome experiments were carried out in self-made glass chambers. Three glass slides of 1 mm thickness were glued together with NOA 61 UV-glue (Norland Products). Several holes of 3 mm diameter were bored with a diamond drill and a 150-µm-thick coverslip (Menzel-Gläser) glued to the bottom with NOA 61. The chambers were cleaned before experiments by sequential washings consisting of 10 minutes of sonication in chloroform/methanol (1:1 volume), 2% Hellmanex® III (Hellma), 1 M KOH, ethanol and milliQ water. In case of SLB experiments, the glass chambers were additionally treated every second experiment with acid piranha solution. For some liposome experiments, aluminium chambers were used, which were fabricated in the same manner as described for the glass chambers and cleaned the same way, except for the KOH and piranha wash which was omitted.

Preparation of lipid-coated beads, SUVs, and vesicles for flotation assay

The lipid mixture utilized for liposome swelling from lipid beads consisted of 50 mol% DOPC, 36 mol% DOPE, 12 mol% DOPG, 2 mol% 18:1 cardiolipin, 0.2 mol% DHPE-TexasRed and 1 mass% DSPE-PEG-biotin. All lipids were dissolved in chloroform and supplied by Avanti Polar Lipids, except for the DHPE-TexasRed, which was from Invitrogen. Lipids were mixed in a 10 ml round-bottom glass flask and a solution of 100 mM rhamnose in methanol was added (2.5:1 chloroform-to-methanol volume ratio). Next, 0.6 g of 212-300 µm glass beads (acid washed, Sigma Aldrich) were added. Subsequently, the chloroform and methanol was removed from the lipid-bead mixture by rotary evaporation (200 mbar, 2 hours, RT). The lipid-coated beads were then aliquoted, desiccated overnight and stored under argon at –20°C.

Small unilamellar vesicles (SUVs) for SLB and vesicles for sedimentation experiments consisted of DOPC, DOPE, DOPG, cardiolipin and DHPE-TexasRed in a volume ratio of 50:36:12:2:0.2. Thus being the same lipid composition as described for the preparation of lipid beads, except

without addition of DSPE-PEG-biotin. For SUVs, these lipids were mixed and dried to a lipid film of 500 µg which was subsequently rehydrated with 400 µl of water. This yielded a lipid emulsion of 1.25 mg/ml, which was vortexed for 2 minutes to create SUVs. To separate SUVs from larger lipid structures, a two-step extrusion was carried out using a mini extruder and 250 µl Hamilton syringes (both from Avanti Polar Lipids). The sample was run through two filters (drain disc 10 mm diameter, Whatman) and a polycarbonate membrane. The membrane had a pore size of 0.2 µm for the first and 0.03 µm for the second passage. Vesicles for sedimentation experiments were formed from a dried lipid film of 895 µg of the aforementioned lipid composition, which was dissolved and vortexed in 90 µl of 0.9 M sucrose. Both vesicle solutions were kept at - 20°C until use.

Vesicles for the flotation assay were prepared from a dried lipid film identical to the one used for the generation of SUVs. To 1000 µg of lipid film 100 µl of a 1:3 dilution of PURE*frex*2.0 with milliQ water was added and the solution was vortexed for 5 minutes to receive a 10 µg/µl solution of lipid vesicles. The solution was stored at - 20°C.

Filament assembly on SLB

First, the surface of washed glass chambers was activated by oxygen plasma treatment (basic plasma cleaner, Harrick Plasma) for 15 min. Directly after plasma cleaning, 6 µl SUV solution and 12 µl 6 mM $CaCl_2$ were added to the chamber. The chamber was covered with a coverslip, placed on a 0.5 mm thick adhesive silicone sheet (Life Technologies), and incubated for 30 minutes at 37°C. After incubation, the formed SLB was washed four times with MRB80 buffer (80 mM K-Pipes, 4 mM $MgCl_2$, 1 mM EGTA) and incubated 10 minutes with 0.5 mg/ml k-Casein in MRB80.

For experiments with purified BtubA/B, 20 µl of a solution containing PURE*frex*2.0, 0.05% (w/v) methylcellulose, 4 µl MRB80 (3 µl H_2O) and purified BtubA/B and Atto488/Atto561-labelled BtubA/B was added to the glass chamber and imaged at either 25 or 30°C. Activity check of synthesized protein was conducted by combining BtubA and BtubB, which were beforehand separately expressed at 37°C for 3 hours. Then, 8.5 µl expression solution of BtubA and 1.5 µl of 1 µM labelled BtubA/B-Atto488 were added to the SLB and imaged for 30 minutes at 30°C. Subsequently, 5 µl of BtubB expression mix were added during imaging.

Flotation assay

A 20-µl PURE*frex*2.0 mix was incubated for 3 hours at 37°C. Subsequently, 12 µl of vesicle solution were added and the sample was incubated for 20 minutes at 30°C. Afterwards, 80 µl of a 1:1 dilution of PURE*frex*2.0 Solution-I with water was added and the sample was spun down at 8.000 g for 2 minutes. Due to the lighter weight of the vesicles compared to the PURE solution, a pellet of vesicles formed during centrifugation at the top of the solution. From under the pellet, 80 µl of solution was harvested. After a second centrifugation of the pellet, another 15 µl were removed from under the pellet and the pellet was resuspended by pipetting up and down. Of this liposome fraction, 10 µl were taken for analysis. The 80 µl of previously removed bottom fraction was as well spun down again and 10 µl were taken for analysis from the middle of the tube to avoid collection of vesicles and filaments. For analysis, equal amounts of liposome and bottom fractions were run on a 12% SDS-protein gel.

Protein synthesis in liposomes

A swelling solution with a volume of 20 µl and consisting of PURExfrex2.0, 1 µl DnaK mix (GeneFrontier Corporation), 100 nM Atto488-BtubA/B, 3.75 nM BtubA and 2.5 nM of BtubB DNA construct was prepared. 20 ug of lipid beads were added and the solution incubated on ice for 2 hours to enable natural swelling without significant expression activity. During incubation, the tube was gently manually rotated a few times. To further enhance encapsulation efficiency, four freeze-thaw cycles were applied by dipping the tube into liquid nitrogen followed by thawing at RT. In the meantime, the glass chamber was sequentially incubated for 5 minutes with a solution of BSA and BSA-biotin (1:1 molar ratio, 1 mg/mL, Thermo Fisher Scientific) and with Neutravidin (1 mg/mL, Sigma Aldrich) to later immobilize the biotinylated liposomes. Next, 4 µl of swelling solution and 12 µl of dilution buffer (PURExfrex2.0 Sol I and milliQ (7:4 volume ratio) supplemented with 83 mg/l Proteinase K) were added to the chamber. Imaging was performed with a confocal microscope (A1+ from Nikon, ×100 oil immersion objective) using a 488 nm laser for tubulin and a 561 nm laser for membrane detection. During imaging the liposomes were incubated at 37°C.

4.5 Supplementary information

Sequence of *btubA* (5'→ 3', complete linear construct)

CAGTCACGACGTTGTAAAACGACGGCCAGTCGCGAAATTAATACGACTCACTATAGGGGAATTG
TGAGCGGATAACAATTCCCCTCTAGAAATAATTTTGTTTAACTTTAAGAAGGAGATATACATATG
AAAGTTAATAATACAATTGTAGTTAGTATTGGTCAGGCGGGCAACCAAATCGCGGCGAGCTTCT
GGAAAACCGTGTGCCTGGAGCACGGTATTGACCCGCTGACCGGTCAGACCGCGCCGGGCGTTGC
GCCGCGTGGTAACTGGAGCAGCTTCTTTAGCAAGCTGGGCGAGAGCAGCAGCGGTAGCTACGTG
CCGCGTGCGATCATGGTTGATCTGGAACCGAGCGTGATTGACAACGTTAAAGCGACCAGCGGCA
GCCTGTTCAACCCGGCGAACCTGATTAGCCGTACCGAGGGCGCGGGTGGCAACTTTGCGGTTGG
TTACCTGGGTGCGGGTCGTGAGGTGCTGCCGGAAGTTATGAGCCGTCTGGATTATGAAATCGAC
AAGTGCGATAACGTGGGTGGCATCATTGTTCTGCATGCGATCGGTGGTGGCACCGGCAGCGGTT
TTGGCGCGCTGCTGATCGAGAGCCTGAAGGAAAAATACGGCGAGATTCCGGTGCTGAGCTGCGC
GGTTCTGCCGAGCCCGCAGGTGAGCAGCGTGGTTACCGAGCCGTATAACACCGTTTTTGCGCTGA
ACACCCTGCGTCGTAGCGCGGATGCGTGCCTGATCTTCGATAACGAAGCGCTGTTTGACCTGGCG
CACCGTAAATGGAACATTGAGAGCCCGACCGTGGACGATCTGAACCTGCTGATCACCGAAGCGC
TGGCGGGCATTACCGCGAGCATGCGTTTCAGCGGTTTTCTGACCGTGGAAATCACCCTGCGTGAG
CTGCTGACCAACCTGGTTCCGCAACCGAGCCTGCACTTCCTGATGTGCGCGTTTGCGCCGCTGAC
CCCGCCGGATCGTAGCAAGTTCGAGGAACTGGGTATCGAGGAAATGATTAAAAGCCTGTTCGAC
AACGGCAGCGTGTTTGCGGCGTGCAGCCCGATGGAAGGTCGTTTTCTGAGCACCGCGGTTCTGTA
TCGTGGCATCATGGAGGATAAACCGCTGGCGGATGCGGCGCTGGCGGCGATGCGTGAAAAGCTG
CCGCTGACCTACTGGATTCCGACCGCGTTCAAAATTGGCTATGTTGAGCAGCCGGGTATTAGCCA
CCGTAAAAGCATGGTGCTGCTGGCGAACAACACCGAAATCGCGCGTGTTCTGGATCGTATTTGC
CACAACTTCGACAAGCTGTGGCAACGTAAAGCGTTTGCGAACTGGTATCTGAACGAGGGTATGA
GCGAGGAACAGATCAACGTGCTGCGTGCGAGCGCGCAAGAACTGGTGCAGAGCTATCAAGTTGC
GGAGGAAAGCGGCGCGAAGGCGAAAGTTCAAGACAGCGCGGGTGATACCGGTATGCGTGCGGC
GGCGGCGGGTGTGAGCGACGATGCGCGTGGTAGCATGAGCCTGCGTGACCTGGTTGATCGTCGT
CGTTAAGCGATCACTAGCATAACCCCTTGGGGCCTCTAAACGGGTCTTGAGGGGTTTTTTGGGCG
TAATCATGGTCATAGCTGTTTCCTGTGTG

Sequence of *btubB* (5'→ 3', complete linear construct)

CAGTCACGACGTTGTAAAACGACGGCCAGTCGCGAAATTAATACGACTCACTATAGGGGAATTG
TGAGCGGATAACAATTCCCCTCTAGAAATAATTTTGTTTAACTTTAAGAAGGAGATTTGAAAATG
AGAGAAATATTAAGTATACATGTAGGTCAATGCGGCAACCAGATCGCGGATAGCTTTTGGCGTC

TGGCGCTGCGTGAACACGGCCTGACCGAGGCGGGCACCCTGAAGGAAGGTAGCAACGCGGCGG
CGAACAGCAACATGGAAGTGTTCTTCCACAAGGTTCGTGACGGTAAATACGTGCCGCGTGCGGT
GCTGGTTGATCTGGAGCCGGGCGTTATCGCGCGTATTGAAGGTGGCGACATGAGCCAGCTGTTT
GATGAAAGCAGCATCGTGCGTAAAATCCCGGGTGCGGCGAACAACTGGGCGCGTGGTTATAACG
TGGAGGGCGAAAAAGTTATCGACCAGATTATGAACGTGATCGATAGCGCGGTTGAGAAGACCA
AAGGTCTGCAAGGCTTCCTGATGACCCATAGCATCGGTGGCGGTAGCGGCAGCGGTCTGGGCAG
CCTGATTCTGGAACGTCTGCGTCAGGCGTACCCGAAGAAACGTATCTTCACCTTTAGCGTGGTTC
CGAGCCCGCTGATTAGCGACAGCGCGGTGGAGCCGTATAACGCGATCCTGACCCTGCAACGTAT
TCTGGACAACGCGGATGGTGCGGTTCTGCTGGACAACGAAGCGCTGTTCCGTATCGCGAAGGCG
AAACTGAACCGTAGCCCGAACTACATGGATCTGAACAACATCATTGCGCTGATTGTGAGCAGCG
TTACCGCGAGCCTGCGTTTTCCGGGCAAGCTGAACACCGATCTGAGCGAGTTCGTGACCAACCTG
GTTCCGTTCCCGGGCAACCACTTTCTGACCGCGAGCTTCGCGCCGATGCGTGGTGCGGGTCAGGA
AGGTCAAGTGCGTACCAACTTTCCGGACCTGGCGCGTGAAACCTTTGCGCAGGACAACTTCACC
GCGGCGATCGATTGGCAGCAAGGTGTTTATCTGGCGGCGAGCGCGCTGTTCCGTGGCGATGTGA
AGGCGAAAGACGTTGATGAAAACATGGCGACCATTCGTAAGAGCCTGAACTACGCGAGCTATAT
GCCGGCGAGCGGCGGTCTGAAACTGGGCTATGCGGAAACCGCGCCGGAAGGTTTTGCGAGCAGC
GGCCTGGCGCTGGTGAACCACACCGGTATCGCGGCGGTTTTCGAGCGTCTGATCGCGCAATTCG
ACATTATGTTTGATAACCACGCGTACACCCACTGGTATGAAAACGCGGGTGTTAGCCGTGACAT
GATGGCGAAAGCGCGTAACCAGATTGCGACCCTGGCGCAGAGCTATCGTGATGCGAGCTAAGCA
ATAACTAGCATAACCCCTTGGGGCCTCTAAACGGGTCTTGAGGGGTTTTTTGGGCGTAATCATGG
TCATAGCTGTTTCCTGTGTG

Sequence of *btubC* (5'→ 3', from T7 promotor to T7 terminator)

TAATACGACTCACTATAGGGGAATTGTGAGCGGATAACAATTCCCCTCTAGAAATAATTTTGTTT
AACTTTAAGAAGGAGATATACATATGGGCAGCAGCCATCATCATCATCATCACAGCAGCGGCCT
GGTGCCGCGCGGCAGCATGGACTCCCCTCTCGATCGTCAGCTCGCTGCCGCCTCTCGCAGTGTCG
AAGAGGCGCGGAGAATGGCTTATCACGACGATTCGAAGATCGGGTATCTGGTGGAGCAGATCAG
CGTGCTGGCAGATCTGCGGCAGAAAGAGGGAGACTTCCGCAAGGCCGAGTCGCTGTATCGTGAG
GCGCTATTCAGCGCTCAGGAGCAGCGTAAGCCGGACCCGGAGTTGCTGACGGGCATCCATTCCT
TGCTGGCGCATCTGTATGATCGCTGGGGCCGGATGGATCTCGCCTCGCAGTTTTATGAGAAAGCC
CTGAAGATCGCCGAGCGAGGCGGCATCGCCCAGAGTGATAAGGTGGCGATCATCAAAAACAAT
CTGGCGATGATCTTCAAGCAGCTCCGTGACTACACCCGTGCGGAGCAGCACTACCAAGAGGCGC
TGGAAATCTTCCGCAAAACGGATGGTGAATACAGCGCTCGGGTGGCTAGCGTTTTTAACAATCTC
GGGGTGCTATATTACAGCAACCTGGAGGTCGAGCAGGCGCAGGAGATGCATGAGCATGCGTTGA
CGATTCGGCAGAGCCTTTCGAATGATCAGGCGGACTCGGGGGATCTCTCACAGACCTACATCAA
TCTCGGCGCTGTTTATAAAGCGGCGGGAGATTTTCAGAAAGCTGAGGCCTGTGTGGATCGTGCTA
AGAAGCTGCGGGCCAGCATGAATGGCTACCACCCGCAGCCGCGCCGTGCGGCGTCTTTGCTTGT
CGATAAATCCCTGTGACAAAGCCCGAAAGGAAGCTGAGTTGGCTGCTGCCACCGCTGAGCAATA
ACTAGCATAACCCCTTGGGGCCTCTAAACGGGTCTTGAGGGGTTTTTTG

Table 4.1: List of primers used

Primer	FW/RV	Sequence 5' → 3'
ChD 365	FW	CAGTCACGACGTTGTAAAACGAC
ChD 173	RV	CACACAGGAAACAGCTATGAC

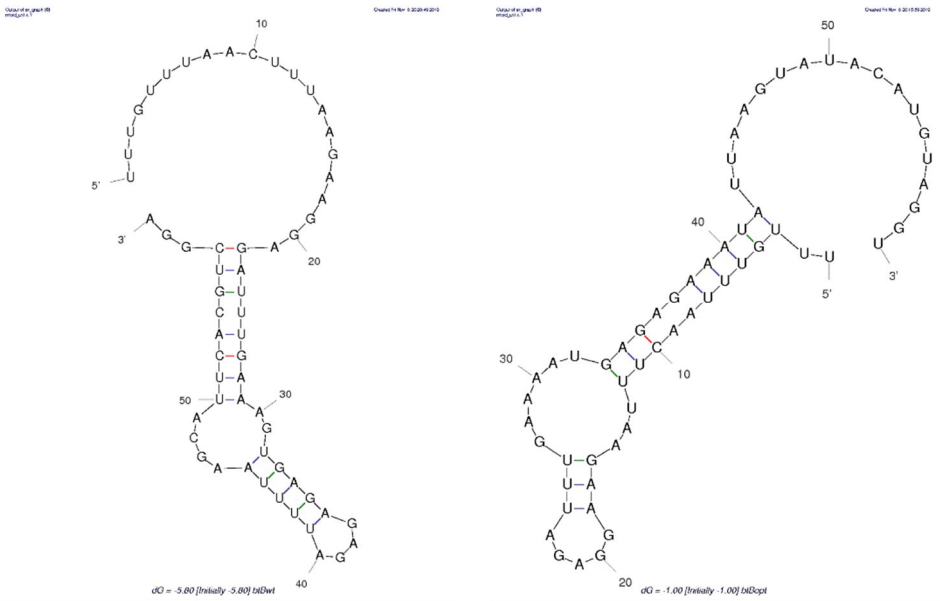

Figure 4.7: Possible RNA structures of the 30 basepairs before and after the start codon (including start codon, 60 bp total). The folds with the lowest • G values were calculated with mfold [26] for the sequences around the RBS in combination with the wildtype sequence (left image, • G = -5.8 kcal/mol) and in combination with the optimized sequence (right image, • G = -1.0 kcal/mol).

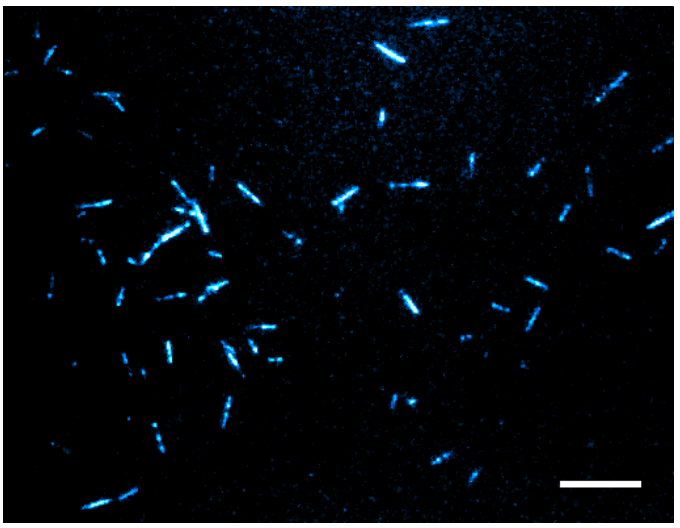

Figure 4.8: Bacterial microtubules on an SLB, formed by 1 µM of purified bacterial tubulin. Scale bar: 10 µm.

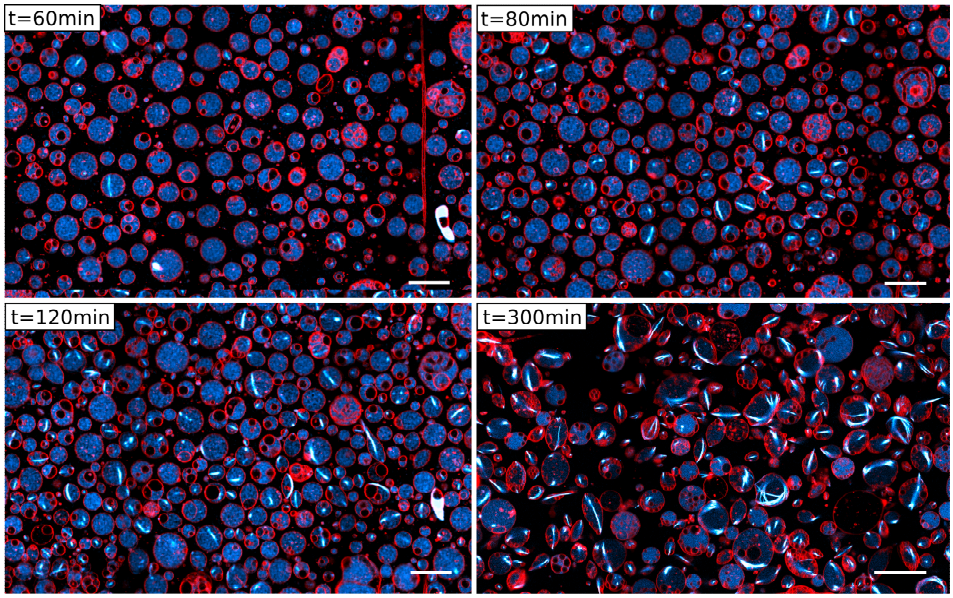

Figure 4.9: Expression of bacterial tubulin inside liposomes over time. Incubation was conducted at 37°C. Scale bars: 20 µm.

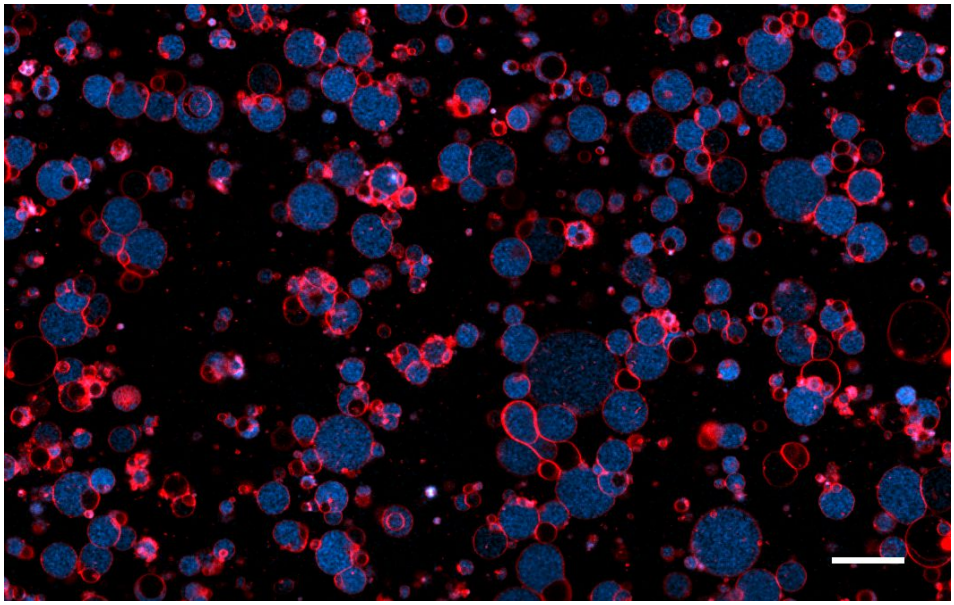

Figure 4.10: Negative control for expression of BtubA/B in liposomes. Instead of bacterial tubulin, the yeast protein Vps2 was expressed in presence of 100 nM labelled tubulin. Image acquired after 4 hours of incubation at 37°C. Scale bar: 20 µm.

References

[1] Wagstaff J, Lowe J. Prokaryotic cytoskeletons: protein filaments organizing small cells. Nat Rev Microbiol 2018;16:187–201.

[2] Rosati G, Lenzi P, Franco V. 'Epixenosomes': Peculiar epibionts of the protozoon ciliate Euplotidium itoi: Do their cytoplasmic tubules consist of tubulin? Micron 1993;24:465–71.

[3] Petroni G, Spring S, Schleifer KH, Verni F, Rosati G. Defensive extrusive ectosymbionts of Euplotidium (Ciliophora) that contain microtubule-like structures are bacteria related to Verrucomicrobia. Proc Natl Acad Sci U S A 2000;97:1813–7.

[4] Jenkins C, Samudrala R, Anderson I, Hedlund BP, Petroni G, Michailova N, et al. Genes for the cytoskeletal protein tubulin in the bacterial genus Prosthecobacter. Proc Natl Acad Sci U S A 2002;99:17049–54.

[5] Pilhofer M, Ladinsky MS, McDowall AW, Petroni G, Jensen GJ. Microtubules in Bacteria: Ancient tubulins build a five-protofilament homolog of the eukaryotic cytoskeleton. PLoS Biol 2011;9.

[6] Deng X, Fink G, Bharat TAM, He S, Kureisaite-Ciziene D, Lowe J. Four-stranded mini microtubules formed by Prosthecobacter BtubAB show dynamic instability. Proc Natl Acad Sci U S A 2017;114:E5950–8.

[7] Diaz-Celis C, Risca VI, Hurtado F, Polka JK, Hansen SD, Maturana D, et al. Bacterial Tubulins A and B Exhibit Polarized Growth, Mixed-Polarity Bundling, and Destabilization by GTP Hydrolysis. J Bacteriol 2017;199.

[8] Schlieper D, Oliva MA, Andreu JM, Lowe J. Structure of bacterial tubulin BtubA/B: Evidence for horizontal gene transfer. Proc Natl Acad Sci 2005;102:9170–5.

[9] Akendengue L, Trepout S, Grana M, Voegele A, Janke C, Raynal B, et al. Bacterial kinesin light chain (Bklc) links the Btub cytoskeleton to membranes. Sci Rep 2017;7:45668.

[10] Lee K-C, Webb RI, Janssen PH, Sangwan P, Romeo T, Staley JT, et al. Phylum Verrucomicrobia representatives share a compartmentalized cell plan with members of bacterial phylum Planctomycetes. BMC Microbiol 2009;9:5.

[11] Noireaux V, Libchaber A. A vesicle bioreactor as a step toward an artificial cell assembly. Proc Natl Acad Sci U S A 2004;101:17669 LP – 17674.

[12] Nourian Z, Roelofsen W, Danelon C. Triggered gene expression in fed-vesicle microreactors with a multifunctional membrane. Angew Chem Int Ed Engl 2012;51:3114–8.

[13] Shimizu Y, Inoue A, Tomari Y, Suzuki T, Yokogawa T, Nishikawa K, et al. Cell-free translation reconstituted with purified components. Nat Biotechnol 2001;19:751–5.

[14] Sadler FW, Dodevski I, Sarkar CA. RNA Thermometers for the PURExpress System. ACS Synth Biol 2018;7:292–6.

[15] Cortese JD, Schwab B 3rd, Frieden C, Elson EL. Actin polymerization induces a shape change in actin-containing vesicles. Proc Natl Acad Sci U S A 1989;86:5773–7.

[16] Hotani H, Miyamoto H. Dynamic features of microtubules as visualized by dark-field microscopy. Adv Biophys 1990;26:135–56.

[17] Tanaka S, Takiguchi K, Hayashi M. Repetitive stretching of giant liposomes utilizing the nematic alignment of confined actin. Commun Phys 2018;1.

[18] Lee J, Park B, Woo S-G, Lee J, Park J. Prosthecobacter algae sp. nov., isolated from activated sludge using algal metabolites. Int J Syst Evol Microbiol 2014;64:663–7.

[19] Bisson-Filho AW, Hsu Y-P, Squyres GR, Kuru E, Wu F, Jukes C, et al. Treadmilling by FtsZ filaments drives peptidoglycan synthesis and bacterial cell division. Science 2017;355:739–43.

[20] Yang X, Lyu Z, Miguel A, McQuillen R, Huang KC, Xiao J. GTPase activity-coupled treadmilling of the bacterial tubulin FtsZ organizes septal cell wall synthesis. Science 2017;355:744–7.

[21] Fernandez C, Giraldo R. Modulation of the Aggregation of the Prion-like Protein RepA-WH1 by Chaperones in a Cell-Free Expression System and in Cytomimetic Lipid Vesicles. ACS Synth Biol 2018;7:2087–93.

[22] Blanken D, van Nies P, Danelon C. Quantitative imaging of gene-expressing liposomes reveals rare favorable phenotypes. Phys Biol 2019;16:45002.

[23] Tsai F-C, Koenderink GH. Shape control of lipid bilayer membranes by confined actin bundles. Soft Matter 2015;11:8834–47.

[24] Litschel T, Ramm B, Maas R, Heymann M, Schwille P. Beating Vesicles: Encapsulated Protein Oscillations Cause Dynamic Membrane Deformations. Angew Chem Int Ed Engl 2018;57:16286–90.

[25] Godino E, Lopez JN, Foschepoth D, Cleij C, Doerr A, Castella CF, et al. De novo synthesized Min proteins drive oscillatory liposome deformation and regulate FtsA-FtsZ cytoskeletal patterns. Nat Commun 2019;10:4969.

[26] Zuker M. Mfold web server for nucleic acid folding and hybridization prediction. Nucleic Acids Res 2003;31:3406–15.

[27] Schindelin J, Arganda-Carreras I, Frise E, Kaynig V, Longair M, Pietzsch T, et al. Fiji: an open-source platform for biological-image analysis. Nat Methods 2012;9:676–82.

Chapter 5

De novo synthesis of the ESCRT-III complex

When a man lies he murders some part of the world.

Clifford Lee Burton, adapted from Paul Gerhardt

The ESCRT system plays vital roles in eukaryotic vesicle budding and cell division. In this Chapter we explored if we can reconstitute the membrane modulating functions of the ESCRT-III system by cell-free expression of the respective proteins. After confirming full-length synthesis of the ESCRT-III proteins by the PURE system, we investigated interaction of the synthesized proteins with lipid membranes. Binding of expressed ESCRT-III proteins to SLBs and liposome membranes was analysed by fluorescence and electron microscopy, as well as by flotation assays. Results indicate that the proteins are binding to lipid membranes and are forming spiral structures typical for ESCRT-III filaments. Autoinhibition regarding membrane binding, as described in literature for full-length ESCRT-III proteins, was not observed. Vesicle budding was not observed either, which is in alignment with recent findings that ESCRT-III proteins are on their own not capable of inducing membrane scission and require additionally the protein Vps4 to exert this function. Vps4 is expressed at full length as well, but activity of the synthesized protein has not been confirmed. Further, protein purification of the ESCRT-III proteins was attempted.

5.1 Introduction

The endosomal sorting complex required for transport (ESCRT) machinery is a functional group of protein complexes that are a main actor in a multitude of essential membrane remodelling processes in eukaryotic cells. It was originally discovered as a group of proteins required for the biogenesis of multivesicular bodies (MVBs) in yeast endosomes [1–3]. The main task of endosomes is to separate proteins that will be degraded by lysosomes from those that will be recycled. Transmembrane proteins destined for degradation are marked by ubiquitination and will be sorted and aggregated on the membrane of the endosome by the first three protein complexes ESCRTs-0, I, and II. The ESCRT-II complex will also act as a recruiter for the ESCRT-III complex, which will facilitate formation and release of the vesicle. Thus, the proteins marked for degradation are encapsulated in intraluminal vesicles (ILVs) inside the MVB. Eventually, the MVBs will fuse with a lysosome in which all proteins are degraded.

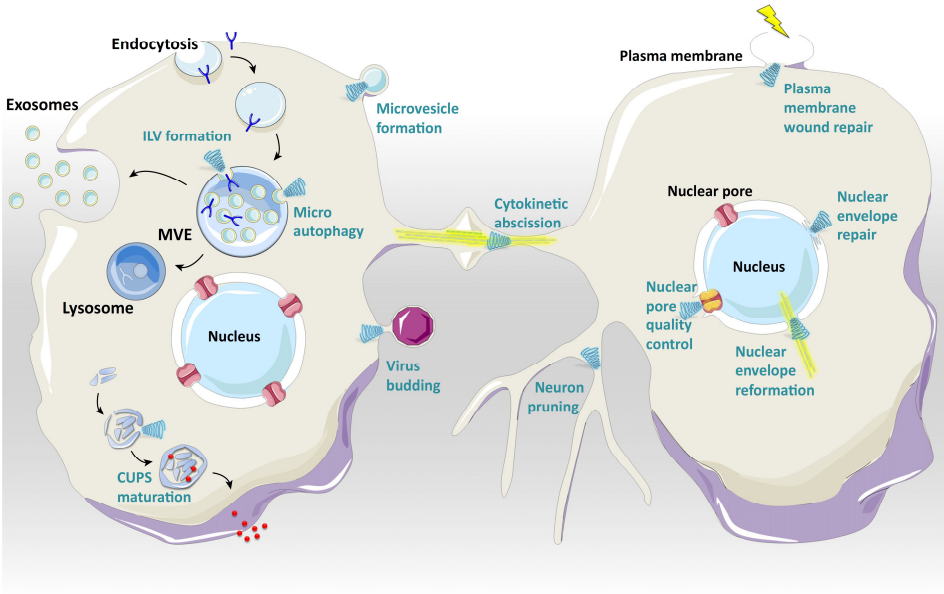

Figure 5.1: Overview of ESCRT-dependent processes. The ESCRT-III machinery is indicated as blue spirals. Abbreviations: CUPS, compartment for unconventional protein secretion; MVE, multivesicular endosome/body. Taken from Christ et al. 2017.

Since this discovery, it has been revealed that the ESCRT system is as well involved in various other cellular processes (Figure5.1) such as: release of HIV-1 and other viruses from host cell [4,5]; neural pruning [6]; plasma membrane repair [7]; sealing of the nuclear envelope [8]; extraction of defective nuclear pore complexes [9]; and biogenesis of microvesicles and exosomes [10,11]. Furthermore, during the final step of eukaryotic cell division two ESCRT-III complexes are formed at the constricted abscission side between the two daughter cells where they will induce scission of the cell membrane and thus finalize division [12,13]. In this variety of cellular processes, the ESCRT-III system is responsible for the constriction of the membrane and the severing of the membrane neck from within the cytoplasm through the formation of a filament complex. The other

ESCRT subsystems 0, I and II are mainly responsible for positioning and recruitment of the ESCRT-III machinery and are not involved in some of the mentioned cellular mechanisms.

The ESCRT-III complex is composed of the four core subunits Vps20, Snf7, Vps24 and Vps2 which all share similar biochemical properties and molecular architecture. Vps20 is recruited by ESCRT-II and will subsequently recruit Snf7, which is the main component of the complex in terms of quantity. Snf7 polymerizes into curved filaments on the membrane which have been shown to form spiral structures on SLB membranes and liposomes *in vitro* (Figure5.25)[14,15]. Vps24 and Vps2 bind to the filaments of Snf7 and inhibit further polymerisation of the same as well as changing the filament structure [16]. Moreover, Vps2 recruits the AAA-ATPase Vps4 which disassembles and recycles the ESCRT filaments. Until polymerisation, the ESCRT proteins exists predominantly in an autoinhibited state as monomers in solution.

All four ESCRT-III proteins contain a core domain of four helices (• 1-4), which are responsible for membrane binding and filament polymerisation (Figure5.2). Another • -helix (• 5) is mediating autoinhibition by binding to the core domain, thus preventing it from interacting with other subunits and binding to the membrane [17]. The autoinhibition can be lifted by recruitment to already active subunits. Membrane binding is mediated by two mechanisms. One is the electrostatic attraction between positive amino acid residues of the core domain and the negatively charged membrane [18,19]. The second is the insertion of a hydrophobic anchor domain into the membrane, which is positioned at the N-terminus (• 0) [18].

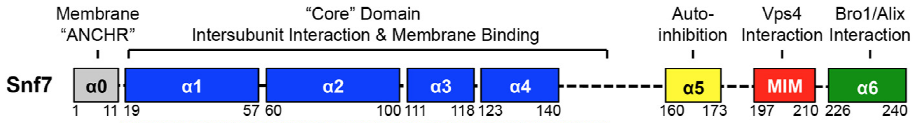

Figure 5.2: Structural organisation of the Snf7 subunit. The core domain is responsible for membrane recruitment and protein polymerisation. The α2 and α3 helices are positively charged, which allows them to bind to negatively charged membranes. Autoinhibition is mediated by the negatively charged α5, which folds onto the core domain. C-terminal domains (MIM,α6) are recruiting and interacting with other proteins like Vps4. Taken from Tang et al. 2015.

What is most intriguing about the ESCRT machinery, compared to other membrane remodelling system such as clathrin or SNARE complexes, is that it facilitates outward rather than inward budding. As a consequence it is able to enforce membrane scission on the very compartment it is confined to. This imposes the challenge on the ESCRT-III complex to exert the necessary force for scission of the membrane neck without blocking membrane fusion by being located in the membrane neck itself. Several mechanisms of how the ESCRT is nevertheless capable of remodelling cell membranes have been proposed. One has been the sequential dome model, which assumes that Snf7 forms a conical cylinder inside of the membrane neck. Vps24 and Vps2 then form hemisphere caps on the end of the cylinder to form a highly curved protein dome at the constriction side that could facilitate membrane scission [20]. Another model suggested the formation of a Snf7 spiral around the membrane neck that would close the membrane neck by inward polymerization and capping by Vps24 and Vps2 [21]. In both these older models, the subunits form the ESCRT complex in a sequential manner. The ATPase Vps4 is recruited last and is either only necessary for recycling of the complex after scission or the release of accumulated tension in the complex and thus finalizing the abscission. However, these models have recently

been contradicted by evidence demonstrating that abscission and membrane neck constriction during vesicle biogenesis and cell division are dependent on Vps4 activity [16,22,23]. It was further shown that, rather than having to be recruited sequentially, the ESCRT components likely act simultaneously. Snf7 forms filaments to which Vps2 and Vps24 cause alteration of filament structure and inhibition of filament growth, but through subunit turnover by Vps4 the inhibition is constantly lifted again [16]. This allows the complex to grow while being constantly altered by the removal and addition of components. The turnover leads to reduction in spiral diameter and thus constriction and finally abscission of the membrane neck (Figure5.3A). It is, however, still unclear if the complex ends in a dome or cone-like shape [24]. The dynamic dome model model is supported by evidence from *in vitro* experiments in which Vps4 could depolymerize ESCRT-III spirals into dome-caped segments [25].

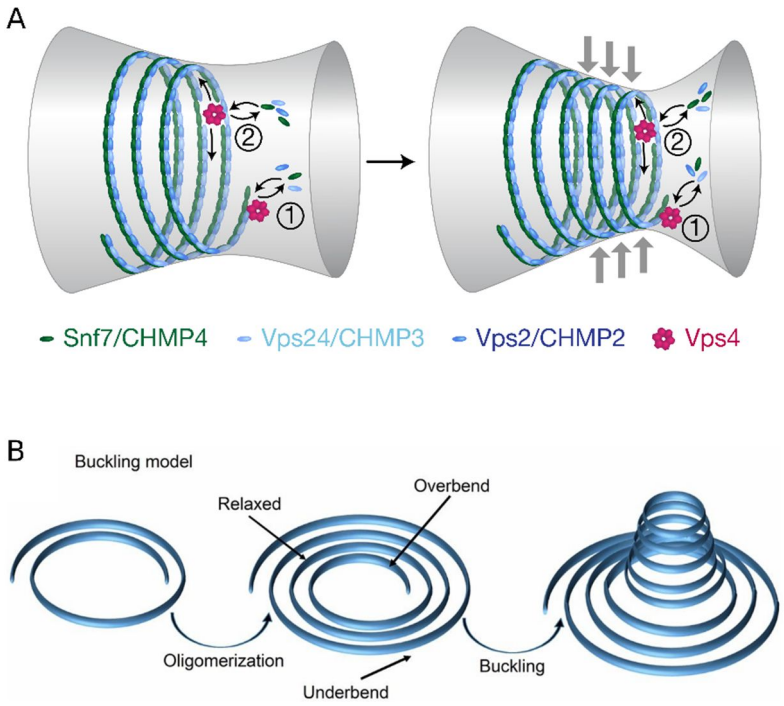

Figure 5.3: Two models for ESCRT membrane remodelling. **(A)** Schematic of the dynamic turnover model. Vps4 mediates continuous subunit turnover in ESCRT-III assemblies during growth and constriction. (1) At the tip, dynamic turnover of growth-inhibitory Vps2 and Vps24 subunits may result in polymerization of inward-curving filaments. (2) At the core of the complex, Vps4-mediated subunit turnover may result in sliding of neighbouring helical turns to promote constriction. Taken from Mierzwa et al. 2017. **(B)** Schematic of the buckling model. Tension is created by a spiraling filament growing beyond its preferred radius of curvature which upon release can remodelling of the membrane. Taken from Caillat et al. 2019.

Another possible mechanism for membrane remodelling is that through polymerization of ESCRT-III into a spiral elastic tension is created, as part of the filaments are over- and others underbend, which is released through buckling of the structure into a cone (Figure5.3B). Indeed, it has been demonstrated on flat membranes *in vitro* that ESCRT filaments can create tension which upon

release can deform the membrane [15]. This might be a possibility of how the ESCRT system could create the membrane evagination required as a first step for vesicle budding independent of other mechanisms. However, this model does not account for the mechanism of membrane abscission or the formation of the ESCRT complex inside of the abscission side during cell division and can therefore be seen as a partial model for ESCRT activity.

Our aim was to reconstitute the ESCRT system by *de novo* synthesis of the ESCRT-III proteins, and should this be successful to explore its possibilities for cell-division of a minimal system. In 2009, the group of Hurley were the first to report that they achieved the reconstitution of a functional ESCRT-III machinery *in vitro* and that it was capable of facilitating vesicle budding when the four ESCRT-III proteins were added sequentially to the outside of GUVs [21]. They further reported, that the addition of Vps20, Snf7 and Vps24 was sufficient for the generation of vesicles, while Vps4 was reported to be unnecessary for budding but did enhance repetitive budding events (Figure5.4). However, these results have been invalided by the recent findings that Vps4 is essential for membrane abscission [13,16,22,23,26]. At the time point at which the project was started, this crucial role of Vps4 was not yet clear.

We initially worked in collaboration with the lab of Philippe Bastiaens (Max-Planck institute for molecular physiology Dortmund). They worked with ESCRT-III constructs they received from the Hurley lab and gave account of having achieved the same results as reported by them, namely vesicle budding caused solely by the activity of the four ESCRT-III proteins. Our hypothesis was thus that we might be able to achieve the generation of vesicles by *de novo* synthesis of the four ESCRT-III proteins following the established protocol. As it became clear during the project that this would be highly improbable without addition of Vps4, we started to include it in our investigation as well.

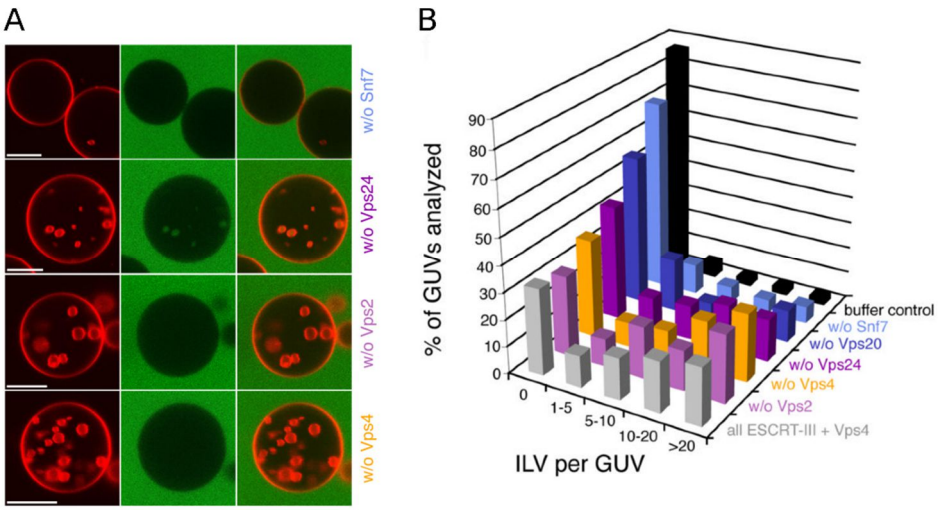

Figure 5.4: In vitro vesicle budding reported by Wollert et al.. **(A)** Microscopy images of several different conditions in which a protein was omitted. **(B)** Analysis of number of ILVs generated per condition. Number of vesicles does not decrease if either Vps4 or Vp2 are omitted. Taken from Wollert et al. 2009.

We initially worked in collaboration with the lab of Philippe Bastiaens (Max-Planck institute for molecular physiology Dortmund). They worked with ESCRT-III constructs they received from the Hurley lab and gave account of having achieved the same results as reported by them, namely vesicle budding caused solely by the activity of the four ESCRT-III proteins. Our hypothesis was thus that we might be able to achieve the generation of vesicles by *de novo* synthesis of the four ESCRT-III proteins following the established protocol. As it became clear during the project that this would be highly improbable without addition of Vps4, we started to include it in our investigation as well.

5

5.2 Results and discussion

5.2.1 Correction of Snf7 construct and creation of His-tag constructs

During the project we noticed that the Snf7 construct that we have received from the lab of Philippe Bastiaens contained a mutation. Positioned 712 bp after the start codon and 11 bp before the stop codon, the deletion of an A-T base pair caused a frameshift of the sequence downstream (Figure 5.5). As a consequence, the original stop codon was not recognized, causing the actual stop codon to be positioned 135 bp downstream. This results in a translational product containing 45 additional amino acids (circa 5 kDa) which might differ in properties and activity from the wildtype protein. We therefore corrected the frameshift by a PCR in which adenosine was added through the applied primers (Figure5.5). A few of the experiments we performed have at least partly been conducted with the faulty Snf7 construct containing the frameshift. In these cases, Snf7 will be mentioned as Snf7^{F}. Further, we added a 6xHis-tag to the Vps20• C, Vps2 and corrected Snf7 construct to facilitate labelling of the expressed proteins. The addition of a 6xHis-tag to Vps24 was not successful.

Figure 5.5: Sequence correction of frame shift in the Snf7 constructs. Top: The first line corresponds to the wild-type sequence, the second line is the sequencing result before and after the correction. A deletion of an adenosine, 712 bp after the start codon and 11 bp before the stop codon (marked in red), has caused a frameshift for the sequence downstream. Bottom: Method for correction of Snf7

sequence. Two primers were used tail by tail for a PCR of the whole plasmid with one primer containing an additional basepair to correct the deletion.

5.2.2 ESCRT-III genes are synthesized at full length by the PURE system.

The first step to reconstruct a functional ESCRT-III system by *de novo* synthesis was to confirm that the corresponding genes are fully transcribed and translated by the PURE system. The four ESCRT-III genes which we have received from the lab of Philippe Bastiaens were already under a T7 promotor and terminator. The sequence for Vps4, including a T7 promotor, RBS and T7 terminator sequence, was sent for gene synthesis to GenScript (United states) and was received in the pUC57 plasmid. After we confirmed by IVT assay that transcription was positive for all four ESCRT-III genes (Figure5.27), we investigated the translation products. The four ESCRT-III genes and Vps4 were expressed with PURE*frex* and with addition of Greenlys. Additionally, the terminal protein of the phi29 virus (TP) and a PURE*frex* mix without added DNA served as positive and negative controls respectively. Distinct expression products were visible for all of the ESCRT-III constructs with minor amounts of side products visible (Figure 5.6). Intensity of the Snf7^{F}, Vps2 and Vps20• C bands were comparable with the expression of TP. The Vps24 band was slightly more faint than the other bands. Vps4 was unlike the other constructs synthesized *de novo*. In this case the sequence was optimized in the same manner as for the bacterial tubulin genes in chapter 4.4. The IVTT of Vps4 yielded a clear band on the SDS-PAGE (Figure 5.7). Compared with the expressed Snf7, the intensity of the Vps4 band was significantly stronger on the GreenLys signal and the Coomassie staining. The larger size of Vps4 would likely lead to a slightly stronger signal with the same number of proteins expressed, but is unlikely to account for such a distinct difference. The codon optimization of the construct could explain the difference as it might aid with the translation initiation of the tRNA.

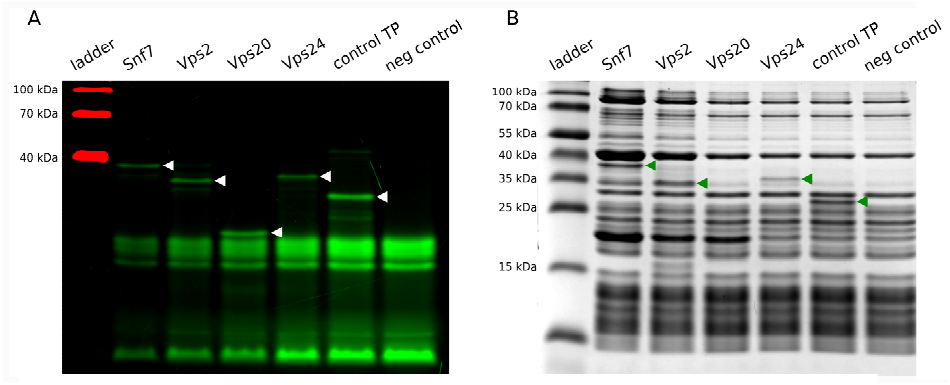

Figure 5.6: SDS-PAGE of ESCRT-III proteins expressed *in vitro*. A. GreenLys fluorescence signal of expression products. Expression of the terminal protein (TP) was used as a positive control and expression without DNA construct as a negative control. Synthesized full-length proteins are marked by white arrowheads. Note: The intensity of the GreenLys signal increases in the image from the left to the right. This can be considered as an artefact of the imaging. B. Coomassie staining of the same gel. Synthesized full-length proteins that are visible above PURE system background are marked by green arrowheads.

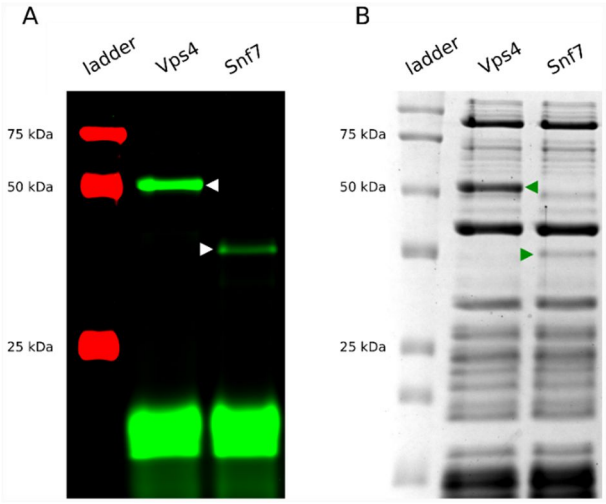

Figure 5.7: SDS-PAGE of expressed Vps4 and Snf7^{His}. A. GreenLys fluorescence signal of expression products. Synthesized full-length proteins are marked by white arrowheads. B. Comassie staining of the same gel. Synthesized full-length proteins are marked by green arrowheads.

Besides qualitative control, we quantified the amount of Snf7^{His} synthesized by PURE*frex*. This was important, as we had to validate if the amount of protein synthesized would be sufficient to reconstruct results received with purified proteins in literature. We choose Snf7 for quantification, because it is reported to be the main component of the ESCRT-III complex and was in previous studies added at higher concentrations than the other proteins. For a total of three Western Blots, average Snf7 concentration has been estimated to equal 2.4 ± 0.6 µM (Table 5.10). An example of a Western Blot is shown in Figure 5.8A with the respective calibration line depicted in Figure 5.8B. Membrane scission was claimed to be observed with a total amount of 1.2 µM of ESCRT proteins [21] and Snf7 polymerisation on a SLB was observed at 300 nM of Snf7 [15]. Therefore, as long as the majority of the expressed ESCRT proteins are active, the amount of them should be sufficient to replicate these results.

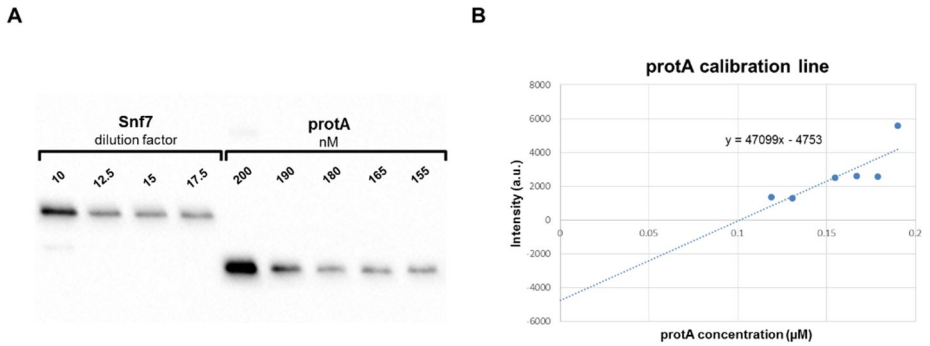

Figure 5.8: Western blot for Snf7 quantification. A. Bands for Snf7 and protA dilutions. Snf7 concentration was determined for dilution factor 10x, 12.5x, 15x and 17.5x by means of the protA

calibration curve. B. Calibration curve of protA which was received from the intensity values of the western blot.

5.2.3 Membrane recruitment capabilities of cell-free expressed ESCRT-III proteins

Membrane binding is a prerequisite for the ability of ESCRT-III to remodel the membrane. Therefore, we investigated the membrane binding capabilities of the synthesized ESCRT proteins. To this end, two methods were applied, namely the addition of the proteins to a supported lipid bilayer (SLB) and a flotation assay with lipid vesicles. For the flotation assay, we expressed ESCRT proteins and added to them a solution of liposomes. After a short incubation time, the suspension was centrifuged, which resulted the liposomes to float on top of the solution as they contained a buffer solution lighter than PURE*frex*. If the ESCRT proteins were able to bind to the membrane, they were expected to collocate with the vesicles. The top fraction was separated from the remaining solution, diluted and both fractions put on a SDS-PAGE. We performed a flotation assay with Snf7 in the presence of Vps20• C (Figure 5.A) and observed that the band of Snf7 was distinctly stronger in the liposome fraction (LF) compared to the bottom fraction (BF). This indicates that under the given condition, the expressed Snf7 was able to bind to the membrane of the liposomes. However, this was as well the case for the sample containing no Vps20• C. Here the Snf7 was to the same degree enriched in the liposome fraction compared to the bottom fraction, indicating that Snf7 did not require Vps20• C in order to bind to the membrane. In literature, it is described that Snf7 does bind to negatively charged membranes by itself. However, only relatively slowly and under prolonged incubation. In contrast, the addition of Vps20 with a deleted C-terminus greatly enhances the rate at which Snf7 binds to the membrane by offering a nucleation point for the polymerization of the Snf7 filament [15]. Therefore, our observation does seemingly contradict what would be expected for the membrane binding of Snf7.

Further, it was checked if binding of the expressed Snf7 to the membrane was dependent to the presence of DnaK in the expression mix, which was not the case. Omission of DnaK yielded the same result of enrichment in the liposome fraction (Figure 5.9B). The easiest way to label a protein expressed by the PURE system is the incorporation of GreenLys. We therefore checked if the labelling affects the membrane binding capabilities of the synthesized Snf7. Again, Snf7 was clearly enriched in the top fraction (Figure 5.9B). Having confirmed that GreenLys should not interfere with recruitment to the membrane, we applied it to investigate the membrane binding of Vps20• C. We focused here on the GreenLys signal, because the Vps20• C band is otherwise overshadowed by the PURE system background. Close to all of Vps20• C was located in the liposome fraction, confirming a strong binding to the membrane (Figure 5.10A). Vps24 was added to lipid vesicles without Vsp20• C or Snf7. It was enriched in the lipid fraction, but not as clearly as Vps20• C or Snf7 (Figure 5.10B). It should, however, be taken into account that some of the Vps24 might have been lost in an additional washing step, in which the lipid fraction was diluted 10 times and then separated again. No such washing step has been performed for the flotation assays with Snf7.

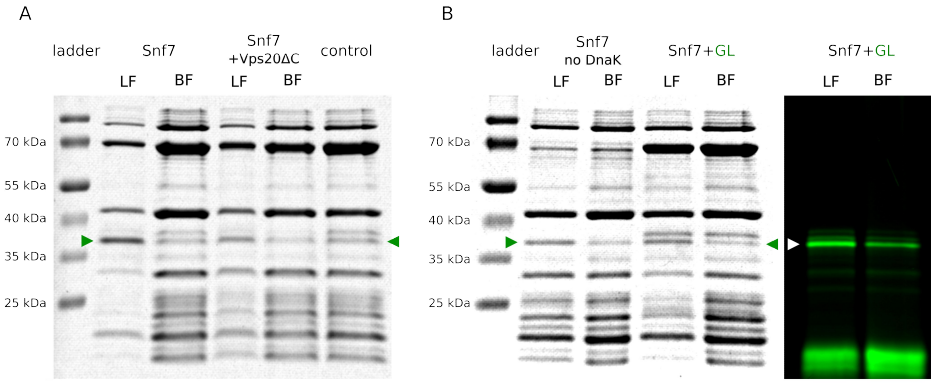

Figure 5.9: Flotation assays of Snf7 **(A)** Flotation assay of Snf7 with and without Vps20• C. Staining of the lipid fraction (LF), which is the phase containing the lipid vesicles, is right next to the bottom fraction (BF), the solution that was removed from beneath the vesicles. The lipid fraction was diluted after separation, which results in a lower PURE system background signal. Despite this, the Snf7 signal is clearly stronger in the lipid fraction in both conditions, indicating a binding to the lipid vesicles. The Vps20• C signal is not clearly visible. Likely due to the low amount used for the assay and the overlap with the PURE system background. **(B)** Second flotation assay of Snf7. Once without addition of DnaK and once with addition of GreenLys. Enrichment of Snf7 in the lipid fraction is visible in both cases. Height of Snf7 is marked by green and white arrows. A standard expression mix of Snf7 with DnaK was used as a positive control.

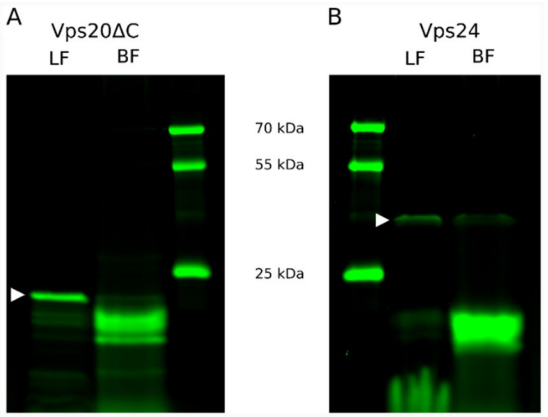

Figure 5.10: : Flotation assay of Vps20• C **(A)** and Vps24 **(B)**. In both cases after removal of the bottom fraction (BF) the remaining solution was diluted with PURE buffer. About 5 times in the case of Vps20• C and about 10 times in case of Vps24. After a second centrifugation step, a the solution was removed again from under the pellet and the diluted lipid fraction gathered. Both proteins collocate with the lipid fraction.

To further investigate membrane recruitment of the expressed ESCRT proteins, we incubated them on a SLB membrane while imaging it by confocal and TIRF microscopy. In order to visualize recruitment, the ESCRT proteins were labelled with GreenLys during gene expression and the membrane was labelled with DHPE-Texas Red. To make sure that GreenLys itself does not preferably bind to the membrane, we added a solution of GreenLys without expression products to the SLB (Figure 5.11). In this case, there was no colocalization of the GreenLys and the red membrane patches. Contrary, when synthesized Snf7 labelled with GreenLys and unlabelled Vps20• C were added to the membrane a clear overlap of the GreenLys and the membrane signal was visible (Figure 5.12). This strongly indicates binding of the ESCRT-III proteins to the membrane. Crosstalk can be excluded as sole reason for the colocalization as the GreenLys signal varied sufficiently from the one of the Texas-Red channel. As in the flotation assay, when Vps20• C was omitted binding of Snf7 to the membrane was still occurring (Figure 5.13). When Vps24 labelled with GreenLys was added to the membrane with and without addition of Snf7, there was colocalization of Vps24 and the membrane in both cases.

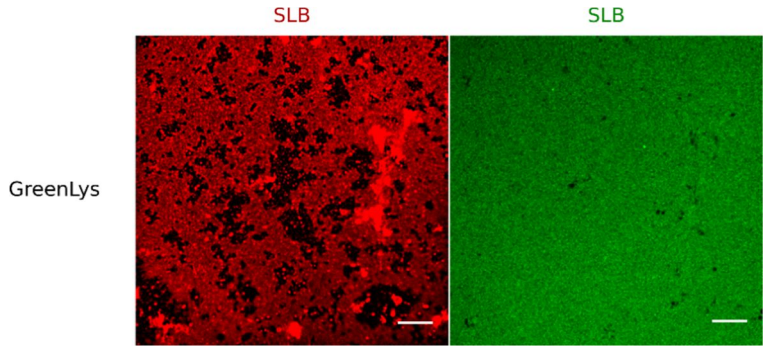

Figure 5.11: Confocal microscopy of GreenLys-tRNA in presence of a SLB. The GreenLys-tRNA channel and Texas Red membrane channel are shown from left to right. Dark areas in the membrane channel imply incomplete formation of the SLB. GreeLys signal does not colocalize with the membrane. GreenLys was added in a 200x dilution. Scale bar: 10 µm.

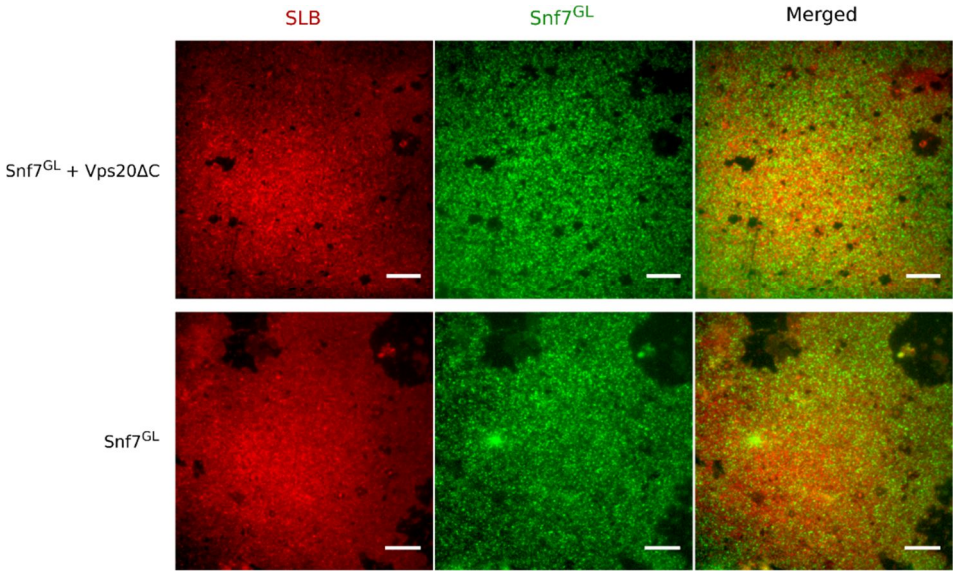

Figure 5.12: TIRF microscopy of Snf7^{GL} membrane recruitment in the presence and absence of Vps20• C. Texas Red membrane channel, GreenLys-tRNA channel and the merge image of both are shown from left to right. Snf7^{GL} colocalizes with the Texas Red membrane in both conditions. Ratio of expression mixes was 3:7 of Vps20• C and Snf7^{GL} respectively. Scale bar: 10 µm.

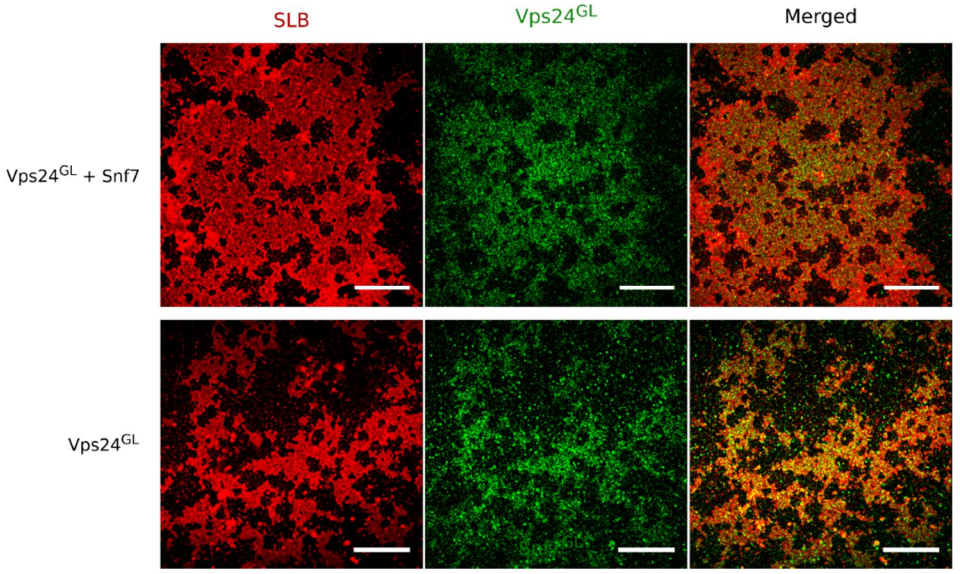

Figure 5.13: Confocal microscopy of Vps24^{GL} membrane recruitment with and without Snf7. Texas Red membrane channel, GreenLys-tRNA channel and the merged image of both are shown from left to right. Colocalization of Vps24^{GL} and the membrane was visible with and without the addition Snf7. The solution consisted of the expression mixes of Vps24^{GL} and Snf7, as well as PURE buffer in a respective ratio of 1:2:2. Scale bar: 20 µm.

The nucleation and growth of Snf7 patches have been shown by Chiaruttini et al.[15] on supported membranes by time-lapse images using TIRF microscopy. In this work, a similar approach has been attempted with the expressed Snf7^{GL}. Applying the estimated concentration received by the Western Blots, we prepared three conditions. In the first two we added expressed Snf^{GL} on top of a SLB at concentrations of what resemble 0.7 µM and 1.4 µM based on our estimates. For the third condition, we added Vps20• C and 1.4 µM Snf7. SLB quality was overall good, with only few holes and lipid vesicles interrupting it. Acquired time-lapse images indicated an increase in the fluorescent signal in the sample with 1.4 µM Snf7 and Snf7+Vps20• C (Figure 5.28), but no patch formation in either of the three samples (Figure 5.14). That binding to the membrane was still occurring can as well be seen by the strong signal of Snf7^{GL} on the surface of lipid aggregates attached to the membrane (Figure 5.15). In fact, preferred binding to small vesicles with high positive membrane curvature over larger vesicles has been reported in the past [18], which seemingly contradicts another report about preferred binding to negative membrane curvatures [27].

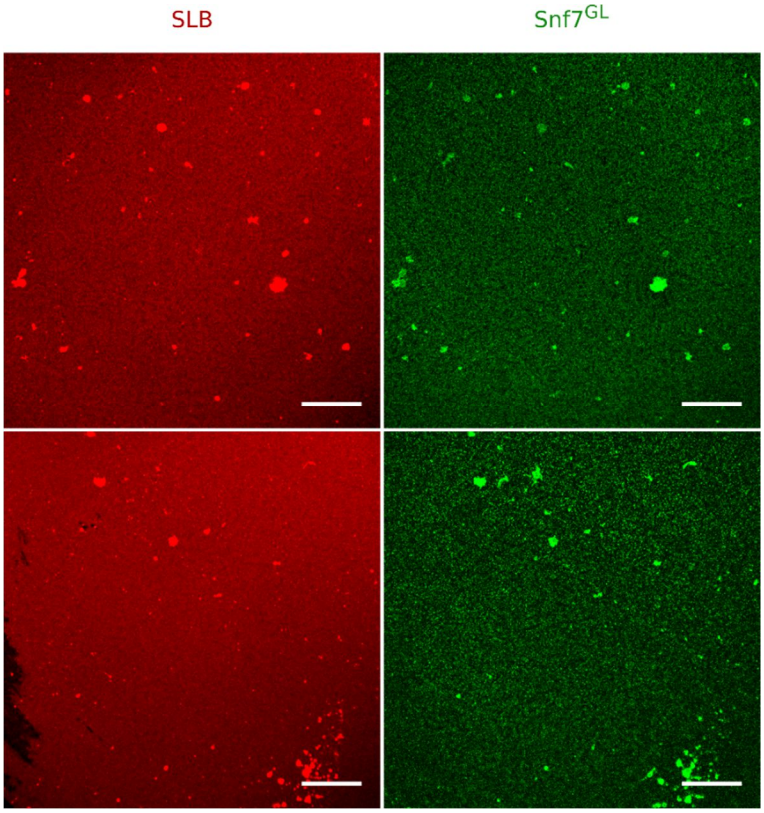

Figure 5.14: Absence of patch formation through Snf7^{GL} recruitment. Left: Texas-RED membrane channel; Right: GreenLys-tRNA channel. Snf labelled with GreenLys has been added to membranes with only minor irregularities. Unlike reported for purified Snf7, no patch formation was observed with expressed Snf7 of which about 0.7 µM (upper images) and 1.4 µM (lower images) were added. Snf7^{GL} signal was mostly evenly distributed over the membrane, except for more intense signals colocalizing with lipid vesicles and agglomerations on top of the membrane. Scale bar: 20 µm.

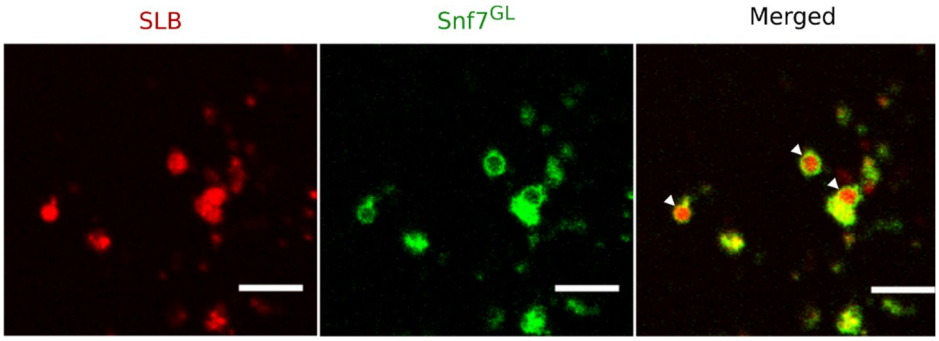

Figure 5.15: Snf7^{GL} binds to the outside of SUVs. Zoom in of lower image from Figure 5. (0.7 µM Snf7). Snf7^{GL} (green) is recruited to lipid aggregates (red), bound on top of a SLB. Scale bar: 5 µm.

We attempted as well to apply an alternative labelling method by using an NTA dye. In order to label components of the ESCRT system with it, we have created constructs with a 6xHis-tag at the C-terminus for three of the four ESCRT-III constructs. However, when the expression product of Snf7-His was added to the membrane together with the NTA-dye, no colocalization was observed (Figure 5.31). The most likely explanation is that the NTA dye was diluted before use in distilled water instead of buffer solution. In absence salt ions, the nickel ions essential for the binding, might have dissociated from the NTA group. Another possibility is that the 6xHis-tag of the protein was sterically not accessible, although this is unlikely considering that the C-terminal end of Snf7 is not incorporated in the folded protein. Moreover, for an additional negative control, we synthesized the terminal protein (TP) with GreenLys and added it to an SLB. To our surprise, a slight colocalization was here observed as well (Figure 5.29). When further analysed, this colocalization appears to be less strong than what we observed with Snf7 (Figure 5.30). Our conclusion is that the terminal protein itself seems to have a certain affinity for the membrane and was likely not a good choice for a negative control. We did not test a second negative control due to time limitations.

As mentioned, the Snf7 and the other ESCRT proteins are reported to be auto-inhibited in absence of the protein prior in the cascade. However, it has been described that the auto-inhibition is leaky to a certain degree and does primarily increase the time until the nucleation of the filament assembly. Both in the SLB and the flotation experiments, Snf7 is able to bind the membrane in the absence and presence of Vps20• C in a comparable manner. When added at a presumably low amount, instead of forming patches from a few nucleations, Snf7 appears to bind immediately to the membrane. This suggests that the auto-inhibition mechanism is not fully conserved in PURE expressed Snf7. The same holds true for Vps24 in the flotation and SLB assay.

It should be considered that in the SLB assay, the incorporation of GreenLys might affect the folding and properties of the expressed protein. Snf7 binds to the membrane by electrostatic interactions of the lysine (K) amino acid [19]. The incorporation of the GreenLys could promote or inhibit binding of the Snf7 protein to the lipid membrane by either blocking it from membrane or by affecting autoinhibition. In Figure 5.16 the extent of lysines present in the 18-141 amino acid residue of Snf7 are depicted. Next to its influence in binding affinity, the combination with GreenLys might cause alterations in protein folding. The interaction between the two Snf7 • -helices highlighted in Figure 5.16B is mediated by a lysine. It has been hypothesized that GreenLys incorporation can modify this interaction and result in misfolding of the protein. Still, it can be argued whether GreenLys greatly influences membrane recruitment, as the GreenLys sidechain has

a size in the order of magnitude of a tryptophan residue. Additionally, only a certain percentage of the lysines in expressed proteins will be labelled by GreenLys as it competes with the unlabelled Lys-tRNA.

However, this does not explain the results of the floating assay in which no GreenLys was added (Figure 5.A). On the other hand, we do have in this case no insight into the dynamics of binding. There was no difference visible between addition and omission of Vps20• C, but the rate of recruitment might have been different and a point of saturation reached in both samples after the 30 minutes of applied incubation time. In summary, the results are not final but strongly indicate that the auto-inhibition of Snf7 and Vps24 is not present in the expressed proteins. This is supported by the results of two different methods. What can be confirmed is that the synthesized ESCRT proteins Vps20• C, Snf7 and Vps24 are able to bind to the membrane and that on their own.

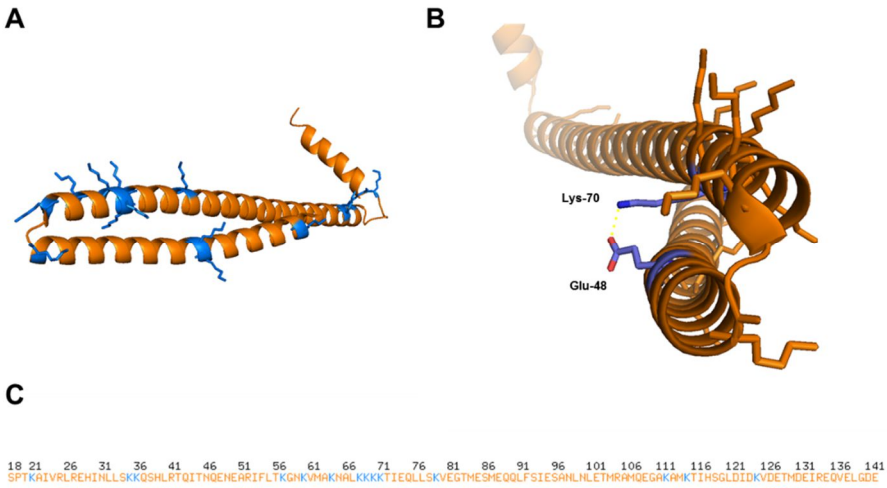

Figure 16: Visualisation of Snf7 protein residue 18-141. A. The Snf7 protein structure shown in orange with lysine residues coloured in blue. B. Zoom in of interaction between Lysine-70 and Glutamate-48 of the two Snf7 α-helices. C. Amino acid sequence of Snf7 residues 18 to 141. The lysine residues (K) is coloured in blue.

5.2.4 Cell-free expressed ESCRT-III proteins do not cause membrane budding on liposomes

We conducted an assay according to the protocol of Wollert et al. in which all four ESCRT proteins were added on the outside of liposomes. In our experiment, liposome swelling was performed in sucrose solution. In parallel, ESCRT proteins were expressed separately and added sequentially to the liposomes sample after swelling. Vps20• C, Snf7^{F}, Vps24, and Vps2 were added with incubations of 5 minutes in between to the liposomes in the given order. During and after the addition several liposomes were observed with a confocal microscope (Figure 5.17A). No budding events were observed and the number of intraluminal vesicles was not increasing. In the publication of Wollert et al. it is claimed that not all ESCRT proteins are required for budding. Moreover, it has been reported that although Snf7 alone is not able to perform vesicle budding it is able to deform the liposome membrane in drastic manners [15]. We decided therefore to co-express two of the

proteins Vps20• C and Snf7^{F} in presence of the liposomes. By reducing the number of proteins we can limit the competition for the expression machinery. Therefore, the yield of the two proteins should be in this case higher than if all four ESCRT-III proteins were to be expressed. Imaging started right after the expression solution that contained the DNA of Vps20• C and Snf7^{F} was added. Again, no budding events, membrane remodelling, or increase in number of intraluminal vesicles was detected (Figure 5.17B).

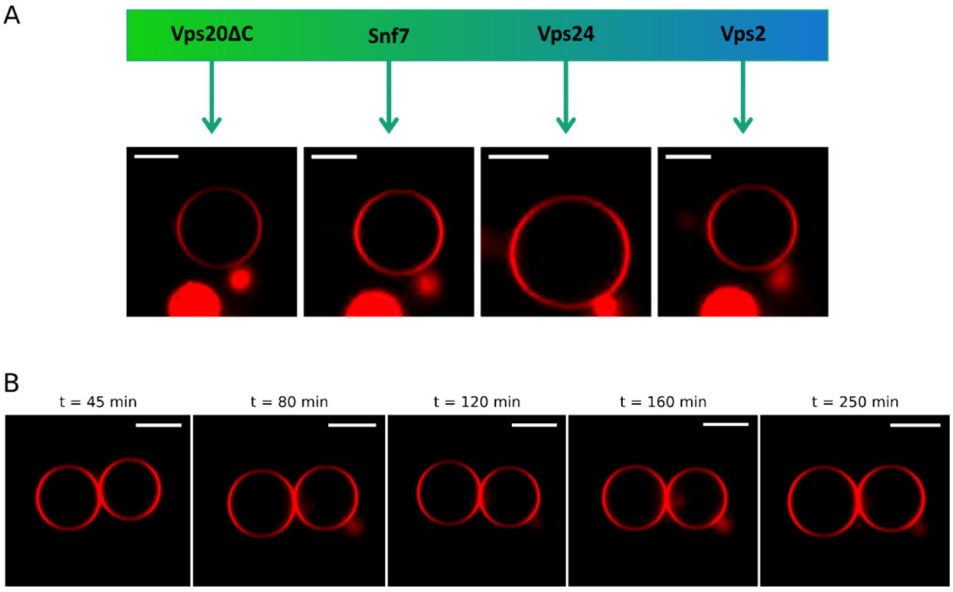

Figure 5.17: Sequential addition of the ESCRT-III proteins to liposomes. **(A)** Sequence of addition. Liposomes were incubated with Vps20• C, Snf7^{F}, Vps24, and Vps2 consecutively. After each protein was added the liposomes were incubated for 5 minutes before the addition of the next one. No budding events were observed. Scale bar = 5 µm. **(B)** Expression of Vps20• C and Snf7^{F} in presence of liposomes. Two liposomes (in red) are tracked over time. No signs of membrane deformation by co-expression of Vps20• C and Snf7^{F} were detected. Lipid composition was DOPC/DOPS at a ratio of 6:4. Scale bar = 5 µm.

After we detected and corrected the frameshift of Snf7, we repeated the experiment of sequential addition. In this case, however, we limited it to the addition of the first three proteins (Vps20• C, Snf7 and Vps24) and used PURE*frex*2.0 instead of 1.0 for the expression of the proteins. The yield of PURE*frex*2.0 is considerably higher than the one of its processor. Additionally, we added a dye right after the addition of the last ESCRT protein to the liposome solution to which all intact liposomes would be impermeable. If budding occurs, all generated intraluminal vesicles should be labelled with the dye. We could thus discern vesicles that have been generated after the addition of the ESCRT proteins from those which were already present inside of the liposomes beforehand. This allowed us to analyse a larger amount of liposomes over time. If the absence of vesicle budding in the previous experiments was a result of either too low protein concentrations, too few liposomes observed, or of the longer Snf7^{F} product than we should have now obeserved budding events to take place. Nevertheless, when we checked on the sample 90 minutes after the addition of the ESCRT

proteins, not a single labelled intraluminal vesicle was observed (Figure 5.18 and Figure 5.). Z-stacks of several liposomes were taken before and after the addition and in them no newly formed intraluminal vesicles were observed either.

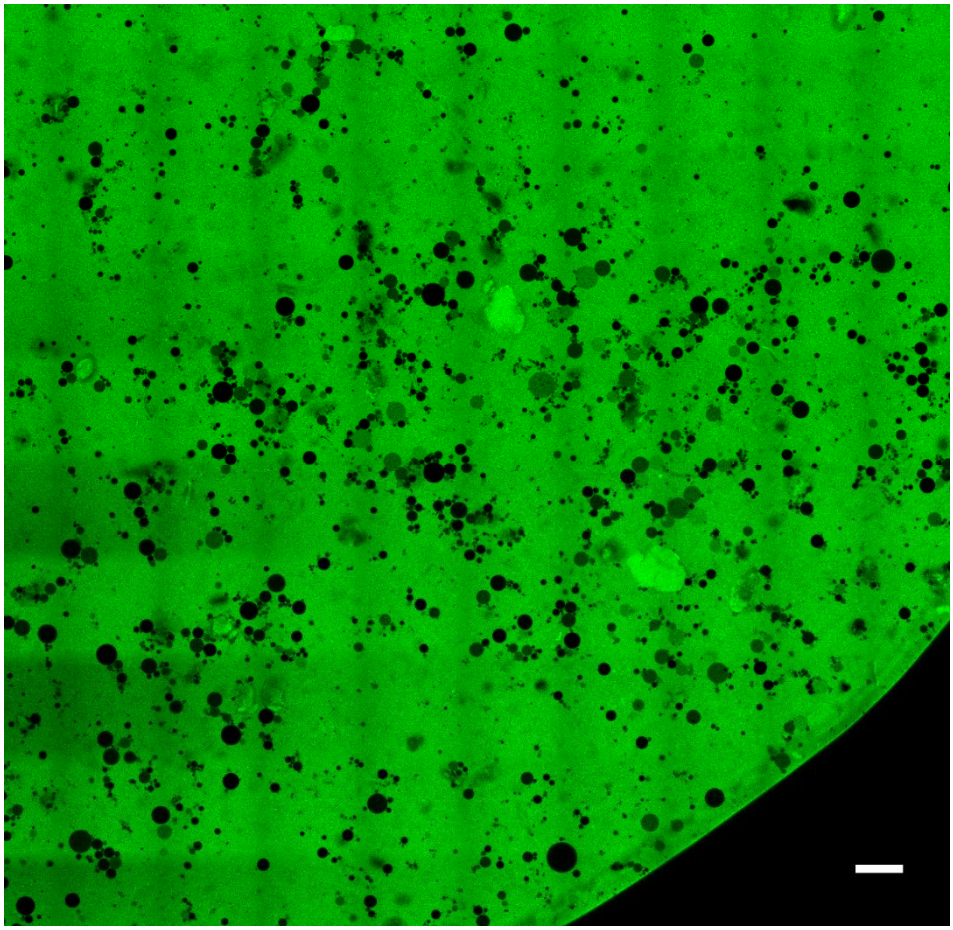

Figure 5.18: Addition of Vps20• C, Snf7 and Vps24 synthesized with PURE*frex*2.0 to liposomes. The three expression mixes have been added in the given order and with incubation breaks of 5 minutes. After the addition of Vps24, Alexa-488 dye was added to label the outside solution. Image of the Alexa-488 signal was taken 90 minutes after addition of the dye. Some of the liposomes where leaky and took up some of the outside solution or completely exchanged their content with it. A certain percent remained impermeable and can be seen as black circles. Any intraluminal vesicle containing the dye inside of such a liposome would indicate that it was formed after the addition of the dye and might have been the result of budding caused by the three ESCRT protein. In the depicted image, no such vesicles were detected. Lipid composition was DOPC/DOPE/DOPS at a ratio of about 10:7:2. Scale bar = 50 µm.

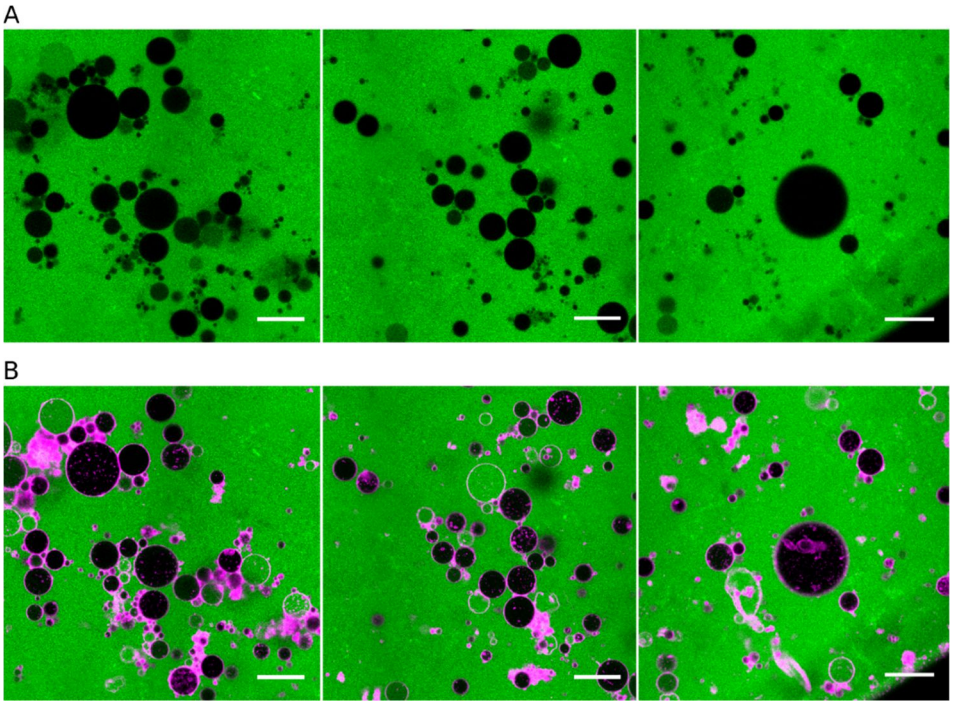

Figure 5.19: Close-up of Figure 5.18. On top is the dye channel and on the bottom the merge of dye and liposome signal. Scale bars = 20 µm.

None of the conditions tested yielded any indication for any membrane remodelling activity of the synthesized ESCRT proteins. From the assumptions we started with there would be two possible reasons for this. The first is that the proteins were active, but the conditions for membrane deformation were unfavourable. The creating of a bud for the formation of the vesicle requires to overcome the tension of the membrane. If the membrane tension in our experiments was too high, it might be impossible for a functional ESCRT system to generate vesicles. We do not have direct control of the membrane tension as is the case for example in experiments using micropipettes. Consequently, we cannot rule out that the membrane tension was too high. We do know, however, that under the second condition with PURE system inside and outside of the liposome, the membrane tension should be low and that the membrane can be deformed by filaments like bacterial or eukaryotic microtubules in the given condition. The second possibility is that some or all of the expressed ESCRT-III proteins are partly or completely non-functional. The only function that we can be entirely sure of to be present in the synthesized proteins is the capability to bind to membranes.

However, we do know by now that it would have been in fact highly unlikely to observe vesicle budding. As described in the introduction, it has become very clear towards the end of the project due to progress in the field that the ESCRT-III system is on its own not capable of generating budding and fission of vesicles. The collaboration with the lab of Philippe Baestiens ended shortly after it started as they ceased working on the ESCRT system due to low reproducibility. In fact, since the publication of Wollert et al. in 2009, no other lab has reported successful vesicle budding

in vitro by the ESCRT system. In experiments with bacterial microtubules we have observed accumulation of ILVs in liposomes in our samples under certain osmotic conditions. It is possible that the ILVs reported by Wollert et al. were as well the result of membrane remodelling due to osmotic pressure. The group of Hurley, who was one of the main authors, has by now retracted their claim that ESCRT-III on its own is sufficient for membrane budding and vesicle abscission. In a recent publication they are instead claiming that combining three of the ESCRT-III proteins and Vps4 can lead to scission of a membrane tube *in vitro* [26]. In this latter publication, a nanotube was pulled out from a GUV, which contained the ESCRT components, by optical tweezers. Upon light activation, caged ATP was released which together with Vps4 caused a pulling force on the bead and in some cases a severing of the membrane tube. However, there was no evidence presented that the ESCRT proteins formed a functional complex or that there was any specific constriction formed as observed *in vivo*. It was already reported before that Snf7 alone is able to deform the membrane of a liposome to the point of rupture of the liposome. Therefore, it might be that the increased tension observed was the result of unspecific membrane remodelling in the GUV and not the formation of a functional complex in the membrane tube. Moreover, the slow increase in membrane tension and the constriction of the whole membrane tube do not fit with the current model of ESCRT-III function in which the membrane is constricted rather rapidly at a narrow side [23].

In short, there is no final proof of the ESCRT system being capable to cause budding of the membrane and severing the vesicle the membrane neck *in vitro*. Moreover, even *in vivo* it is unclear if the ESCRT system is on its own able to perform these two steps necessary for vesicle generation. There is sufficient evidence that the ESCRT-III system combined with Vps4 is potent to cause the later. On the other hand, it might be that the ESCRT system is either not responsible for the initial budding of the membrane or that it requires cofactors like cargo proteins or lipid rafts [28]. Unlike in yeast, ILV genesis is only partly disrupted by deletion of ESCRT-III components in human cells [29] and there exist several ESCRT-independent mechanisms for ILV formation present in eukaryotic cells. One is for example based on the sphingolipid ceramide [30] and might also aid the ESCRT system during vesicle budding [31]. To conclude, if ESCRT system activity would be capable to trigger membrane budding in a minimal system is currently unclear.

5.2.5 Protein purification of Snf7

We faced the problem that, when we could not reproduce results reported in literature for purified ESCRT proteins with our synthesized ones, it was unclear if this was due to the conditions of the experiment or the properties of the expressed protein. Therefore, it was crucial to attain purified ESCRT-III proteins ourselves to use them as positive controls. Moreover, this would also have given us additional possibilities for labelling. First, we tried to express and purify the ESCRT-III proteins by using the original construct ESCRT-III plasmids we have received and the protocol for purification by Wollert et a. 2009, who allegedly used the same plasmids. These contained the sequence for a cleavable maltose binding protein (MBP) that can be used for purification and should avoid aggregation of the protein. However, purification failed for all four proteins (data not shown). Next, linear constructs of the ESCRT-III genes were prepared by PCR and inserted into the pRSET B expression vector for protein purification. Expression vectors of Vps20• C, Snf7, and Vps24 were transferred to RosettaTM(DE3) cells and IPTG added to induce protein expression. Overexpression of the corresponding proteins failed however in all three samples (Figure 5.20). It was concluded that the incubation conditions (20°C, 1 mM IPTG) were likely not ideal for overexpression of the

proteins. Therefore, several conditions were tested with the Snf7 vector at low cell culture volumes, including two different cell strains (RosettaTM(DE3) and C41(DE3)). Protein overexpression of both strains was induced with two different IPTG concentrations (1 mM and 0.2 mM IPTG) and at two different temperatures (37°C for 3 hours and 20°C overnight). Additionally, we tried again as well with the original construct of $Snf7^{F}$ coupled with a MBP.

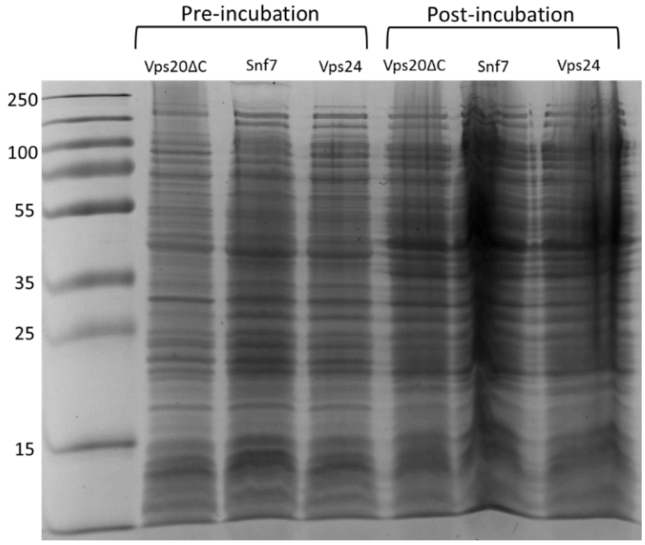

Figure 5.20: Protein gel of cell lysates before and after incubation under IPTG. Constructs of Vps20• C, Snf7, and Vps24 in pRSET B were expressed in RosettaTM(DE3) cells.

Figure 5. shows the eluates of the protein purifications from all incubation conditions. The eluate of Vps20• C purification is shown as a negative control. The red arrow shows where the Snf7 bands should be. The size of Snf7 is 27 kDa, but it has been found constantly up higher in protein gels (Figure 5.). In the C41(DE3) cells there are two faint bands that could represent the Snf7. Also, in the RosettaTM(DE3) incubated at 20°C overnight with 1 mM IPTG, a faint band can be found. To determine whether these bands are Snf7, a western blot was performed. ProteinA was used as a positive control for the western blot. In contrast to the proteinA, which was clearly visible on the gel, the five samples that were tested showed nothing (data not shown). From this result, it was concluded that the bands did not represent Snf7. Thus, Snf7 was either not expressed by the cells or completely lost during purification. It is known that ESCRT-III proteins tend to aggregate, which might have led to removal of Snf7 together with the cell debris. Eventually, after having tried these different conditions we decided to not continue our efforts to receive purified ESCRT proteins.

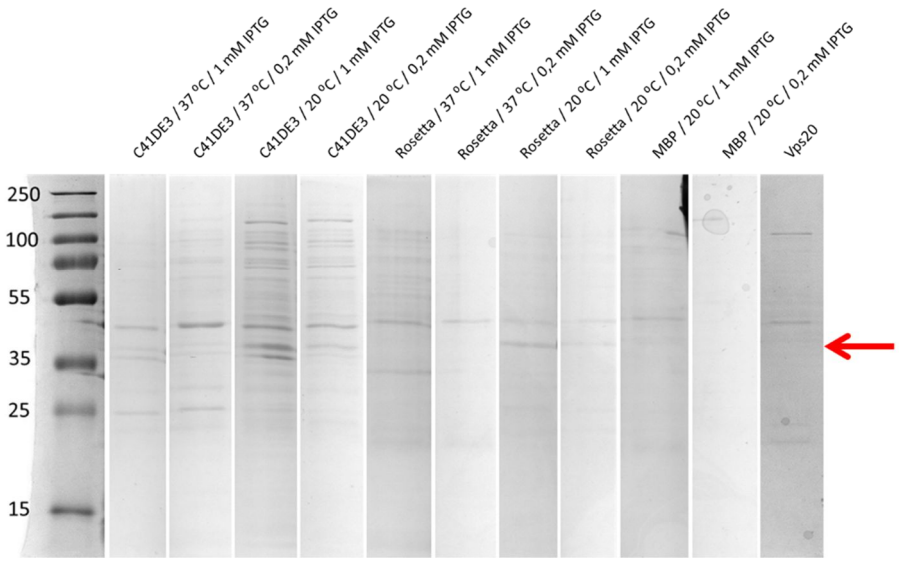

Figure 5.21: Eluates of the Snf7 purification from all incubation conditions. The eluate of the Vps20ΔC purification is used as a negative control. The red arrow marks the size where Snf7 bands are found in expression gels.

5.2.6 EM imaging reveals structures formed by synthesized Vps20• C and Snf7

It has been shown by electron microscopy that the ESCRT-III system forms spiral-like filaments on the surface of liposomes [15,16]. Accordingly, we have investigated by TEM if there are structures formed by the *de novo* synthesized proteins on liposomes membranes. Two different methods have been applied for the sample preparation. For the first attempt, we used liposomes with a DOPC/DOPS lipid composition generated by swelling from glass beads as done for the experiments described previously in section 5.2.4. Snf7 and Vps20• C were expressed by PURE*frex*. The liposomes were incubated with the expression mix of either Snf7 or Snf7 and Vps20• C in three different compositions (see materials and methods) for 20-25 minutes and were then added onto the EM grid. Staining was achieved by incubation with uranyl acetate. Sample quality was overall sub-standard and the number of liposomes per sample was very low, indicating that they did either not bind to the membrane of the grid or where mostly removed during the washing steps. The few observed liposomes did not show any filament structure or protein patterns (Figure 5.22). In the images the presence of many small dark dots in the background and on the liposomes is noticeable. These are probably constituents of the PURE system, most likely ribosomes as they contain rRNA to which the uranyl acetate can bind.

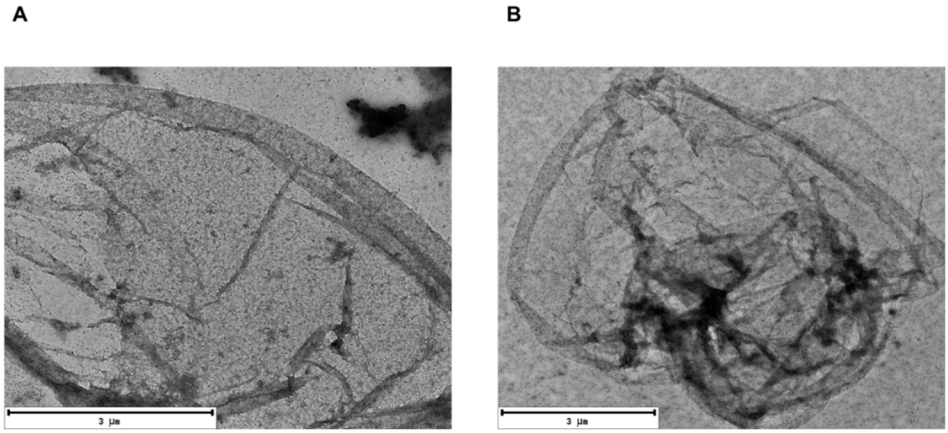

Figure 5.22: TEM images of liposomes incubated with ESCRT proteins expressed by PURE*frex*. A. Liposome incubated with expressed Snf7 and Vps20 (composition III). B. Liposome after incubation with only Snf7 (composition II). No signs of filament formation on the surface of the liposomes could be identified.

For the second condition, we created the liposomes by natural swelling combined with sonication and used PURE*frex*2.0 for the expression of the proteins. We observed in the sample with expressed Snf7 and Vps20• C, despite a suboptimal staining quality, structures on the liposomes that were distinctively different from what we observed in the other samples (Figure 5.24 and 5.32). These structures mostly resembled densely packed spirals or parallel filaments which were in immediate proximity to each other. The spirals were elongated and have average dimensions of 90 nm x 55 nm. These structures were not present in a sample in which only Snf7 was expressed (Figure 5.23).

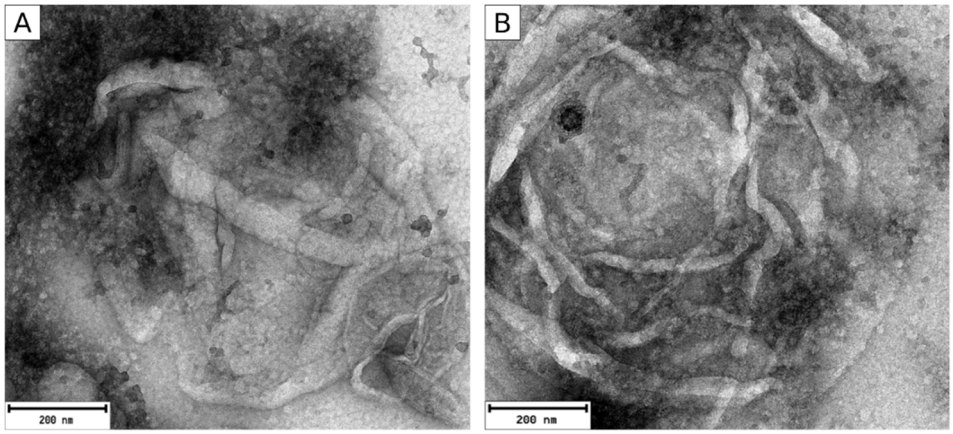

Figure 5.23: TEM images of liposomes incubated exclusively with Snf7 synthesized by PURE*frex*2.0. No filament-like structures are visible.

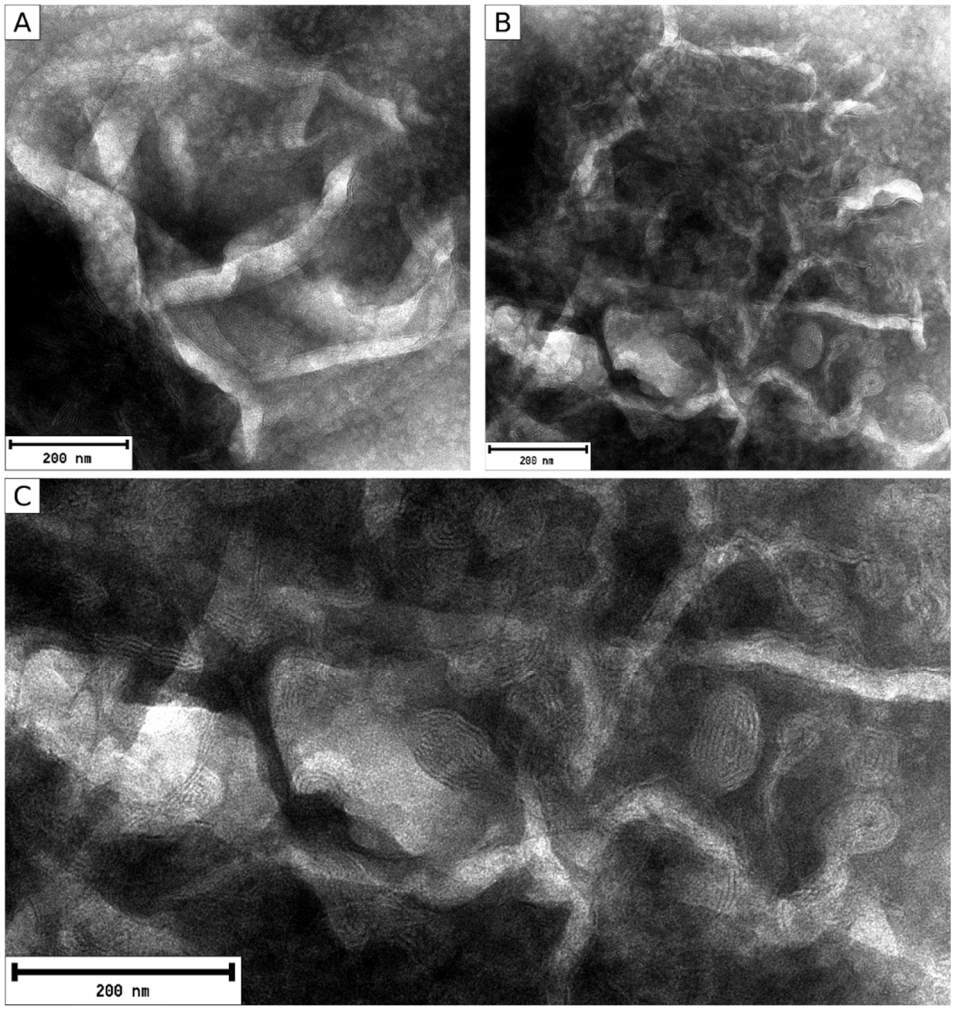

Figure 5.24: TEM images of liposomes incubated with Vps20• C and Snf7 synthesized by PURE*frex*2.0. A. Liposome displaying parallel filament structures. B and C. Liposome containing parallel and spiral filament structures, which can be seen in the magnification of the lower half of the liposome in picture C.

Plot analysis of the filament structures (Figure 5.) yielded a mean distance between filament peaks of 4.8 nm (± 0.4 nm). It is with the given sample quality not possible to infer an accurate diameter of the filaments themselves, but we would guess that it would range between 3.5 and 4.5 nm. Most of the filaments observed appear to be packed immediately next to each other. Overall, no single filaments could be detected, indicating that the filaments have a strong tendency to bond to each other. The reported diameter of Snf7 filaments is about 4.5 nm [14,15,19] and thus in the range of what we observed. Moreover, ESCRT-filaments can form tight interfilament bonds that results in a diameter of 9-10 nm of two adjacent filaments [14,15,19] which is the diameter we observed as well inside the structures. Hence, the observed filament size and distance fit overall quite well to

what is reported about the structural dimensions of connected ESCRT filaments. However, the spacing between the filaments of the spirals we observed is smaller than what was previously reported for Snf7 [15] or human CHMP4 [32]. Filament spiral reported by Chiaruttini et al. consist of rather loose filaments which are either single or double-stranded (Figure 5.25A. In comparison, the space between the filaments in our experiment is minimal and very even. Maybe this is due to the presence of Vps20• C in our condition, which might affect the spatial organisation of the filaments. It has for example been shown that Snf7 spirals when Vps2 and Vps24 are added as well display a stronger bundling of the filaments (Figure 5.25B)[16]. However, it cannot be ruled out that the observed filaments and spirals do not consist of Snf7, but solely of Vps20• C. Another cause might be differences in the buffer solution like pH or salt concentrations. The observation that Snf7 did not form complexes on the liposomes on its own is surprising. For once, because as mentioned it has been reported that Snf7 is capable of forming spirals on its own under similar conditions. Moreover, this might contradict the results described in 5.2.3 which indicated that autoinhibition is not present in the expressed proteins. The most forward explanation is that while membrane recruitment is not inhibited in the expressed proteins, subunit polymerization is still deactivated. It could be that unlike reported in literature, inhibition of membrane recruitment is in this case not directly linked with inhibition of polymerization. However, the fact that the EM results are based on single experiments prevents any firm conclusion for now.

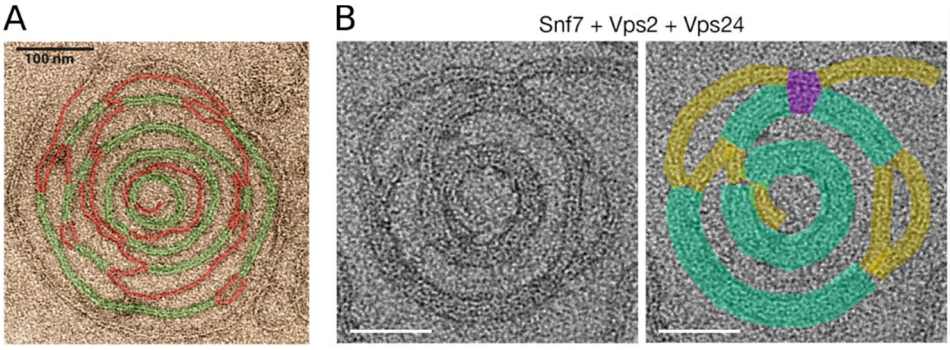

Figure 5.25: Previously reported EM images of ESCRT on liposome membranes. **(A)** Spiral consisting of Snf7 filaments. Single filaments are marked in red and double-stranded ones in green. Taken from Chiaruttini et al. 2015. **(B)** ESCRT spiral formed by Snf7, Vp2 and Vps24. Double-stranded filaments are marked in yellow and quadruple bundles in green. Scale bar = 50 nm. Taken from Mierzwa et al. 2017.

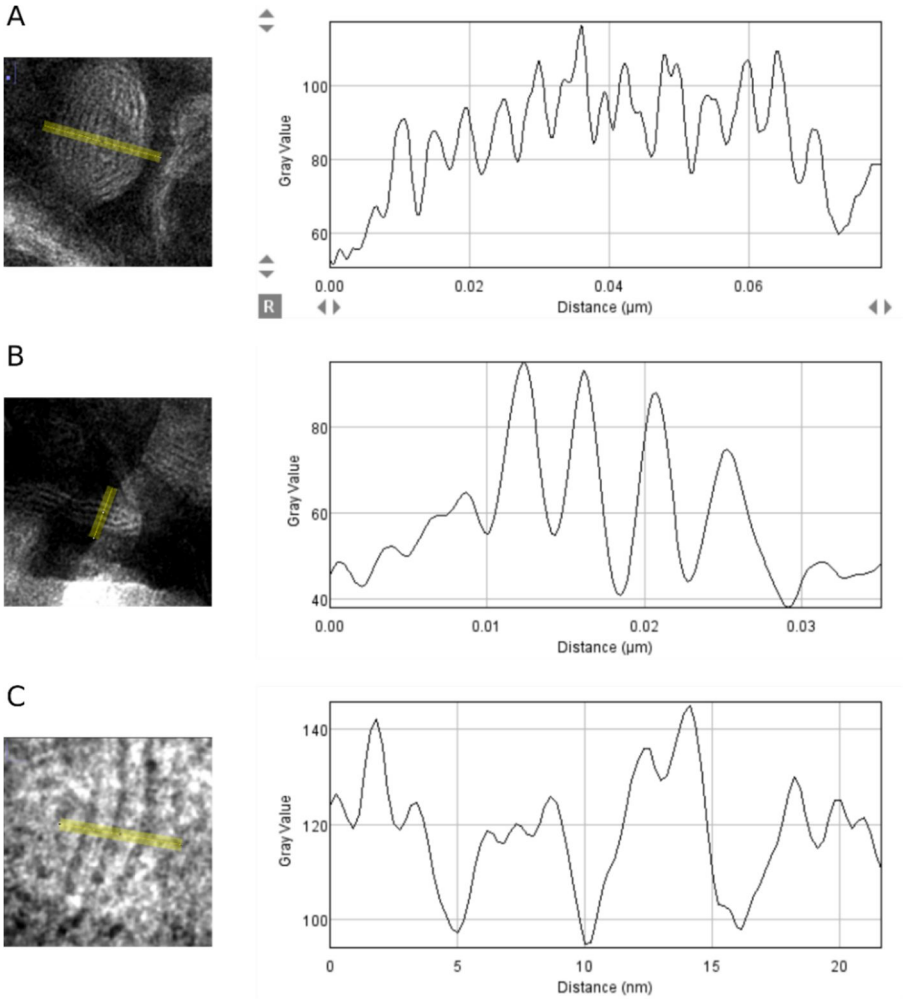

Figure 5.26: Plot analysis of filament structures. Examples of structures analysed with ImageJ plot analysis plug-in are given on the left with the respective plot profile on the right. A. Plot through a spiral. B. Plot through parallel filaments or elongated spiral. C. Plot through parallel filaments.

5.3 Conclusions

We were able to demonstrate that we can synthesize the four ESCRT-III proteins and Vps4 at full length with the PURE system and that at least three of the expressed ESCRT-III proteins are able to bind to lipid membranes. Further, our results indicate that expressed Vps20• C and Snf7 form a protein complex on lipid membranes similar, but not identical to what has been reported in literature. However, this evidence needs to be further verified. It also remains unclear to what degree membrane binding was the result of recruitment to a filament complex and if it was autoinhibited. Flotation and colocalization assays indicated that autoinhibition is not taking place in the expressed proteins. Moreover, even if the structures observed would later be confirmed to be ESCRT filaments, we still could not conclude that they inherited the confirmation and functionality of an active ESCRT complex. Overall, we faced the problem that we lacked purified proteins as a positive control, which made it difficult to investigate the properties of expressed proteins and if they were functional. This is especially true for Vps4. All we could do was to verify that Vps4 is expressed at full length. The only option we currently have to verify Vps4 activity is to it add to the EM liposome assay and check for changes in filament structure. However, it is not clear that these changes would be of major qualitative difference and conclusions might again be feeble without a positive control. Additionally, we currently lack a reliable method for reconstituting and reliably verifying complete ESCRT function, which means that even if our system would be completely functional we might not be able to detect it with the methods we currently have at hand. It is possible that ESCRT-III and Vps4 are on their own not able to form the evagination of the membrane as a first step of vesicle budding and in this case it would be necessary to create a membrane neck a priory to be severed by the ESCRT complex. If severing would be observed, it further would be important to reliably confirm the presence of an ESCRT complex at the abscission side by EM or super-resolution fluorescence microscopy in order to avoid attributing a functional ESCRT system to nonspecific effects or artefacts.

If the ESCRT system could be reconstituted by cell-free synthesis, it would offer two basic functions for application in a synthetic cell: the budding of vesicles from the liposome into the outside solution and finalization of division by severing of the membrane neck. In the context of a minimal cell, the excretion of vesicles would only be a sensible aim if it represents a form of asymmetrical division as in yeast. For this to be the case, the released vesicles must be able to potentially encapsulate a sufficient amount of the cell-machinery to exert all key functions for growth and replication. Considering the average size of ILVs formed by ESCRT *in vivo* it is doubtful that this would be the case. ILVs formed by the ESCRT system have a diameter of 20-30 nm in yeast [22] and 40-60 nm in human cells [33]. In comparison, the smallest verified bacteria are non-symmetrical with minimal diameters of 0.2 µm [34] and it is hypothesized that the minimal volumina for bacteria might be 0.013 μm^3 [35,36], which would mean about a 0.3 µm diameter in case of a sphere. On the other side, it might be that the ESCRT machinery can be tuned in regard of the size of vesicles formed as mutations in ESCRT genes resulted for example in increased vesicle diameters [22]. Nevertheless, even if the diameters could be increased to 0.3 µm, it would be still unlikely that a vesicle would contain enough components for reproduction. The rarity of bacteria with average diameters smaller than 0.5 µm indicates that it requires a certain degree of adaptation. The probability that any synthetic minimal system in the near future would be accurate enough to encapsulate exactly the number of components necessary for reproduction is more than unlikely. If we will create a minimal system, it will require a very tolerant setting that can compensate for its lack of precision and organisation compared to organisms that were fine-tuned

over extensive time periods by evolution. Vesicle diameters above 0.5 µm are therefore likely necessary to allow for a sufficient chance of encapsulating all necessary components. As a consequence of all these aspects, true division might be more achievable if another system is deforming the liposome into two compartments connected by a membrane neck, which could then be severed by the ESCRT complex. In this case, ESCRT function might depend on correct positioning, which might be achieved by preference to certain curvatures. Otherwise, a recruiter would be needed. Once the complex starts polymerizing in the membrane neck, it might orientate itself into the correct position to facilitate abscission. As reported in section 3.2.3 and in literature [37], liposomes encapsulating microtubules will in rare cases divide along the microtubule into a dumbbell shape. If this morphology could be enhanced, the ESCRT system could be utilized in the same manner as it acts in eukayotic cytokinesis. The ESCRT system could stabilize the membrane neck while the microtubules are depolymerized to allow for abscission of the membrane. However, this would be already a rather complicated process, requiring well timed transitions. Hence, it is not obvious that this would be a feasible mechanism for a minimal cell.

Another interesting candidate for asymmetrical division might be the viral protein VP40 which is involved in the release of the Ebola virus. It has been reported to be capable of inducing vesicle budding *in vitro* without any other cofactors [38]. The reported vesicle diameters vary and are partially rather large virions (up to about 2 µm) compared to Ebola virions. The mechanism of VP40 mediated budding is not known and therefore it is inconclusive how much the reported results *in vitro* reflect the situation *in vivo*. If it could be applied, a system consisting of a single protein would surely be advantageous compared to more complex multicomponent systems like ESCRT-III, as it would tend to require less organisation and resources. Nevertheless, if VP40 is a suitable candidate for a minimal division is unclear with the current amount of information available. Yet another candidate would be the Cdv system, which will be discussed in the next chapter.

5.4 Materials and Methods

Preparation of linear constructs

Linear constructs were obtained by PCR reactions of the four ESCRT-III genes, present in the Pet11a plasmid and of Vps4 in the pUC57 plasmid. PCRs were conducted with the reaction mixture displayed in Table 5.1 and utilizing the primers 25 ChD and 118 ChD for ESCRT-III proteins as well as 173 ChD and 365 ChD for Vps4. The Phusion polymerase (Finnzymes) was added last to the mix. The temperature settings are reported in Table 5.2. Afterwards, the PCR-generated linear constructs were purified by a PCR clean-up kit (Wizard® SV Gel and PCR Clean-Up System), provided by Promega according to the manufacturers protocol. Concentration and purity of the DNA constructs was determined by spectrophotometer measurement (NanoDrop 2000, Thermo Scientific) and they were checked for full length and side products by gel electrophoresis on 1% agarose gels.

Table 5.1: Components of PCR mixture.

Component	Amount (µL)	Concentration
5x HR buffer	10	-
MilliQ water	35.5	-
FW primer	1.0	10 µM
RV primer	1.0	10 µM
PCR Nucleotide mix	1.0	10 mM
DNA Template	1.0	1-10 ng/µL
Phusion polymerase	0.5	2 U/µL
Total volume	50	

Table 5.2: Applied PCR temperature cycle.

Step	Temperature (°C)	Time	Number of cycles
Initial denaturing	98	30 s	1
Denaturing	98	10 s	
Annealing	Min (Tm)	20 s	30
Elongation	72	1min/kb	
Final elongation	72	8 min	1

Correction of Snf7 construct and addition of a 6xHis-tag

A comparison of the construct we received from the Lab of Phillipe Baestiens and the wild-type Snf7 sequence revealed the deletion of an A-T pair, which caused a shift in the reading frame. In order to correct for the frameshift we performed a PCR reaction using primer 729 ChD and 730 ChD that were oriented tail to tail for transcription of the whole plasmid. Moreover, the 729 ChD primer contains a phosphorylated 5'-end and an additional single nucleotide for the addition of the missing base pair (Figure 5.5). The PCR was performed as described in the previous section, including an elongation time of 6 minutes and 30s. Next, 30 µL of PCR product were incubated at 37°C for 1 hour with 1 µL of DpnI (20 U/µL), 4 µL of Smartcut buffer and 5 µL of MilliQ water. The resulting sample was purified using the PCR clean-up kit. Hereafter, 7 µL of sample were incubated with 1 µL of ligase enzyme (3 U/µL), 1 µL of ligase buffer and 1 µL of MilliQ water for 6 hours at 20°C. This resulted in circular plasmids containing a corrected version of the Snf7 gene. The plasmids were transformed into an *E. coli* top10 bacteria strain and plated on an agar plates containing ampicillin (100 µg/mL) for overnight growth at 37°C. Colonies were picked and grown in LB medium with ampicillin at 37°C for 16 h. Finally, plasmids were extracted from the grown colonies, DNA concentration was measured and the plasmids were send for sequencing. The corrected plasmid was stored in glycerol solution and by PCR a linear fragment of the sequence was obtained for further experiments, applying primers 310ChD and 25ChD. C-terminal addition of the 6x-His tag was conducted by PCR as well. The forward primer was 731Chd for each reaction with the reverse primers 732ChD, 733ChD, 734ChD and 735ChD for Snf7, Vps2, Vps20• C and

Vps24, respectively. Otherwise, the procedure was identical to what has been conducted for the correction of the Snf7 construct, including PCR protocol, DpnI digestion and ligation.

In vitro transcription and translation

Cell-free expression for SDS-PAGE and other experiments was performed with PURE*frex* or PURE*frex*2.0 (GeneFrontier Corporation) according to the supplier's protocol and 5 nM of respective linear DNA. In case of subsequent gel analysis, 1 µl of GreenLys solution (FluoroTect™, Promega) was added. In other other experiments 1 µl of DnaK was added unless noted otherwise. For details, see Table 5.3. Gene expression conducted in PCR tubes incubated at 37°C for 3 hours with subsequent denaturing of the proteins with SDS and incubation at 90°C for 10 minutes.

Table 5.3: Expression mixes PUREfrex

Component	Standart	+ DnaK	+ GreenLys
B (solution I)	10 µl	10 µl	10 µl
E (solution II)	1 µl	1 µl	1 µl
R (solution III)	1 µl	1 µl	1 µl
DnaK	-	1 µl	-
GreenLys	-	-	1 µl
MilliQ water	7 µl	6 µl	6 µl
DNA construct	1 µl	1 µl	1 µl

Western Blot

An SDS-PAGE gel is made according to section 3.4. The gel was loaded with 10 µl of sample in a ratio of 5:4:1 of protein, Laemmli buffer, and DTT (100mM) respectively. Next, the gel was run and transferred to nitrocellulose at 1.3 A and 20 V for 10 min in Bio-Rad Trans-Blot TURBO. The program for high molecular weight proteins was used. Under shaking the blot membrane was blocked in 5% skim milk for 1 h, ensuing 1 hour of incubation with anti-His-HRP antibody (1:10,000 dilution). Hereafter, the blot was washed 3x for 10 minutes with TBS-T solution under shaking. Finally, 5 mL 1:1 mix of Supersignal West Pico Stable Peroxide Solution and Supersignal West Pico Enhancer Solution was pipetted onto the membrane blot and it incubated for 5 minutes at room temperature. For imaging of the Blot, a Biorad Gel Imager was used. Western Blot analysis and band quantification has been conducted with ImageQuant TL.

Flotation assay

The flotation assay protocol was based on a previously described protocol by Loose et al. [39]. First, lipid vesicles were generated. Therefore, the lipid mixture described in Table 5. was desiccated and the lipid film was rehydrated with 63 µl of 1x G-buffer under vortexing for 2-3 minutes and 5 minutes of sonication. This results in 10 µg/µl lipid mixture of vesicles. As a next step, a 40-µl PURE*frex* expression mix of the corresponding protein was expressed for 3 hours at 37°C and 10 µl of the vesicle emulsion added. For the combination of Snf7 and Vps20, the vesicle mix is first incubated with 5 µl expression mix of Vps20• C for 5 min at 25°C and then 35 µl of Snf7 expression mix added. Samples were incubated at 25°C for 30 min in a heat block and subsequently centrifuged for 2 minutes at 20.000 g. This resulted in a pellet of lipids formed on top

of the solution as the vesicles were lighter than the PURE*frex* solution. About 47 µl were removed from under the pellet (bottom fraction) and the pellet (lipid fraction) resuspended in 11.5 µl MilliQ water, DTT (final concentration of 10 mM) and SDS buffer to a final volume of 15 µl for loading onto the gel. Of the bottom fraction, 11,5 µl were combined with DTT and SDS buffer as described before. In case of Vps20• C and Vps24 an additional washing step was performed to further remove background. Therefore, 50 µl of 1x G buffer (=10x diluted G buffer, see 2.5) were added to the lipid fraction of Vps20• C and 100 µl to the one of Vps24. The lipid fraction was then spun down for 2 minutes at 20.000 g. In this case, a pellet formed at the bottom of the tube due to the lower density of the 1x G buffer. Samples were run on a 12% SDS-protein gel according to section 3.4.

Table 5.4: Lipid composition for flotation assay

Lipid	Mol%	Concentration (g/l)	Volume (ul)
DOPC	~ 60	10	37,5
DOPS	~ 40	10	25
DHPE-Texas Red	-	1	3

Binding to SLB

First, the surface of washed glass chambers was activated by oxygen plasma treatment (basic plasma cleaner, Harrick Plasma) for 15 min. Directly after plasma cleaning, 6 µl SUV solution and 12 µl 6 mM $CaCl_2$ were added to the chamber. The chamber was covered with a coverslip, placed on a 0.5 mm thick adhesive silicone sheet (Life Technologies), and incubated for 30 minutes at 37°C. After incubation, the formed SLB was washed four times with MRB80 buffer (80 mM K-Pipes, 4 mM MgCl2, 1 mM EGTA). The respective proteins were expressed as described before under addition of GreenLys, with the only deviation being that a 10x lower concentration of GreenLys was used. Expression mixes were added to the chamber and the sample imaged either by confocal or TIRF microscopy. In case of the experiment in which the estimated concentrations of 0.7 µM and 1.4 µM of Snf^{GL} were applied, the Snf7 expression mix was diluted with PURE*frex* buffer (solution I and MilliQ water in a ratio of 1:1) in a ratio of 3:7 for 0.7 µM and 3:2 for 1.4 µM.

Liposome budding assay

Two different methods were applied for the preparation of liposomes. For the first method, glass beads (212-300 µm) were poured into a clean beaker. The beads were spread out over the surface to create a single layer and were heated to approximately 50°C. Then, the lipid mix (DOPC/DOPS) listed in Table 5.5 was added to the beads in a dropwise manner. Hereafter, the beaker with the lipid-coated beads was desiccated for one hour. Finally, the beads were flushed with argon and stored at -20°C. The swelling of liposomes occured in 50 µl of a 0.5 M sucrose solution, to which 15 µg of lipid beads were added. Sucrose is used as swelling solution as it is a polar, non-charged disaccharide known to produce desirable liposomes and to counter the osmolarity of the PURE system. Swelling occurred for two hours put on ice, after which the sample was diluted 1:1 with 0.5 M sucrose solution and added to the imaging chamber.

Table 5.1: Lipid compositions for first liposome swelling method.

Lipid	Mol%	Concentration (g/l)	Volume (ul)
DOPC	~ 60	10	75
DOPS	~ 40	10	50
DHPE-Texas Red	-	1	12
DSPE-PEG-biotin	-	10	4

Lipid bead preparation and liposome swelling for the second method were conducted with the same technique as described in detail in section 4.4. The lipid mixture shown in Table 5.6Table 5.2 was prepared in a 10 mL round-bottom flask. Next, 254 µl of 100 mM rhamnose and 0.6 g of 425 - 600 µm glass beads were added. The chloroform was removed by rotary evaporation (200 mbar, 2 hours, RT) after which the beads were desiccated and stored under argon at -20°C. For the swelling of liposomes, 20 mg of the lipid-coated beads were added to the swelling solution, which consisted of the complete PURE*frex*2.0 expression mix without DNA. The swelling solution which was incubated for 2 hours on ice and subsequently underwent four freeze-thaw cycles.

Table 5.2: Lipid compositions for second liposome swelling method.

Lipid	Mol%	Concentration (g/l)	Volume (ul)
DOPC	50	10	101.6
DOPE	36	10	67.1
DOPG	12	10	23,2
Cardiolipin	2	10	8
Texas Red	0,2	1	10
PEG-biotin	0,26	10	2

As described in 3.4, a glass chamber was washed and sequentially incubated for 5 minutes with a solution of BSA and BSA-biotin (1:1 molar ratio, 1 mg/mL) and with Neutravidin (1 mg/mL) to later immobilize the biotinylated liposomes. For addition of proteins to the sample, three approaches were explored. The sequential approach comprises addition of the four pre-expressed ESCRT-III proteins to the liposomes which were incubated with each protein for 5 min at room temperature. The order of addition was Vps20• C, Snf7, Vps24, and then Vps2 with volumes of 1 µl, 4.2 µl, 1.4 µl and 1.4 µl added respectively. The ratios between the aforementioned volumes were derived from Wollert et al. [21]. Here, the assumption has been made that equal concentrations of each protein were expressed. Co-expression of Vps20• C and Snf7 are PUREfrex co-synthesized in situ, outside immobilized liposomes prepared by the first method. Here, 0.72 µl of linear Vps20• C (25 ng/µl) and 3.0 µl linear Snf7 (50 ng/µl) were added to the liposome expression mix. The mixture was supplemented to the chamber and expression in presence of immobilized liposomes was observed for 3 hours. In both experiments, proteins were expressed with the standard PURE*frex* mix shown in Table 5.3 and liposomes were prepared by the first method. The samples were

incubated at room temperature. The experiment conducted with addition of Vps20• C, Snf7 and Vps24 expressed by PURE*frex*2.0 was conducted as described in section 4.4. Liposomes were added to the chamber, which was kept at 30°C. Then 10 µl Vps20• C, 15 µl Snf7, 10 µl Vps24, and 0.75 µl Alexa-488 dye were added sequentially with 5 minutes of incubation time in between except for the dye which was immediately added. When the next solution was added, the corresponding amount of solution was removed beforehand from the chamber. For all experiments a confocal microscope (Nikon A1R) was used.

Protein purification

For protein purification, the purified plasmids were transformed into RosettaTM(DE3) competent cells and into C41(DE3) cells. RosettaTM(DE3) cells were grown on plates containing ampicillin and chloramphenicol (both 100 µg/mL). The C41(DE3) cells were grown on ampicillin (100 µg/mL) plates. A colony was grown in 20 mL LB-medium with the corresponding antibiotics (100 µg/mL). At OD600 of 0.6 - 0.9, expression was induced with 1 mM or 0.2 mM Isopropyl-• -D-thiogalactopyranosid (IPTG). The cultures were either incubated for 3 hours at 37°C or overnight at 20°C (both in shaker incubator at 250 rpm). After pelleting down the cells, they were resuspended in lysis buffer (ESCRT proteins: 20 mM Hepes, 100 mM NaCl, pH 8.0). The cells were lysed using sonication (Qsonica Sonicators, PTS technics), 10 sec pulse, 30 sec rest, 30% amplitude, 10 cycles. After spinning down at 16.000 g for 20 min at 4°C, the supernatant was applied to a QIAGEN Ni-NTA column. The column was then washed twice with a washing buffer with low concentration imidazole (20 mM Hepes, 100 mM NaCl, 10 mM imidazole, pH 8.0). Next, the proteins were eluted in an elution buffer with high concentration imidazole (20 mM Hepes, 100 mM NaCl, 100 mM imidazole, pH 8.0). Since imidazole can affect the activity of the proteins, the buffer is exchanged with a desalting column from Thermo Fisher. The buffer that is used for the exchange is 50 mM Hepes/KOH, 100 mM K-glutamate, 6 mM $Mg(OAc)_2$, 7 mM • -ME, pH 7.6. This product was further purified by applying it to a QIAGEN Ni-NTA column.

Sample preparation for TEM imaging and analysis

The first condition for TEM imaging was conducted with liposomes generated by natural swelling from glass beads and with expression of ESCRT proteins by PURE*frex*. Glass beads were coated with a lipid mix of 60% DOPC, 40% DOPS and a fraction of DHPE-Texas Red as described for the first method of the liposome budding assay. Swelling took place for 2 hours after addition of 20 µL of 1x G buffer (=10x diluted G buffer, see section 2.4) to 15 mg of coated beads. Gene expression of Vps20• C and Snf7 were conducted as described in section 4.4. After the swelling, the liposomes were diluted by 1x G buffer and for the respective samples Vps20• C was added and incubated for 5 minutes at RT. Next, Snf7 was added and the sample incubated for 20 minutes at RT. Five conditions were exploited, but only three yielded samples on which liposomes were found. These three conditions are listed in Table 5.7. TEM grids (Carbon support films, grids: Cu 400) were plasma cleaned for 90 seconds and each grid incubated with 3 µL of sample for 1 minute. Hereafter, the sample was washed 3x in MilliQ water drops and dried with filter paper. Finally, each sample was incubated with 3 µL of uranyl acetate for 30 s, while residual was removed by filter paper. The grids were imaged with a JEM-3200 FSC.

Table 5.7: First compositions of liposome samples for TEM.

Components	Compositions		
	I	II	III
Liposomes	4 µl	1 µl	4 µl
1x G buffer	2 µl	5 µl	3.5 µl
Snf7	4 µl	4 µl	1.5 µl
Vps20• C	-	-	1 µl

In the second condition for TEM imaging we utilized liposomes generated by vortexing and size extrusion. The proteins, Vps20• C and Snf7 were synthesized with PURE*frex*2.0 according to the protocol in section 4.4. Composition of the lipids was the same as in Table 5.5 except for Texas Red (DOPC, DOPE, DOPG, Cardiolipin). Lipids were added to vial and dried first under Argon flow and subsequently in the desiccator for 30 minutes. The lipid pellet was rehydrated in 800 µl 0.6 M sucrose to a final concentration of 1.25 mg/ml. Small Unilamellar Vesicles (SUVs) were obtained by vortexing for about 2 minutes. Subsequently, GUVs and aggregates were removed from the emulsion by extrusion through a 0.4 µm pore size membrane with 11 passages.

Two conditions were tested. One with only expressed Snf7 and another one with expressed Snf7 and Vps20• C. Both samples were incubated for 20 minutes at 30°C to facilitate polymerization and binding to the liposomes. Grids were made slightly hydrophilic through plasma cleaning for 10 seconds. The grids were incubated for 10 min with 4 µl of the solutions, and washed with MilliQ water twice. Excess liquid was removed with filter paper and the samples stained with 4 µl 2% uranyl acetate for 1 minute. After drying the samples again with filter paper, they were imaged on a JEOL JEM-1400 plus. Plot analysis was performed with the ImageJ plot analysis plug-in. Beforehand, a Gaussian blur filter was applied to reduce noise.

Table 5.8: Second compositions of liposome samples for TEM.

Components	Compositions	
	I	II
Liposomes	4 µl	10 µl
Snf7	10 µl	8 µl
Vps20• C	-	2 µl

5.5 Supplementary information

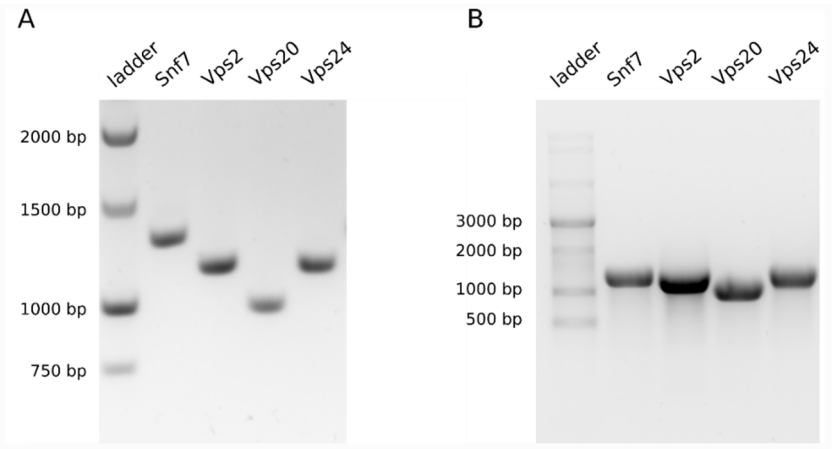

Figure 5.27: Check of ESCRT-III DNA constructs and RNA transcripts on 1% agarose gels. A. Linear DNA constructs of the ESCRT-III system. B. RNA transcripts transcribed by the viral T7 polymerase.

Table 5.9: Primer list for ESCRT experiments

Primer	Description	Sequence
25 ChD	Pet11a RV	GATGCTGTAGGCATAGGCTTGG
118 ChD	Pet11a FW	GAATGGTGCATGCAAGGAGATG
173 ChD	pUC57 RV	CACACAGGAAACAGCTATGAC
310 ChD	Pet11a FW	GGATCTCGACGCTCTCCCTTATG
365 ChD	pUC57 FW	CAGTCACGACGTTGTAAAACGAC
729 ChD	snf7 correction FW	(P)-AATGGGGCTTTGAGCGGCCG
730 ChD	Snf7 correction RV	TCTGCTTGTAGTTCTCTTAATGCTTTTTCATCTTCATCT
731 ChD	FW addition of HIS-tag	(P)-TGAGCAATAACTAGCATAACC
732 ChD	add. HIS-tag Snf7 RV	CTAGTGGTGATGGTGATGATGTCCACCTCCAAGCCCCATTTCTGCTTGTAGTTC
733 ChD	add. HIS-tag Vps2 RV	TCAGTGGTGATGGTGATGATGACCTCCACCAGTCTGCTTCTTCAAAGTGTTCAAC
734 ChD	add. HIS-tag Vps20• C RV	CTAGTGGTGATGGTGATGATGTCCACCTCCATTGAGTTCACTTTCGAGAGCATCC
735 ChD	Add. HIS-tag Vps24 RV	TCAGTGGTGATGGTGATGATGTCCACCTCCGTTTTGCAAAGCTCTCAGCCTTTC

Table 5.10: Estimated Snf7 concentrations from western blots.

Experiment	Measured concentration (µM)
I	1.80
	2.79
II	1.55
	2.20
	2.31
III	3.14
	2.57
	2.95
Mean	2.41

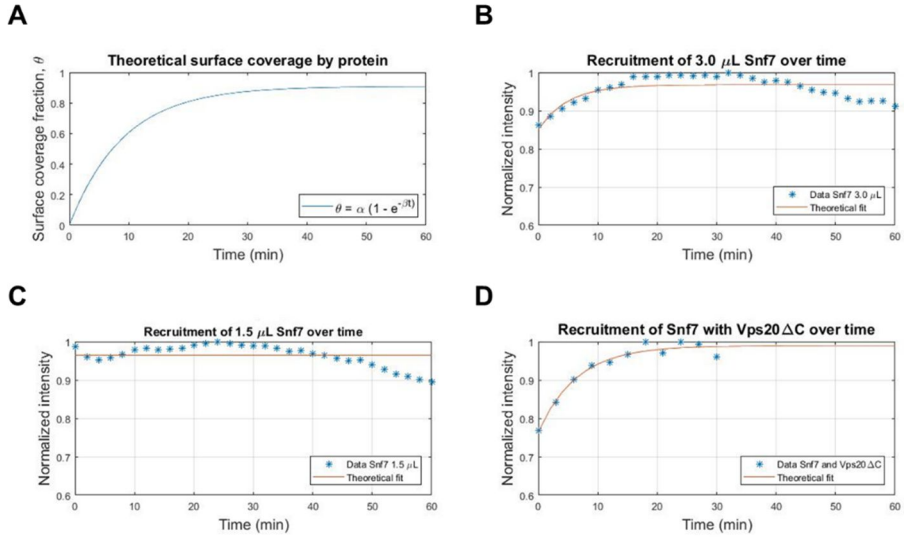

Figure 5.28: Fit of Snf7GL recruitment to a lipid membrane over time. A. The theoretical curve of surface coverage has been calculated for ka = 0.2 s^{-1}, kd = 0.01 s^{-1} and [P] = 0.5 M. B. Normalized intensity for 3.0 µl of Snf7 (=1.4 µM) in blue and the theoretical fit in red C. Normalized intensity for 1.5 µl of Snf7 (=0.7 µM) in blue and the theoretical fit in red D. Normalized intensity for 3 µl of Snf7 (=1.4 µM) and 1.5 µl of Vps20C in blue and the theoretical fit in red.

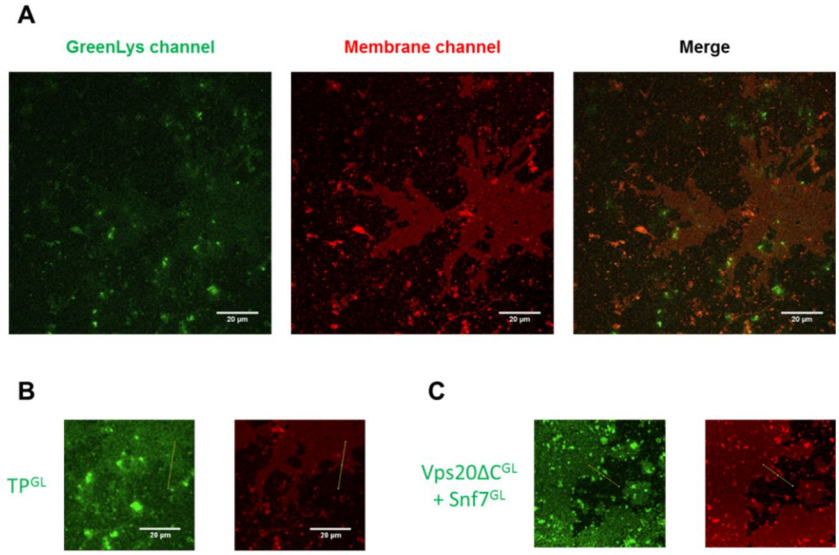

Figure 5.29: Confocal microscopy of TP^{GL} membrane recruitment. A. TP^{GL} signal co-localizes with the membrane signal. B./C. A yellow line is drawn from the membrane to the glass surface. The intensity profile on this line is measured for TP^{GL} and Vps20• C^{GL} + $Snf7^{GL}$. Intensity profiles are made for both membrane and protein channel. Scale bar = 20 µm.

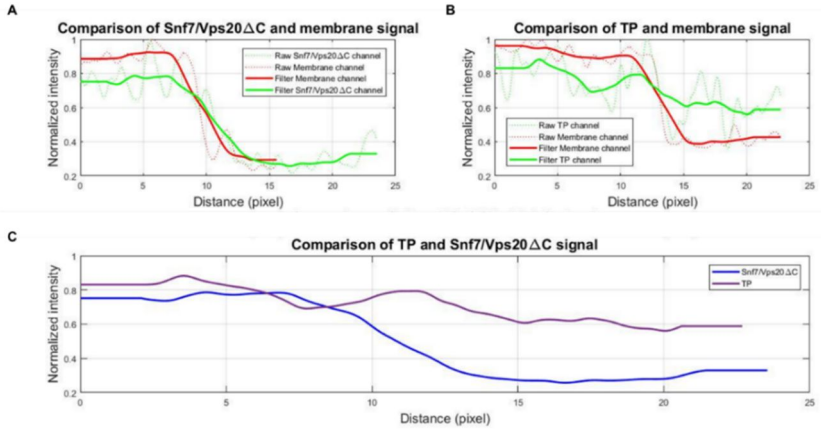

Figure 5.30: Comparison between membrane recruitment of TP^{GL} and $Vps20C^{GL}$ + $Snf7^{GL}$. A. Dashed raw membrane (red) and protein (green) data are smoothened by the Savitsky Golay filter. A comparison is made between the membrane signal and protein signal of Vps20• C^{GL} + $Snf7^{GL}$. B. Dashed raw membrane (red) and protein (green) data are smoothened by the Savitsky Golay filter. A comparison is made between the membrane signal and protein signal of TP^{GL}. C. Comparison of TP^{GL} (purple) signal and $Snf7^{GL}$ + Vps20• C^{GL} (blue) signal.

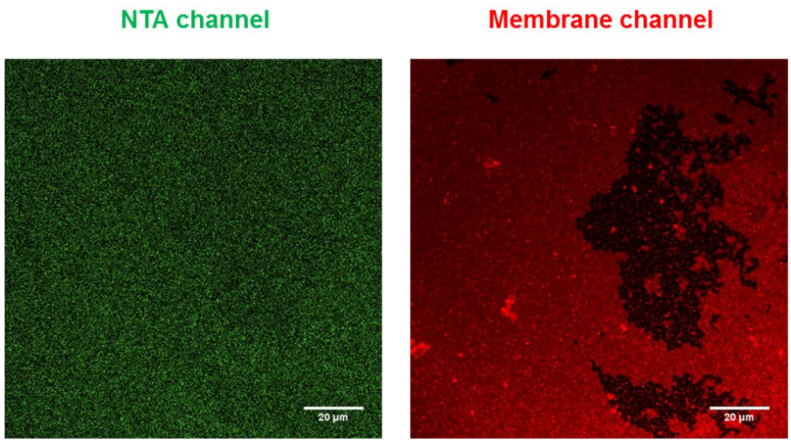

Figure 5.31: Snf7-His and 488-NTA dye on SLB membrane. No colocalization of the dye and the membrane was observed.

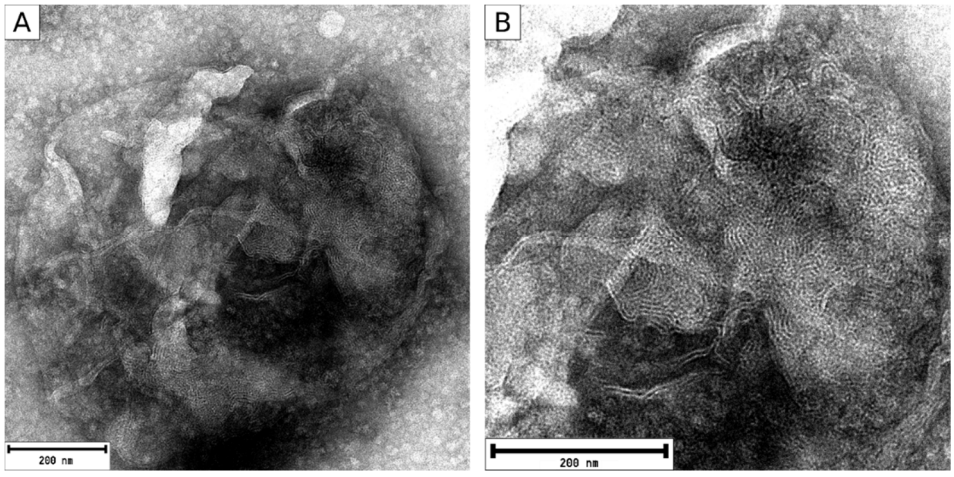

Figure 5.32: TEM images of liposomes incubated with Vps20• C and Snf7 synthesized by PURE*frex*2.0. Image B is a magnification of image A.

Sequence of *vps4* (including T7 promotor and terminator)

TAATACGACTCACTATAGGGGAATTGTGAGCGGATAACAATTCCCCTCTAGAAATAATTTTGTTT
AACTTTAAGAAGGAGATATAGATATGAGCACGGGAGATTTTTTAACTAAGGGAATCGAGCTGGT
TCAGAAAGCGATTGACCTGGATACCGCGACCCAATACGAAGAAGCGTACACCGCGTACTACAAC
GGCCTGGACTACCTGATGCTGGCGCTGAAGTATGAGAAAAACCCGAAAAGCAAGGACCTGATCC
GTGCGAAGTTTACCGAGTACCTGAACCGTGCGGAACAACTGAAAAAGCACCTGGAAAGCGAGG
AAGCGAACGCGGCGAAAAAGAGCCCGAGCGCGGGTAGCGGCAGCAACGGTGGCAACAAGAAA
ATCAGCCAAGAAGAGGGTGAAGATAACGGTGGCGAGGACAACAAAAAGCTGCGTGGTGCGCTG

AGCAGCGCGATTCTGAGCGAGAAACCGAACGTTAAGTGGGAAGACGTGGCGGGTCTGGAGGGT
GCGAAAGAGGCGCTGAAAGAGGCGGTTATTCTGCCGGTTAAATTCCCGCACCTGTTCAAGGGTA
ACCGTAAACCGACCAGCGGTATTCTGCTGTACGGTCCGCCGGGCACCGGTAAAAGCTACCTGGC
GAAGGCGGTGGCGACCGAAGCGAACAGCACCTTCTTCAGCGTTAGCAGCAGCGATCTGGTTAGC
AAATGGATGGGCGAGAGCGAAAAGCTGGTGAAACAGCTGTTCGCGATGGCGCGTGAAAACAAA
CCGAGCATCATTTTTATCGACGAGGTTGACGCGCTGACCGGCACCCGTGGTGAAGGTGAAAGCG
AGGCGAGCCGTCGTATCAAAACCGAGCTGCTGGTGCAGATGAACGGCGTTGGTAACGATAGCCA
AGGTGTTCTGGTGCTGGGTGCGACCAACATCCCGTGGCAGCTGGATAGCGCGATTCGTCGTCGTT
TCGAACGTCGTATCTACATCCCGCTGCCGGACCTGGCGGCGCGTACCACCATGTTTGAGATCAAC
GTGGGTGATACCCCGTGCGTTCTGACCAAGGAAGACTACCGTACCCTGGGTGCGATGACCGAAG
GTTATAGCGGCAGCGATATTGCGGTTGTGGTTAAAGACGCGCTGATGCAGCCGATTCGTAAGAT
CCAGAGCGCGACCCACTTCAAGGATGTGAGCACCGAAGACGATGAGACCCGTAAACTGACCCCG
TGCAGCCCGGGCGACGATGGTGCGATCGAGATGAGCTGGACCGACATCGAAGCGGATGAGCTG
AAGGAACCGGATCTGACCATTAAAGACTTCCTGAAGGCGATTAAAAGCACCCGTCCGACCGTTA
ACGAGGACGATCTGCTGAAACAGGAACAATTTACCCGCGATTTTGGTCAGGAAGGCAACTAATG
AGCAATAACTAGCATAACCCCTTGGGGCCTCTAAACGGGTCTTGAGGGGTTTTTTG

References

[1] Katzmann DJ, Babst M, Emr SD. Ubiquitin-Dependent Sorting into the Multivesicular Body Pathway Requires the Function of a Conserved Endosomal Protein Sorting Complex, ESCRT-I. Cell 2001;106:145–55.

[2] Babst M, Katzmann DJ, Snyder WB, Wendland B, Emr SD. Endosome-Associated Complex, ESCRT-II, Recruits Transport Machinery for Protein Sorting at the Multivesicular Body. Dev Cell 2002;3:283–9.

[3] Babst M, Katzmann DJ, Estepa-Sabal EJ, Meerloo T, Emr SD. ESCRT-III: An endosome-associated heterooligomeric protein complex required for MVB sorting. Dev Cell 2002;3:271–82.

[4] Garrus JE, von Schwedler UK, Pornillos OW, Morham SG, Zavitz KH, Wang HE, et al. Tsg101 and the vacuolar protein sorting pathway are essential for HIV-1 budding. Cell 2001;107:55–65.

[5] Votteler J, Sundquist WI. Virus budding and the ESCRT pathway. Cell Host Microbe 2013;14:232–41.

[6] Loncle N, Agromayor M, Martin-Serrano J, Williams DW. An ESCRT module is required for neuron pruning. Sci Rep 2015;5:8461.

[7] Jimenez AJ, Maiuri P, Lafaurie-Janvore J, Divoux S, Piel M, Perez F. ESCRT Machinery Is Required for Plasma Membrane Repair. Science (80-) 2014;343:1247136.

[8] Raab M, Gentili M, de Belly H, Thiam H-R, Vargas P, Jimenez AJ, et al. ESCRT III repairs nuclear envelope ruptures during cell migration to limit DNA damage and cell death. Science (80-) 2016;352:359 LP – 362.

[9] Webster BM, Colombi P, Jager J, Lusk CP. Surveillance of nuclear pore complex assembly by ESCRT-III/Vps4. Cell 2014;159:388–401.

[10] Olmos Y, Carlton JG. The ESCRT machinery: new roles at new holes. Curr Opin Cell Biol 2016;38:1–11.

[11] Christ L, Raiborg C, Wenzel EM, Campsteijn C, Stenmark H. Cellular Functions and Molecular Mechanisms of the ESCRT Membrane-Scission Machinery. Trends Biochem Sci 2017;42:42–56.

[12] Guizetti J, Schermelleh L, Mantler J, Maar S, Poser I, Leonhardt H, et al. Cortical constriction during abscission involves helices of ESCRT-III-dependent filaments. Science 2011;331:1616–20.

[13] Goliand I, Adar-Levor S, Segal I, Nachmias D, Dadosh T, Kozlov MM, et al. Resolving ESCRT-III Spirals at the Intercellular Bridge of Dividing Cells Using 3D STORM. Cell Rep 2018;24:1756–64.

[14] Henne WM, Buchkovich NJ, Zhao Y, Emr SD. The endosomal sorting complex ESCRT-II mediates the assembly and architecture of ESCRT-III helices. Cell 2012;151:356–71.

[15] Chiaruttini N, Redondo-Morata L, Colom A, Humbert F, Lenz M, Scheuring S, et al. Relaxation of Loaded ESCRT-III Spiral Springs Drives Membrane Deformation. Cell 2015;163:866–79.

[16] Mierzwa BE, Chiaruttini N, Redondo-Morata L, von Filseck JM, Konig J, Larios J, et al. Dynamic subunit turnover in ESCRT-III assemblies is regulated by Vps4 to mediate membrane remodelling during cytokinesis. Nat Cell Biol 2017;19:787–98.

[17] Bajorek M, Schubert HL, McCullough J, Langelier C, Eckert DM, Stubblefield W-MB, et al. Structural basis for ESCRT-III protein autoinhibition. Nat Struct Mol Biol 2009;16:754–62.

[18] Buchkovich NJ, Henne WM, Tang S, Emr SD. Essential N-terminal insertion motif anchors the ESCRT-III filament during MVB vesicle formation. Dev Cell 2013;27:201–14.

[19] Tang S, Henne WM, Borbat PP, Buchkovich NJ, Freed JH, Mao Y, et al. Structural basis for activation, assembly and membrane binding of ESCRT-III Snf7 filaments. Elife 2015;4.

[20] Schoneberg J, Lee I-H, Iwasa JH, Hurley JH. Reverse-topology membrane scission by the ESCRT proteins. Nat Rev Mol Cell Biol 2017;18:5–17.

[21] Wollert T, Wunder C, Lippincott-Schwartz J, Hurley JH. Membrane scission by the ESCRT-III complex. Nature 2009;458:172–7.

[22] Adell MAY, Vogel GF, Pakdel M, Muller M, Lindner H, Hess MW, et al. Coordinated binding of Vps4 to ESCRT-III drives membrane neck constriction during MVB vesicle formation. J Cell Biol 2014;205:33–49.

[23] Adell MAY, Migliano SM, Upadhyayula S, Bykov YS, Sprenger S, Pakdel M, et al. Recruitment dynamics of ESCRT-III and Vps4 to endosomes and implications for reverse membrane budding. Elife 2017;6.

[24] Caillat C, Maity S, Miguet N, Roos WH, Weissenhorn W. The role of VPS4 in ESCRT-III polymer remodeling. Biochem Soc Trans 2019;47:441–8.

[25] Maity S, Caillat C, Miguet N, Sulbaran G, Effantin G, Schoehn G, et al. VPS4 triggers constriction and cleavage of ESCRT-III helical filaments. Sci Adv 2019;5:eaau7198–eaau7198.

[26] Schoneberg J, Pavlin MR, Yan S, Righini M, Lee I-H, Carlson L-A, et al. ATP-dependent force generation and membrane scission by ESCRT-III and Vps4. Science 2018;362:1423–8.

[27] Lee I-H, Kai H, Carlson L-A, Groves JT, Hurley JH. Negative membrane curvature catalyzes nucleation of endosomal sorting complex required for transport (ESCRT)-III assembly. Proc Natl Acad Sci U S A 2015;112:15892–7.

[28] Babst M. MVB vesicle formation: ESCRT-dependent, ESCRT-independent and everything in between. Curr Opin Cell Biol 2011;23:452–7.

[29] Stuffers S, Sem Wegner C, Stenmark H, Brech A. Multivesicular endosome biogenesis in the absence of ESCRTs. Traffic 2009;10:925–37.

[30] Trajkovic K, Hsu C, Chiantia S, Rajendran L, Wenzel D, Wieland F, et al. Ceramide triggers budding of exosome vesicles into multivesicular endosomes. Science 2008;319:1244–7.

[31] Juan T, Furthauer M. Biogenesis and function of ESCRT-dependent extracellular vesicles. Semin Cell Dev Biol 2018;74:66–77.

[32] Cashikar AG, Shim S, Roth R, Maldazys MR, Heuser JE, Hanson PI. Structure of cellular ESCRT-III spirals and their relationship to HIV budding. Elife 2014;3:1–17.

[33] Edgar JR, Eden ER, Futter CE. Hrs- and CD63-dependent competing mechanisms make different sized endosomal intraluminal vesicles. Traffic 2014;15:197–211.

[34] Luef B, Frischkorn KR, Wrighton KC, Holman H-YN, Birarda G, Thomas BC, et al. Diverse uncultivated ultra-small bacterial cells in groundwater. Nat Commun 2015;6:6372.

[35] Velimirov B. Nanobacteria, Ultramicrobacteria and Starvation Forms: A Search for the Smallest Metabolizing Bacterium. Microbes Environ 2001;16:67–77.

[36] Ghai R, Mizuno CM, Picazo A, Camacho A, Rodriguez-Valera F. Metagenomics uncovers a new group of low GC and ultra-small marine Actinobacteria. Sci Rep 2013;3:2471.

[37] Emsellem V, Cardoso O, Tabeling P. Vesicle deformation by microtubules: A phase diagram ´ 1998;58:4807–10.

[38] Soni SP, Stahelin R V. The Ebola virus matrix protein VP40 selectively induces vesiculation from phosphatidylserine-enriched membranes. J Biol Chem 2014;289:33590–7.

[39] Loose M, Mitchison TJ. The bacterial cell division proteins FtsA and FtsZ self-organize into dynamic cytoskeletal patterns. Nat Cell Biol 2014;16:38–46.

Chapter 6

De novo synthesis of Cdv proteins

"If two people agree on everything, one of them is unnecessary."

Winston Churchill

The archaeal Cdv system possesses homologues to the eukaryotic ESCRT system and is assumed to be heavily involved in the cell division processes of several archaea. In this chapter, we synthesized the proteins CdvA, CdvB and CdvC of *Sulfolobus acidocaldarius* to investigate their potential for deforming and dividing liposomes. All three genes can be expressed at full-length, but membrane binding of CdvA was not observed. Protein purification of CdvA and CdvB was attempted but did not deliver sufficient fractions of the respective protein.

6.1 Introduction

In the previous chapter we have investigated the potential of the ESCRT-III system for division of a minimal synthetic cell. However, recent findings suggest that the ESCRT system might on its own not have the potential for efficient liposome division. Therefore, we looked for alternative cell division machineries and decided that the Cdv (cell division) proteins, which are found in a subgroup of archaea, would be interesting candidates.

Archaea constitute one of the three basic domains of life besides Bacteria and Eukaryotes, although their distinctive difference from bacteria in genome and morphology has been recognized comparatively late in the 1970s [1], 300 years after the discovery of bacteria. Archaea are most commonly known for their ability to strive in extreme environmental conditions like hypersaline waters or at temperatures above 120°C [2,3]. Nevertheless, they can be found in moderate environmental niches as well and the human microbiome is for example populated by several different species of archaea [4]. Taxonomic sampling has led rather recently to the split of archaea into Euryarchaea and the superphyla of the TACK group [5]. Interestingly, it is now believed the divergence of Archaea and Eukaryotes has occurred after this split and that archaea of the TACK group are closer related to Eukaryotes than was anticipated in the past [6] (Figure 6.1A). Indeed, it has been discovered that several of their characteristics are more similar to Eukaryotes than to Euryarchaea, for example in regards of their cell-cycle organisation and chromosome copy number [7,8].

Regarding cell division, it is notable that almost all Euryarchaea possess homologues of the bacterial cell division protein FtsZ, while archaea of the phylium Crenarchaeota, which is part of the TACK superphylum, completely lack any such homologues [8] (Figure 6.1B). In general little is known about the division machinery of archaea and it was therefore even more exiting that homologues of ESCRT-III and Vps4 were discovered in hyperthermophilic crenarchaea of the genus *Sulfolobus* [9,10]. *Sulfolobus* possesses four ESCRT-III homologues (CdvBs) and one homologue of Vps4 (CdvC). While the three homologues CdvB1, CdvB2 and CdvB3 are distributed over the chromosome, the two homologues CdvB and CdvC as well as the non-homologous protein CdvA are located together on an operon-like locus. All four CdvB genes are homologues of the Vps2/Vps24 class of ESCRT proteins. In contrast, no homologues have been found of Snf7, the supposedly main component of the eukaryotic ESCRT system. The secondary structure of CdvB is reported to be similar to other ESCRT proteins, containing four core • -helices and an • 5 helix that likely acts as an inhibitor. However, CdvB lacks several of the positively charged residues at its core domain that are important for membrane binding in eukaryotic ESCRT proteins (see previous chapter) and it has indeed been shown that CdvB is on its own unable to bind to archaeal membranes [11]. In CdvB1 and CdvB2, the corresponding domain is more positively charged than in CdvB, but less than in the eukaryotic homologues. Therefore, these two proteins might be able of membrane binding, but no experimental evidence is currently available [12]. CdvA is no ESCRT homologue and unique to the TACK superphylum, but contains a sequence at its C-terminus that is able to bind CdvB. Binding is mediated by a wH-domain of CdvB, which is absent in the other ESCRT-III homologues CdvB1-3. Most importantly, CdvA binds to archaeal membranes and has been shown to recruit CdvB to liposomes *in vitro* [11].

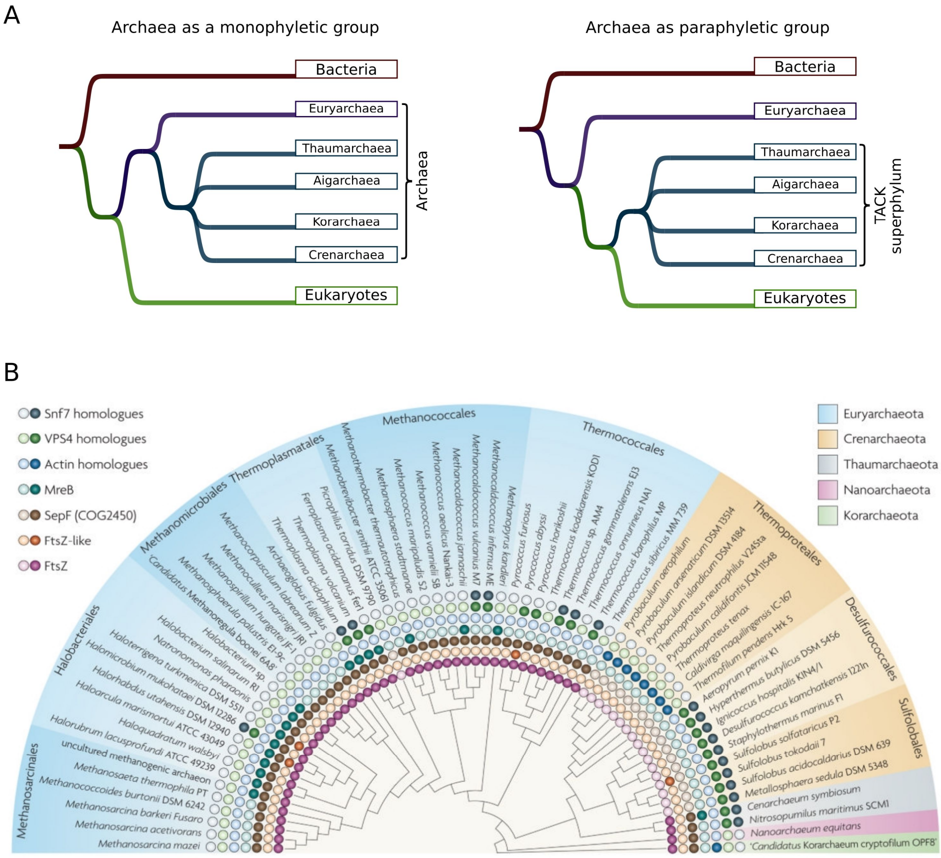

Figure 6.1: **(A)** Two alternative phylogenetic trees for the three domains of life. The left tree depicts the classical model with all three domains of life as monophyletic groups. The right tree follows the recent proposal that eukaryotes have split from archaea after the divergence from Euryarchaea, which would make the Archaea a paraphyletic group. **(B)** Distribution of cytoskeletal and cell division proteins across the different archaeal phylia. Filled-in circles indicate the presence of one or more genes encoding homologs of the respective protein class. In case of the Crenarchaeota, the respective shown homologues of Snf7 are actually closer homologues to Vps2/Vps24. Taken from Makarova et al. 2010 [13].

As mentioned in the previous chapter, the ESCRT system plays a key role in cell division in mammalian and other eukaryotic cells. However, this is not the case for yeast, which led to the hypothesis that this role might be a later addition to the functions of the machinery [14]. However, there is strong evidence that the archaean ESCRT system, also called the Cdv system, is playing a key role in cell division of crenarchaea. In synchronised *Sulfolobus acidocaldarius* cells, ESCRT homologues are maximally abundant in populations undergoing division [14]. Single deletion mutants of the homologues CdvB1-3 lead to moderate or severe impairment of growth, the formation of enlarged cells and defects in DNA segregation, while deletion of CdvB was lethal [15]. When recruitment of CdvB to CdvA was blocked *in vivo* by over-expression of the CdvB wH domain it resulted in enlarged and nucleoid-free cells, indicative of failed cell division [11]. A similar effect was observed by over-expression of an ATP-hydrolysis-deficient CdvC mutant [14].

These results indicate that CdvA, CdvB and CdvC are crucial for cell division in *S. acidocaldarius*, while the homologues CdvB1, CdvB2 and CdvB3 are involved but not essential for it. Additionally, there are indications that in thaumarchaea, which encode for both Cdv and FtsZ, cell division is primarily based on Cdv proteins rather than on FstZ [16]. These results are further supported by the colocalization of fluorescently labelled CdvA, CdvB, CdvB1 and CdvB2 to the constriction side before and during cell division (Figure 4.2A-C). Furthermore, cryo-electron tomography of dividing *S. acidocaldarius* cells revealed a protein belt located at the division furrow during different stages of cytokinesis (Figure 6.2D). The protein belt fits the fluorescence signal rather well, and thus indicates that CdvA and CdvB are forming protein rings or helices on the membrane at the constriction side (Figure 6.2E). Nevertheless, to what degree and how exactly the Cdv system is promoting cell division is still unknown. It has been shown that when CdvA is incubated on liposomes it forms filaments wrapped around the them [17] and there have been reports claiming that if CdvA and CdvB are added to liposomes together they are able to deform them into tubes (Figure 6.2F). In Eukaryotes, constriction of the ESCRT complex at the abscission side is dependent on Vps4 and it might be that depolymerisation of Cdv filaments by Cdv through CdvC is the driving force for reducing the diameter of the protein ring. However, there is so far no evidence for such a mechanism.

Here, we have explored the potential of the Cdv system as a candidate for the division of a minimal cell by investigating the *de novo* synthesis of the CdvA, CdvB and CdvC proteins. Archaea are not as complex as eukaryotes cells, which increases the chances that we can reconstitute an archaean system in an *in vitro* environment. Additionally, reconstitution of the Cdv system *in vitro* might help us understand how it facilitates division in Archaea.

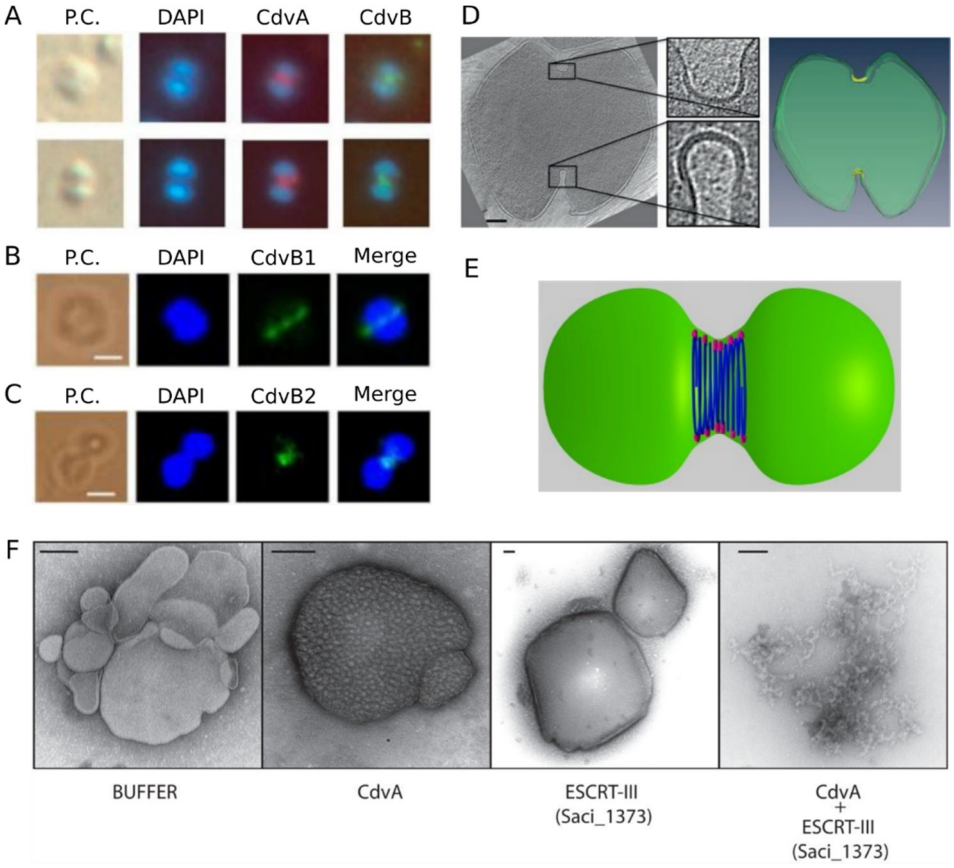

Figure 6.2: Imaging of the Cdv system *in vivo* and *in vitro*. (A-C) Immunofluorescence microscopy of Cdv proteins. **(A)** Localization of CdvA and CdvB during *S. acidocaldarius* cytokinesis. Taken from Lindås et al. 2008 [18]. (B,C) Localization of *S. islandicus* CbvB1 **(B)** and CdvB2 **(C)** to the division site. Scale bars represent 1 µm. Taken from from Liu et al. 2017 [19]. **(D)** Cryo-EM image of a dividing *S. acidocaldarius* cell. The cell membrane and soma are denoted in green and the protein belt at the cleavage furrow is denoted in yellow. Insets represent zoom in of the two sides of the cleavage furrow. Scale bars = 150 nm. Taken from Dobro et al 2013 [17]. **(E)** "Hourglass" model of the Cdv system during cytokinesis, showing CdvB polymers (blue) that are connected to the membrane via CdvA (purple). Taken from Caspi and Dekker 2018 [12]. **(F)** Negative stain electron microscopy of liposomes incubated with CdvA and CdvB (called here ESCRT-III). When both proteins were added, liposomes seemed to be deformed into tubular structures. Scale bar = 100 nm. Taken from Samson et al 2011 [11].

6.2 Results and discussion

6.2.1 Expression of Cdv proteins and membrane binding assay

Templates for gene expression were *cdvA*, *cdvB* and *cdvC* from *Sulfolobus acidocaldarius*. All three genes were synthesized *de novo* with an optimized sequence as described for the bacterial tubulin genes in section 4.4. We investigated expression products by an IVTT assay with gene expression by PURE*frex* and visualisation by SDS-PAGE and GreenLys. Corresponding expression products were visible for all three genes with minor amounts of side products visible (Figure 6.3). Intensity of the CdvB and CdvC bands was distinctively higher than in the positive control of $Snf7^{His}$. CdvA had a slightly lower intensity than $Snf7^{His}$, although it should be considered that its smaller size might be partly responsible for that.

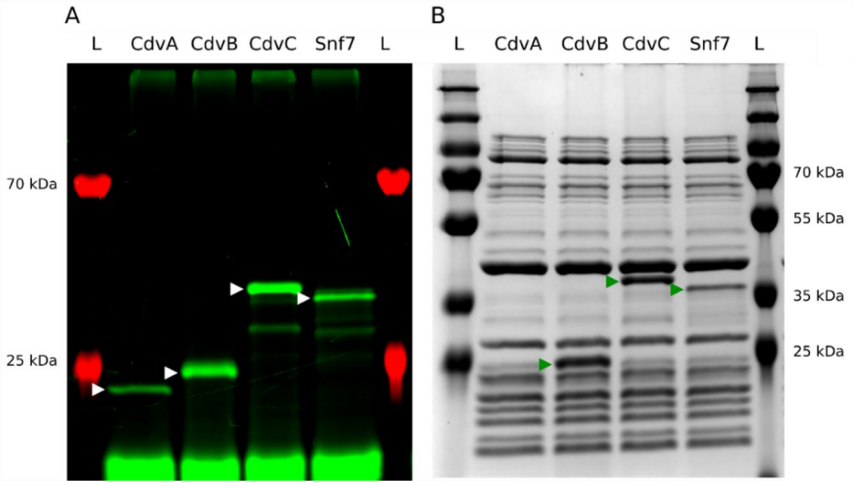

Figure 6.3: SDS-PAGE of Cdv proteins expressed *in vitro*. **(A)** GreenLys fluorescence signal of expression products. Expression of $Snf7^{His}$ was used as a positive control. Synthesized full-length proteins are marked by white arrowheads. **(B)** Coomassie staining of the same gel. Synthesized full-length proteins that are visible above PURE system background are marked by green arrowheads.

Analogue to the approach taken in the previous chapter, we next checked for membrane binding capabilities of expressed CdvA. This was not done for CdvB and CdvC because from has been reported they are not expected to bind to membranes at all. First, we added expressed CdvA to liposomes of the same lipid composition used in most of our experiments (DOPC, DOPE, DOPG, cardiolipin) and performed a sedimentation assay identical to the one described in 5.4. As can be seen in Figure 6.4A, CdvA did not colocalize with the liposome fraction. We repeated the same experiment with liposomes composed of *E. coli* polar lipids (Figure 6.4B), but obtained the same result. This strongly indicates that CdvA is not recruited to liposomes with a bacterial lipid composition.

The absence of membrane binding might be connected to the fact that the lipids of archaeal membranes are distinctively different to those found in Prokaryotes and Eukaryotes. While lipids in bacterial and eukaryotic membranes consist of fatty acid chains that are ester linked to glycerol-3-phosphate, most of the archaeal lipids are composed of fully saturated acyl chains (isoprenoids),

ether linked to glycerol-1-phosphate (Figure 6.4). In addition, although most archaea growing under moderate condition possess bilayer membranes like bacteria or eukaryotes, monolayer membranes formed by tetraether lipids are found in extreme thermophiles and acidophiles, including *Sulfolobus acidocaldarius* [20]. These lipids have C_{40} isoprenoid acyl chains which span the entire membrane (Figure 6.4) and can contain cyclopentyl or cyclohexyl rings [21,22].

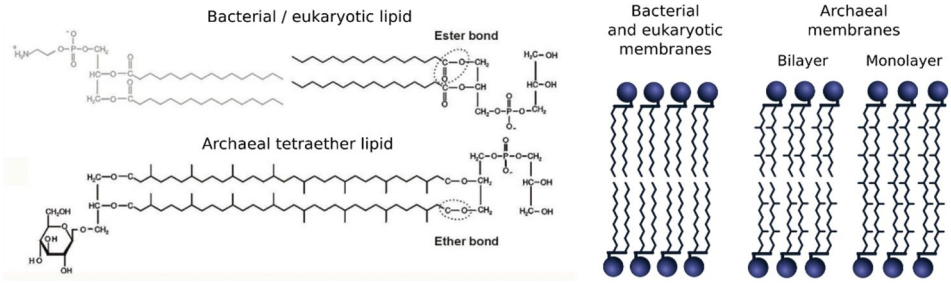

Figure 6.4: Comparison of lipids and membrane structure between bacteria/eukaryotes and archaea. Some Archaea form a membrane from a bilayer of lipids like bacteria or eukaryotes while others possess a monolayer membrane composed of tetraether lipids. Lipid structure images taken from Albers et al. 2000 [21].

Given these differences in membrane composition and morphology, it is well possible that the membrane binding of CdvA is specific to archaeal membranes. If this is the case, then there would be two possible ways to enable recruitment *in vitro*. The first is the application of archaeal lipids for which it already has been shown that CdvA can bind to liposomes made from them [11]. This would maybe solve the problem of membrane binding, but would bring with it a set of uncertainties, as archaeal lipids are not very well explored for the self-assembly of membrane model systems. It is for example not clear how well liposomes generated from them could be applied for encapsulation of an *in vitro* transcription and translation system or how much adjustment and optimization our protocols would require. Additionally, there is the problem of compatibility with other systems (see conclusions). We have therefore decided not to investigate the application of archaeal lipids for our experiments. The second option would be to artificially link CdvA or CdvB to membranes. The classical approach would be to add a His-tag to the protein, which could then facilitate recruitment to NTA-lipids of the liposome. Our standard lipid composition for encapsulation of the PURE system already contains NTA-lipids and therefore this would not require any adaption of existing protocols. In case of CdvA, the primary concern would be to attach the His-tag in a manner that would not interfere with recruitment of CdvB, as this seems to be its primary and maybe sole function apart from its recruitment to the membrane. In case that CdvA is only responsible for recruitment of CdvB, it might be sufficient to directly recruit CdvB to the membrane, although this might be more problematic as it is not known how exactly CdvB forms a functional filament complex and what domains are involved. An alternative explanation of our results would be that the expressed CdvA is not expressed in a functional manner and might for example not be folded correctly and unable to bind to the membrane. To check if this is the case, however, we would need purified CdvA as a positive control. This was one of the motivations for our attempt to purify the Cdv proteins as described in the next section.

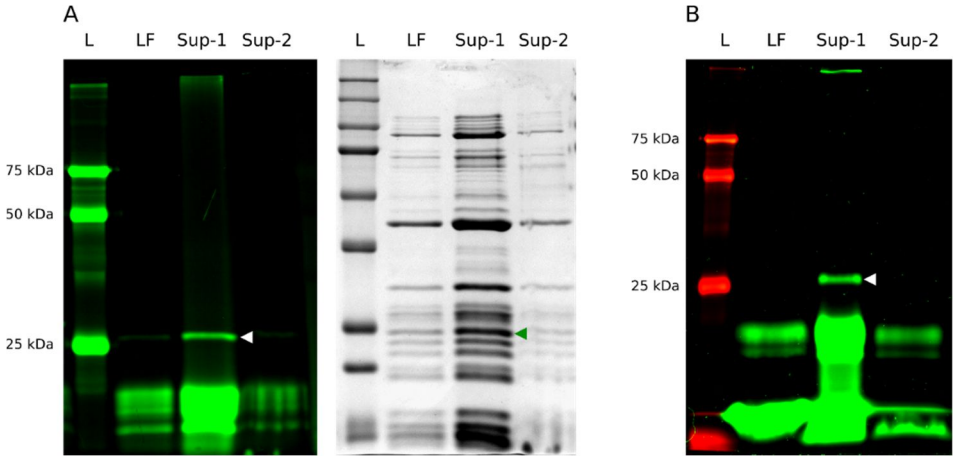

Figure 6.4: Sedimentation assays of CdvA. **(A)** Sedimentation with DOPC/DOPG liposomes. On the left side is the GreenLys signal and on the right the coomassie staining. **(B)** Sedimentation with liposomes formed from *E. coli* polar lipid extract. Liposomes containing sucrose were spun down and the supernatant (Sup-1) was removed. After a washing step and second spin-down, the supernatant was removed again (Sup-2) from the final lipid fraction (LF). The band of CdvA is marked with white and green arrow heads respectively.

6.2.2 Protein purification of Cdv proteins

As for the ESCRT project, we tried to obtain purified proteins of the Cdv system, because we would need to have a positive control to assert the activity of synthesized protein. The genes of CdvA, CdvB and CdvC were transferred into the expression vector pRSET B and transformed into C41(DE3) and RosettaTM(DE3) cells. First, the optimal condition for expression was determined by testing several different conditions with CdvB at low media volumes. The different conditions have been in more detail described in section 5.2.5. Here as well, the cell lysates were put on a SDS-PAGE which showed a strong accumulation of protein at the height expected for CdvB (Figure 6.5A). This was not observed in the lysates of RosettaTM(DE3). They only showed a faint band at the corresponding height for CdvB. As a consequence of these results, we chose to conduct the protein purification of CdvB with C41(DE3) cells, 0.2 mM IPTG and incubation at 37°C. However, when the intermediate products of proteins purification were analysed, it became clear that after cell lysis almost all CdvB was located in the pellet together with the cell debris, indicating aggregation of the protein (Figure 6.5B). CdvB is proposed to be the main component of the filament complex and to polymerize with its own subunits. A protein containing domains for polymerisation is more likely to aggregate with itself and this might have been the reason for the aggregation of CdvB. In addition, it has been reported that CdvB cannot purified due to insolubility of the protein [17]. This problem could be addressed in future experiments by linking CdvB to a maltose-binding protein as done for ESCRT-III purification in literature.

For purification of CdvA and CdvC, we chose the same condition for gene expression as for CdvB. Unlike in case of CdvB, they were both found in the supernatant instead of the pellet after cell-lysis. The supernatant was split into two fractions of which one was submitted to heat treatment.

Afterwards, both fractions were purified using Ni-NTA columns. Contrary to expectations, analysis of the eluates and the intermediate products revealed that the CdvA and CdvC were apparently not binding to the Ni-NTA column. In both the heat-treated and untreated fraction, most of the respective protein was present in the flow-through and the rest was almost completely washed out of the column with only minute fractions left in the eluate (Figure C). One explanation for a lack of binding is that the His-tag is not exposed to the Ni-NTA column, but is folded inside the protein. This could be addressed by inserting a linker sequence or changing the position of the His-tag to the N-terminus. However, we decided at this point to put the project to a halt.

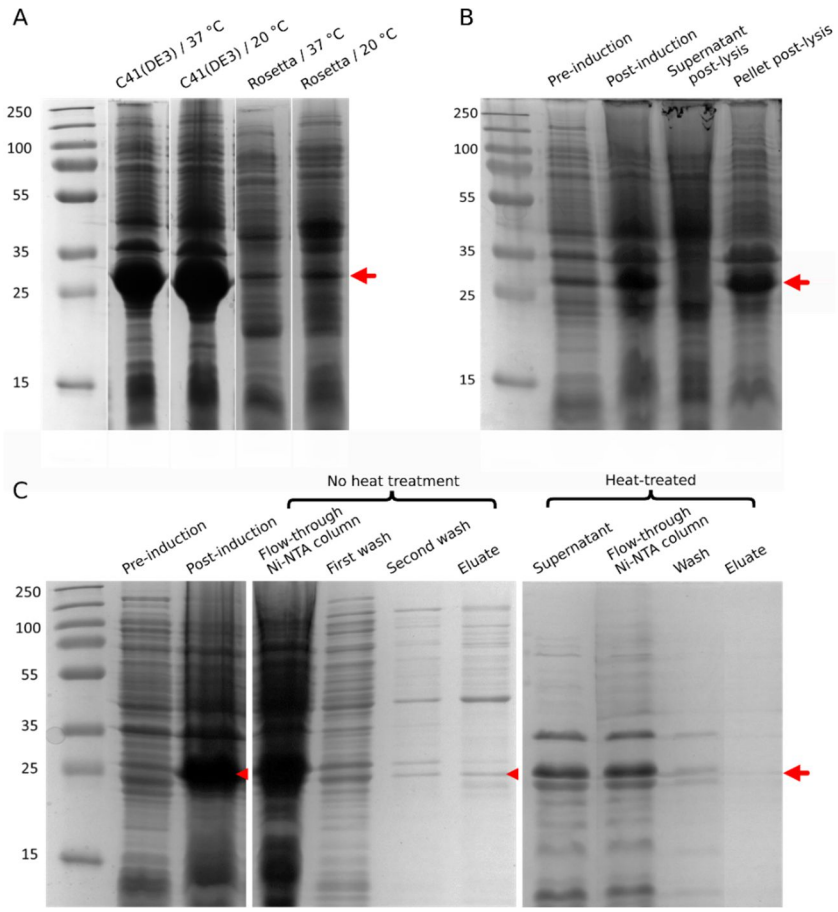

Figure 6.5: Products of protein for purification of Cdv proteins visualized by SDS-PAGE. **(A)** Cell lysates of different conditions (cell lines and temperatures) for CdvB expression. **(B)** Products of the first steps of CdvB purification from C41(DE3) cells incubated at 37°C for 3 hours with 0.2 mM IPTG. **(C)** Products of protein purification steps of CdvA. CdvA was expressed by C41(DE3) cells incubated at 37°C for 3h with 0.2 mM IPTG. (All) Red arrow marks the size of the respective band of CdvA and CdvB.

6.3 Conclusions

We investigated the Cdv system with the aim to assess its potential for division of a minimal synthetic cell. Based on the presented results, we decided rather early after the start of the project to stop it. Although full-length expression by the PURE system was confirmed, membrane binding to liposomes was clearly negative. If this was due to the difference between prokaryotic and archaeal lipids or due to misfolding of the expressed protein can only be addressed by either conducting the experiment with purified protein or with liposomes formed from archaeal lipids. We have decided against including archaeal lipids in our investigations as they might not be compatible with our established protocols and, even more important, would not be compatible with our approach of the creation of a minimal cell, as it involves the synthesis of a basically prokaryotic lipid membrane. Moreover, protein purification failed for all three Cdv proteins. We already experienced great difficulties in our effort to investigate *de novo* synthesis of the ESCRT-III system without having purified proteins as a positive control and supplement available. Without purified protein, it would be very difficult to access to what degree our expressed proteins are active and to link our results to the ones in literature. Therefore, we discontinued on this project. If one would want to continue the investigation of the Cdv system *in vitro* with the primary focus on its function *in vivo*, it would be crucial to utilize archaeal lipids for that purpose. There are protocols for the purification of archaeal lipid extracts, although they are currently not commercially available. If the project would be continued with the aim to apply the Cdv system in a minimal cell based on a prokaryotic machinery, the next step would be to successfully purify the corresponding proteins and to attach them to the membrane by His-tag binding to NTA-lipids. In both cases, it should be considered that the ESCRT homologues CdvB1-3 are likely involved in the cell division process as well and that omission of all three proteins might prevent reconstitution of a functional machinery.

Aside these practical challenges, the question remains to what degree the Cdv system is actually able facilitate cell division. Although it is clear that it plays a crucial role in cytokinesis of archaea, this does not mean that there are no other essential components involved. All things considered, little is known about the mechanisms by which archaea divide. In case of Cdv mediated division there is still the mystery of size proportions. The Cdv complex has a starting diameter of over 1 µm and it is not clear if it could work with the same mechanism as the ESCRT complex which is more than one order of magnitude smaller. In the end, only future advances in the field will reveal if the Cdv system is truly such a powerful mediator of cell division as proposed.

6.4 Materials and methods

Gene expression

Optimized sequences of CdvA, CdvB and CdvC of *Sulfolobus acidocaldarius*, including a T7 promotor, RBS and T7 terminator sequence (see supplementary information), were sent for gene synthesis to GenScript (United states) and were received in the pUC57 plasmid. Linear constructs for expression were obtained by PCR reactions, utilizing the primers173 ChD and 365 ChD. Cell-free gene expression was conducted with PURE*frex* and addition of GreenLys. For detailed information see section 5.4.

Sedimentation assay

Two lipid mixtures were applied. The lipid mix of DOPC/DOPG (Table) was desiccated and the lipid film rehydrated with 63 µl of 0.9 M sucrose solution under vortexing for 2-3 minutes and 5 minutes of sonication. This resulted in a 15 µg/µl lipid mixture of SUVs. The second lipid mix was prepared by solving 2 mg of *E. coli* polar lipids (Avanti) in 100 µl 0.9 M sucrose under vortexing, yielding a lipid mixture of 20 µg/µl. The given sucrose concentration was chosen under the assumption that its osmolarity would be close enough to the PURE system to avoid bursting of the liposomes and at the same time sufficiently heavier than the PURE system to allow for sedimentation of the liposomes. As a next step, a 40-µl PURE*frex* expression mix of the corresponding protein was expressed for 3 hours at 37°C and 10 µl of the respective SUV emulsion added. Samples were incubated at 25°C for 15 minutes in a heat block and subsequently centrifuged for 4 minutes at 20.000 g. This resulted in a pellet of lipids formed on the bottom of the tube, confirming that the SUVs were heavier than the PURE*frex* solution. About 47 µl of supernatant (Sup-1) was removed without disrupting the pellet. Then, 40 µl of 1x G buffer was added and the sample spun down a second time. Afterwards, 35 µl of the supernatant (Sup-2) was removed and the pellet (LF) resuspended in 7 µl MilliQ water. Of each of the two supernatants and the lipid fraction 11,5 µl were mixed with DTT (final concentration of 10 mM) and SDS buffer to a final volume of 15 µl for loading onto the gel. Samples were run on a 12% SDS-protein gel according to section 3.4.

Table 6.1: DOPC/DOPG lipid mixture for sedimentation assay of CdvA

Lipid	Mol%	Concentration (g/l)	Volume (µl)
DOPC	~ 60	10	56
DOPG	~ 40	10	37.5
DHPE-Texas Red	-	1	4.5

Protein purification

For protein purification, the purified plasmids were transformed into RosettaTM(DE3) and into C41(DE3) competent cells. Cells were grown according to the protocol described in 5.4. The pelleted cells were resuspended in lysis buffer (20 mM Tris, 300 mM NaCl, pH 8.0) and lysed using sonication (Qsonica Sonicators, PTS technics) with a 10 second pulse, 30 second rest, 30% amplitude, and 10 cycles. After spinning down at 16.000 g for 20 minutes at 4°C the samples were split in two and one fraction was as a heat treatment incubated for 20 minutes at 75°C followed by a second spin down for 15 min at 16.000 g. Afterwards each supernatant was applied to a QIAGEN Ni-NTA column. The column was then washed twice with a washing buffer with low concentration imidazole (20 mM Tris, 300 mM NaCl, 10 mM imidazole, pH 8.0) and the proteins were eluted in an elution buffer with a high concentration of imidazole (20 mM Tris, 300 mM NaCl, 100 mM imidazole, pH 8.0).

5.5 Supplementary information

Sequence of *cdvA* (including T7 promotor and terminator)

TAATACGACTCACTATAGGGGAATTGTGAGCGGATAACAATTCCCCTCTAGAAATAATTTTGTTT
AACTTTAAGAAGGAGATATACATATGGGTATCCCGGTGGAAGTGCTGACCAAGTTCATCGGCCA
GAAGGTGAAAGACGTTTACGGTCGTGACGCGGGTGTGATTGTGCATGTGTACACCGAGATCGAT
GGCACCATCACCGGCATTGAACTGTTCAAGGGCGAGGAAATTAAAACCTATAGCCCGAACAGCG
TGAAAGTTGACGGCGATAGCGTGGTTATCCTGCCGGATTGGAAGACCGACAGCCTGAAAGTTCT
GGGTCAGATGGAGAAGATCCGTAAACGTCAACGTGCGCTGGAGGAACTGTACAGCCGTCAGGA
GATTCCGAAAAGCACCTATGAAGATATGAAGCGTAAACTGGACAGCGAGCTGCTGAAGATCCGT
GATGAACACAGCCGTCTGAAGGGTCGTCTGAAAGACCGTCTGAACAGCATTGAAGATCAGGTGG
CGCAAATCGACCGTGCGATGATTGCGCTGAAAATCAACTACATTAGCGGCGAGATCCCGGAACT
GGCGTATAAGAACAGCATGGAGATTCTGCGTCTGAGCCGTGACAGCTACGCGCTGGAACGTGAC
GATATCAAGAAAACCCTGGACAAGCTGGATGGCCTGGACAAAGAGGTTATTGAACTGAAGCCG
AGCGCGAGCCTGAACACCAGCACCGAGCAAAGCAACAAGAACGAAGGTAATAAGAGCGAAGTG
AGCGTGCCGATTCCGGTGCGTGTGATCAATACCCTGTAATGAGCAATAACTAGCATAACCCCTTG
GGGCCTCTAAACGGGTCTTGAGGGGTTTTTTG

Sequence of *cdvB* (including T7 promotor and terminator)

TAATACGACTCACTATAGGGGAATTGTGAGCGGATAACAATTCCCCTCTAGAAATAATTTTGTTT
AACTTTAAGAAGGAGATATACATATGTTCGATAAGCTGAGCATCATTTTCAATAGCGACCGCAA
GCGCAAGGTTCATCTGAGCAAGGCGATTACCGAGATTAGCCTGAAGCTGAAGGAGCAGCAAGA
CCGTCTGGATGAAGCGATCCGTCGTCTGCGTGAGCGTGACAAGGACCTGTTCGAAAAAGTGATC
CGTAGCCAGATTGAGGGTGACATCGCGCGTGCGACCATTTACGCGCAAGAAATCAGCGATATCC
GTAAGATGATCAAGATCATCTACACCGCGTATCTGGCGATCGAGAAAGTGCGTCTGAAACTGGA
CACCGTTCAGGAACTGCAAGGCGTGAGCCTGGTTCTGTTCCCGGTGATGCGTATTCTGGGCGAGC
TGAAAGAACAGGTTCGTGGTATTGCGCCGGAAGTGGCGCTGGCGCTGGACAGCATTACCAGCAG
CGTTAACAGCATCGCGATTGAAACCGGTGCGCTGAGCGAAAAGACCTTTGTGCCGACCGTTGCG
GATGAGCAGGCGAAACAAATCATGGAGGAAGCGCAAAAGATGGCGGAAGTGAAAGTTCGTGAG
CTGCTGCCGGAACTGCCGCACCCGCCGAGCGAGCTGCCGAAGCGTGTGGCGAAACAGGTTCAAA
GCAGCAACAAGAAAAGCCTGAGCGAAGATATGATTCTGAACTACATCAAGACCACCGGTGGCTT
CATTGACGTGGATTATATCGCGAAGAACTTTGACGTTAGCAAAGATGAAGTGTTCAATGTTCTGC
GTCGCCTGGAGGAGAAAGGTCTGATCGTGCTGGAGGGCTAATGAGCAATAACTAGCATAACCCC
TTGGGGCCTCTAAACGGGTCTTGAGGGGTTTTTTG

Sequence of *cdvC* (including T7 promotor and terminator)

TAATACGACTCACTATAGGGGAATTGTGAGCGGATAACAATTCCCCTCTAGAAATAATTTTGTTT
AACTTTAAGAAGGAGATATACATATGAGCGCGCAGGTGATGCTGGAGGAGATGGCGCGTAAGT
ATGCGATCAATGCGGTGAAGGCGGATAAAGAAGGCAATGCGGAGGAAGCGATCACCAACTACA
AGAAAGCGATTGAAGTGCTGGCGCAGCTGGTTAGCCTGTATCGTGACGGTAGCACCGCGGCGAT
CTACGAACAAATGATCAACGAGTACAAGCGTCGTATCGAGGTGCTGAAGGAACTGATTCCGGCG
GATGGTGCGGGTAACGGTAACGGTAAACACAGCCAGGTGAGCGTTGACGATCTGGTGATGAAG
GAGAAACCGAAGGTTAACTTCAACGACATCGTGGGTCTGGAGGATGTTAAAGAAGCGCTGAAA
GAGGCGATTGTTTACCCGACCCGTCGTCCGGACCTGTTTCCGCTGGGTTGGCCGCGTGGCATCCT
GGTGTATGGTCCGCCGGGTTGCGGCAAGACCATGATTGCGGCGGCGGTGGCGAACGAAATCGAC
AGCTACTTCATTCAAGTGGATGCGGCGAGCGTTATGAGCAAATGGCTGGGCGAGGCGGAGAAGA
ACGTGGCGAAAATCTTCAACAGCGCGCGTGAACTGAGCAAGAAAGATGGCAAGCCGGTTATCAT

TTTTATCGACGAGATTGATGCGCTGCTGGGCACCTACAACAGCGAAAACGGTGGCGAGGTGCGC
GTTCGTAACCAGTTCCTGAAAGAAATGGACGGTCTGCAAGATAAAAGCGAGAACTTTAAGGTGT
ATGTTATCGGCGCGACCAACAAGCCGTGGCGTCTGGACGAACCGTTCCTGCGTCGTTTTCAGAAA
CGTATCTACATTCGTCTGCCGGATATTGAGCAGCGTAAGAGCCTGCTGCTGCACTATACCAGCAA
AATCAAGATGGACAACGTGAACATTGATGAACTGGCGAAAATGACCGAGGGTTATACCGCGAG
CGACATCAAGGATATTGTTCAGGCGGCGCACATCCGTGTGGTTAAAGAAATGTTCGACAAGAAA
CTGGAGCAACCGCGTGCGGTGAACATGGAAGATTTTAAGGAGATCCTGAAAATTCGTAAGCCGA
GCGTGAATAGCGAAGTGATTAAAGTGTACGAAGCGTGGCATGAGAAGTATAAAGCGCTGTAATG
AGCAATAACTAGCATAACCCCTTGGGGCCTCTAAACGGGTCTTGAGGGGTTTTTTG

References

[1] Woese CR, Fox GE. Phylogenetic structure of the prokaryotic domain: the primary kingdoms. Proc Natl Acad Sci U S A 1977;74:5088–90.

[2] Oren A. Molecular ecology of extremely halophilic Archaea and Bacteria. FEMS Microbiol Ecol 2002;39:1–7.

[3] Kashefi K, Lovley DR. Extending the upper temperature limit for life. Science 2003;301:934.

[4] Bang C, Schmitz RA. Archaea associated with human surfaces: not to be underestimated. FEMS Microbiol Rev 2015;39:631–48.

[5] Guy L, Ettema TJG. The archaeal "TACK" superphylum and the origin of eukaryotes. Trends Microbiol 2011;19:580–7.

[6] Williams TA, Foster PG, Cox CJ, Embley TM. An archaeal origin of eukaryotes supports only two primary domains of life. Nature 2013;504:231–6.

[7] Samson RY, Bell SD. Cell cycles and cell division in the archaea. Curr Opin Microbiol 2011;14:350–6.

[8] Samson RY, Dobro MJ, Jensen GJ, Bell SD. The Structure, Function and Roles of the Archaeal ESCRT Apparatus. Subcell Biochem 2017;84:357–77.

[9] Obita T, Saksena S, Ghazi-Tabatabai S, Gill DJ, Perisic O, Emr SD, et al. Structural basis for selective recognition of ESCRT-III by the AAA ATPase Vps4. Nature 2007;449:735–9.

[10] Hobel CF V, Albers S V, Driessen AJM, Lupas AN. The Sulfolobus solfataricus AAA protein Sso0909, a homologue of the eukaryotic ESCRT Vps4 ATPase. Biochem Soc Trans 2008;36:94–8.

[11] Samson RY, Obita T, Hodgson B, Shaw MK, Chong PL-G, Williams RL, et al. Molecular and structural basis of ESCRT-III recruitment to membranes during archaeal cell division. Mol Cell 2011;41:186–96.

[12] Caspi Y, Dekker C. Dividing the Archaeal Way: The Ancient Cdv Cell-Division Machinery. Front Microbiol 2018;9:174.

[13] Makarova KS, Yutin N, Bell SD, Koonin E V. Evolution of diverse cell division and vesicle formation systems in Archaea. Nat Rev Microbiol 2010;8:731–41.

[14] Samson RY, Obita T, Freund SM, Williams RL, Bell SD. A role for the ESCRT system in cell division in archaea. Science 2008;322:1710–3.

[15] Yang N, Driessen AJM. Deletion of cdvB paralogous genes of Sulfolobus acidocaldarius impairs cell division. Extremophiles 2014;18:331–9.

[16] Pelve EA, Lindas A-C, Martens-Habbena W, de la Torre JR, Stahl DA, Bernander R. Cdv-based cell division and cell cycle organization in the thaumarchaeon Nitrosopumilus maritimus. Mol Microbiol 2011;82:555–66.

[17] Dobro MJ, Samson RY, Yu Z, McCullough J, Ding HJ, Chong PL-G, et al. Electron cryotomography of ESCRT assemblies and dividing Sulfolobus cells suggests that spiraling filaments are involved in membrane scission. Mol Biol Cell 2013;24:2319–27.

[18] Lindas A-C, Karlsson EA, Lindgren MT, Ettema TJG, Bernander R. A unique cell division machinery in the Archaea. Proc Natl Acad Sci U S A 2008;105:18942–6.

[19] Liu J, Gao R, Li C, Ni J, Yang Z, Zhang Q, et al. Functional assignment of multiple ESCRT-III homologs in cell division and budding in Sulfolobus islandicus. Mol Microbiol 2017;105:540–53.

[20] De Rosa M, Gambacorta A, Gliozzi A. Structure, biosynthesis, and physicochemical properties of archaebacterial lipids. Microbiol Rev 1986;50:70–80.

[21] Albers S V, van de Vossenberg JL, Driessen AJ, Konings WN. Adaptations of the archaeal cell membrane to heat stress. Front Biosci 2000;5:D813-20.

[22] Koga Y, Morii H. Biosynthesis of Ether-Type Polar Lipids in Archaea and Evolutionary Considerations. Microbiol Mol Biol Rev 2007;71:97 LP – 120.

Chapter 7

Applications and riscs of synthetic cells and an extendend definition of life

We are but whirlpools in a river of ever-flowing water.
We are not the stuff that abides, but patterns that perpetuate themselves.

Norbert Wiener, The Human Use of Human Beings

7.1 Outlook on reconstituting cell division in a minimal cell

In chapter 5 and 6 of this thesis we have reported our attempts to reconstitute the ESCRT-III and the Cdv systems for division of liposomes. In both cases, the results were inconclusive as to how promising these systems could be for achieving division in synthetic cells. It appears likely that the ESCRT-III system in combination with Vps4 is responsible for severing of membrane necks, but requires other systems for prior formation of the necks. In eukaryotic cells, actin mediates the constriction of the membrane until sufficiently narrow membrane necks are formed [1,2]. Simultaneous reconstitution of the actin ring and the ESCRT-III system, as well as their orchestration to perform division, would be a daunting challenge that very likely requires a higher level of understanding and control than we currently possess in regard of synthetic cell-like systems. Further, it would introduce by itself a comparatively high level of complexity. However, combining these systems would at the same time be highly promising for gaining and verifying knowledge about eukaryotic cell division, making it highly relevant for medical research. Therefore, such an integrative approach should be seriously considered once we have learned more about how to recreate the individual systems. Alternatively, FtsZ has so far been the most prominent candidate for division. However, it is not clear how dependant its function is on a cell wall synthesis machinery. A system including a reconstituted bacterial cell wall would likely not be as minimal as theoretically possible, but would on the other hand be at the same time much more relevant as a model system to study prokaryotic cell processes. The Min system, *in vivo* responsible for correct localisation of the FtsZ ring, has turned out to be able by itself to generate pulsing deformations of liposomes when reconstituted with encapsulated purified [3] or expressed [4] proteins. It has been hypothesized that these deformations might be potent enough for division, making the Min system a candidate for liposome polarisation as well as for division.

Expression of bacterial tubulin (Chapter 4) could play a secondary role in division by modulating liposome morphology prior to division. The Min system as well as other division related mechanisms might require an elongation of the liposome for optimal function. Bacterial microtubules might be able to support such a morphology. As observed with eukaryotic tubulin, the ability of filaments to elongate liposomes and the resulting morphologies are highly dependent on the osmotic pressure across the vesicle membrane. Incorporation of membrane pores might help to decrease membrane tension and reliably avoid hyper- or hypotonic conditions. At the same time, the supply of nutrients from a feeding solution, like NTPs or amino acids would be enabled. Moreover, low membrane tension would likely also be beneficial for a protein-based cell division machinery. If bacterial tubulin indeed becomes a useful tool in synthetic biology will primarily depend on the discovery of further interaction partners. Until efficient regulators of bacterial microtubule are found and applied, it would be possible to regulate microtubule length and integrity by high intensity laser illumination (Section 4.2). Depolymerisation of bacterial microtubules will especially be a necessary function prior to division to enable fusion of the membranes.

At last, it is possible to envisage protein-free mechanisms for liposome division. Budding could be triggered solely from lipid synthesis and membrane growth as explained in Chapter 1. If so, this approach would be the most minimal mechanism and thus most suitable for a true minimal cell. Therefore, for the realisation of a minimal cell it will be crucial to develope efficient reconstitution of lipid synthesis. Moreover, if efficient membrane growth is achieved, the division process itself could be achieved instead mechanically in microfluidic systems [5]. Such an approach would not create a cell system that is alive in regards of the here applied definition and will likely not teach

us much about division processes *in vivo*. Nevertheless, it could substitute intermittently for a true cell division machinery. If other essential processes like DNA replication and liposome growth are already reconstituted separately, such an external approach for division could allow us to effectively start evolution experiments and improve the synthetic cell system before solving the problem of internally orchestrated division.

7.2 Applications of a minimal cell

It is not uncommon in the field of synthetic cell research to claim that a minimized synthetic living system would offer a more efficient platform regarding the conversion of energy and the production of drugs than existing organisms [6,7]. The argument often made is that the redundancy and complexity of existing organisms is hampering our ability to alter them to our needs and to perform at a high efficiency. Therefore, the design of a synthetic cell able of reproduction is claimed to have enormous potential for biotechnological processing and therapeutic purposes. This theory is supported by the finding that moderate reduction of genome size (15-20%) can lead to promotion of cell growth and protein production [8–10].

Generally speaking, the complexity and degree of redundancy found in biological systems is the product of continuous adaptations to a complex environment and the competition with other organisms. Constant or periodic changes in the environment require naturally evolved cells to maintain a set of seemingly redundant genetic components to create a sufficient degree of robustness and adaptability. This differs starkly from the demands that biotechnology has on the applied organisms, as the environment is in this case man-made and kept stable. Consequently, it is in the industrial context important that the organism is well adapted to the provided and specific environment. Thus, it is reasonable to assume that for such applications, organisms with lower complexity and a lower amount of functionally redundant components would be highly favourable. However, we do not know exactly to what degree the given complexity is also involved in making the system efficient and how comparatively inefficient a minimal system would therefore be. After all, a component that is deemed non-essential can still be beneficial for the function of the system. As a consequence, the removal of many non-lethal genes will result in a decrease of efficiency regarding processes like rate of division or cell vitality, especially in cases of accumulative loss of genetic material. The results of stepwise genome reduction of *E. coli* suggest a quantitative linkage between the amount of genomic sequences and growth fitness [11]. In case of the semi-synthetic cells created by the Craig Venter Institute, removal of genes led to vital, but slowly replicating organisms even in the hyper-stable environment of the lab [12]. This relationship between complexity and efficiency is as well reflected by the superior protein yield of cell extracts compared to purified expression system. Here, it seems likely as well that many cellular components not essential for gene expression nevertheless enhance the efficiency of the involved processes and the robustness of the expression machinery.

Therefore, the efficiency of an organism for biotechnological purposes does not necessarily improve with its simplicity and the question arises how much complexity can be removed without impairing the function of the cellular system. A minimal cell, at least in the true sense, would perform almost by definition extremely poorly regarding any given task. If we then would add to an absolutely minimal system the genetic circuits necessary for the given application and for a sufficient efficiency and vitality, we would meet the complexity of existing organisms at least half-way. Therefore, the successful creation of a minimal cell would be a significant scientific

breakthrough, but it will not result in a platform that can be immediately used for industrial purposes. Instead, receiving a synthetic system able to compete with the efficiency of existing organisms by starting from a minimal system will be a significant effort in itself. When it comes to applications for therapeutical purposes, this holds even more true. After all, the human body is not a simplistic and static environment and it would be a more reasonable approach to modify existing organisms that have evolved over millions of years adapting to it than to start with a system that is barely able to survive in an optimized laboratory environment. Note that this does not apply for non-living artificial cells (mimetic cells), which can for example be utilized as drug carriers. The situation is different as well in regards of abiological cells, meaning living cells designed with components and mechanisms absent in nature. The previous arguments are based on the notion that a minimal cell will be predominantly based on mechanisms already found in existing organisms and will therefore be subject to the same limitations as those set-upon those organisms in general. If we imagine a living artificial entity that significantly deviates from these mechanisms and principles, for example by relying on components for encoding information and enzymatic reactions different than DNA, RNA, or protein, then it might well be possible that it can rather rapidly exceed the efficiency of existing organisms in regards of specific tasks and environments. Evolution is highly conservative and does rarely abandon fundamental mechanisms. The fact that DNA and RNA were the first molecules on earth to establish themselves as stable information carriers of living organisms does not mean that they are the most efficient ones. The same is true for proteins and any other biological components and mechanisms. On the macroscopic scale, man-made devices have already surpassed biological systems in many regards and there is no reason to assume that the same cannot be achieved on the microscopic scale.

This opens up the question why we would even try to stick to existing systems for cellular processes, if this limits us to create something that already exists. Why inventing the wheel twice? One answer is that the creation of a minimal cell is effectively less of a goal in itself, as it is a pathway to understand what already exists in every living organism. If we use for example a completely synthetic method for division of a synthetic cell, then this might make the process easier to control, but it will teach us less about the processes taking place in living organisms. By applying naturally existing systems, we simultaneously learn more about them. And if we are successful in creating a minimal cell, then this system will be a superb platform and model system for adding and studying a vast number of biological processes in the absence of the complexity present in any other organism. Thus, the minimal cell can be seen primarily as an endeavour to gain knowledge than to create directly an alternative production machinery. However, the knowledge gained this way will significantly increase the effectiveness and precision with which we can manipulate existing organisms and treat diseases. The minimal cell project is therefore still highly relevant in general for advances in biotechnology and medicine. Farther into the future, once we have vastly increased our knowledge and improved our methods, we most likely will be able to create completely synthetic organisms based on classical biological mechanisms that will outperform natural organisms. Till then, humanity will continue to do what it has done for millennia and adjust existing organisms to its needs.

7.3 Risks of developing synthetic cells

A question that comes up frequently in regard of the development of synthetic cells is if they could potentially pose a risk for the environment and for humanity. The short answer to this question is: No. At least if we constrain the question to the definition of a minimal cell we applied in this thesis, meaning a cellular organism of minimal complexity and overall composed of existing biological components.

To illustrate why a minimal cell would not be a serious threat, let us imagine applying the same principle to a multicellular organism like a dog. As with the minimal cell, it could be discussed at length what would be the minimal components of a dog, but let us apply the definition of something that is able to survive and reproduce in the most benign environment. This could be a combination of a stem brain, lung, heart, blood circulation, intestine, and reproductive organs based on canine cells and swimming in a nutrient solution. All other components like teeth, eyes, skin, limbs, or higher brain functions could be seen as adaptions to the native environment and not necessary for reproduction in a laboratory. Besides the possible ethical and aesthetic problems attached to such a creation, there would hardly be any concern regarding its potential to escape the laboratory and to cause damage. After all, it would demand meticulous care by its human creators in order to survive. The argument, that it could evolve does not apply in this scenario. In order to evolve, a biological organism has to undergo several changes over a multitude of generations, but in this case the number of generations would not surpass one or two. And even if it could miraculously survive somehow and create offspring over several generations, there would be thousands of beings more adapted to the given environment. It would be outmatched and selective pressure would terminate its chances of proliferating long enough to evolve. Basically, the same applies to a minimal cell. All nutrients are constantly supplied to it; of which several would be near non-existent in a normal environment. Parameters like acidity, salt concentrations, and temperature would be kept stable constantly and factors like UV damage would be avoided in the laboratory. If we are speaking strictly of a minimal cell as defined previously, it will not have any additional systems to compensate for fluctuations or absence of these parameters. When exposed to the natural world, it would not be able to adapt before the system would break down. As with the minimal dog or a human being left on the moon naked, there would be no time to adapt to an environment which is almost immediately deadly to the system. The direct potential of danger of a minimal cell, again, as previously defined as such, is therefore negligible.

However, what if we create a minimal cell, and then increase its complexity again? Implying it would technically not be a minimal cell anymore of course. In this case it could admittedly become dangerous. Nevertheless, as long as we add only existing biological modules, it will likely not be more dangerous than the organisms that do already exist. Further, whatever potentially dangerous modules we can add to it, we can add most likely to other, already established organisms as well. And we could select the organism that is already best adapted to the environment in which it would be released. As discussed in the previous section, even if we create a minimal cell and use it as a platform, for a long time it will likely be more easy to manipulate existing organisms. For example, when it comes to biological warfare, it would be extremely difficult to implement all the complex mechanisms that are necessary for an organism to survive and replicate in the human body. On the other hand, this problem can be largely skipped if the module is inserted into a pathogen already adapted to proliferate in the human body such as a flu virus. Further, concerns have been voiced that so called biohackers might start creating life forms outside of any governmental control. Quote:

"Imaging a world where practically anybody with an average IQ would have the ability to create novel organisms in their home garage" [13]. To put this into perspective, we should remind ourselves that it takes even today a multitude of scientific groups, many years and an extensive budget to at least understand the basic functions and properties of a single cellular organisms. Not to mention the *in vitro* creation of such a complex entity. In short, the complexity of living entities makes a creation by amateurs extremely unlikely. An exception to this might be viruses, as they can be basically made from nothing else but RNA or DNA and are much more simple in their function as they rely on the complicated and tuned systems present in their host cells. Nevertheless, the biggest danger is here as well the synthesis and manipulation of known viruses instead of completely new ones.

What appears to create uneasiness about the idea of a minimal cell is not the actual danger of an overly simplified organism assembled *in vitro*. It is the idea of creating something foreign and different to what we know. However, as long we stick to existing components, what we will create will not be that different to what already exists. This being said, everything about the previous statement changes as soon as we would apply components and modules that are not homologous to what exists in nature. This could be significant changes made to existing biological systems or the design of completely novel ones.

Ultimately, it is possible to design proteins that are fundamentally different to the ones existing in biological organisms. Especially if we consider additional components that are simply not present in nature. The 20 amino acids for example are almost ubiquitous, but only in biological organisms. Recently, the synthesis of a *E. coli* bacterium with a simplified genetic code has been achieved by removal of three codons from the genome, thus leaving them available for coding other amino acids [14]. Further, the genetic code itself can be expanded by adding new bases. For example, a DNA consisting of six different nucleotides has been created and yielded promising results in *in vitro* evolution experiments [15,16] and recently DNA made from even eight compatible bases was achieved [17]. Moreover, we might part with the central dogma itself for future creations of artificial organisms. There is no reason to assume that there are no molecules other than DNA, RNA, and protein that can be utilized for the creation of life. After all, these three classes of molecules had to emerge under very constraint conditions and after life evolved it was apparently restricted in its capacity to change the fundamental elements of its own functions. Moreover, researchers gain continuously access to an unknown number of possible candidates for evolvable information carriers, some of which might have never appeared on this planet outside of a laboratory [18]. Organisms made from such components of an entirely new kind could have different attributes than life as we know it, such as high heat resistance or increased energy efficiency. When released such lifeforms might be able to outcompete existing organisms due to their unique and novel properties. Therefore, forms of life that are in their very nature *de novo* might very well represent a serious danger at some point in the future.

7.4 Defining life

The question about the very nature of life is often touched upon in synthetic biology. Nevertheless, there exists little agreement among scientists on what exactly life is or if even the attempt of reducing it to a distinct principle is reasonable [19–21]. Many different definitions have been proposed which vary widely in what characteristics they attribute to be exclusive to living entities [20,22–25]. Yet, in most cases these definitions either include phenomena that can also be applied

to non-living entities or exclude organisms that would otherwise be judged with certainty to be alive.

7.4.1 An unscientific category

First, it is important to remember that the terms of “life” and “alive” have not emerged from scientific fields, but have evolved in historical, religious, medical and philosophical contexts. Thus, it is not surprising that there are fundamentally different views on what constitutes life and at what point an entity becomes alive. Additionally, as with many categories the boundary at which life starts seems more than anything else dependent on the subject defining it. An anecdote to illustrate the point:

A general once invited a professor, who did his service in the reserve, to join him for dinner in his shelter during world war I. During the conversation the professor began to lose himself more and more in a topic of abstract concepts and the general became severely tired of it. Then, suddenly, the general asked the professor: “If I would attach 500 bristles in rows to a hand-big board, would I not be correct to call it a brush?” The professor answered perplexed: “Yes, surely.” The general continued to ask if it would still be brush with 200 bristles and the professor agreed again. Thus, the general kept getting lower with the number, until the professor exclaimed awkwardly that ten bristles are definitely not sufficient to consider it a brush anymore. The general then proclaimed amused: “Very well, I learned something new today. The concept of a brush requires a minimal number of eleven bristles!”.

When looking at entities that might be considered alive or not, we apparently face the same problem as the professor does with the brush. Namely, that although there appears to be a difference between living and non-living entities it does appear completely arbitrary where we draw the line between those two states. In case of what is alive, it appears to be common sense that all humans, animals, and cells are clearly living entities as long as their basic vital functions are present. However, when we start stripping one component at a time from these entities, it is at least questionable that we would reach a point at which the removal of a single enzyme or carbon atom would suddenly mark the border between alive and dead. The same is true considering creating a living organism bottom-up and adding one component at a time. When would a synthetic cell be alive? After completing a single successful reproduction cycle? Or after completion of two cycles, or three cycles, or eleven cycles?

The same issue manifests itself if we consider the range of existing living and non-living entities with different degrees of complexity ranging from multicellular organisms down to inorganic matter (Figure 7.2). Biologists would generally define with certainty multicellular organisms as well as single cell organisms like bacteria as alive. This becomes more a topic of debate if parasitic or symbiotic bacteria are considered, since they require other cells for their metabolism as they lack the ability to produce certain essential components themselves. The argument can be made that such an organism should not be considered alive as it requires another organism for survival and reproduction. However, the same argument can be made in regards of all heterotrophic organisms. After all, neither zebras nor humans can survive and reproduce in absence of other organisms like plants and gut bacteria. Further reducing complexity and independence, we may assess mitochondria, which have evolved from bacterial endosymbionts of eukaryotic ancestors [26]. Mitochondria contain their own specific DNA, albeit it is not encoding for all of their components.

Here, the arguments against them being alive would mainly be that they are just part of another organism and that they do not encode all of their components themselves. However, if we would rewind the evolution of mitochondria and have them regain gradually their former genes one by one, would we encounter a specific transition point between dead and alive by adding a single gene? Again the question appears reminiscent of the paradox with the bristle.

Viruses are minimal in their complexity, rely completely on host cells for replication, and are by many considered not to be alive. Nevertheless, in many cases they encode the complete information for all of their components. Further, a virus might require a living cell for all of its functions, but we already explored that most organisms are dependent on other organisms in order to function. The difference between a virus hijacking a complete metabolism and a cell consuming the products of another cell's metabolism could be seen as one of magnitude rather than of principle. Moreover, viruses can in some cases contain genomes larger than those of some bacteria [27] and some viruses can even be infected by other viruses [28], raising the question if an entity that can become sick can be considered dead?

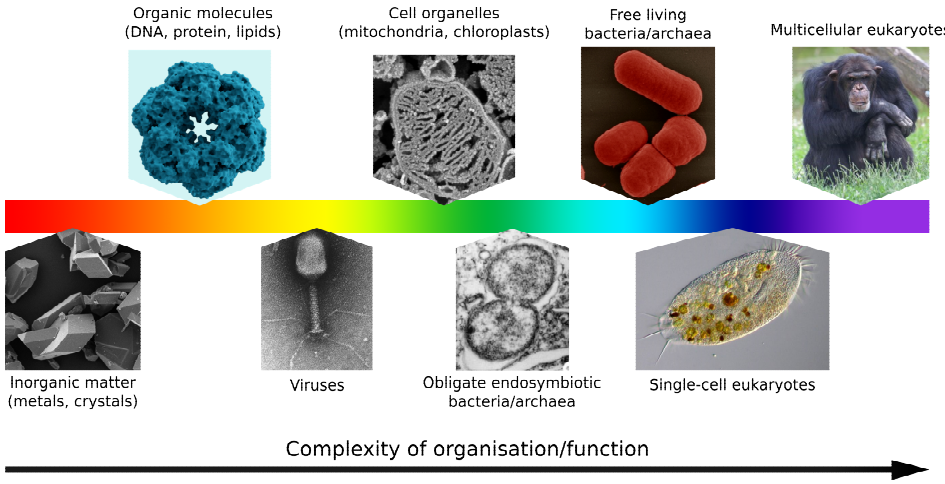

Figure 7.2: Spectrum of entities arranged from non-organic matter to highly complex organisms. Images from left to right: **(1)** SEM image of crystals from an explosive compound. Taken from Pelikan et al. 2014 [29]; **(2)** Glutamine synthetase. Taken from Wikimedia. Author: Thomas Splettstoesser; **(3)** TEM image of a T4 phage. Taken from Miller et al. 2003 [30]; **(4)** SEM image of a broken-up mitochondria. Taken from MacDonald et al. 2018 [31]; **(5)** TEM image of an chlamydiae endosymbiont. Taken from Collingro et al. 2005 [32]; **(6)** SEM image of *Acinetobacter baumannii*. Source: Robert Koch Institute, created by Gudrun Holland and Michael Laue; **(7)** Amoeba Stylonychia putrina. Taken from Wikimedia. Author: Picturepest; **(8)** Male chimp. Source: Biomedical Primate Research Centre, Rijkswijk.

At the end, there appears to be no discrete line between living and non-living entities and it could be suggested that life, as illustrated, is in practical terms a continuum of complexity and function, rather than a distinctive state of matter. As with the concept of a brush, the term life is in most cases applied as a pragmatic concept and relative to the subject applying it. When biologists gather up a list of subjectively satisfying attributes to define life in accordance with their field of research [19,21,33], then this is generally done to help creating a framework to work with. Such definitions are useful for specific applications, but should not be misinterpreted as objective facts. Instead of

identifying any system capable of replication or movement alive, it would be more precise and scientifically sufficient to term them for example replicators [34] or motile machineries respectively. Researchers working on different kinds of synthetic cells should define what their specific model system represents, rather than to fall back to a term that is in its current application not a scientific one. After all, from a pragmatic point of view, no overarching classification of the phenomena of life is required to investigate distinct biological processes [21].

7.4.2 Looking for a general principle

As elaborated in the previous paragraph, the term of life as it is generally applied has primarily not emerged from an objectively existent principle, but rather from subjective observations and pragmatic applications. Nevertheless, this does not mean necessarily that there might not be a fundamental principle inherent to life at all. It only means that we cannot trust our pragmatic usage of the term to be identical with such a principle. In order to find such a principle, two fundamental attributes of life should be taken into account.

First, whatever life represents, it is not a state, but a process. If a cell is rapidly frozen under sufficient pressure, the water it contains will vitrify and its structure will be almost perfectly maintained [35,36]. If we define life as a specific arrangement of matter (lipid membrane, DNA helix, etc.) then the frozen bacteria would have to be considered alive, as no significant change to its structure occurred. However, as long as this cell would not thaw up, it would show absolutely no characteristics different from any non-living structure and basically be a piece of ice containing some contamination of carbon. Although biological structures are essential for the fitness of an organism, without taking into account the dimension of time there is no inherent difference between them and non-living matter. If of two systems in which all molecules are arranged identical one breaks down immediately and the other starts to replicate and evolve, we would inevitably deem the first one to be dead and the second one to be alive.

Second, the concept of life makes only sense if it entails a lifeform and its environment. The examples of parasites, endosymbionts, and organelles given previously demonstrate the different degrees to which lifeforms are dependent on their environment. Moreover, every living entity requires a source of nutrients for survival and reproduction and often other factors like oxygen. A human being on the moon is in a way as alive as the spacesuit it wears is intact. Gram-positive bacteria and cyanobacteria are forming spores under adverse conditions which are virtually biochemically inert [37,38]. On their own, these spores possess no life-like attributes. Only upon entering a suitable environment, they will start to regain such life-like characteristics.

Having restricted life to a process dependent on the environment, we may examine several processes, that have been proposed to be characteristic for life on their own or in combination with others:

Growth
Reproduction
Absorption of matter or energy
Reduction of entropy
Movement
Metabolism
Evolution
Self-maintenance
Originating from a living entity

To analyse if these are valid candidates for being unique to living entities, we can start by simply asserting if inanimate matter can display the same properties. The phenomenon of fire displays growth, reproduction and the absorption of matter, while a growing crystal displays growth and absorption of matter, as well as a local reduction of entropy. Further, it seems reasonable to state that no ordinary form of machine should be considered alive. The machines we can create currently are able to perform movement, local reduction of entropy (fridges) and metabolism (bioreactors). Moreover, humanity has already been able to create machines that can replicate themselves in a primitive way from mechanical components [39]. This has been demonstrated 15 years ago by a robot arm which is made from cubes and is able to assemble another robot arm identical to itself (Figure 7.3). Although it is true that the replication of the robot requires the addition of already highly complex components, this does not negate that the robot assembled a copy from components less complex than itself, which is in principle not very different from living organisms absorbing components they cannot produce themselves for replication.

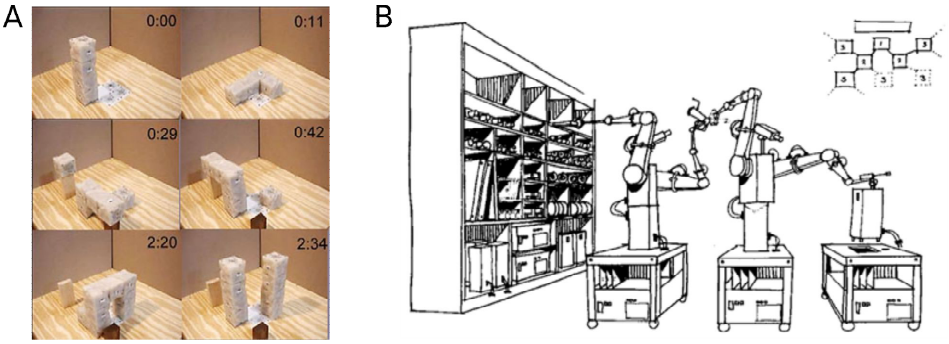

Figure 7.3: **(A)** Self-replicating robot. The robot consists of several cubes capable of bending and rotation. The arm can detach one of the cube attached to its end and utilize it to construct an identical arm to itself by adding cubes provided in its vicinity. Taken from [39]. **(B)** Principle of Self-replicating robots. Taken from: NASA Conference Publication 2255 Advanced Automation for Space Missions, Proceedings of the 1980 NASA Summer Study, June1980.

Considering self-maintenance, it should be considered that all living systems breakdown eventually and thus ultimately fail to maintain themselves. Moreover, many lifeforms even actively perform

mechanisms such as apoptosis that will destroy them for the sake of enabling the passing of their genes through other entities of the belonging organism or species. The restriction that all life originates from other life might sound sensible but is a non-sequitur as the first living entity could not have had a living ancestor by definition. However, if we do not consider the first living organism as truly alive, following this logic its descendants can neither be alive. Such a definition does not allow for start.

As a consequence, the attribute that would remain of the given list is the principle of evolution. Evolution basically arises as a consequence of the imperfect replication of a system and one proposed definitions of life is: *Life is self-reproduction with variations* [20]. However, this does not very clearly separate life from other phenomena capable of replication. The telling difference between the replication of a lifeform and the replication of a phenomenon like fire is that living entities replicate based on an intrinsic information. While changes of genes can create different lifeforms, the nature of a fire will always depend on external factors like the amount of available oxygen or the substrate. Therefore, a more specific definition could be: *Life is self-reproduction with variations, based on an internal information carrier.*

This definition can be equated with the principle of evolution and does include all forms of life that are generally considered to be alive, while being absent in all apparently inanimate matter and all simple version of machines. Moreover, as an emergent phenomenon, evolution possess characteristics and dynamics that exceed those inherent to its physical requirements. However, while it does apply to the origin of all known forms of life, it seems not to apply to certain individual lifeforms. After all, a sterile animal or human being is not capable of reproduction and thus would not be part of Darwinian evolution. As a response, it could be argued that such an animal or human would still be the result of evolution and reproduction. However, we could question this argument with a thought experiment. Assuming further technological progress, it is at least possible that humanity might be in the future able to create even complex forms of life completely *de novo*. If a sterile human being would be grown from chemically synthesized cells, then this human being would neither be the result of reproduction or evolution, nor capable of it. However, if this human being would still be fully capable of eating, thinking, and completing a PhD, then it would seem very obscure to not affirm it as being alive. The main aspect of this paradox is that the way multicellular beings are alive appears to be inherently different from how single cell organisms are alive. It could therefore be proposed that they should be treated as two fundamentally different categories of lifeforms and that the aforementioned principle of evolution for example is perfectly suitable for any kind of unicellular lifeform, but not necessarily for every multicellular one.

A counterargument that could be made is that a multicellular organism is just as alive as the cells it is made of. However, if we would cut a mammal into many pieces so fast and delicately that we can transfer each piece or even each cell in a nutrient solution without killing a single cell, would we say that the respective animal would be still alive distributed over a dozen petri dishes? It appears to be only reasonable to conclude that the property of alive assigned to a multicellular organism is a specific and emergent phenomenon. Thus, multicellular organisms appear to be alive on two levels simultaneously.

Overall, a definition that covers all the different aspects of unicellular and multicellular life will likely have to be very general in order to cover these very different systems. What is common in all known organisms is that they possess an internal information carrier. This would be RNA or DNA

in case of cells. In multicellular organisms the task of the conservation and processing of information is not only mediated by genetic information carriers, but as well by the nervous system. Therefore, information storage and adaptation is present on both levels of complexity. However, neither artificial DNA databanks nor a hard disc drive appears to share much commonality with biological organisms beyond the storage of information itself. It is reasonable to assume that a certain dynamic has to act on the information carrier to lead to the emergence of life. The most obvious dynamic process connected to genetic information is of course evolution, but we already established that Darwinian evolution cannot act on the level of a single, non-reproductive individual. However, we could instead consider a more general concept akin to the one of evolution. Removing the criteria of reproduction and multiple generations, we could describe life as *the change of the internal information of an entity through interactions of the entity with its environment.*

In short, life as an inherent principle could be proposed as: *A pattern which is evolving.*

Examples of interactions between the internal pattern of an organism and its environment could be natural selection, active adaption, or learning. In case of such a broad definition, all kinds of multicellular organisms which possess a neural network capable of reacting and adapting to the environment would be alive based on this capability. All multicellular organisms too primitive for such processing mechanisms would only be as alive as its individual cells. Contrary, a phenomenon such as fire, which possess many of the formerly discussed attributes of life, lacks any kind of intrinsic information carried over during the process of combustion. The colour of a flame will always depend solely on the conditions in which the fire is burning. It has no dynamic intrinsic nature that can change and cause it to glow green when burning paper instead of yellow. Crystals do possess the stable internal information of their components defining the structure of their lattice. However, this information remains static. Hence, a crystal is not able to evolve in the given sense and would be just as fire a phenomenon that is excluded in the given definition. There are of course many other principles that have been proposed to be inherent to life and which have not discussed here, such as the hierarchical definition [23] or the well-known one brought forth by Erwin Schrödinger in 1944 [22].

7.4.3 Implications of an overarching principle

The second elaborated principle of live being in its essence any evolving pattern is rather fundamental and basic. This brings with it a certain vagueness and it is admittedly likely of little use for any direct scientific application. As mentioned earlier, it appears that distinct definitions that do not claim to encompass all aspects of life are more useful for specific scientific fields. The given definition is excluding phenomena like fire, but at the same time it does lead to the description of a large variety of processes as being alive which we would normally not consider to be so, with potentially interesting implications.

Artificial intelligence, machine learning, and computer viruses

For instance, an artificial intelligence would be included as alive under this definition as well as any kind of machine learning programme (Figure 7.4A). After all, the program changes its internal information in adaption to the input of the environment and evolves in order to solve given tasks. Further, not only would the given principle include common viruses, but also any kind of electronic virus that is able to evolve in the environment of the internet. This strongly challenges our understanding of life as a biological phenomenon. Here, it should be considered that every

biological organism consists of ultimately non-biological components and that only because life has evolved in the past in specific ways, this does not mean that a general principle of life would be bound to them.

Memes

In his well-known book The Selfish Gene, Richard Dawkins has argued for the existence of cultural units that can be understood as replicators in a cultural background just as genes act as replicators in organisms [40]. These cultural units have been termed as memes and it has been theorized that cultural developments have been strongly influenced by the evolution and spreading of memes [40,41]. This concept has already been proposed in several variations before, as for example by Huxley attributing evolution and natural selection to ideas in 1880, writing that: “A theory is a species of thinking, and its right to exist is coextensive with its power of resisting extinction by its rivals” [42]. Recently, the concept of memes as cultural replicators has become so popular that based on it the discipline of memetics has emerged [43]. Just as genes encoded by DNA, ideas that qualify as memes appear to possess the capability of replication, mutation, high-fidelity copying, and the formation of lineages in the cultural domain [41]. In regards to their human hosts, memes can be of symbiotic, neutral, or parasitical nature. They can spread through the behaviour they generate in their hosts, for example by containing a moral imperative that the respective idea has to be spread. As in case of parasites and viruses, transmission and replication of memes can occur effectively even when the induced behaviour is detrimental to their hosts [44]. Defined as such an evolvable entity, a meme would as well fit the proposed overarching principle of life. It might appear rather strange to assign the attribute of being alive to a mental construct. However, if we do accept the existence of such cultural or social replicators, their resemblance to genes and biological organisms reliant on a host, and that life as a principle is not correlated to a specific substrate, then the concept that these replicating ideas themselves are alive is not inherently illogical. After all, if genes and memes behave fundamentally in the same way, how much does it matter that the substrate is DNA for one and neural circuits for the other?

It is noteworthy that in regards of the spreading of ideas considered as potentially harmful, the term of social contagion has emerged already at the end of the 19th century and appears to be closely related to the concept of a meme [45]. Further, it could be stated that just as bacteria and viruses have been applied as biological weapons, memes recognized as social contagions have been attempted to be utilized in the same manner. A prominent case that could be interpreted as such an incident was the decision of the German government to assist Lenin in reaching Russia in 1917, speculating that the revolutionary ideas of Lenin could disrupt the Russian state. This proved to be successful, as the October Revolution led to the exit of the Russian empire from the war. Further comparing memes and diseases, when added together the estimated number of deaths allegedly caused by the ideologies of national socialism and communism exceeds the estimated number of deaths caused by the Spanish flue by a factor between 1 and 7 [46–48]. Considering memes as being alive might influence the very way we consider how ideologies affect individuals and societies. If harmful and contagious ideologies would be assessed to share a common principle with parasites and viruses, then this might change how we judge and treat people affected by them. Victims of ideological possession might in the future be treated with a similar understanding and compassion as we treat today people suffering from an infection. At the same time, it should be kept in mind that the categorization of a phenomenon as pathological can also be utilized in harmful manners, as done for example in the past by lobotomizing the frontal cortex of hysteria patients.

On the other hand, a meme can as well enhance its own replication chances by enhancing the fitness and well-being of its host. The scientific method and mind-set might be seen as such a symbiotic meme, which has primarily spread by boosting host capabilities and by attracting imitation through a promise of progress.

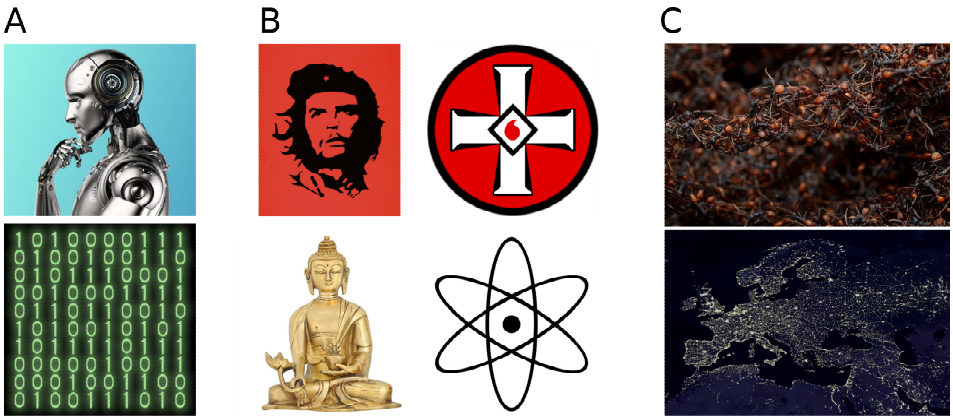

Figure 7.4: Phenomena included in an extended principle of life. **(A)** Artificial intelligence, machine learning, as well as adaptive computer viruses. **(B)** Symbols representing different types of memes. Top left: Che Guevara portrait. Top right: Symbol of the KKK. Bottom left: Buddha statue. Bottom right: Atom sign as symbol for science. **(C)** Examples of superorganisms. Top: Ant colony of army ants. Taken from Wikimedia. Author: Geoff Gallice. Bottom: Satellite image from Europe and western Asia at night. Taken from www.NASA.gov.

Superorganisms

Last, if we consider multicellular organisms alive in their own right, that means beyond the level of its singular living cells, then the possibility arises that entities composed of a connected multitude of multicellular organisms are alive in their own right as well. Typical examples for such potential superorganisms are ant colonies or bee hives, in which the colony behaves like an organism and is subject to selective pressure as a whole despite the physical individuality of each animal [49,50]. If such entities indeed operate as organisms in the real sense, then to what degree does the same apply to human cultures and nations? Very similar to an ant colony, a nation for example resembles several aspects of multicellular organisms, as it consists of living entities, which are specialized to operate certain vital tasks like energy production, acquisition of resources, and organisation. Moreover, it is able to evolve in response to changes by changing its internal information encoded by laws as well as cultural patterns. On the one hand, the concept of human societies as organisms has already been assessed to be a useful metaphor [51], but it is at least an interesting question to what degree societies might be actually alive as an emergent phenomenon. Moreover, advances in transportation and communication have led to the development of strong trade and cultural connections between many human societies. Especially the internet has created a dense information network connecting a large proportion of humanity. Therefore, it could be assumed that humanity as a whole might at some point start to exhibit the emergent behaviour of a superorganism.

References

[1] Mabuchi I. Biochemical aspects of cytokinesis. Int Rev Cytol 1986;101:175–213.

[2] Miller AL. The contractile ring. Curr Biol 2011;21:R976–8.

[3] Litschel T, Ramm B, Maas R, Heymann M, Schwille P. Beating Vesicles: Encapsulated Protein Oscillations Cause Dynamic Membrane Deformations. Angew Chem Int Ed Engl 2018;57:16286–90.

[4] Godino E, Lopez JN, Foschepoth D, Cleij C, Doerr A, Castella CF, et al. De novo synthesized Min proteins drive oscillatory liposome deformation and regulate FtsA-FtsZ cytoskeletal patterns. Nat Commun 2019;10:4969.

[5] Deshpande S, Spoelstra WK, van Doorn M, Kerssemakers J, Dekker C. Mechanical Division of Cell-Sized Liposomes. ACS Nano 2018;12:2560–8.

[6] Jewett MC, Forster AC. Update on designing and building minimal cells. Curr Opin Biotechnol 2010;21:697–703.

[7] Xu C, Hu S, Chen X. Artificial cells: from basic science to applications. Mater Today (Kidlington) 2016;19:516–32.

[8] Morimoto T, Kadoya R, Endo K, Tohata M, Sawada K, Liu S, et al. Enhanced Recombinant Protein Productivity by Genome Reduction in Bacillus subtilis. DNA Res 2008;15:73–81.

[9] Mizoguchi H, Sawano Y, Kato J, Mori H. Superpositioning of Deletions Promotes Growth of Escherichia coli with a Reduced Genome. DNA Res 2008;15:277–84.

[10] Pósfai G, Plunkett G, Fehér T, Frisch D, Keil GM, Umenhoffer K, et al. Emergent Properties of Reduced-Genome Escherichia coli Science (80-) 2006;312:1044 LP – 1046.

[11] Kurokawa M, Seno S, Matsuda H, Ying B-W. Correlation between genome reduction and bacterial growth. DNA Res 2016;23:517–25.

[12] Hutchison CA 3rd, Chuang R-Y, Noskov VN, Assad-Garcia N, Deerinck TJ, Ellisman MH, et al. Design and synthesis of a minimal bacterial genome. Science 2016;351:aad6253.

[13] Schmidt M. Diffusion of synthetic biology: a challenge to biosafety. Syst Synth Biol 2008;2:1–6.

[14] Fredens J, Wang K, de la Torre D, Funke LFH, Robertson WE, Christova Y, et al. Total synthesis of Escherichia coli with a recoded genome. Nature 2019;569:514–8.

[15] Zhang L, Yang Z, Sefah K, Bradley KM, Hoshika S, Kim M-J, et al. Evolution of functional six-nucleotide DNA. J Am Chem Soc 2015;137:6734–7.

[16] Georgiadis MM, Singh I, Kellett WF, Hoshika S, Benner SA, Richards NGJ. Structural basis for a six nucleotide genetic alphabet. J Am Chem Soc 2015;137:6947–55.

[17] Hoshika S, Leal NA, Kim M-J, Kim M-S, Karalkar NB, Kim H-J, et al. Hachimoji DNA and RNA: A genetic system with eight building blocks. Science (80-) 2019;363:884 LP – 887.

[18] Pinheiro VB, Taylor AI, Cozens C, Abramov M, Renders M, Zhang S, et al. Synthetic Genetic Polymers Capable of Heredity and Evolution. Science (80-) 2012;336:341 LP – 344. [19] Tang B. A Minimal or Concise Set of Definition of Life is Not Useful. J Biomol Struct Dyn 2012;29:613–4. https://doi.org/10.1080/073911012010525003.

[20] Trifonov EN. Vocabulary of definitions of life suggests a definition. J Biomol Struct Dyn 2011;29:259—266.

[21] Ruse M. Ernst Mayr. The growth of biological thought: Diversity, evolution, and inheritance. Cambridge, Mass., and London: Belknap Press of Harvard University Press, 1982. xiii + 974 pp. $30.00 (cloth). J Hist Behav Sci 1984;20:220–4.

[22] Schrödinger E. What is Life? The Physical Aspect of the Living Cell. Cambridge University Press; 1944.

[23] Jagers op Akkerhuis GAJM. Towards a Hierarchical Definition of Life, the Organism, and Death. Found Sci 2010;15:245–62.

[24] Emmeche C. Defining life, explaining emergence 1997.

[25] Zhu TF, Szostak JW. Coupled growth and division of model protocell membranes. J Am Chem Soc 2009;131:5705–13.

[26] Roger AJ, Munoz-Gomez SA, Kamikawa R. The Origin and Diversification of Mitochondria. Curr Biol 2017;27:R1177–92.

[27] Van Etten JL, Lane LC, Dunigan DD. DNA viruses: the really big ones (giruses). Annu Rev Microbiol 2010;64:83–99.

[28] La Scola B, Desnues C, Pagnier I, Robert C, Barrassi L, Fournous G, et al. The virophage as a unique parasite of the giant mimivirus. Nature 2008;455:100–4.

[29] Pelikan V, Zeman S, Yan Q-L, Erben M, Elbeih A, Akstein Z. Concerning the Shock Sensitivity of Cyclic Nitramines Incorporated into a Polyisobutylene Matrix. Cent Eur J Energ Mater 2014;11:219–35.

[30] Miller E, Kutter E, Mosig G, Arisaka F, Kunisawa T, Rüger W. Bacteriophage T4 Genome. Microbiol Mol Biol Rev 2003;67:86–156, table of contents.

[31] MacDonald JA, Fowle WH, Shin E, Woods DC. A method for freeze-fracture and scanning electron microscopy of isolated mitochondria. MethodsX 2018;5:593–8.

[32] Collingro A, Toenshoff E, Taylor M, Fritsche T, Wagner M, Horn M. “Candidatus Protochlamydia amoebophila”, an endosymbiont of Acanthamoeba spp. Int J Syst Evol Microbiol 2005;55:1863–6.

[33] Schwille P, Spatz J, Landfester K, Bodenschatz E, Herminghaus S, Sourjik V, et al. MaxSynBio: Avenues Towards Creating Cells from the Bottom Up. Angew Chem Int Ed Engl 2018;57:13382–92.

[34] Dawkins R. Replicators and Vehicles. Cambridge Univ Press 1982:45–64.

[35] Gilkey JC, Staehelin LA. Advances in ultrarapid freezing for the preservation of cellular ultrastructure. J Electron Microsc Tech 1986;3:177–210.

[36] Huebinger J, Han H-M, Grabenbauer M. Reversible Cryopreservation of Living Cells Using an Electron Microscopy Cryo-Fixation Method. PLoS One 2016;11:e0164270–e0164270.

[37] Adams DG. Heterocyst formation in cyanobacteria. Curr Opin Microbiol 2000;3:618–24.

[38] Koonin E V, Starokadomskyy P. Are viruses alive? The replicator paradigm sheds decisive light on an old but misguided question. Stud Hist Philos Sci Part C Stud Hist Philos Biol Biomed Sci 2016;59:125–34.

[39] Zykov V, Mytilinaios E, Adams B, Lipson H. Robotics: self-reproducing machines. Nature 2005;435:163–4.

[40] Dawkins 1941- R. The selfish gene. New edition. Oxford ; New York : Oxford University Press, 1989.; 1989.

[41] Gers M. The Case for Memes. Biol Theory 2008;3:305–15.

[42] Huxley TH. The Coming of Age of the Origin of Species. Nature 1880;22:1–4.

[43] Heylighen F, Chielens K. Evolution of Culture, Memetics BT - Encyclopedia of Complexity and Systems Science. In: Meyers RA, editor., New York, NY: Springer New York; 2009, p. 3205–20.

[44] Kelly K. Out of Control. 1994.

[45] Marsden P. Memetics and Social Contagion: Two Sides of the Same Coin? J Memet 1998;2:171–85.

[46] Ikenberry G, Valentino B. Final Solutions: Mass Killing and Genocide in the 20th Century. Foreign Aff 2004;83:164.

[47] Rudolph J. R. Death by Government. New Brunswick; 1994.

[48] Johnson NPAS, Mueller J. Updating the accounts: global mortality of the 1918-1920 "Spanish" influenza pandemic. Bull Hist Med 2002;76:105–15.

[49] GARDNER A, GRAFEN A. Capturing the superorganism: a formal theory of group adaptation. J Evol Biol 2009;22:659–71.

[50] Dawkins R. The extended phenotype. 1999.

[51] Kesebir S. The Superorganism Account of Human Sociality: How and When Human Groups are Like Beehives. SSRN 2011.

Summary

Humanity has achieved to decipher the most fundamental mechanics of cellular life. Nevertheless, despite intense efforts there are still considerable gaps in our understanding of cellular processes. Traditionally, biologists investigate life by observation of existing lifeforms. In order to assign functions to biological components, it is common practice to remove components from the system and then note the effect this has on the organism. Done repeatedly, this top-down approach allows for the creation of lifeforms with a reduced complexity, which makes it easier to fully map and model their cellular processes. In contrast, more and more additional effort is now exerted by the scientific community to recombine *in vitro* biological components in order to form a cellular lifeform. This bottom-up approach might not only yield in the end a minimal cellular system created *de novo*, but will further challenge us to verify and sophisticate our knowledge about cells.

Gene expression through transcription and translation is the probably most fundamental process present in all cells existing today and any attempt of designing a minimal cellular system mimicking a real cell faithfully will have to involve these processes at its core. Thus, cell-free gene expression constitutes a key tool for the creation of a minimal cell. In this thesis we applied the bottom-up approach to investigate eukaryotic and prokaryotic microtubules, as well as the yeast ESCRT-III (endosomal sorting complex required for transport) and archaeal Cdv (cell division) system regarding their potential for cell-free expression and synthetic cell research.

Overall, all proteins utilized in this thesis for cell-free expression (Mal3, BtubA, BtubB, BtubC, Vps20• C, Snf7, Vps2, Vps24, Vps4, CdvA, CdvB, and CdvC) have been synthesized by the PURE system at full-length. Therefore, expression itself was not a problem for any of the applied systems and the most critical step for each protein system was to evaluate if the expressed proteins were active regarding their functions and interactions. A key factor for each project was thus to find reliable testing conditions for the respective protein activity.

For cell-free protein synthesis, we applied the commercially available PURE system, which is comprised exclusively of reconstituted components. A current drawback this system suffers from is that expression stops after a few hours due to unknown causes. This time interval is too short to reconstitute certain cellular functions and in the long run the design of a minimal cell will require a translation system that is more stable over time. Therefore, we attempted to enhance the expression lifetime of the PURE system by implementation of a semi-open system. However, no changes in duration of expression or yield was observed **(Chapter 2)**. This result supports the hypothesis that neither accumulation of toxic waste products, nor the depletion of NTPs or amino acids are primarily responsible for break-down of PURE system activity over time.

Another question we investigated was if it would be possible to regulate eukaryotic microtubules by expression of microtubule associated proteins (MAPs). We chose to attempt expression of the end-binding MAP Mal3 due to its ability to be expressed functionally in *E. coli* and its crucial role in organizing protein recruitment at the plus-end of microtubules. To visually confirm activity of expressed Mal3, we added it to microtubules together with the purified proteins Tea2 and Tip1, which are recruited by Mal3 to the microtubule plus-end **(Chapter 3)**. In this plus-end tracking assay distinctive prove of the activity of expressed Mal3 was visually given by formation of comets at microtubule tips.

A restriction faced with eukaryotic tubulin is that it cannot be synthesized by any prokaryotic expression system such as the PURE system. However, the tubulin homologues BtubA and BtubB have been previously discovered in bacteria of the genus *Prosthecobacter*, in which they form filaments similar to microtubules. We synthesized BtubA/B with the PURE system and were able to show that it was expressed at full-length and was fully capable of forming dynamic bacterial microtubules **(Chapter 4)**. Assembly took mostly place on top of a supported lipid bilayer (SLB) to which the filaments were binding without addition of any cofactors. A fraction of labelled bacterial tubulin, which would not result in any filaments on its own, was added for visualization. Further, the capability of synthesized BtubC to recruit bacterial microtubules to lipid membranes beyond the tendency for binding already observed could be confirmed by flotation assays. Moreover, when expressed inside liposomes BtubA and BtubB formed filaments that were deforming the vesicles similar to what is known of encapsulated tubulin or actin. The encapsulated filaments could be disintegrated by intense laser illumination upon which vesicles appeared to reverse into their former shape. Overall, bacterial microtubules have the potential to become a useful tool for engineering synthetic cells under the premise that more proteins associated their regulation and function will be discovered.

One of the challenges for the creation of a minimal cell is to achieve cell division and we explored the yeast ESCRT-III system in respect to its potential to facilitate division in a minimal cell setup **(Chapter 5)**. However, assessing the activity of the four ESCRT-III proteins turned out to be difficult because of a lack of purified proteins. Nevertheless, we could assert membrane binding capabilities of the ESCRT proteins by flotation assays and colocalization to SLB membranes. The formation of filament complexes composed of expressed Vps20• C and Snf7 was confirmed by transmission electron microscopy. However, it is not certain if these structures are truly resembling ESCRT filaments. Membrane deformation initiated by expressed ESCRT-III proteins could not be achieved, which is in line with more recent literature that proved the dependency of the ESCRT complex on the ATPase Vps4 for this function. Vps4 can be expressed by the PURE system, but its ATPase activity was not analyzed, as consumption of ATP cannot be reliably detected in the PURE system and depolymerization of filaments would require more efficient visualization of filaments or filament complexes.

Activity of expressed Cdv proteins could not be confirmed or analyzed **(Chapter 6)**. It could only be determined that expressed CdvA, which is responsible for anchoring the Cdv complex to the membrane in archaea, did not bind to the lipid membranes we used in our settings. A possible reason for this could be differences in membrane composition between bacteria and archaea.

As elaborated in Chapter 1 and 7, the terms and definitions that entail synthetics cells and the phenomenon of life are generally not very concise and rather arbitrary. We proposed that in most scientific work the respective definitions should be orientated with respect to the aim of the research and explicitly be restricted to the applied framework. Regarding a more general definition of lifeforms, we suggested that life is characterized by self-reproduction with variations, based on an internal information carrier. This definition excludes no lifeforms in general, but certain representatives of living entities which are uncapable of reproduction. Therefore, an even more basic and fundamental principle was proposed, according to which any kind of pattern which is capable of evolving could be considered alive. This definition not only includes all organisms generally considered alive but as well several other phenomena.

Samenvatting

De mensheid is er in geslaagd de fundamentele mechanismen van cellulair leven te ontcijferen. Er zijn echter, ondanks intensieve inspanningen, nog aanzienlijke gaten in ons begrip van cellulaire processen. Biologen bestuderen van oudsher het leven door bestaande levensvormen te observeren. Om functies aan bepaalde biologische componenten toe te kennen is het gebruikelijk om deze componenten weg te halen en het effect dat dit heeft op het organisme te beschouwen. Door dit herhaaldelijk te doen kunnen met de zogenaamde top-down aanpak minder complexe levensvormen gecreëerd worden. De cellulaire processen van deze vereenvoudigde organismen kunnen eenvoudiger volledig in kaart gebracht en gemodelleerd worden. De wetenschappelijke gemeenschap levert echter meer en meer inspanningen om een cellulaire levensvorm te creëren door in vitro biologische componenten samen te voegen. Deze contrasterende bottom-up aanpak zal niet alleen een minimaal cellulair systeem opleveren dat de novo is gecreëerd, maar zal ons ook verder uitdagen om onze kennis over cellen te verifiëren en uit te breiden.

Genexpressie via transcriptie en translatie is waarschijnlijk het meest fundamentele proces dat plaatsvindt in alle hedendaagse cellen, en elke poging om een minimaal cellulair systeem te maken dat een waarheidsgetrouwe afspiegeling is van een echte cel dient dit proces als uitgangspunt te nemen. Celvrije genexpressie is daarom een essentieel gereedschap om een minimale cel te bouwen. In deze thesis hebben we de bottom-up aanpak toegepast om eukaryote en prokaryote microtubuli te bestuderen. Bovendien is het potentieel van het ESCRT-III systeem van gist (endosomal sorting complex required for transport, endosomaal sorteercomplex noodzakelijk voor transport) en het Cdv systeem van archaea (cell division, celdeling) onderzocht met betrekking tot celvrije expressie en onderzoek naar synthetische cellen.

Alle eiwitten die in deze thesis zijn gebruik voor celvrije genexpressie (Mal3, BtubA, BtubB, BtubC, Vps20ΔC, Snf7, Vps2, Vps24, Vps4, CdvA, CdvB, and CdvC) zijn in hun volledige lengte gesynthetiseerd in het PURE-systeem. Expressie zelf was dus geen probleem voor alle toegepaste systemen, en daarom was de meest kritische stap voor elk eiwitsysteem om te evalueren of de tot expressie gebrachte eiwitten actief waren qua functies en interacties. Het vinden van betrouwbare testcondities voor de eiwitten was daarom een essentiële factor in de respectievelijke projecten.

Voor celvrije eiwitsynthese hebben we het commercieel verkrijgbare PURE-systeem toegepast, dat exclusief bestaat uit gereconstitueerde componenten. Een huidig nadeel van dit systeem is dat eiwitexpressie na een paar uur stopt, en dat de oorzaak hiervan onbekend is. Dit tijdsinterval is te kort om bepaalde cellulaire functies te reconstitueren. Op de lange termijn zal een translatiesysteem dat meer stabiel is over tijd nodig zijn voor het ontwerp van een minimale cel. We hebben daarom gepoogd de expressietijd van het PURE systeem te verlengen door een halfopen systeem te implementeren. Een verandering van expressieduur of -opbrengst is echter niet geobserveerd (Hoofdstuk 2). Dit resultaat ondersteunt de hypothese dat noch de accumulatie van giftige afvalstoffen, noch het opraken van NTPs of aminozuren, verantwoordelijk is voor de afname van activiteit van het PURE-systeem over tijd.

Een ander vraagstuk dat we hebben bestudeerd was of het mogelijk is om eukaryotische microtubuli te reguleren door de expressie van microtubuli-geassocieerde eitwitten (MAPs). We hebben gekozen om te proberen de MAP Mal3, die aan het einde van de microtubulus bindt, tot expressie te brengen, aangezien dit eiwit functioneel tot expressie kan worden gebracht in E. coli en het een cruciale rol heeft in het organiseren van het rekruteren van eiwitten aan het plus-einde van microtubuli. Om de activiteit van tot expressie gebracht Mal3 visueel te bevestigen, hebben we het samen met de gepurificeerde eiwitten Tea2 en Tip1, die door Mal3 gerekruteerd worden aan het

pluseinde, toegevoegd aan microtubuli. Duidelijk visueel bewijs van de activiteit van tot expressie gebracht Mal3 werd gegeven door de vorming van kometen aan de uiteinden van microtubuli in deze plus-end tracking analyse.

Een beperking die wordt opgelegd door te werken met eukaryote microtubuli is dat deze in geen enkel prokaryoot expressiesysteem, zoals het PURE systeem, gesynthetiseerd kunnen worden. Echter zijn in bacteriën van het genus Prosthecobacter de tubulinhomologen BtubA en BtubB ontdekt, waar ze aan microtubili gelijkende filamenten vormen. We hebben BtubA/B gesynthetiseerd met het PURE-systeem en waren in staat te laten zien dat het in volledige lengte tot expressie gebracht werd en in staat was dynamische bacteriële microtubuli te vormen (Hoofdstuk 4). De vorming van microtobuli vond voornamelijk plaats bovenop een supported lipid bilayer, waar de filamenten zonder toevoeging van enige cofactor aan bonden. Een beetje gelabeld bacterieel tubulin, dat zelf geen filamenten kon vormen, was toegevoegd om visualisatie mogelijk te maken. De geschiktheid van tot expressie gebracht BtubC om bacteriële microtubuli aan lipide membranen te binden, bovenop de eerder geobserveerde neiging tot binding, is bovendien bevestigd met behulp van flotatietesten. Daarnaast vormden BtubA en BtubB, wanneer tot expressie gebracht in liposomen, filamenten die het membraan van het blaasje vervormden, zoals bekend is van tubulin of actin. Intense belichting met een laser kon de ingekapselde filamenten uiteen doen vallen, waarna de blaasjes in hun oorspronkelijke vorm terug leken te keren. Samenvattend hebben bacteriële microtubuli het potentieel om een nuttig gereedschap te worden om synthetische cellen te bouwen, er vanuit gaande dat er meer eiwitten ontdekt worden die betrekking hebben op hun regulatie en functioneren.

Het bereiken van celdeling is een van de uitdagingen bij het maken van een minimale cel. We hebben het ESCRT-III systeem van gist bestudeerd met betrekking tot zijn potentieel om celdeling van een minimale cel te faciliteren (Hoofdstuk 5). Het beoordelen van de activiteit van de vier ESCRT-III-eiwitten bleek echter lastig te zijn vanwege een gebrek aan opgezuiverde eiwitten. Niettemin konden we met flotatietesten en co-lokalisatie op SLB-membranen de membraanbindingsmogelijkheden van de ESCRT-eiwitten aantonen. De formatie van complexen van filamenten bestaande uit tot expressie gebracht Vps20ΔC en Snf7 werd bevestigd door transmissie-elektronenmicroscopie. Het is echter niet zeker of deze structuren echt ESCRT-filamenten nabootsen. Vervorming van het membraan, geïnitieerd door tot expressie gebrachte ESCRT-III-eiwitten, kon niet worden gerealiseerd, in overeenstemming met meer recente literatuur waarin bewezen wordt dat het ESCRT complex afhankelijk is van de ATPase Vps4 voor zijn functie. Vps4 kon tot expressie gebracht worden in het PURE-systeem, maar zijn ATPase-activiteit is niet geanalyseerd, aangezien de consumptie van ATP niet nauwkeurig gedetecteerd kan worden in het PURE systeem, en studie van het depolymeriseren van filamenten een meer efficiënte visualisatie van de filamenten dan wel filamentcomplexen nodig heeft.

De activiteit van tot expressie gebrachte Cdv-eiwitten kon niet worden geanalyseerd of bevestigd (hoofdstuk 6). Het enige dat vastgesteld kon worden was dat tot expressie gebracht CdvA, verantwoordelijk voor het verbinden van het Cdv-complex met het membraan in archaea, niet aan de door ons gebruikte lipide membranen bindt. Het verschil in membraancompositie tussen bacteriën en archaea is hier een mogelijke oorzaak van.

Zoals uitgeweid wordt in hoofdstuk 1 en 7, zijn de terminologie en definities waarmee synthetische cellen en het verschijnsel ‘leven’ worden beschreven in het algemeen niet erg precies en betrekkelijk willekeurig. We hebben voorgesteld dat in het gros van het wetenschappelijke werk de respectievelijke definities georiënteerd dienen te worden met betrekking tot het doel van het onderzoek, en expliciet beperkt tot het toegepaste kader. Met betrekking tot een meer algemene

definitie van levensvormen hebben we voorgesteld dat leven wordt gekarakteriseerd door zelf-reproductie met variaties, gebaseerd op een interne drager van informatie. Deze definitie sluit in het algemeen geen levensvormen uit, maar wel bepaalde vertegenwoordigers van levende systemen die niet in staat zijn tot reproductie. Derhalve is een meer fundamenteel principe voorgesteld, waarmee elk soort patroon dat in staat is te evolueren als levend beschouwd zou kunnen worden. Deze definitie omvat niet alleen alle organismen die doorgaans als levend beschouwd worden, maar ook enkele andere fenomenen.

Acknowledgements

During the last 5 years I encountered so many good people of whom the company I enjoyed and who helped me in the lab and outside. I could not have succeeded without them. There have been so many of those, that I will not be able to mention all of them here. My apologies for that.

Christophe, thank you for giving me the opportunity to work in such a great group with such a dedicated supervisor. Your love for science, your scientific integrity, your enthusiasm, and the vigor with which you pursue science are inspirational. You made sure I would finish my PhD, even if this entailed hijacking a Bavarian boat. Thank you for your continuous support during the last 5 years.

Marileen, thank you for your support and patience. And thank you as well for your trust that I will find my way. **Arjen** and **Wiel**, thank you for your help with the electron microscope.

My dear Mofos and Paranymphs, **Ali** and **Mehran**. You two have been true friends through all this time. I am not exaggerating that without your love and support I surely would not have had the strength to finish this. I am blessed to be able to call myself your friend. **Mehran**, there is no measurement for the value of what you have taught me and all the encouragement you have given me to go my path. I can only hope to inspire one day someone in a way as you inspired me. Thank you for your wise kindness. **Ali**, thank you so much for all the compassion that you are overflowing with. It is such a joy to see how you lose yourself when engaging in the things you are interested and the people you care for. Thank you for every smile and laughter you shared. You brought a happiness and liveliness to the office that lifted all of us out of our daily struggles.

Jonas, my double/alter ego. Thank you for your support, your generosity, the many great discussions we had, and of course for your Koningsdag dating guide! I hope we will soon have again shots together. **Duco**, thank you for your humour and the rich kindness hidden under your sharp tongue. You are a great Tutor and I hope you will always have some students around that can look up to you. And thanks for all the help you readily gave. If it was with translating the summary or exhausting yourself on my staircase. **David**, thank you for opening up the ground for all the dirty borderline jokes. I wish you all the best for you and your family! **Elisa**, your perseverance is remarkable and I hope it will carry you well through the rest of your PhD! A big thanks to **Anne** for her essential help in the different projects! I just wish I could have given you more thankful proteins to work with. **Ilja**, thank you for protecting the lab from the laws of entropy. **Pauline**, I was always impressed by your knowledge and thoroughness of thinking, but even more I admired your positivity and enthusiasm. The best of luck now with starting a family! And a big thanks of course to the former lab members **Andrew**, **Huong**, and **Fabrizio** who welcomed me kindly when I started. Good luck to **Zhanar** and **Anna** who joined the lab when I was about to finish. **Wouter**, may the PURE and filaments be with you!

Maurits, thank you for the delightful conversations and your expertise on Scotch. **Reza**, thank you for your interest in bacterial microtubules. I wish you success in their investigation! Many thanks to **Louis**, **Nuria**, **Kim**, **Vladimir**, **Esengül**, **Renu**, **Celine**, **Eli**, and the other current and former members of Marileens group for their help with the microtubules and their kindness. I hope you will continue to have many game nights in the future!

A great thanks to my students **Gabriele**, **Anna, Mats, and Kabir** for contributing significantly to this work. Being your supervisor was the most fun part of it!

Roland, thank you for your honesty and for being simply a great guy. There is nobody who can imitate somebody brushing their teeth without using an actual brush as good you can. And thank you for bringing our PhD movie projects to a whole new level! **Nicole** and my dirty Nerdies, thank you for all the highly inappropriate insider jokes!

Patrick, it was an honor to rub swords with you. I hope you are soon out the *dangerzone!* **Carsten**, another great teacher. Thank you for all the great conversations in which you played the devils advocate with genuine understanding of the other side. **Benjamin**, thank you for the sparring match. And thank you for not beating all of us up for all these Arnold Schwarzenegger comments. Thanks to **George** and **Sonja** for staying till the middle of the night to discuss the intrinsic nature of morality. **Richard**, thank you for the chats in front of BN. **Dimitri**, thank you for the chambers and allowing me to have some me-time in your workshop. Thanks to **Fede**, **Becca**, **Jochem**, **Anthony** and all the other people at BN who I had the pleasure to share drinks with!

Irina, thank you for all the delicious food and joining me on my adventure trip to St. Petersburg. My gratitude to my **Hungarian sparring partner** who crippled me for almost a year. It was a good fight, no regrets. Greetings to my former fencing partner **Mark**, who always makes us look so fancy during our final PhD moments. **Nathalie**, thank you for welcoming me to the society of psychologists! **Saskia**, you will not read this, but thank you nevertheless for the inspiration that sometimes all that keeps us from doing what we want is simply doing it. And a thanks to **Jordan** for encouraging me to clean up my room (at least once in a while) and to **Sam** for reminding me to meditate in it once in a while. My gratitude to the **Dutch landscape**, which made me appreciate how much joy I receive from simply having hills around me.

Flo, du alter Hund. Ich werde nie vergessen wie wir das erste Mal zusammen gespielt haben und ich deine schöne Eisenbahn habe entgleisen lassen. Wir haben seit damals einiges zusammen durchgemacht und ohne deine Kameradschaft wäre die Schulzeit oft nicht ertragbar gewesen. Seitdem habe ich deine Geradlinigkeit, Verlässlichkeit, und Loyalität bewundert. Du suchst und gehst deinen eigenen Weg, unbeirrt und ohne Kompromisse. Alleine dafür liebe ich dich und ich wünsche dir alle Kraft dies weiter zu tun. Egal wie chaotisch meine Situation, ich wusste immer, dass deine Freundschaft wie ein Fels unberührt von all dem bleiben würde. Genauso wie weder Entfernung noch Zeit ihr etwas anhaben konnten. Solch eine Sicherheit zu besitzen, solch einen Freund den meinen nennen zu können ist ein Privileg für welches ich nicht dankbar genug sein kann.

Nelli, nicht dankbar genug kann ich sein für die wundervolle Zeit die wir miteinander hatten. Vielen Dank für jeden guten Tag. Alle Kraft und viel Mut wünsche ich dir für deine Zukunft! **Phillip** du zarte Seele, ich hoffe wir werden bald wieder ordentlich ein Bierchen zusammen zischen. Einen großen Dank an die alte Gang (**Marcel, Chrissi**, **Phillip**, **Anja**) und an **Stephanie** die mir meine Studienzeit so versüßt haben. Hoffentlich begegnen wir uns bald wieder am Main. Dank an **Felix** und **Ben** für all die geile Zeit die wir in der Schule hatten. Vielen Dank den Leuten vom Insel Survival für dieses einmalige Erlebnis. Dank auch an meine neuen Mitbewohner **Andi**, **Silja** und **Katharina** die mich inmitten der Seuche aufgenommen und mir herzliche Gesellschaft gegeben haben.

An meinen Vater, es ist schade, dass du dies nicht mehr lesen wirst. Ich habe erst spät realisiert was ich Alles von dir erhalten habe.

An meine Mutter, leider bin ich nicht imstande in Worte zu fassen was ich dir Alles verdanke. Du hast mich immer unterstützt und das auf so viele Arten gleichzeitig. Dein Rückenhalt hat mir den Mut gegeben hinaus in die Welt zu gehen und mein Glück zu versuchen. Ohne deinen Glauben an mich und deine Liebe hätte ich dies nie geschafft.

Curriculum Vitæ

Johannes Michael Kattan

15.09.1989	Born in Lauf, Germany

Education

2000 - 2009	Highschool Melanchton Gymnasium Nürnberg, Germany
2009 - 2015	B.Sc + M.Sc. Biology JMU Würzburg, Germany
2015-2020	Ph. D. in synthetic biology Department of Bionanoscience, Delft University of Technology, Netherlands *Thesis:* Biosynthesis of protein filaments for the creation of a minimal cell *Supervisor:* Dr. C. J. A. Danelon *Promotor:* Dr. C. J. A. Danelon *Co-Promotor:* Prof. dr. M. Dogterom

List of publications

Doerr A, de Reus E, van Nies P, van der Haar M, Wei K, **Kattan J**, et al. **Modelling cell-free RNA and protein synthesis with minimal systems**. Phys Biol 2019;16:25001.

Kattan J, Doerr A, Dogterom M, Danelon C **Shaping liposomes by de novo synthesis of bacterial microtubules**. *in preparation.*